" NON-LINEAR ANALYSIS

OF

REINFORCED CONCRETE FRAMES "

by

RICHARD HUGH DEEBLE

A THESIS SUBMITTED FOR THE DEGREE

of

DOCTOR OF PHILOSOPHY

DEPARTMENT OF CIVIL ENGINEERING,

UNIVERSITY OF ASTON IN BIRMINGHAM

September 1973

THE AUTHOR

The author graduated from the Civil Engineering Department of the University of Aston in Birmingham in July 1969. The following year, he was employed as an Assistant Engineer in the Structural Department of Wallace Evans & Partners, Consulting Engineers in Penarth, Glamorgan. During this period, he was engaged in the design and detailing of reinforced concrete structures.

The work presented in the thesis was carried out in the course of three calender years of full-time research under the supervision of Professor K. I. Majid.

No part of this work has been submitted in support of an application for another degree or qualification.

SYNOPSIS

The work presented in this thesis constitutes an investigation into the use of computer methods for the non-linear analysis of reinforced concrete frames. Two computer methods are proposed, both of which use a concept of gradually reducing flexural rigidity of a section upto collapse. The change in stiffness and properties along a frame are accounted for by dividing it into smaller submembers of constant stiffness.

The first method uses an incremental technique to account for the non-linearity of the material. A series of linear analyses are performed for each increment of proportional loads applied to a frame upto collapse, the stiffnesses of all submembers are modified at every increment according to their induced curvatures. In this method, the instantaneous flexural rigidity-curvature diagram of the material is used.

For the second method, the smooth non-linear moment-curvature relationship of reinforced concrete is assumed to consist of a series of straight lines. The points joining these lines are termed critical points. An iterative technique is adopted to predict load factors at which these critical points are attained for each submember upto collapse.

To verify the accuracy of these analyses, a set of twelve pin-ended reinforced concrete frames were tested subject to proportional loading upto collapse. The moment-curvature relationships of each section used in the frames are obtained from tests performed on beams of identical section. A method is also presented whereby these relationships can be found from the properties of a section and its constituent materials. The effect of axial load on these relationships is also examined.

Comparison of the results shows that the non-linear behaviour of reinforced concrete frames can be predicted successfully by computer analysis.

ACKNOWLEDGEMENTS

The author would like to thank his supervisor, Professor K. I. Majid, for his help and encouragement during the last three years.

Thanks are also expressed to the laboratory technical staff of the Department for their assistance in the preparation of the reinforced concrete specimens, and construction of the test rigs.

In the preparation of this thesis, the author would like to thank his wife for typing a difficult script.

Finally, the author would like to thank the staffs of the Computer Centres at Aston University and the Atlas Computer Laboratory for their prompt service and the Science Research Council for their financial support.

CONTENTS

			Page
SYNOPSIS			(i)
ACKNOWLEDGEMENTS			(ii)
CONTENTS			(iii)
NOTATION			(vii)
CHAPTER 1		INTRODUCTION AND HISTORICAL REVIEW	
	1.1	General Introduction	1
	1.2	Analysis of Structures	2
	1.3	Non-linearity in structures	3
	1.4	Failure of structures	7
	1.5	Historical Review	8
	1.6	The developments in reinforced concrete frame analysis	14
	1.7	Scope of the present work	27
CHAPTER 2		MOMENT CURVATURE RELATIONSHIP OF REINFORCED CONCRETE	
	2.1	Introduction	30
	2.2	Properties of reinforced concrete sections	30
	2.3	Determination of the moment-curvature relationship of a reinforced concrete section	33
	2.4	Properties required for constructing the moment-curvature diagram	43
	2.5	Instantaneous flexural rigidity	44
	2.6	Representation of the (EI) - Ø diagram	44
	2.7	Axial load effect on moment-curvature relationships	46

		Page
CHAPTER 3	THE NON-LINEAR ANALYSIS OF REINFORCED CONCRETE FRAMES BY AN INCREMENTAL TECHNIQUE	
3.1	Introduction	51
3.2	Numerical techniques for the non-linear analysis of structures	51
3.3	Non-linear analysis of reinforced concrete frames by an incremental technique	57
3.4	Particular factors to be considered in the formation of the incremental computer analysis for reinforced concrete frames	64
3.5	A computer program for the non-linear incremental analysis of reinforced concrete frames	76
3.6	Results	79
3.7	General discussion of the incremental method	79
CHAPTER 4	NON-LINEAR ANALYSIS OF REINFORCED CONCRETE FRAMES BY AN ITERATIVE LOAD FACTOR METHOD	
4.1	Introduction	85
4.2	Properties of reinforced concrete	85
4.3	Difficulties arising in the non-linear analysis of reinforced concrete frames	86
4.4	Non-linear analysis by the iterative load factor method	87
4.5	The computer program	92
4.6	Conclusions and discussion	95

			Page
CHAPTER 5		TESTS ON REINFORCED CONCRETE PORTAL FRAMES	
	5.1	Introduction	101
	5.2	Details of the frames	101
	5.3	Manufacture of frames and beams	108
	5.4	Instrumentation	110
	5.5	The test rig	111
	5.6	Testing the apparatus	118
	5.7	Test procedure	118
CHAPTER 6		TESTS ON REINFORCED CONCRETE BEAMS TO DETERMINE THEIR MOMENT-CURVATURE RELATIONSHIPS	
	6.1	Introduction	121
	6.2	Details of the beams	121
	6.3	Manufacture of beams	122
	6.4	Test arrangement	122
	6.5	The test rig	127
	6.6	Test procedure	130
	6.7	Comparison of measured and theoretical moment-curvature relationships	131
	6.8	Moment-curvature relationships of the sections	134
	6.9	Conclusions	137
	6.10	Tests on reinforced concrete sections subject to axial load	137
	6.11	Results of axial load tests	138

Page

CHAPTER 7 COMPARISON OF RESULTS AND GENERAL REMARKS

7.1 Introduction 163

7.2 The consistency of the results in sets 1, 2 and 3 163

7.3 Description of experimental results with particular regard to their failure modes 166

7.4 Comparison of results by experiment and computer 177

7.5 The effect of axial load in the columns on the results of frame F13 197

CHAPTER 8 GENERAL CONCLUSIONS

8.1 Summary 201

8.2 Conclusions 203

8.3 Suggestions for future research 207

APPENDIX 1 210

APPENDIX 2 228

REFERENCES 235

NOTATION

A_c	Area of concrete section
A_s	Area of tensile steel reinforcement
A'_s	Area of compressive steel reinforcement
C	Total compressive force
C_c	Concrete compressive force
C_s	Compressive steel force
E_c	Modulus of elasticity of concrete
E_s	Modulus of elasticity of steel
EI	Flexural rigidity
$(EI)_c$	Flexural rigidity in the cracked state
$(EI)_t$	Instantaneous flexural rigidity
$(EI)_u$	Flexural rigidity after steel yield
$(EI)_{un}$	Flexural rigidity in the uncracked state
F	Load factor
I_e	Transformed second moment of area
I_G	Gross second moment of area
M	Bending moment
M_c	Moment at first cracking of concrete
M_{crit}	Moment at a critical point
M_k	Modified moment
M_p	Fully plastic moment
M_u	Moment at ultimate state
M_y	Moment at first yield of steel
P	Axial load
P_u	Ultimate axial load
T	Total tensile force

Y_c	Centroid of total compressive force
b	Breadth of a section
d	Effective depth of a section
d'	Depth to centroid of compressive reinforcement
e	Strain
e_{cc}	Strain in concrete at extreme compressive fibre
e_{cu}	Ultimate compressive strain in concrete
e_{sy}	Yield strain in tensile reinforcement
e'_{sy}	Plastic strain in steel
f	Stress
f_{cc}	Stress in concrete at extreme compressive fibre
f_{ct}	Ultimate tensile strength of concrete
f'_{cu}	Ultimate compressive stress in concrete
f_{sc}	Stress in compressive reinforcement
f_{sy}	Yield stress of tensile reinforcement
f'_{sy}	Increased tensile stress in steel
f_{su}	Ultimate tensile stress of steel
h	Depth of a section
k	Bending moment factor
r	Percentage of tensile reinforcement
x	Depth of neutral axis
z	Lever arm
z_G	Gross section modulus

Matrices and vectors

$\underline{K}$	Overall stiffness matrix of a frame
$\underline{L}$	Load vector of a structure

$\underline{X}$	Joint displacement vector
$\underline{P}$	Member force vector
$\Delta \underline{L}$	Increment of load
$\Delta \underline{M}$	Increment of bending moment
$\Delta \underline{P}$	Increment of member force
$\Delta \underline{X}$	Increment of joint displacements
$\Delta \underline{\phi}$	Increment of curvature

Greek symbols

Δ	Increment
ϕ	Curvature
ϕ_c	Curvature at first cracking of concrete
ϕ_y	Curvature at yield of tensile reinforcement
ϕ_u	Curvature at the ultimate state
θ	Rotation

CHAPTER 1

INTRODUCTION AND HISTORICAL REVIEW

1.1 General Introduction

1.1.1 In recent years, rapid advancements have been made in the analysis and design of engineering structures. The more sophisticated developments have been associated with the analysis of steel structures. These developments include facilities to deal with many non-linear effects prevalent in all types of structure. Reinforced concrete is now becoming a widely used material in the construction of many types of structure. There is, therefore, a need to develop methods of analysis for reinforced concrete structures parallel in sophistication to those existing for the analysis of steel structures.

1.1.2 The prime requirement of any analysis is to predict the behaviour of real frames as accurately as possible. To accomplish this, the combined and overall behaviour of all the members of a frame, and a true representation of their properties must be known. The new unified code of practice (1) in its general requirements for analysis states :

" The methods of analysis used in assessing compliance with the requirements of the various limit states should be based on as accurate a representation of the behaviour of the structure as is practicable. "

1.1.3 It is possible in certain cases to analyse reinforced concrete structures by simplifying them into simple sub-frames. These simplified sub-frames are then analysed by the classical methods such as moment-distribution, or the slope-deflection equations. If, however, a true prediction of overall structural behaviour of frames with many degrees of freedom is required, resort must be made to use of matrix methods of analysis in conjunction with a digital computer. It is, thus, desirable to formulate techniques which fully define the complete behaviour of any reinforced concrete frame and which utilise the actual properties of its members.

A more convenient method of expressing the property of reinforced

concrete is by its bending moment-curvature relationship. This relationship has been used in the work covered by this thesis. An analysis must also be capable of coping with special situations which occur in a loaded reinforced concrete frame, such as cracking of the concrete, the effect of axial loading and the attainment of ultimate bending moment at various sections prior to collapse.

1.1.4 The work presented in this thesis is an investigation to determine whether an analysis is possible for predicting the non-linear behaviour of reinforced concrete frames upto collapse. To verify the practicality of any new analysis, it is necessary to perform investigations into the real behaviour of frames, and then compare the results with those obtained by the analysis. In this thesis, the results obtained from the computer analyses have been compared with the results obtained by a series of tests performed on reinforced concrete frames loaded proportionally to collapse. The moment-curvature properties of the different sections employed in these frames were determined from tests carried out on reinforced concrete beams of identical sections. In addition, an analytical method for determining these relationships based upon the properties of the concrete and steel has been presented, using the relationships obtained by both these methods, the frames were analysed.

1.2 Analysis of Structures

1.2.1 Before any structural analysis can be performed accurately, a great deal of information regarding the behaviour of a material and its response to loading must be investigated. The more important considerations of these are now discussed.

1.2.2 The behaviour of structural materials are generally taken to fall into three idealised forms. For the work described throughout this thesis, flexural deformations are predominant in members, and therefore, their bending moment-curvature relationships are utilised to define the behaviour. The three most common

idealisations of material behaviour are :-

1) Elastic

2) Rigid-Plastic

3) Elastic-Plastic

The elastic response is shown in fig. 1.1(a). In this idealisation, the range of interest is confined to the point at which the elastic limit of the material is attained, denoted by a, c, in the figure. An analysis performed using this philosophy assumes factored values of yield stress and strain to ensure no section of a frame reaches its elastic limit, whilst subject to working loads.

The rigid-plastic form is shown in fig. 1.1(b). This assumes no deformation of a structure until plasticity is reached at point a. The deformation is then purely plastic a - b. This concept has been utilised in the development of the rigid-plastic and ultimate load theories.

The final idealisation is the elastic-plastic theory shown in fig. 1.1(c). This is the most representative of the three concepts, since it includes both the elastic and rigid-plastic behaviour of the material, and so defines the overall behaviour. These idealisations, however, apply mainly to steel and most metal materials, and are not representative of the non-linear behaviour of reinforced concrete.

1.3 Non-linearity in structures

1.3.1 Before dealing with the non-linearity of structures, it is important to mention that most practical structures behave in an approximate linear manner under their working loads. Linearity does suffer from certain drawbacks, in that no consideration is made of the significant reserve of strength to be gained from materials after yield takes place. No attempt can be possible to define the behaviour when a structure is subject to high loading by an elastic

(linear) analysis. The assumption of linear behaviour is very uneconomic from the material aspect.

1.3.2 If an analysis is performed by any of the above three idealisations, simplifying assumptions are nearly always necessary to render the analysis practicable. These assumptions are concerned with the three main causes of non-linearity in engineering structures which are :

1) The non-linear behaviour of the material used in the manufacture of the structure.

2) The effect of large deformations compared with the undeformed structure, i.e. the change in geometry of a structure under loading.

3) The effect of heavy compressive axial loads in members on their bending stiffness, and on the distorted structure of 2) above. The effect can be so significant that there is a real likelihood of a structure becoming unstable whilst still in the elastic state. Some other causes of non-linearity in structures manufactured from steel and reinforced concrete are given below :-

(a) Steel

(i) Spread of plasticity in members

(ii) Stress reversal

(iii) Strain hardening of the material

(b) Reinforced Concrete

(i) Cracking of the concrete and yield of the reinforcement

(ii) Spread of plasticity in both the reinforcement and concrete

(iii) The effect of creep in the concrete

(iv) Falling branch effects

1.3.3 The property of steel may be represented by the idealised elastic-plastic relationship of fig. 1.2. The behaviour is assumed to be elastic upto

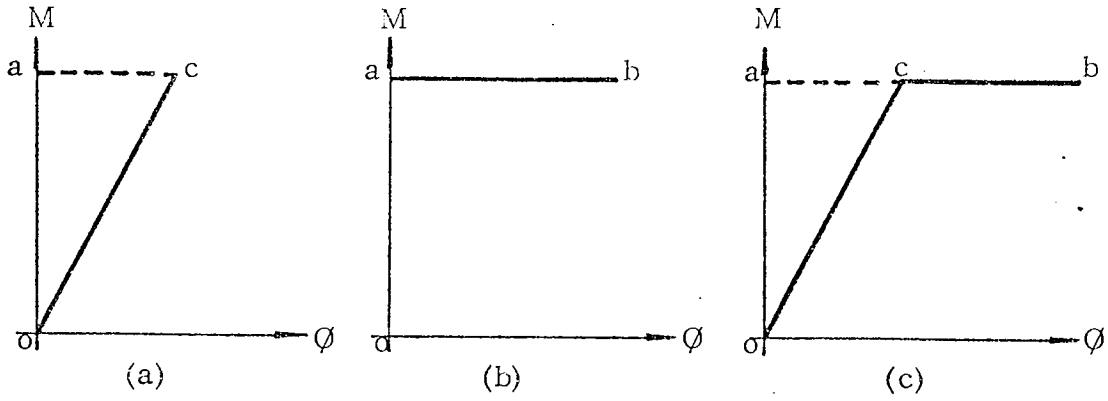

Figure 1.1 Idealised moment-curvature diagrams
(a) elastic
(b) rigid-plastic
(c) elastic-plastic

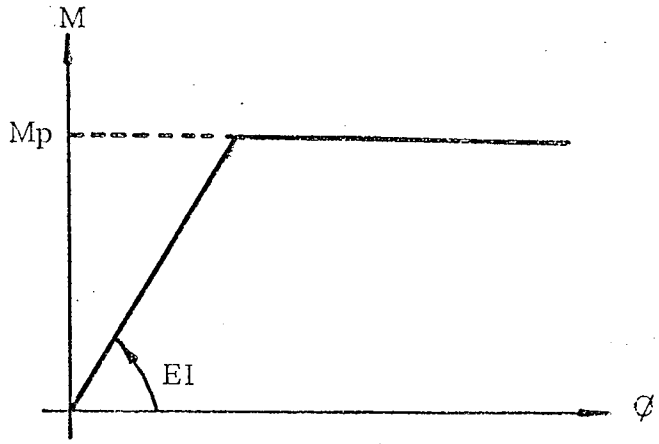

Figure 1.2 Idealised elastic plastic moment-curvature relationship of steel

the attainment of the fully plastic moment M_p of the section, after which, the behaviour is purely plastic. The effect of strain hardening of steel on the carrying capacity of small structures is considerable, and an allowance for this should be made if an accurate analysis is required. In large, multi-storey structures, heavy axial loading occurs in the lower columns, and the effect of the instability is greater than that of strain hardening, for this type of structure the latter effect may thus be neglected. The moment-curvature property of reinforced concrete is highly non-linear, and this will be discussed fully in Chapter 2. A brief outline of the main problems will be given here. It is well known that concrete is weak in tension and develops cracks when subjected to tensile flexure. This results in a reduction of flexural rigidity of the material, after which, the behaviour is essentially elastic, until the steel reinforcement yields. The stiffness of the section is then reduced gradually until the maximum bending moment of the section is reached. The curve then remain reasonably constant until the concrete crushes and then falls. For under-reinforced concrete sections consisting of reinforcement which exhibits strain hardening, a further increase in moment after yield of steel is present. For over-reinforced concrete sections, the moment-curvature relationship falls immediately after the attainment of maximum moment. This is referred to as 'falling branch' behaviour. In practical structures, it is not always necessary to consider this behaviour as constituting collapse. In most cases, any extra loading from these falling branch sections as they unload is transferred to other parts of the structure. Both these above situations should be allowed for in an accurate analysis.

1.3.4 In a linear analysis, it is assumed that the deformations of a structure are small compared with its overall dimensions. The equilibrium equations are thereby formed using the undeformed geometry of a structure. For most practical frames, especially those manufactured from reinforced concrete, the

deformations produced by loading, do not in fact alter their overall geometry significantly, even near the collapse state. The loss in accuracy resulting from the assumption of small deflections is not significant for these cases. However, where tall, slender sway frames are subject to heavy compressive axial loading, use of the undistorted structure in the solution of the equilibrium equations may well lead to an overestimation of overall structural stiffness. This is because the bending moments throughout the structure increase due to the PΔ effect.

Use of the distorted frame geometry is, therefore, necessary for an analysis of this type of frame.

1.3.5 Axial loading also affects the moment-curvature properties of materials. In steel sections, the presence of compressive axial loads cause a reduction in their fully plastic moment value. Compressive axial loads also affect the moment-curvature relationship of reinforced concrete sections, this effect will be described later in the thesis.

1.4 Failure of Structures

1.4.1 Structural failure can be defined in many ways. The attainment of ultimate bending moment at one section may be deemed as failure, even though the structure may be capable of supporting further loading. In a rigid-plastic analysis, failure is defined as that state when sufficient plastic hinges have formed in a structure to transform it into a mechanism. The most generally accepted form of failure, however, is taken as that when a structure loses all its stiffness, and is incapable of withstanding further loading.

1.4.2 Modern ideas concerning the analysis and design of reinforced concrete structures has led to the concept of Limit States (1). In a 'design' of a reinforced concrete structure, a combination of these limit states must be considered. These limits are concerned with the state of a structure in its ultimate condition,

and with its serviceability state such as extent of cracking and its durability.

1.5 Historical Review

1.5.1 For many years, the elastic approach to analysis was used as the basis for all the early work, the most prominent of these being the use of the slope deflection equations, and the more recent moment distribution method. The manual use of either of these methods, even for the analysis of structures with few redundancies, requires a great deal of effort and time on behalf of the analyst. Elastic methods, however, are still used by engineers, but many simplifying assumptions are necessary for a frame analysis. In an elastic analysis or design, member sizes are selected on the basis that they do not develop stresses greater than certain permissible values when the structure is subject to its working loads. These loads represent the maximum values which a structure is expected to carry in its working life.

1.5.2 For an elastic analysis, therefore, no load factor against collapse can be obtained, only safety factors are imposed to ensure no part of a structure reaches its elastic limit. Most structural materials, however, exhibit a great deal of reserve strength, even after the attainment of yield. This led to an investigation for a more rational approach to the analysis and design of frames. For steel structures, the result was the formation of the rigid-plastic theories of structural analysis by J. F. Baker and his team (2)(3). These theories are based upon the state of a frame at collapse. At this ultimate state, the bending moment distribution in a frame must satisfy three main conditions.

(i) The equilibrium condition, for which the internal bending moments must be in equilibrium with the externally applied loading.

(ii) The mechanism condition, where the bending moments must be equal

to the fully plastic moments at a sufficient number of sections for the whole or part of a structure to become a mechanism with plastic hinges.

(iii) The yield condition where the ultimate (fully plastic) moment must not be exceeded at any part of a structure.

Other conditions which must be adhered to are that plastic hinges possess unlimited rotational capacity, whilst the bending moment there remains constant at the fully plastic value. Also, premature collapse does not occur due to member instability. Finally, the deflections of a frame are negligible until the collapse state is reached. The rigid-plastic theory yields a more economical design, as the full range of properties of a material are utilised, and a specified load factor against collapse can be imposed.

Horne (4) developed a plastic moment distribution method which utilised most of the above conditions. By this method, a structure could be designed so that a given set of loads would just cause collapse. The object of this method was to establish various distributions of bending moments throughout the structure that are in equilibrium with the given loads. Another method which makes use of the above characteristics of the distribution of bending moments to determine the collapse load of a trial design, is that due to Neal and Symmonds (5). In this method, individual mechanisms were combined to determine the actual collapse mechanisms.

1.5.3 The foregoing rigid-plastic approaches to analysis and design cannot be universally applied to all steel structures, in particular, tall, slender, multi-storey sway frames, where the effect of instability may cause collapse at loads far below those predicted by a rigid-plastic analysis. For the analysis of low steel frames and continuous beams in which the non-linear effects of axial load and gross deflections are small the rigid-plastic theory can be used with a high degree of accuracy. The effect of instability in the elastic-plastic range

of behaviour of a steel frame was the subject of most of the subsequent research on the design and analysis of frames. Wood (10) discussed the importance of frame instability in cases where sway was unrestrained. He stressed that failure may well take place before a mechanism is formed.

1.5.4 Methods which include an allowance for instability in the ultimate load analysis and design of multi-storey steel sway frames have been suggested by Heyman (11) and Holmes and Gandhi (12). Extensive work has also been carried out in the design of tall sway frames subject to instability effects by the Lehigh University Group (13).

1.5.5 In most of the foregoing methods, assumptions of structural behaviour regarding the plastic hinge pattern at failure have been made. A true prediction of this behaviour is only possible if a rigorous analysis is adopted. With the advent of the electronic computer, it was realised that a rigorous analysis of structural frames was possible by means of suitable computer programs, used in conjunction with the matrix displacement method of structural analysis (19). In this method, expressions relating the external loads $\underline{L}$ applied to a frame, to the resulting joint displacements $\underline{X}$ are formed. This is achieved by applying the conditions of joint equilibrium and compatibility to the equilibrium equations of individual members. The equation which relates the loads to the displacements of a frame is given in matrix form as :

$$\underline{L} = \underline{K}\,\underline{X} \qquad (1.1)$$

where $\underline{K}$ is the overall stiffness matrix of a structure. In any analysis by this method, the external loads $\underline{L}$ and the matrix $\underline{K}$ are known, so equation (1.1) can be solved for the unknown joint displacements $\underline{X}$. The member forces $\underline{P}$ of a frame are then found using $\underline{P} = \underline{k}\,\underline{A}\,\underline{X}$, where $\underline{k}$ is the member stiffness matrix and $\underline{A}$ is the displacement transformation matrix.

1.5.6 Livesley was among the first in this country to use a computer for

the analysis of frames. He presented a paper (14) for the computer analysis of rigidly jointed elastic frames in which an allowance was made for the presence of instability. This work was later developed to include the elastic-plastic behaviour of frames, by among others, Livesley (15), Jennings and Majid (16). These developments enabled the complete non-linear load deflection history of a frame to be traced upto and including collapse. Refinements were made to these methods by Anderson (17)and Majid and Anderson (18). By reducing the required storage space for the overall stiffness matrix of a structure, they were able to analyse large multi-storey steel structures elastic plastically.

In (18), the elastic plastic behaviour of a steel frame is examined as plastic hinges develop under increasing proportional loading. Allowance is made of the non-linear effect of axial loads in members at these load factors on the reduction of the stiffness (using the appropriate stability functions (9)) and fully plastic moments of the members, by use of an iterative technique. The axial loads which are expected to occur under the predicted load factors are extrapolated in each cycle of the iteration. A plastic hinge is formed when the predicted load factors at the current and previous cycle of the iteration, satisfy a tolerance test. The hinge is inserted in the frame and the process continued to predict further hinges. At the insertion of each hinge in a frame, the sign of the determinant of the stiffness matrix is found, if it is negative, the frame has lost all its stiffness and has collapsed. The program has facilities to allow for the state where plastic hinges become inactive.

1.5.7 The program described above can deal with the analysis of very large multi-storey frames, by virtue of the reduced computer space required for storage of the overall stiffness matrix, and reduced computation time required for the solution of the stiffness equation (1.1). The overall stiffness

matrix for the frame of fig. 1.3(a) is shown in fig. 1.3(b). In this figure, the non-zero elements of the matrix are shown shaded, it is also noticed that the non-zero elements are grouped around the leading diagonal of the matrix in an irregular band-width. This arrangement is true of the stiffness matrices of most plane frames. The matrix is also seen to be symmetric about the leading diagonal.

For the storage and solution of the stiffness equation (1.1), the compact elimination technique due to Jennings (20) was adopted. In this method, only the elements which lie between the first non-zero one and leading diagonal, inclusive of each row, are stored. The result is a series of half band-widths of elements, for each row of the stiffness matrix. These elements are then stored in vector form in a 'main sequence'. In addition, the positions of each location in the main sequence which stores the leading diagonal element of each row is defined in another vector termed the 'address sequence'. Some zero elements will, however, occur in the main sequence, but these can be reduced by careful numbering of the joints in a frame.

Computer time and storage was further reduced by inserting the rows corresponding to plastic hinges just below the rows corresponding to the joints near to which they develop. With the matrix stored in this main sequence form, Jennings' elimination technique was used to solve the equation:

$$\underline{X} = \underline{K}^{-1} \underline{L} \qquad (1.2)$$

The technique is based on the well known Gaussian elimination method for the direct solution of linear simultaneous equations. A rapid solution is obtained as only the stored elements are operated upon.

This computer method includes most of the significant advances which have been made in the understanding and prediction of the true non-linear behaviour of steel frames. Majid and Anderson have also produced a program (21)

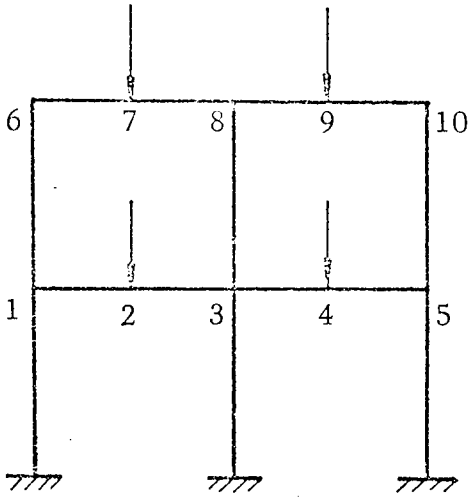

(a)

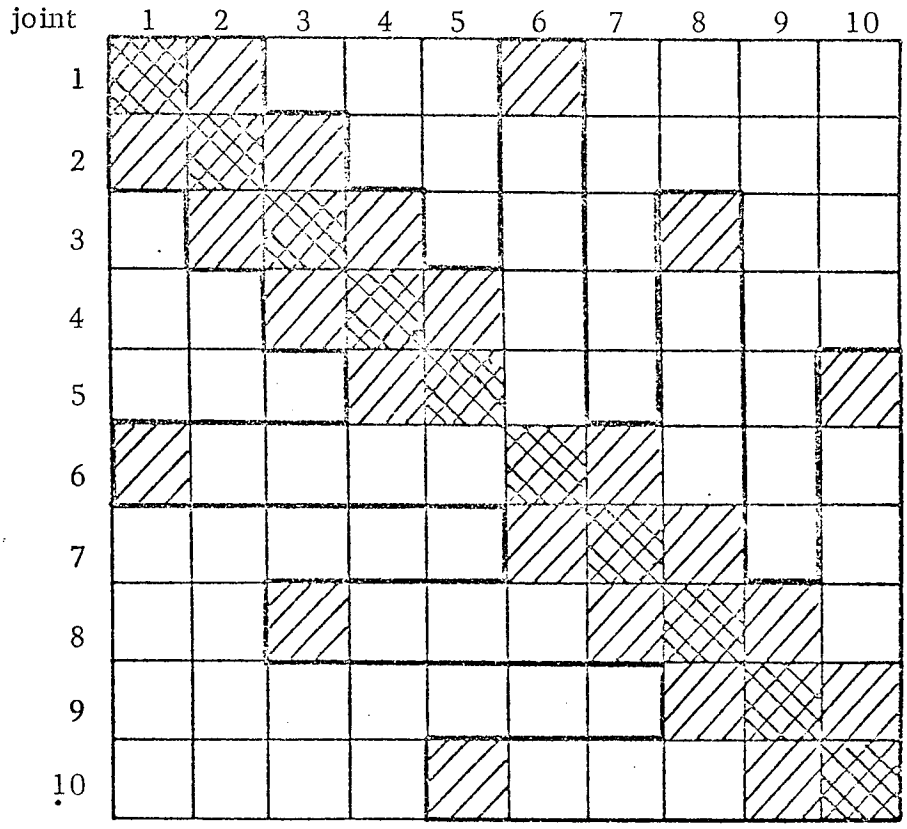

(b)

Figure 1.3 The overall stiffness matrix of the 2-storey 2-bay frame

for the elastic plastic design of steel sway frames. Further work is now in progress (22) (23) (24) which deals with the elastic plastic analysis and design of complete building structures of steel frames with concrete shear walls and slabs, and of frames with infill panels.

1.5.8 The foregoing review shows the developments that have been made for the analysis of steel structures in particular. Most of these methods cannot, however be applied directly for the analysis of reinforced concrete frames. This is because the concept of a plastic hinge cannot be assumed for reinforced concrete in the same way as for steel, since reinforced concrete has a limit on its available plastic deformation. For under-reinforced concrete sections, there is a significant reserve of strength after the tensile steel yields, this is not true, however, for over-reinforced sections which fail as soon as the concrete crushes, with no steel yield taking place. Other differences between reinforced concrete and steel sections are that concrete sections crack prior to the attainment of steel yield, resulting in a reduced stiffness. The properties along a member may also change due to varying percentages of tensile reinforcement. In addition, the strength of concrete varies from mix to mix, even for those with identical constituents. The problem can then be one of statistics in the definition of concrete strength. These factors together with others, such as the effect of joint detailing, contribute to the main differences in the properties and behaviour of reinforced concrete frames.

In any analysis which is to predict the true behaviour of a reinforced concrete frame, the above factors together with those discussed for steel frames must be considered.

1.6 The developments in reinforced concrete frame analysis

1.6.1 The need for an analysis which represented the true behaviour of reinforced concrete frames was realised early. Investigation by Glanville and

Thomas (25), carried out on fixed ended beams, continuous beams and portal frames showed a redistribution of bending moments in the structures as collapse was approached. It was concluded from these tests that reinforced concrete structures were capable of exhibiting some ductility. The extent of this ductility for the redistribution of bending moments in the application to reinforced concrete frame analysis was the subject of subsequent research.

1.6.2 This work was primarily to investigate whether reinforced concrete frames possessed sufficient ductility to redistribute bending moments as collapse was approached, and thus, not fail immediately an ultimate bending moment was reached for the first time in the frame. Parallel to this, research was being undertaken (26) to analyse reinforced concrete sections in the ultimate state. This increased the knowledge of the behaviour of reinforced concrete sections and was incorporated in frame analyses. In this country, Professor A. L. L. Baker pioneered the research on moment redistribution in reinforced concrete frames, his first paper on this subject (27) was published in 1949. He later developed the ultimate load theory for the design of reinforced concrete frames, and published it in book-form (28) in 1956.

In his method, a simple elastic-plastic moment rotation relationship was assumed for the material. This was defined by the initial flexural rigidity EI, the ultimate moment of resistance and a limited plastic rotation capacity. For a frame with n indeterminancies, the load at which the nth hinge forms was termed the ultimate load. The positions of plastic hinges were selected using the bending moments obtained from the slope deflection equations. The rotations of each hinge were calculated by use of virtual work equations in combination with a trial and error prodecure. If rational and safe estimates were made of the moment rotation parameters, design was possible by allowing redistribution of bending moments to such an extent that

the resulting hinge rotations are compatible with the hinge moments, and their magnitudes within safe limiting values. An appropriate relaxation technique was used to check deflections and crack widths.

This method defines the ultimate load of a given structure, but is cumbersome, and no check is made of frame instability prior to the attainment of ultimate collapse load. Improvements have been made to this technique, however, the basic approach outlined above was used in their formation. Baker later presented a method (29) for the ultimate load design of concrete frames, in which the concepts of an idealised frame, an elastic-plastic frame and a practical frame were introduced. The idealised frame is one which based on the assumption of the plastic hinge theory has the correct ultimate strength for a particular case of loading. The calculations in this are based on safe limiting values of parameters that govern strength and deformation. The members of a frame are designed elastically between hinges. The elastic-plastic frame is similar to the idealised frame, with the exception that plasticity is here distributed at hinge sections according to the elastic-plastic bending moment distribution. The practical frame is the actual designed frame. In the design, a frame was assumed to consist of a series of elastic members joined by frictionless hinges. A general arrangement of the frame and its concrete sections appropriate to its loading were assumed. Sufficient hinges were then inserted in the frame to make it statically determinate and resistance moments assumed to act at hinges to yield an economic distribution of bending moments. The positions of hinges and values of rotations were checked at ultimate load by a similar method to that described in reference (28), and adjustments made until a satisfactory solution was obtained for each case of the idealised frame. A practical frame was then designed to be at least as strong in all parts as each of the idealised frames.

This method was an advance on the previous work, but still required a great deal of work on behalf of the analyst. Developments leading to a technique for the design of inelastic space frames (30) were later made. Future developments in Baker's method (31) (32) prompted the European Committee for Concrete (CEB) to initiate an extensive programme of tests into the flexural behaviour of reinforced concrete members, the object of which was to obtain safe limiting values for the parameters necessary in a design by Baker's method. The CEB utilises this method in the proposed limit design philosophy (33). The latest developments of Baker's method are given in his book (8) " Limit Design of Reinforced Concrete."

1.6.3 The ultimate load theory has been accepted as a basis for the analysis and design of reinforced concrete structures for a number of years. The previous code of practice for the structural use of concrete (6), CP114, was amended in 1965 to allow the load factor method to be used as an alternative to the elastic method for design. In this load factor method, a value of 1.8 was suggested as the ratio of the ultimate strength of a member to its working load. The code also allowed a 15% reduction in bending moment in statically indeterminate structures provided the bending moment diagram is redrawn on this basis.

1.6.4 The methods described above are essentially hand methods. The need for a computer analysis of reinforced concrete frames was suggested amongst others by Cranston (34). He carried out his work with the object of developing ultimate load design procedures for reinforced concrete frames upto and beyond maximum load. He followed the work suggested by the Committee set up by the Institution of Civil Engineers (31). He suggested that reinforced concrete shows a further reserve of strength even after the point of first crushing of concrete, and that the rotations which should be allowed for

in reinforced concrete plastic hinges are, in many cases, much greater than those previously considered reasonable. Cranston stressed the need for setting up mathematical models for the simulation of behaviour of real frames. The specific factors which affect the behaviour of reinforced concrete, such as its high non-linearity, were discussed. The behaviour of loaded concrete members is described with particular reference to their moment-rotation (M - θ) relationships. The relation to be expected from an under reinforced member is given by curve A in fig. 1.4 (a). It is shown that the curve flattens out gradually after steel yield and then remains essentially constant until crushing of concrete occurs, it then decreases. If the tension steel exhibits strain hardening, the curve may show an increase in moment when θ becomes large, as indicated by curve B in fig. 1.4 (a). For over-reinforced members, the M - θ relation generally has the form shown in fig. 1.4 (b), where it can be seen that the moment decreases immediately after the maximum moment is attained. This is referred to as falling branch behaviour.

The more important assumptions Cranston made in the formation of his analysis were :-

(i) The curvature at any point is a function of only the moment of that point.

(ii) Deformations of the frame due to axial and shear strains may be neglected.

(iii) Members of a frame can be idealised into a number of segments separated by division points.

(iv) Loads are only applied at division points.

(v) The effect of unloading of zones into the inelastic range can be neglected.

A frame is reduced to the state of statical determinancy by the insertion of sufficient hinge releases. The redundant moment values are proposed, and the

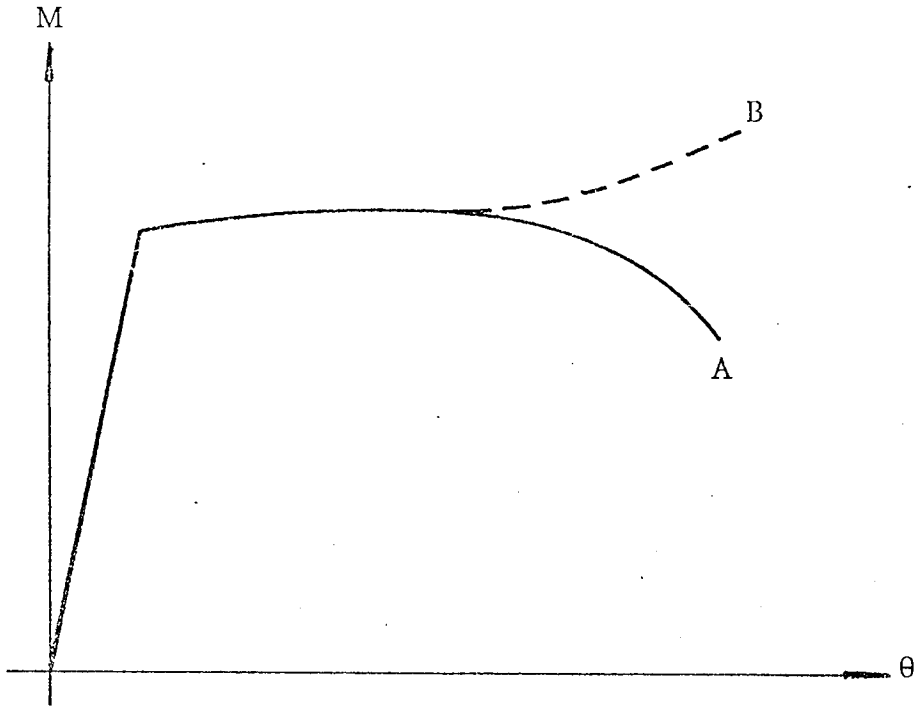

(a)

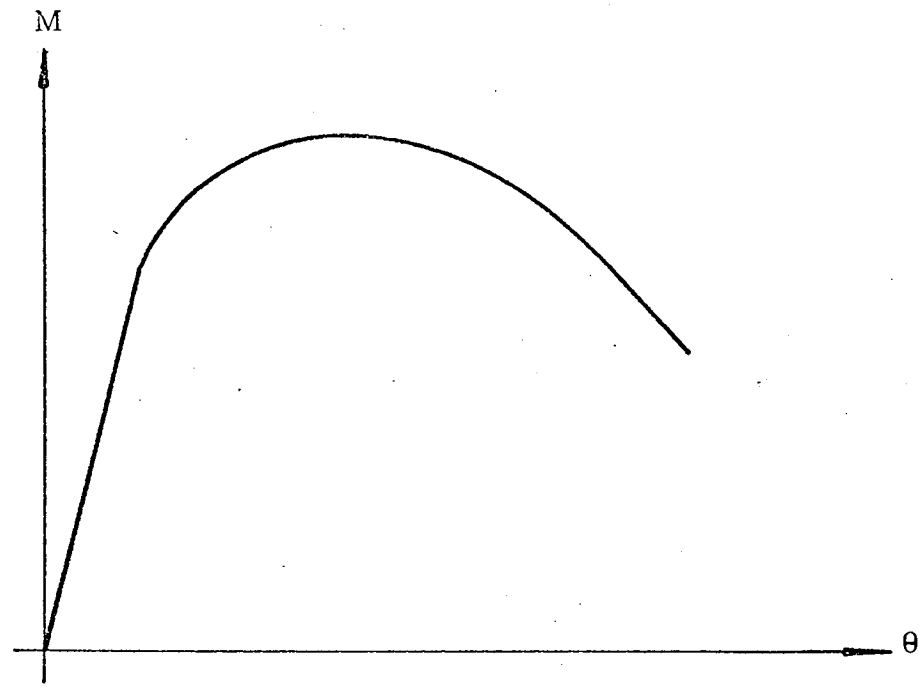

(b)

Figure 1.4 Moment-rotation behaviour
(a) for under-reinforced sections
(b) for over-reinforced sections

resulting deflected shape and discontinuities at the releases are computed by numerical integration. A solution to the proposed shape is found when convergence of the deflected shape is made, this reduces the hinge discontinuities to zero.

1.6.5 To verify the accuracy of this proposed computer analysis, Cranston carried out a series of tests on portal frames (35) (36). The first of these consisted of pin-ended reinforced concrete portal frames, the second was fixed ended portals. In the first set (35), a series of tests on 8 frames are described. The dimensions of a typical frame together with its loading geometry and instrumentation are given in fig. 1.5. The concrete sections were constant throughout, and were reinforced with 2 No. 3/8" diameter bars for compression steel and between 2.2% and 4.4% tension steel at sections where plastic hinges would form. These percentages gave sections in which both the moment-rotation characteristics shown in fig. 1.4 would occur. Deflections and slopes were measured by dial gauges and inclinometers. The frames were tested subject to varying combinations of vertical and sway load.

Two of the 8 frames failed prematurely due to local failures at joints. The remaining 6 frames failed by the expected mechanism. The results of these tests were presented in the form of moment against rotation for each hinge, and load, moment and sway against deflection at mid-transom. The main conclusions drawn from this test series were that the recommendations for the assessment of permissible hinge rotations in (32) were safe. The behaviour of a frame subject to short term loading is predicted with reasonable accuracy by an elastic analysis. Also from this test series, Cranston suggested that further tests were needed on frames with more redundancies to broaden the scope of his conclusions.

Further tests were performed on fixed ended reinforced concrete

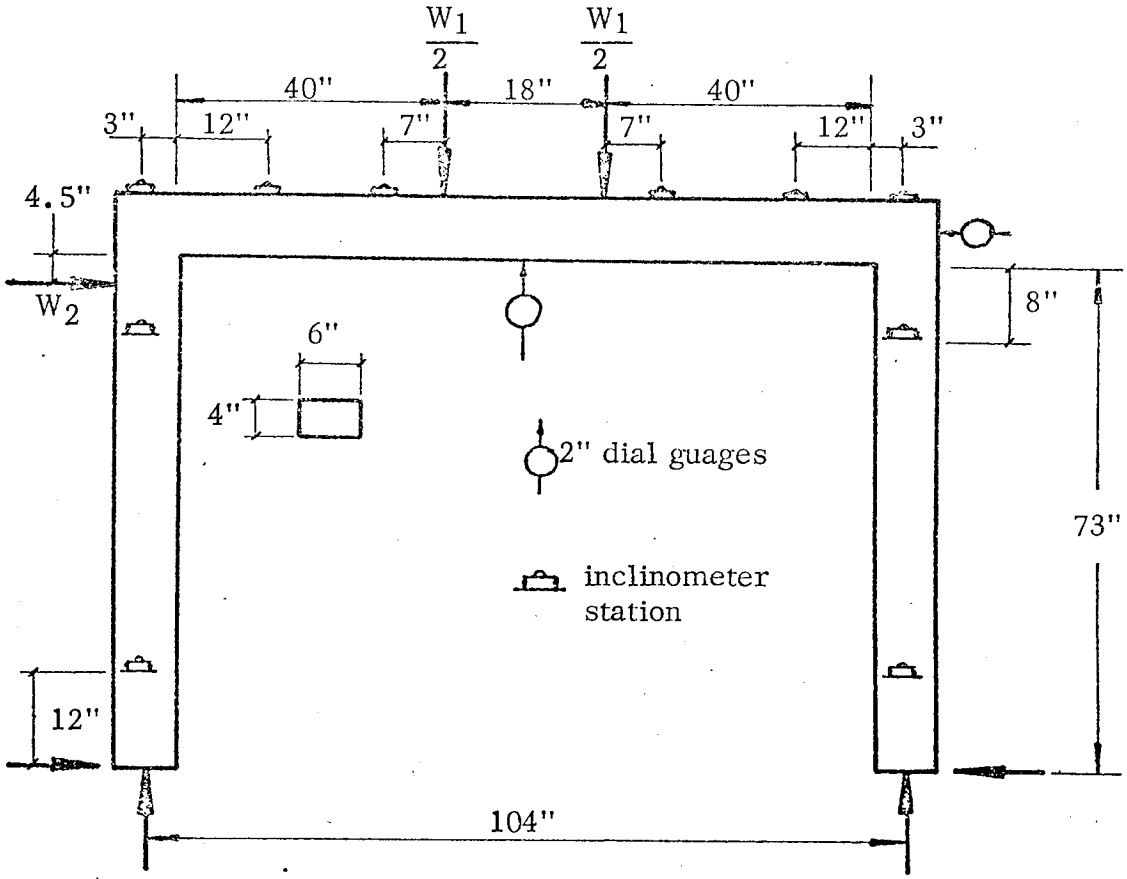

Figure 1.5 Typical Arrangement of a Reinforced Concrete Portal Frame Test by Cranston.

portal frames (36). From these tests, Cranston was able to make more confident conclusions. These were that collapse loads computed on the basis of a mechanism behaviour are reasonable, provided the plastic moments are calculated using the stress block data given in (37). The degree of binding in the compression zone has an influence on the rotation capacity. Special attention must be paid to the stress concentration around joints. He also mentioned that the effects of heavy axial loading in columns and the secondary details around joints, both require further attention.

The computer method presented above is fully comprehensive and can deal with any shaped moment-curvature relationship. The complexity of the method is such, however, that the size of a frame that may be analysed by it is limited. Also, the program requires a great deal of work from the analyst in preparation of data prior to running an analysis by computer.

1.6.6 Much of the Cement and Concrete Association's recent work has been concentrated on the effects of heavy axial loads in columns, and of localised stresses at joints. Cranston (38) presented a method for determining the relationship between bending moment, axial load and curvature in structural members. A numerical technique is proposed for use with a digital computer for determining this relationship. This led to the computer analysis of restrained columns (39). Here, a method is described which can analyse columns of different materials, inelastically. All stages of the column's behaviour upto and beyond maximum load are considered. An iterative procedure was evolved which determines the response of cross sections under specified axial loads and moments. Solutions for a given column are obtained in stages as loading is applied from zero to its maximum value. These solutions correspond to either specified load or deflection. This method was later developed and together with the conclusions of further parallel research and experimental evidence, a

report (40) was published which sets out a practical method for the design of reinforced concrete columns.

The effect of shear on the rotation capacity of reinforced concrete beams has been obtained by a series of tests performed by the C and CA (41). It was shown that the final failure at hinge regions under large shear forces is dominantly of a shear type. However, no significant reduction in available rotation capacity is prevalent, if the shear force is designed for, under the provisions set out in the draft code of practice (7).

1.6.7 The detailing of joints in reinforced concrete frames is of prime importance, if bending moments are to be transmitted to their members. If this detailing is poor, then there is a great likelihood that localised failure will take place at the joints. This has prompted the Cement and Concrete Association to investigate the effect of joint detailing on the strength of reinforced concrete connections.

An investigation into the effects of right angled bends of portal frames subject to opening and closing bending moments was carried out by Swann (42). From his investigations, he concluded that for cases where the bending moments tended to open the corner, the details shown in fig. 1.6 (a & b) performed better than the remaining details. Where the bending moment tended to close the corner, the detail of fig. 1.6(c) was the only one in which bearing failure of the concrete at the bends of the main reinforcement did not limit the strength of the specimens.

Sommerville and Taylor later investigated the influence of reinforcement detailing on the strength of concrete structures (43) and reported on its influence on structural efficiency for half joints, joggled splices in columns, flexural corners and in-situ beam column joints. They concluded from this that the most efficient arrangement of reinforcement can generally be found

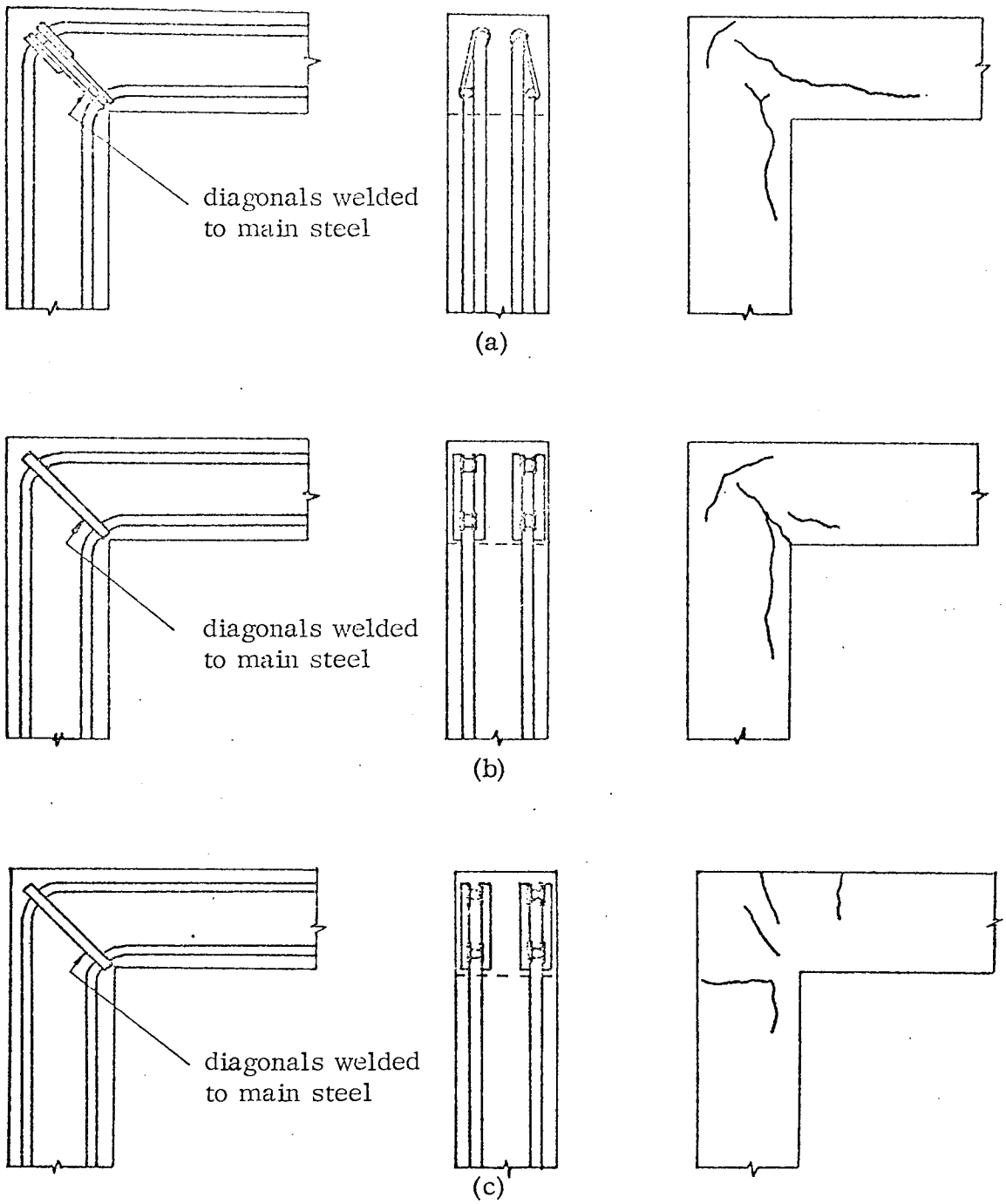

Figure 1.6 Reinforcement details and major crack patterns of best test specimens by Swann

(a) where bending moment tended to open corner
(b) where bending moment tended to open corner
(c) where bending moment tended to close corner

from a simple consideration of the forces involved. Where flexural corners are being opened, their strength depends greatly upon the type, detail and amount of reinforcement being used.

1.6.8 The effect of instability in tall reinforced concrete sway frames is of great importance. Among others, Baker (44) and later Nahhas and Yu (45) studied its effect. In reference (45), the effect of overall frame instability in the elastic-plastic design of reinforced concrete sway frames was discussed. The secondary effect of axial loads in members acting on the deformed structure was suggested as a real threat to the overall stability of tall, slender sway frames. They stated that if a thorough analysis was to be obtained, this effect must be allowed for. They pointed out that even though Baker (8) had extended his method to allow for this action, no attention is paid to the sequence of formation of plastic hinges. The design method is based upon an allowance for the sway $P\Delta$ effects, by means of a magnifying factor applied to the lateral loads. Theoretical moment-curvature relationships are obtained by the known stress-strain curves of the materials based on the assumption of a linear distribution of strain. A brief description of the method is given below.

In a design, if a suitable estimate of the relative lateral sway between two consecutive floor levels Δ is made, and the frame is designed to resist lateral loading of magnified load, allowance would thus be made for the equilibrium of the internal moments and externally applied loads as affected by the sway deflection. Approximate expressions are presented for the calculation of magnifying factor. To satisfy serviceability and ductility requirements, hinges are taken to form at the leeward beam support sections, only at the design load. A check on ductility is made by comparing resultant plastic rotations at hinge sections with safe, permissible values. Compatibility is

checked for which a statically admissible bending moment distribution must be selected in equilibrium with the applied loads, including the magnified lateral loads; also a check that premature instability failure does not take place at the location of critical sections because of a deterioration of stiffness.

The design method was verified by a computer analysis carried out on a 7 storey - 3 bay frame designed by their proposed method. The method can be applied to most practical frames, and also an economic design can be obtained, where there is a limited amount of plastic deformation in members.

1.6.9 Other computer techniques for the inelastic analysis of reinforced concrete frames are presented below. Chin (46) developed a computer method for the non-linear analysis of plane frames subject to proportional loading. The analysis utilises the matrix displacement method and is suitable for a frame with members having an arbitrary moment-curvature relationship. The analysis is split into a main sequence, correction sequence and a prediction sequence. In the main sequence, a set of trial displacements are used to calculate the forces required to maintain equilibrium. If these forces are not sufficiently close to the chosen loading, the trial displacements are corrected using the stiffness properties of the structure. When the forces are close, the prediction sequence forms a new array of trial displacements for the next step of the load-displacement curve.

For this method, the curvature is assumed to be a function of moment only, and shear deformations are neglected. The method includes the non-linear effects of axial loads on the reduction of member stiffness. The program was used to analyse identical frames to those previously analysed by Cranston (34). The results obtained were shown to be in good agreement with those of Cranston's. Chin's analysis requires less work from the analyst, and the computer time

required is small compared with that given in reference (34).

Other methods which analyse reinforced concrete frames inelastically are due to, Nahhas (47), Wilson (48), Cohn (49), and Poologasumdram (50) to list a few.

In 1972, the British Standards Institution published the new code of practice (1) for the Structural Use of Concrete. This code makes use of Baker's work and includes the latest findings of the Institution Research Group.

1.7 Scope of the Present Work

1.7.1 In light of the foregoing review, it is clear that a more rational and universal analysis, similar to those existing for steel, is needed to predict the overall non-linear behaviour of reinforced concrete frames. The majority of the available methods require the selection of hinge positions prior to an analysis, and a constant re-analyse with modified hinge positions. A reliable method is required which will analyse a frame of any configuration comprising of members with any moment-curvature relationship.

1.7.2 The object of the work covered by this thesis is to present computer methods for the non-linear analysis of reinforced concrete frames upto and including the state of collapse, and to test their validity by tests performed on reinforced concrete frames, loaded proportionally to collapse.

1.7.3 The properties of reinforced concrete members are most conveniently defined by their bending moment-curvature (M-ϕ) relationships. Chapter 2 describes this relationship, and a method is proposed by which the M-ϕ relationships may be constructed theoretically from the properties of the concrete and steel. The effect of axial load on the M-ϕ relationships is also discussed here.

1.7.4 The following Chapter describes the incremental approach to the non-linear analysis of reinforced concrete frames. It is shown here that the overall non-linear behaviour can be predicted by summing a series of linear

analyses for small increments of load applied to a frame. A computer program which uses this analysis is described in this Chapter. Reference is also made of an iterative approach for use with the above method.

1.7.5 Chapter 4 details a second analysis and computer program which is a development of that by Majid and Anderson (18), to enable the analysis of reinforced concrete frames to be performed. For this method the M-ϕ relationship of reinforced concrete is represented by a series of short, straight lines connected at points which are termed critical points. At each critical point, a reduction in flexural rigidity occurs. The analysis computes load factors at which these critical points are reached upto collapse of a frame.

In both these computer analyses, the overall stiffness matrix of a frame is constructed and the stiffness equations solved by the method outlined in 1.5.7.

1.7.6 The validity of these analyses have been checked by a series of tests carried out on reinforced concrete portal frames. These are described in Chapter 5. Each frame was proportionally loaded vertically and in sway, upto collapse, and the load-deflection response recorded.

1.7.7 Moment-curvature relationships were obtained for each of the sections used in the portal frames from tests performed on beams of identical sections. These tests are described and the results reported in Chapter 6. A comparison is also made of the relationships obtained by experiment and by the theory of Chapter 2.

1.7.8 The results obtained for the analysis of the reinforced concrete frames of Chapter 5 by the two computer methods are presented and compared with the experimental results in Chapter 7. The results of each test are also described here, and a comparison also made with the collapse loads predicted by the rigid plastic theory.

General conclusions of the validity of the computer analyses are drawn in Chapter 8.

CHAPTER 2

MOMENT-CURVATURE RELATIONSHIP OF REINFORCED CONCRETE

2.1 Introduction

In this chapter, the properties of Reinforced Concrete sections will be investigated. The properties must be known before an analysis of a reinforced concrete frame can be performed. In rigidily jointed frames, it is the ability of members to deform, under the action of bending forces, which gives them their stiffness. A knowledge of the force-deformation characteristics of member sections is necessary. The most convenient method of representing this behaviour for reinforced concrete is by its bending moment-curvature relationship. Before obtaining this, the characteristics of the constituent materials, i.e. concrete and steel, must be investigated.

2.2 Properties of Reinforced Concrete Sections

2.2.1 Reinforced Concrete sections derive their strength in flexure, primarily, by the concrete resisting the high compressive stresses in the compressive zone, and the steel reinforcement resisting the large tensile stresses induced in the tension zone. The extent of the resistance provided by each material is represented by its stress-strain diagram.

2.2.2 The stress-strain characteristics for concrete in uni-axial compression is shown in fig. 2.1. It is seen that the curve is non-linear in shape. The initial stage, however, is reasonably linear and the slope at this point is the short term modulus of elasticity E_c. After reaching the ultimate compressive stress f'_{cu}, the stress decreases until crushing occurs at the ultimate compressive strain e_{cu}.

2.2.3 The stress-strain characteristics of a steel reinforcing bar, subject to a direct tensile force, is shown in fig. 2.2. From this figure, it is seen that the steel behaves linearly from zero stress up to the stress at which it begins to yield (point a). This is the yield stress f_{sy} and yield strain e_{sy}. The slope of the

curve in this linear region is the Young's modulus of elasticity E_s. There may be an increase in stress at point a for certain steels, but if the bar has been "cold-worked", this phenomenon disappears. Between points a and b the stress remains constant for increasing strain, this is termed pure plastic flow. At point b, there is a further increase in stress as the bar strain hardens. At point c, the steel reaches its ultimate tensile stress f_{su}. For further increases in strain, the stress decreases, and the bar ruptures at point d.

2.2.4 The stress-strain diagram of steel can be idealised as the material's moment-curvature relationship by two straight lines, see fig. 2.3. Initially, the behaviour is linear elastic up to the attainment of the fully plastic moment M_p of the section. This state is reached when the yield spreads throughout the depth of the steel section. The second line is horizontal, representing pure plastic deformation on which no limit is imposed. From fig. 2.3, it is seen that only the values of M_p and the initial flexural rigidity EI, (Young's modulus of elasticity * second moment of area) of the section are needed to fully define the relationship. In this idealisation, the effect of strain hardening in the material is neglected as it is assumed that the effect of axial load on the reduction of member stiffness compensates for its omission.

2.2.5 The moment curvature relationship of reinforced concrete is far more complex than that of steel. This relationship defines the combined resistance of concrete and steel to bending. It can therefore be expected that the relationship will be non-linear in nature. A typical moment-curvature diagram for an under-reinforced rectangular concrete section is given in fig. 2.4. It is seen in the diagram that the relationship is in fact smooth and non-linear. Initially, however, the curve is reasonably linear to point a, at which the concrete at the extreme tensile fibre begins to crack. This results in a decrease in flexural rigidity EI, which then remains reasonably constant up to point b. At this stage, the tensile

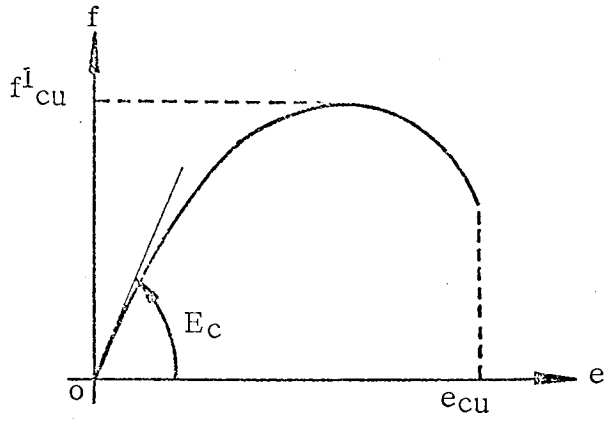

Figure 2.1 Stress-strain diagram for Concrete in Uni-Axial Compression

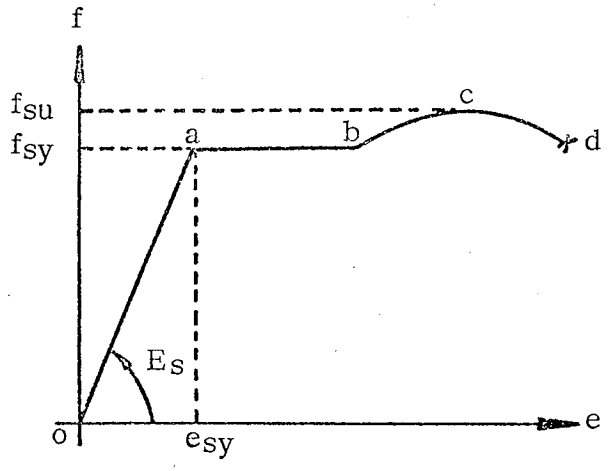

Figure 2.2 Stress-strain diagram for steel under direct tension

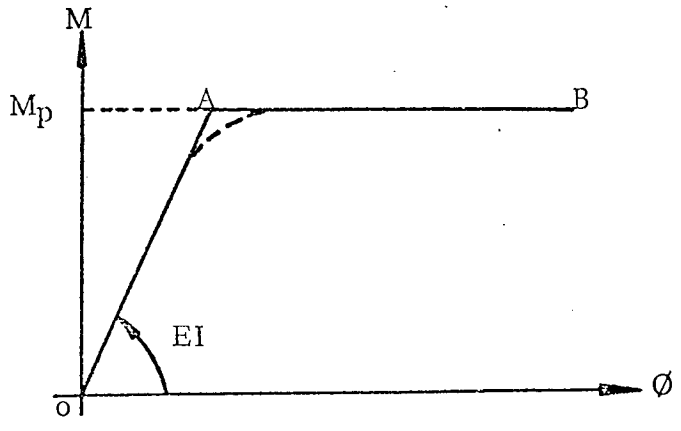

Figure 2.3 Moment-curvature relationship of steel

steel reinforcement begins to yield. Beyond yield, there is a small gradual rise in bending moment up to point c. This is the ultimate bending moment of the section. This increase in moment is primarily due to a rise in the neutral axis of the section, and the increased tensile resistance of the steel at the development of strain hardening. Failure occurs at point d when the concrete reaches its ultimate compressive strain and crushes.

2.2.6 The percentage of tensile reinforcement r present in a section influences its moment-curvature relationship significantly. The extent of this influence is shown in fig. 2.5 where it is seen that for the initial stage of the curves, i.e. up to first cracking of concrete, the percentage of tensile reinforcement r has little effect. In the cracked state, however, an increase in percentage of reinforcement results in increased flexural rigidity EI. This is to be expected since there are larger areas of steel resisting the tensile forces in the section. A section which contains large percentages of tensile reinforcement is termed "over-reinforced". For this type of section, the cracked stiffness does not vary significantly from that in the uncracked state. These sections are dangerous because they fail by crushing of concrete with little or no yielding of the steel. No warning is given of overloading as is prevalent with under-reinforced sections which crack and make use of the ductility of the steel, to supply a reserve of strength.

2.3 Determination of the Moment-Curvature Relationship of a Reinforced Concrete Section

2.3.1 Moment Curvature relationships of reinforced concrete sections can be obtained by two methods. The first is to perform tests on beams of the required section, and to measure curvatures for applied bending moments. This method will be described in Chapter 6. The second method is to determine the values of bending moment and curvature by consideration of the state of stress and strain in a section at points a, b and c in fig. 2.4. This method will be described overleaf.

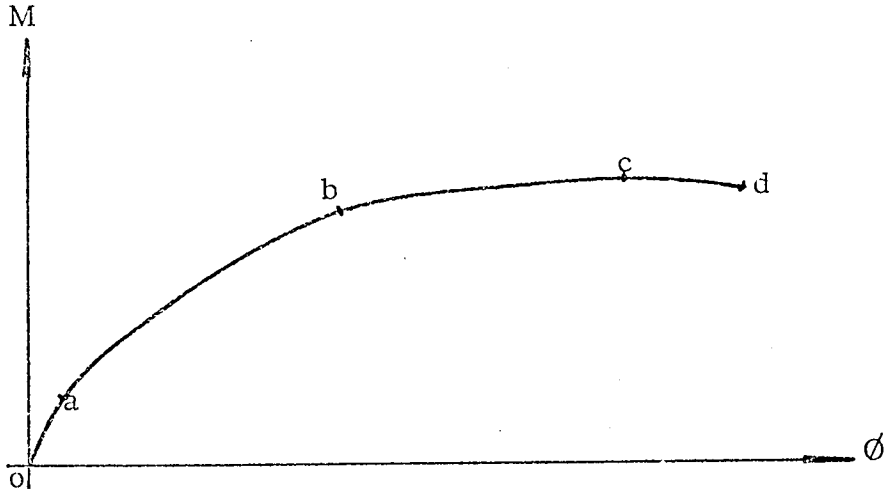

Figure 2.4 Typical Moment Curvature diagram for an under-reinforced concrete section

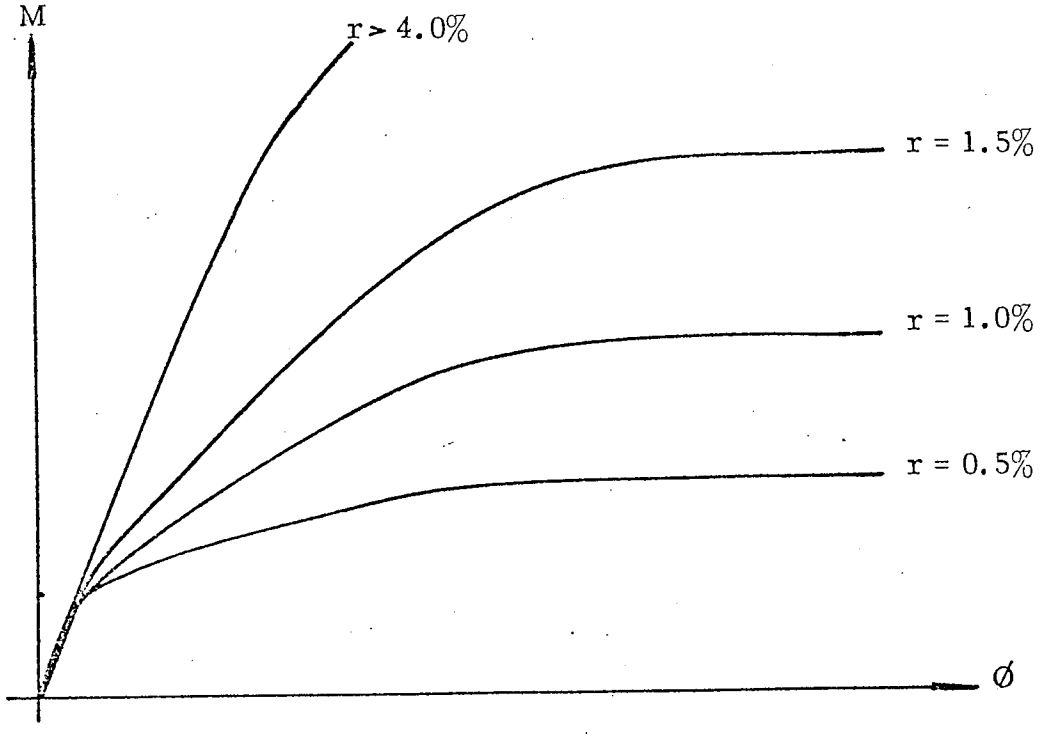

Figure 2.5 The effect of percentage of tensile reinforcement (r) on the moment curvature relationship of a section.

For practical purposes, the moment-curvature diagram of reinforced concrete can be represented by three straight lines. A typical M - Ø diagram of this form is shown in fig. 2.6. In this figure changes in initial flexural rigidity are seen to occur after first cracking of concrete, and first yield of steel. To fully describe this curve, it is necessary to obtain the following parameters : -

M_c ; $\emptyset_c$ - values of bending moment and curvature at which concrete cracks at the extreme tensile fibre of the section.

$(EI)_{un}$ - the flexural rigidity of the section in the uncracked state.

M_y , $\emptyset_y$ - values of bending moment and curvature at which first yield of the tensile reinforcement takes place.

$(EI)_c$ - the flexural rigidity of the cracked section.

M_u , $\emptyset_u$ - values of bending moment and curvature at which the concrete reaches its ultimate state.

$(EI)_u$ - the flexural rigidity of the section between yield and the ultimate states.

2.3.2 One method of obtaining the M - Ø relationship is to use the non-linear stress-strain relationship of reinforced concrete, but a simpler and more practical method is the use of a tri-linear representation. A method for constructing the tri-linear moment-curvature diagram for an "under-reinforced", rectangular concrete section is presented. In addition to the usual reinforced concrete theory assumptions, the following are also made to construct the diagram theoretically :-

(1) The concrete behaves elastically upto the first yield of steel. The value of the elastic constant is taken as the short term modulus of elasticity E_c. (see fig. 2.1).

(2) Cracking of concrete occurs when its ultimate tensile strength f_{ct} is reached. The bending moment at this state depends only upon f_{ct}.

(3) The section modulus z_G and second moment of area I_G in the uncracked state are given by considering the gross area of the section, including the reinforcement.

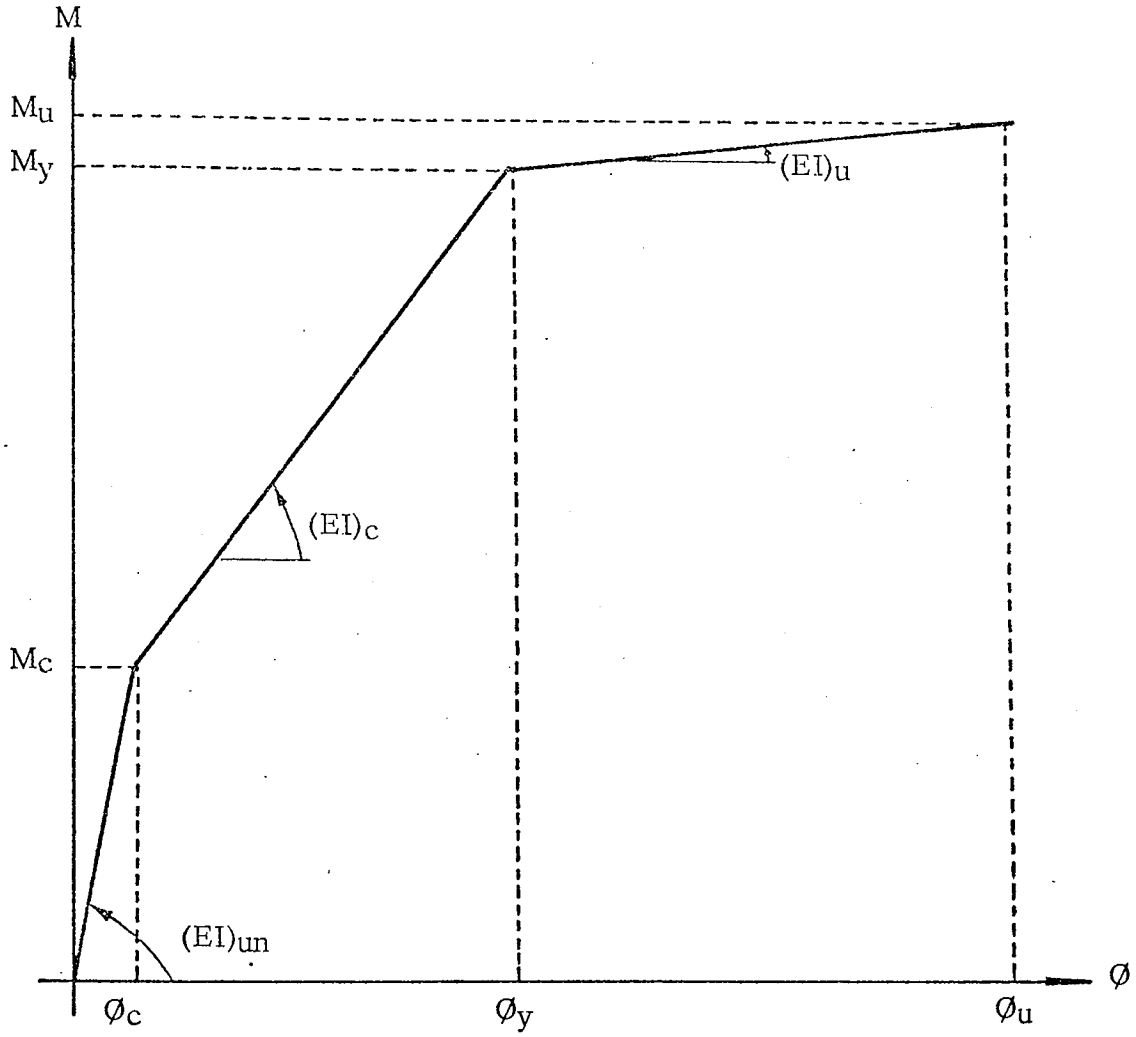

Figure 2.6 Tri-linear representation of the moment curvature relationship of reinforced concrete.

(4) In the cracked state, the stiffness of the section is complex. Empirical formulae are used to evaluate the cracked flexural rigidity $(EI)_c$.

(5) Yield is deemed to occur at first yield of the tensile reinforcement, the stress and strain at this point in the steel are taken as f_{sy} and e_{sy} (see fig. 2.2).

(6) The ultimate moment, M_u, is greater than the yield moment, M_y, due to a rise in the neutral axis, and the increased tensile resistance of the steel as it strain hardens. This condition is reached when the strain in the extreme compressive fibre is e_{cu}, the ultimate compressive strain of the concrete.

(7) The ultimate curvature, $\emptyset_u$, is obtained from the strain diagram at the ultimate state.

(8) At the ultimate state, the neutral axis is at the level of the centroid of the compressive reinforcement.

2.3.3 The uncracked state

The bending moment at which the concrete cracks is in fact fictitious. In reality, the first branch of the M-$\emptyset$ diagram shades off into the second branch. Cracks occur before the value of cracking moment, M_c, is reached. The value of M_c is therefore approximate. Using the usual elastic theory, the bending moment at first cracking of concrete is given by :-

$$M_c = f_{ct} * z_G \qquad (2.1)$$

where: f_{ct} is the ultimate tensile strength of concrete.

z_G is the gross section modulus of the section including the reinforcement.

The flexural rigidity of the uncracked section $(EI)_{un}$ is given by the product of the short term modulus of elasticity of the concrete E_c and the gross second moment of area of the section including the reinforcement, I_G. It is assumed that the material is behaving perfectly elastically in this state. Thus,

$$(EI)_{un} = E_c * I_G \qquad (2.2)$$

The value of E_c may be found experimentally (54), or from CP110(1) where it is related to the cube strength of the concrete. A linear relationship between moment and curvature is assumed up to the first cracking of concrete, and hence the curvature at this point is found from the so-formed triangle in fig. 2.6.

$$\phi_c = M_c / (EI)_{un} \qquad (2.3)$$

2.3.4 The cracked state

The state of a section after cracking of concrete is complex, since there are both cracked and uncracked sections between cracks. To define the flexural rigidity $(EI)_c$ in this state by theory is involved. Empirical relationships, however, exist which define the value of $(EI)_c$. The draft unified code, what is now CP110, suggested the following relationship :-

$$(EI)_c = 0.85\, E_c\, I_e \qquad (2.4)$$

where I_e is the transformed second moment of area of the section

From observations acquired from extensive tests carried out on beams, Monnier et al in the Netherlands (51) was able to relate the flexural rigidity in the cracked state to the percentage of tensile reinforcement r in the section as :-

$$(EI)_c = (-2.5r^2 + 13.9r - 1.1)\, bd^3 * 10^3 \text{ kgfcm}^2 \qquad (2.5)$$

where b - is the breadth of the section in cm

d - is the effective depth of the section in cm

The range of steel percentages for which this expression is valid is between the minimum possible, and that for which the cracked and uncracked flexural rigidities, are equal. Monnier's observations also indicated that the grade of steel, diameter of reinforcing bar used, and the presence of compressive reinforcement, had little effect upon the value of $(EI)_c$.

Both these relationships were used to calculate the magnitude of $(EI)_c$, and a comparison of the results obtained by these and by experimental observation is made in Chapter 6.

The state of stress and strain at first yield of steel in a section is shown in fig. 2.7. The symbols used below in the derivation of the bending moment and curvature at yield are also defined in this figure. To calculate the bending moment at yield, M_y, the lever arm of the couple, z, for the total compressive and tensile forces must be found. This is done by first calculating the depth x of the neutral axis.

For equilibrium $$T = C = C_c + C_s \qquad (2.6)$$

A check must be made to ensure that the compressive reinforcement is within the compressive zone throughout the calculation, if not, its position is allowed for in equation (2.6).

From fig. 2.7

The total tensile force $$T = A_s . f_{sy} \qquad (2.7)a$$

The concrete compressive force $$C_c = (f_{cc} . x . b) / 2 \qquad (2.7)b$$

The compressive steel force $$C_s = f_{sc} . A'_s \qquad (2.7)c$$

From the strain diagram, the strain at the extreme compressive fibre in the concrete is given by : $$e_{cc} = (e_{sy} . x) / (d - x) \qquad (2.8)$$

Now from assumption (1) $$f_{cc} = e_{cc} . E_c \qquad (2.9)a$$

also, $$f_{sc} = e_{sc} . E_s \qquad (2.9)b$$

Thus, $$e_{sc} = e_{cc} . (x - d') / x \qquad (2.10)$$

Substituting equations (2.7) to (2.10) in (2.6) we obtain :

$$A_s f_{sy} = \frac{e_{sy} . x}{d - x} \left(\frac{E_s . A_s' (x - d')}{x} + \frac{E_c . b . x}{2} \right) \qquad (2.11)$$

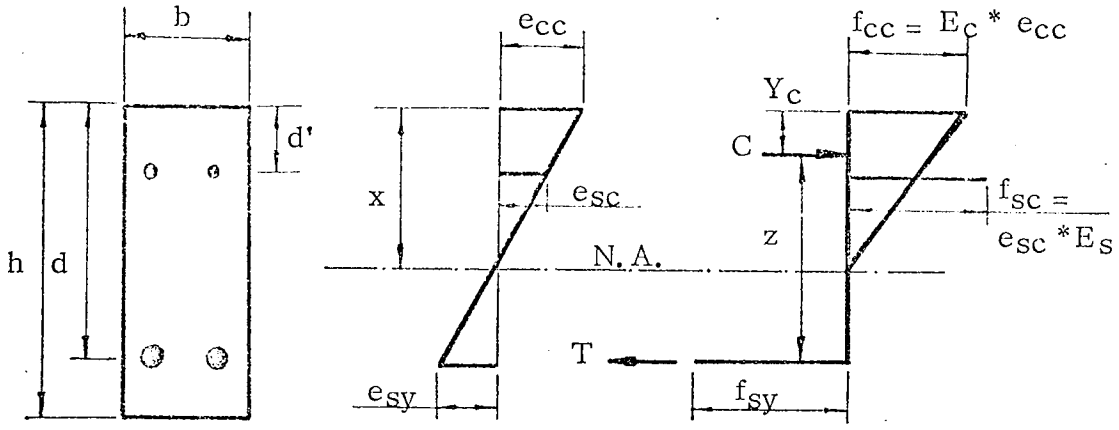

A_s	-	area of tensile reinforcement
A'_s	-	area of compressive reinforcement
b	-	breadth of the section
h	-	depth of the section
d	-	effective depth of the section
d'	-	depth to centroid of compressive reinforcement
x	-	depth of neutral axis from top of section
T	-	total tensile force
C	-	total compressive force
C_c	-	compressive forece due to concrete
C_s	-	compressive force due to compressive reinforcement
Y_c	-	depth of centroid of compressive force
z	-	lever arm of resisting forces
f_{cc}, e_{cc}	-	stress, strain in concrete at extreme compressive fibre
f_{sc}, e_{sc}	-	stress, strain in compressive reinforcement
f_{sy}, e_{sy}	-	yield, stress, strain in tensile reinforcement
E_s	-	modulus of elasticity of compressive reinforcement
E_c	-	short term modulus of elasticity of concrete

Figure 2.7 Stress-strain diagram of a section at first yield of steel

From equation (2.11) the depth x, of the neutral axis from the top of the section, can be found. The centroid of the total compressing force Y_c, and hence the lever arm z, may then be determined. The bending moment at yield is thus given as :

$$M_y = A_s . f_{sy} . z \qquad (2.12)$$

By reference to fig. 2.6, the curvature at yield can be found by considering the triangles formed by the straight lines.

$$\phi_y = ((M_y - M_c) / (EI)_c) + \phi_c \qquad (2.13)$$

N.B. The curvature at yield may also be determined from the state of strain in the section, by :

$$\phi_y = (e_{cc} + e_{sy}) / d \qquad (2.14)$$

where the values are as defined in fig. 2.7.

A comparison is made of the values of ϕ_y, obtained by equations (2.13), (2.14) and experiment, in Chapter 6.

2.3.5. The ultimate state

The bending moment increases from its value at yield to the ultimate value M_u. The ultimate state is assumed to occur when the extreme compressive fibre of the concrete attains its ultimate compressive strain, e_{cu}. The stress-strain diagrams for the section at the ultimate state, together with a definition of the symbols used, is given in fig. 2.8. The neutral axis is assumed to be at the centroid of the compressive reinforcement. It is also assumed that the plasticity in the concrete spreads throughout the depth of the compressive zone. The lever arm of the resisting couple forces of the section is given by :

$$z = d - d' / 2 \qquad (2.15)$$

Owing to the effect of strain hardening in the tensile reinforcement, an increased tensile stress, f'_{sy}, is assumed, the extent of which is taken as a portion of the actual gain of stress from yield f_{sy}, to the maximum value, f_{su}. The ultimate

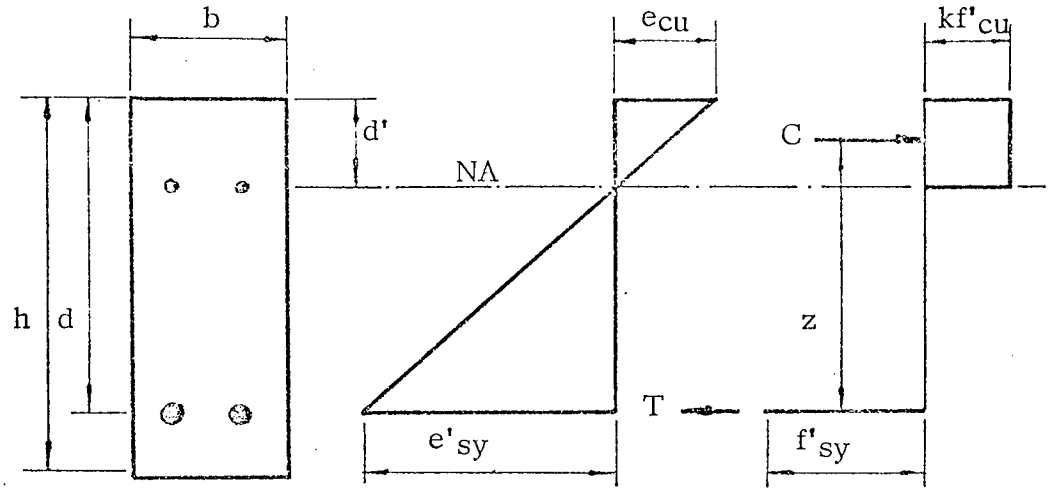

b, h, d, d', C, T, z (defined in fig. 2.7)

f'_{sy}	-	increased tensile stress in steel
e'_{sy}	-	plastic strain in steel
e_{cu}	-	ultimate compressive strain in concrete
kf'_{cu}	-	ultimate compressive stress in concrete for the depth of the compressive zone

Figure 2.8 Stress-strain diagrams of a section at the ultimate state

bending moment of the section is now given by :

$$M_u = A_s . f'_{sy} . z \qquad (2.16)$$

The corresponding curvature is obtained from the state of strain of the section, thus :

$$\emptyset_u = (e_{cu} + e'_{sy}) / d \qquad (2.17)$$

From fig. 2.6 the flexural rigidity $(EI)_u$ of the section in the ultimate state is given by the slope of the third line of the relationship, i.e.

$$(EI)_u = (M_u - M_y) / (\emptyset_u - \emptyset_y) \qquad (2.18)$$

2.4 Properties required for the construction of the theoretical M-Ø diagram

The equations necessary for the theoretical construction of the moment-curvature relationship have been derived. The properties of the concrete and steel required for the construction are :-

(1) The tensile strength of concrete - this can be measured by the split cylinder test as detailed in reference (53), or the modulus of rupture test.

(2) The short term modulus of elasticity of concrete. This may be measured experimentally or related to the cube strength of the concrete as is given in CP110.

(3) The tensile stress, strain curve of the steel, the modulus of elasticity of the tensile and compressive steel. These values are obtained from direct tensile and compression tests of the steel bars.

(4) An estimate of the increased tensile strength due to strain hardening of the steel (found in the same manner described above).

(5) The ultimate compressive strain in concrete. Values set out in codes of practice CP110.

The above method of constructing the M - Ø relationship theoretically is, however, restricted to under-reinforced concrete sections. A comparison of the moment-curvature relationships obtained by the method described in (2.3), and from experimental observations of tests carried out on beams is given in Chapter 6.

* Although the method is essentially semi-empirical, it will be referred to as the theoretical method throughout this thesis.

2.5 Instantaneous flexural rigidity

In a frame analysis, it is the flexural rigidity (stiffness) of a member which is of most importance. It is more convenient to relate the flexural rigidity of a member to its curvature. The instantaneous flexural rigidity $(EI)_t$ is the slope at any point on the moment curvature diagram. For the moment-curvature diagram of fig. 2.9(a), the instantaneous flexural rigidity at point i, is defined as :-

$$(EI)_{ti} = (dM/d\emptyset)_i \qquad (2.19)$$

2.5.1 The instantaneous flexural rigidity-curvature diagram is constructed by measuring the slope at points along the M-$\emptyset$ diagram. This slope is then plotted against the curvature at which it was measured e.g. point i in fig. 2.9(a) and (b). The main advantages in using this diagram are :

(1) the flexural rigidity is given directly for a specific value of curvature.

(2) the accuracy of the diagram can be improved by measuring the slope at points closer together.

(3) A completely smooth M-$\emptyset$ relationship can be represented by a series of short straight lines.

2.6 Representation of the $(EI)_t$ - $\emptyset$ diagram

The $(EI)_t$ - $\emptyset$ diagram is represented for use in a computer analysis by a set of straight lines joining specific points. These points correspond to particular values of flexural rigidity and curvature. For the non-linear M-$\emptyset$ diagram of fig. 2.10(a), the $(EI)_t$ - $\emptyset$ diagram is constructed by measuring the slope of the moment-curvature diagram at, e.g. eight points. These slopes are plotted against the curvature at each of the points. This is shown in fig. 2.10(b). The points are joined by straight lines. More points are selected in the curved regions of the M - $\emptyset$ relationships. Straight regions of the M - $\emptyset$ relationship are shown as horizontal lines on the $(EI)_t$ - $\emptyset$ diagram.

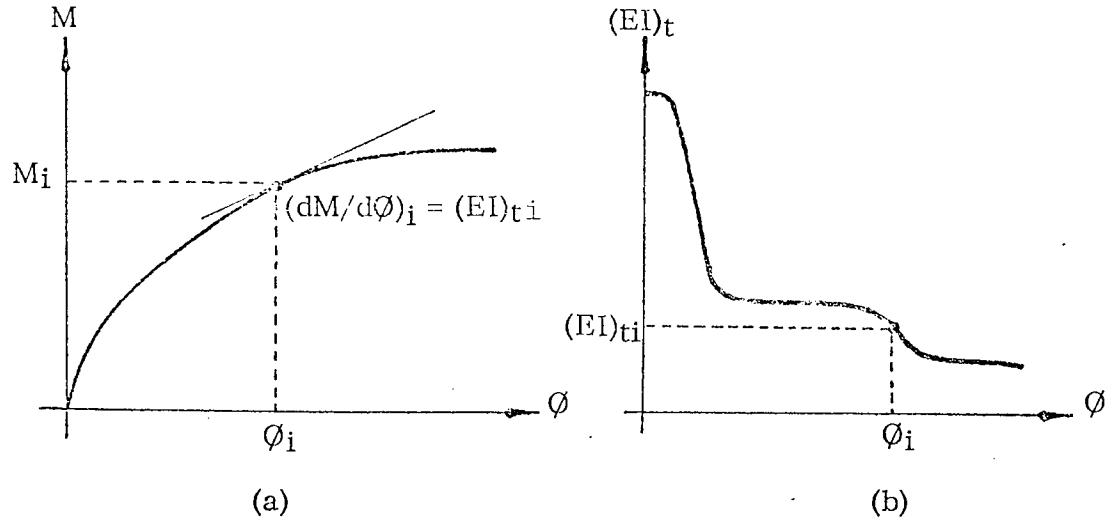

Figure 2.9 Evaluation of instantaneous flexural rigidity on moment curvature diagram

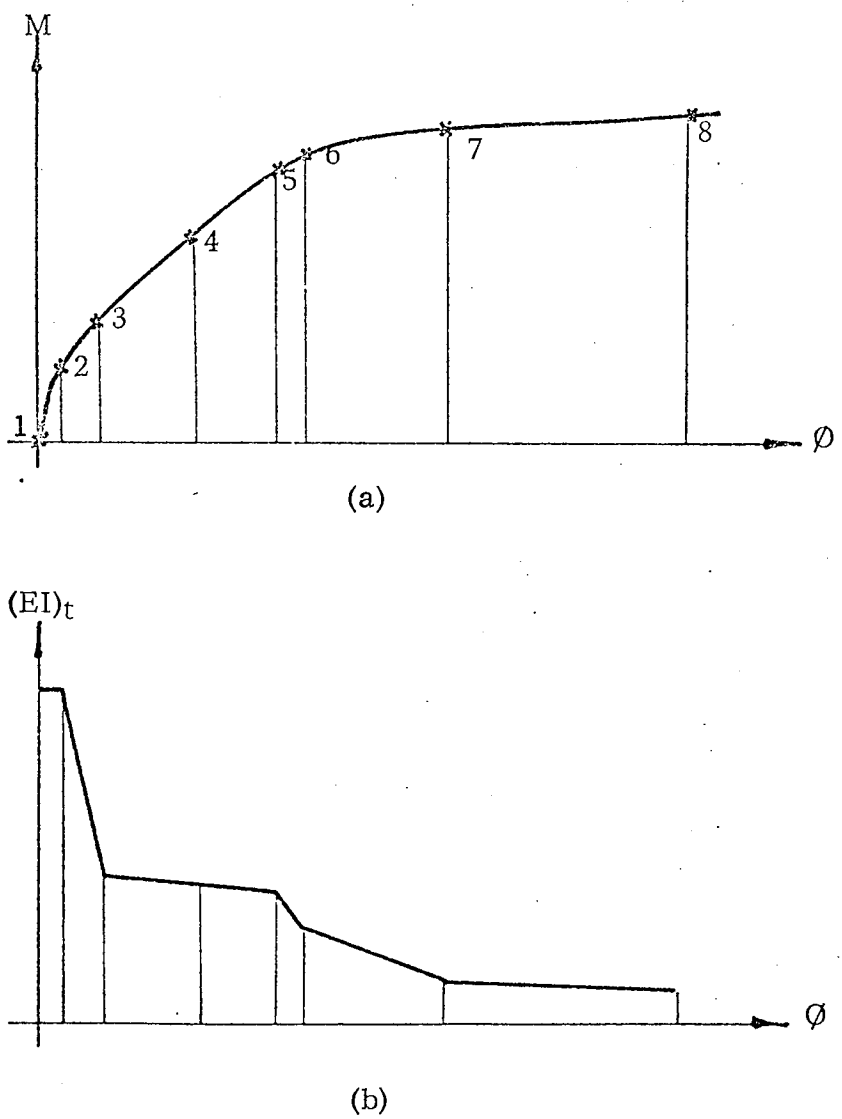

Figure 2.10 (a & b) Construction of $(EI)_t$-$\emptyset$ diagram from a typical moment curvature relationship

To present the $(EI)_t$ - $\emptyset$ diagram in a suitable manner for data in a computer analysis, the following approach is used. A two dimensional array is assigned for both the instantaneous flexural rigidity and curvature values. Each point of the $(EI)_t$ - $\emptyset$ diagram is numbered from one (zero curvature-initial flexural rigidity), upwards. The corresponding values of $(EI)_t$ and $\emptyset$ are assigned to these numbers. The number of points used depends upon the accuracy required for representing the moment-curvature relationship.

For the three line relationship derived in 2.3, the $(EI)_t$ - $\emptyset$ diagram of fig. 2.11 is obtained. From this figure, it is seen that abrupt changes of stiffness occur at the three main stages in the behaviour.

2.7 Axial load effect on moment-curvature relationships

2.7.1 In multi-storey frames, heavy compressive axial loading is present in their lower columns. It is necessary, therefore, to examine the effect of axial load on the moment-curvature relationship of column sections. In the preceding text, the M - $\emptyset$ relationships have been discussed with no axial load present in a section.

2.7.2 In fig. 2.12, the effect of axial load upon the M - $\emptyset$ relationship of a section is shown. The curves are for different ratios of axial load P to the maximum compressive load the section can withstand viz :

$$P_u = A_c f'_{cu} \qquad (2.20)$$

where, Ac is the area of the section

f'_{cu} is the ultimate compressive stress

From this figure it is seen that as this ratio P/P_u increases, the initial stiffness of the section increases. This is because the section is initially in compression and tensile stresses do not develop so quickly. The limit of this ratio for which an increase in initial stiffness always occurs is approximately $P/P_u = 0.4$.

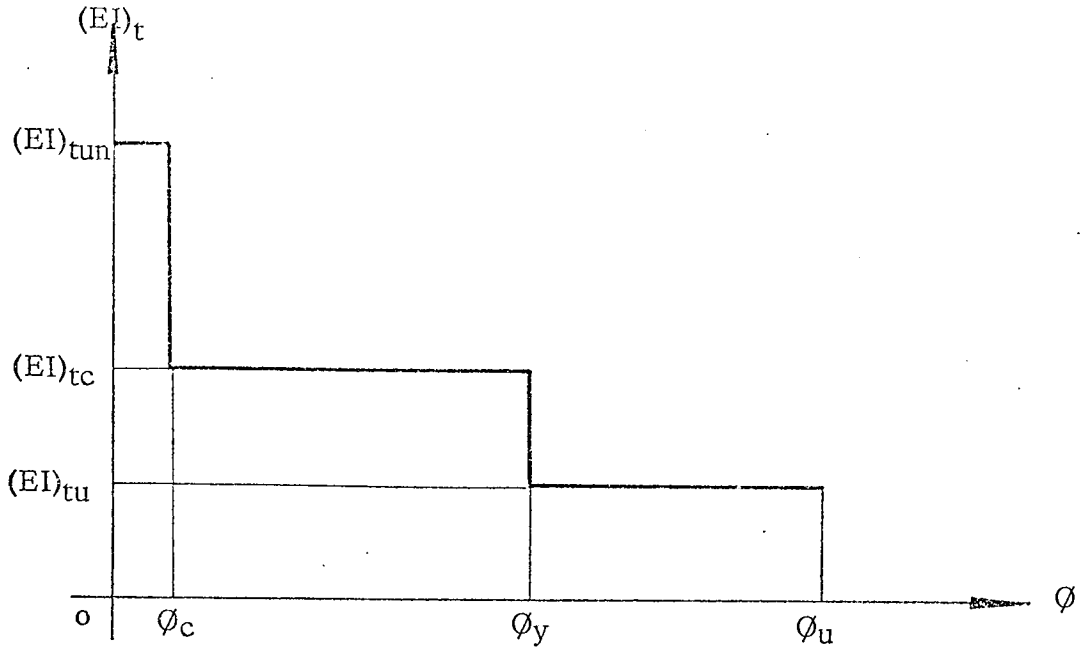

Figure 2.11 $(EI)_t$ - ϕ diagram from the tri-linear M-ϕ relationship of Art. 2.3

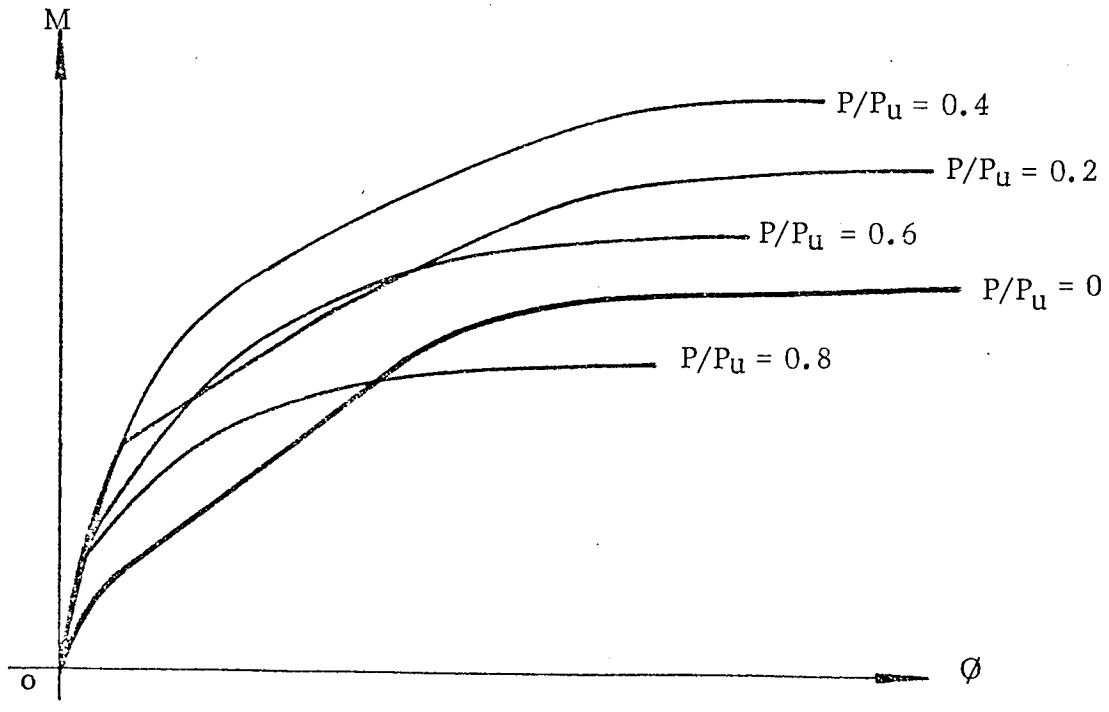

Figure 2.12 The effect of the presence of axial load in a section on its M-ϕ relationship

For values greater than 0.4, it is shown that the extent of plastic deformation is reduced. The percentage of tensile reinforcement present in a section influences the effect of axial load on the M - Ø relationship. This effect is reduced by increasing the percentage of reinforcement.

2.7.3 To allow for the presence of axial load in the lower columns of a structure, a suitable method for adjusting their moment-curvature relationships is needed. In this thesis, the axial load effect is neglected since small axial loads are present in the frames tested. To verify this, tests were carried out for the M - Ø relationship of reinforced concrete beams subject to a constant axial load. These are described in Chapter 6.

A method for determining the relation between axial load moment and curvature (P - M - Ø) for a section has been presented in a report by Cranston (38), where a numerical procedure for determining the relationship is presented. The bending moment and axial strain in a section corresponding to specified values of curvature and axial load are found.

2.7.4 For a reinforced concrete member subject to both compressive axial forces and bending moments, the relationship between its ultimate bending moment M_u and ultimate compressive axial load P_u, can be represented by the interaction curve shown in fig. 2.13,

where P/P_u is the ratio of the axial load in the member to its ultimate axial load

and M/M_u is the ratio of the bending moment in the member to its ultimate bending moment.

Point A on this curve represents a failure of the section in pure compression, i.e. for $P/P_u = 1$ and $M/M_u = 0$. Point D represents a failure in pure bending for which $M/M_u = 1$ and $P/P_u = 0$. Failure with a combination of compressive load and bending moment can be found by drawing a straight line

such as OB through the origin O and with a slope equal to the particular ratio of end load to moment. Point B, where the line intersects the interaction curve, marks failure.

It can be seen from this curve that when low values of compressive axial load exist, the ratio of M/M_u can be greater than unity (at point C), indicating that the member can withstand bending moments in excess of its ultimate bending moment due to the increase in resistance of its section under the action of low axial loading.

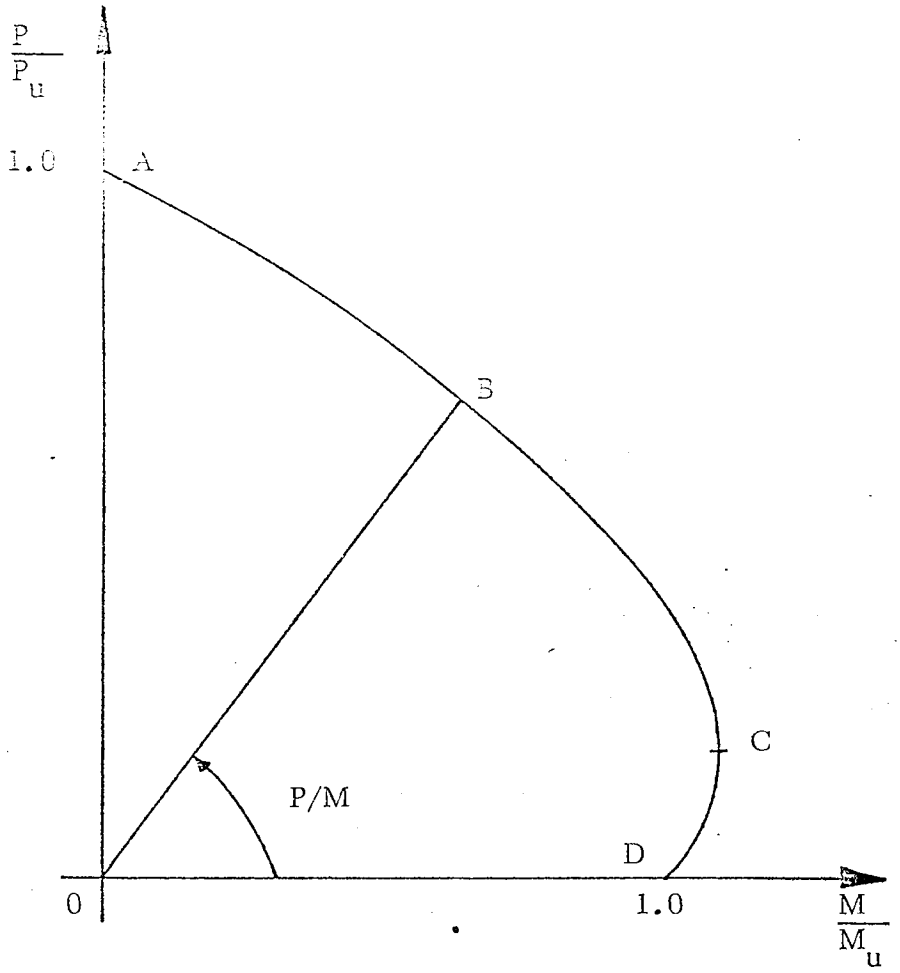

Figure 2.13 Moment-Axial Force Interaction Curve

CHAPTER 3

THE NON-LINEAR ANALYSIS OF REINFORCED CONCRETE FRAMES BY AN INCREMENTAL TECHNIQUE

3.1 Introduction

In this Chapter, an incremental approach for the non-linear analysis of reinforced concrete frames will be presented. A computer technique which utilizes this procedure is then described.

The main causes of non-linearity in reinforced concrete frames have been discussed in the preceding chapters. In the analysis to be presented, it is the non-linear material properties which are assumed to be the dominant cause of non-linearity in reinforced concrete frames.

3.2 Numerical techniques for the non-linear analysis of structures

3.2.1 Structures which exhibit non-linearity in their loaded behaviour may be analysed with a great deal of accuracy by using certain numerical techniques. In this thesis, it is the load-deflection characteristics of frames which are investigated and so these techniques will be discussed with particular reference to the load-displacement of structures.

3.2.2 The overall behaviour of a structure which exhibits non-linearity may be predicted by using an incremental technique. In this method, increments of proportional loading are applied to a structure. The displacements produced by the application of each load increment are then computed. The complete load-displacement history can then be obtained by summating the increments of load and each of the resulting displacements.

To reduce the computational effort in this type of analysis, the stress (f) - strain (e) relationship of each element of a structure is transformed into its instantaneous (tangent) modulus $(E)_t$ - strain diagram. Consider the f - e relationship shown in fig. 3.1 (a), at any value of strain e_i, the slope of the

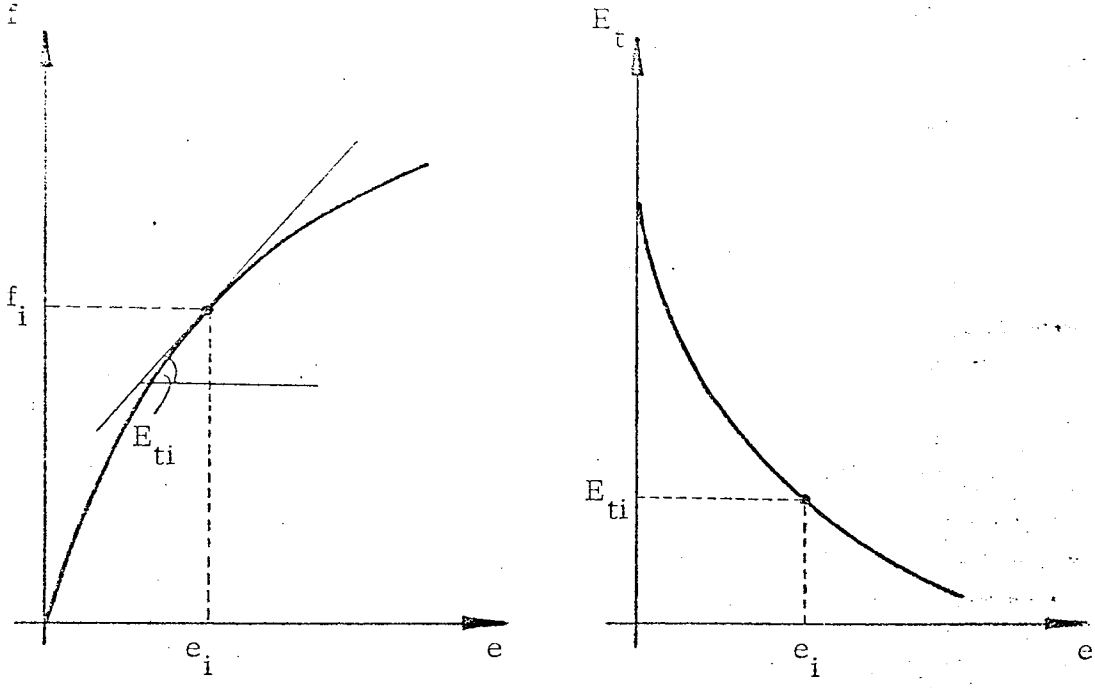

fig. 3.1

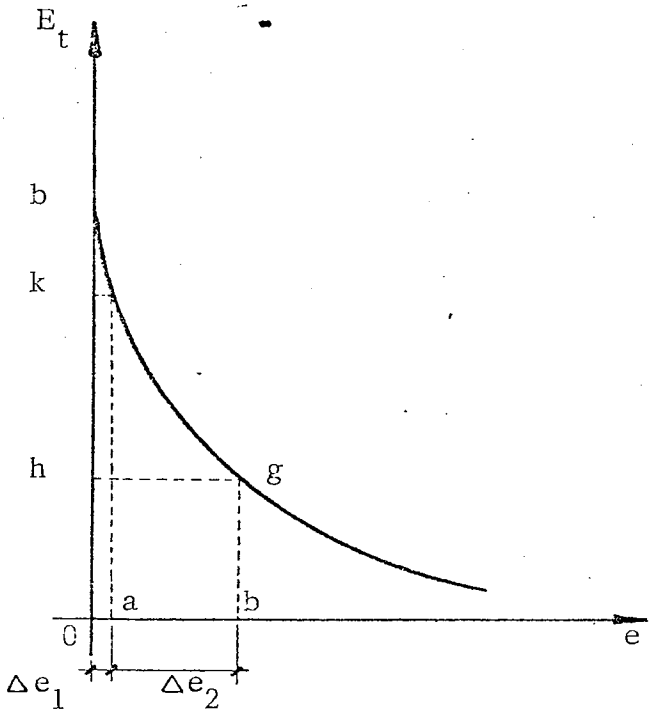

fig. 3.2

curve is the tangent modulus E_{ti}. Hence, a relationship between E_{ti} and e can be obtained by computing the slope at various strains on the f - e curve. A typical relationship of this form is given in fig. 3.1 (b). Using this representation of the properties of a member, the non-linear load-deflection history of a structure may be traced by an incremental method in the following manner.

To simplify the description of this method, the non-linear behaviour of a single member subject to axial extension is considered. The E_t - e diagram of the member is represented by the curve of fig. 3.2. In the unloaded state, the tangent modulus E_{t1} of the member is represented by Ob in the figure. Consider now the application of an increment of load ΔP_1 to the member. This load produces a displacement Δu_1 in the member. The magnitude of this displacement can be found from the solution of the stiffness equation $\Delta u_1 = K_1^{-1} \Delta P_1$. If ΔP_1 is sufficiently small, then the initial tangent modulus E_{t1} can be used to calculate the stiffness coefficient K_1. This is while increasing the load from zero to ΔP_1. Since Δu_1 is known, the increment of stress Δf_1, and hence, strain Δe_1 produced in the member, can be evaluated using the initial value of E_t in the elastic equation. This value of strain is then plotted on the E_t - e curve, and the corresponding value of E_t found. This value is represented by Ok in fig. 3.2.

Consider the application of a further increment of load ΔP_2, then during the analysis of the member subject only to ΔP_2, the new value of tangent modulus E_{t2} given by Ok may be used to represent the tangent modulus of the member. The displacement Δu_2, and hence, strain Δe_2 produced by this new load increment is then computed as before. Under the load $\Delta P_1 + \Delta P_2$, the total strain in the member is $\Delta e_1 + \Delta e_2$, which is

represented by Of in fig. 3.2. Once again, a new E_t for the bar can be obtained from the diagram.

This process of using the current tangent modulus to solve the stiffness equation for an increment of displacement Δu_1, produced by a load ΔP_i acting alone, can be continued upto failure. At the end of each solution to the stiffness and elastic equations, the load, displacement and strain after j increments is given by :-

$$\text{Load } P_j = \sum_{i=1}^{j} \Delta P_i$$

$$\text{Displacement } u_j = \sum_{i-1}^{j} \Delta u_i \qquad (3.1)$$

$$\text{Strain } e_j = \sum_{i=1}^{j} \Delta e_i = \sum_{i=1}^{j} \Delta f_i / E_{ti}$$

In this manner, the overall load-displacement characteristics of the member may be found. It is possible to extend this method enabling complete frames to be analysed. This can be achieved by using the foregoing analysis in conjunction with the matrix displacement method.

It is clear that this method will incur some drifting from the true equilibrium path at the end of each load increment application. This is because the value of tangent modulus $E_{t(i-1)}$ computed from the state of strain in a member after the application of the previous load increment is used to compute the new strain induced by the most recent load increment. The true value of E_t, however, lies somewhere between $E_{t(i-1)}$ and that value corresponding to the total strain of the member after the application of the most recent load increment. It is assumed, however, that this drifting may be reduced to a tolerable level by using small values of load increment throughout the analysis.

3.2.3 A more accurate method of analysing non-linear structures numerically is by using an iterative-incremental approach. This will ensure that equilibrium is being maintained throughout an analysis. One such technique is that referred to as the Newton Raphson procedure. By this method, a set of non-linear equations of the form :

$$\begin{aligned} f_1(x_1 x_2 \;..\;..\;..\;..\; x_n) &= 0 \\ f_2(x_1 x_2 \;..\;..\;..\;..\; x_n) &= 0 \\ &\vdots \\ f_n(x_1 x_2 \;..\;..\;..\;..\; x_n) &= 0 \end{aligned} \qquad (3.3)$$

can be solved by an iterative procedure involving a series of solutions to a "linear" set of equations. In the present context, these are the joint equilibrium equations resulting from the matrix displacement method of structural analysis.

Let the unknowns $(x_1\ x_2\ ..\ x_n)$ be denoted by $\underline{X}$ and the functions $(f_1\ f_2\ ..\ f_n)$ be denoted by $\underline{F}$ where n is the number of unknowns. At any given round of iteration k for which $\underline{F}\,(\underline{X})_k \neq 0$, the value of the function $\underline{F}$ at $(\underline{X} + \Delta\underline{X})_k$ is given in a linearised form by the first two terms of the Taylors series expansion of $(\underline{F})_k$ about $(\underline{X})_k$ as :

$$\underline{F}((\underline{X})_k + \Delta(\underline{X})_k) = \underline{F}(X)_k + \left[\partial \underline{F} / \partial(\underline{X})\right] \Delta(\underline{X})_k \qquad (3.4)$$

where $\underline{X}_k$ are the assumed displacements at the current k^{th} iteration and $\Delta(\underline{X})_k$ are small differences in the values of displacements $(\underline{X})_k$. The first term in the brackets in equation 3.4 is a 1 x n matrix and the second is an n x n matrix. To obtain the values of $\Delta(X)_k$ which will result in an improved approximation of the values of $\underline{X}$, the linearised expansion of $(\underline{X})_k + \Delta(\underline{X})_k$ is equated to zero, i.e :

$$\underline{F}(\underline{X})_k + \left[K\right] . \Delta(\underline{X})_k = 0 \qquad (3.5)$$

where $\left[K\right] = \left[\frac{\partial \underline{F}}{\partial \underline{X}}\right] =$

$$\begin{bmatrix} \frac{\partial f_1}{\partial x_1} & \frac{\partial f_1}{\partial x_2} \cdots \frac{\partial f_1}{\partial x_n} \\ \frac{\partial f_2}{\partial x_1} & \frac{\partial f_2}{\partial x_2} \cdots \frac{\partial f_2}{\partial x_n} \\ \vdots & \vdots \quad \vdots \\ \frac{\partial f_n}{\partial x_1} & \frac{\partial f_n}{\partial x_1} \cdots \frac{\partial f_n}{\partial x_n} \end{bmatrix}$$

and is the Jacobian matrix called the tangent stiffness matrix. Equation 3.5 is called the linear incremental equilibrium equation and it gives the linearised approximation to the relationship between the residual load vector $(\underline{F})_k$ and the resulting increments of displacements $\Delta(\underline{X}_k)$ as :

$$(\underline{X})_k = - \left[K\right]^{-1} (\underline{F})_k \qquad (3.6)$$

from whence a new approximation to the total displacements is given by :-

$$(\underline{X})_{k+1} = (\underline{X})_k + \Delta(\underline{X})_k \qquad (3.7)$$

Equations 3.6 and 3.7 represent the Newton Raphson method of solution to the set of non-linear equations 3.3. The updated solution $(\underline{X})_{k+1}$ is once again substituted into equation 3.6 to obtain a new correction as $(\underline{X})_{k+2}$. At each iteration, the residual loads $(\underline{F})_k$ are calculated, these give a measure of the inbalance and when this is sufficiently small, equilibrium is assumed to be achieved.

To improve numerical stability and also to trace the overall non-linear load-deflection history, the loads can be applied in a series of increments and a solution for $(\underline{X})$ being found for each load increment.

The Newton Raphson process requires a great deal of computational effort, since $\left[K\right]$ has to be recalculated and inverted at each iteration and consequently, some adaptations have been devised for use with the method to reduce the effort. One such approach is to calculate K for the first iteration of the first load increment and then to keep it constant throughout the analysis.

The method is then equivalent to the "initial stress" technique. If the Newton Raphson method is only allowed a single iteration per load increment, the method generates to the "Incremental Stiffness Procedure" which may be characterised by the need for many small increments of load to avoid drifting of the solution from the true equilibrium path.

Other variants of the Newton Raphson process which have been used are to allow two iterations per load increment in the "incremental stiffness procedure" in an attempt to reduce drifting. Another is where three load steps are applied before using the Newton Raphson iteration to achieve equilibrium.

As is prevalent with certain linear problems, ill-conditioning may arise if the functions, in this case the load-displacement curves, are nearly horizontal in the neighbourhood of the solution. This is because a small difference in the applied loading causes a much larger change in the displacements. The Newton Raphson method will not converge if the starting point is too far away from the final solution, and will probably give trouble if the curve has discontinuities.

3.3 Non-linear analysis of reinforced concrete frames by an incremental technique.

In the previous section, an incremental approach to the non-linear analysis of structures was discussed with reference to a single member. In this section, a development of this incremental approach for the non-linear analysis of reinforced concrete frames will be described. Here, the prime cause of non-linearity is that due to material properties, i.e. M-Ø relationship.

3.3.1 Prior to the development of an analysis for any type of structure, the specific factors which influence their behaviour under loading must be considered. There are many factors to be considered when developing an analysis

for reinforced concrete frames and the more important of these will be discussed at the end of this section.

In the development of the analysis, the following assumptions have been made :-

1) In the majority of loading cases, the bending moments in a frame vary along its length. The curvature Ø (which is a function of moment), and flexural rigidity, therefore, also vary. This variation may be accounted for by dividing the members of a frame into smaller submembers, each of which is assumed to have a constant stiffness.

2) All the applied loads act at joints.

3) The loading is proportionally applied to a frame upto collapse.

4) Small deflections compared with the overall geometry of a frame are produced.

5) The effect of axial load on the M-Ø relationship of a section is negligible for the range of loads encountered in this thesis.

6) The properties of the submembers are defined by their instantaneous flexural rigidity-curvature $(EI)_t$ - Ø diagrams.

7) For the purposes of calculation, the curvature Ø of a submember, the bending moment M along its entire length is assumed to be constant. Its value is equal to the larger of the bending moments acting at its ends.

8) The curvature Ø of a submember is a function only of this bending moment M. The curvature at any stage of the loading history is given by :-

$$Ø = M/EI \qquad (3.8)$$

where EI is the current flexural rigidity of a submember.

Adopting these assumptions, the analysis is formulated in the following manner.

3.3.2 Consider the instantaneous flexural rigidity-curvature $(EI)_t$ - Ø

diagram of a typical submember of a frame shown in fig. 3.3. In the unloaded state of the frame, the flexural rigidity of a submember is given by the ordinate Ob, and will be denoted by $(EI)_{to}$. A small increment of loads $\Delta \underline{L}_1$ is then applied to the frame. If ΔL_1 is sufficiently small, the overall stiffness matrix $\underline{K}_o$ of the frame can be constructed using the initial values of flexural rigidity of each submember i.e. $(EI)_{to}$. This matrix $\underline{K}_o$ will represent the stiffness of the frame while the loading increases from zero to ΔL_1.

The joint displacements of a frame $\Delta \underline{X}_1$ produced by the load increment $\Delta \underline{L}_1$ are then found by solving the stiffness equations :-

$$\Delta \underline{X}_1 = \underline{K}_o^{-1} \Delta \underline{L}_1 \qquad (3.9)$$

Using these joint displacements $\Delta \underline{X}_1$, the increment of member forces (bending moment and axial force) in the frame are given by :-

$$\Delta \underline{P}_1 = \underline{k}_o \underline{A} \Delta \underline{X}_1 \qquad (3.10)$$

for which $\underline{k}_o$ is the member stiffness matrix constructed using the $(EI)_{to}$ values.

$\underline{A}$ is the displacement transformation matrix.

For each submember, the larger of the bending moments $\Delta \underline{M}_1$ acting at its ends are then found. The curvature $\Delta \underline{\emptyset}_1$ of each submember resulting from the application of $\Delta \underline{L}_1$ only is computed by the following equation :-

$$\Delta \underline{\emptyset}_1 = \Delta \underline{M}_1 / (EI)_{to} \qquad (3.11)$$

This value of curvature $\Delta \underline{\emptyset}_1$ is then plotted on the $(EI)_t - \emptyset$ diagram. This is shown by Oa in fig. 3.3. The corresponding value of tangent flexural rigidity $(EI)_{t1}$ may then be found and is denoted by Oc in the figure. This value is acquired by interpolating between the points on the $(EI)_t - \emptyset$ diagram.

A further increment of loads $\Delta \underline{L}_2$ is then applied to the frame.

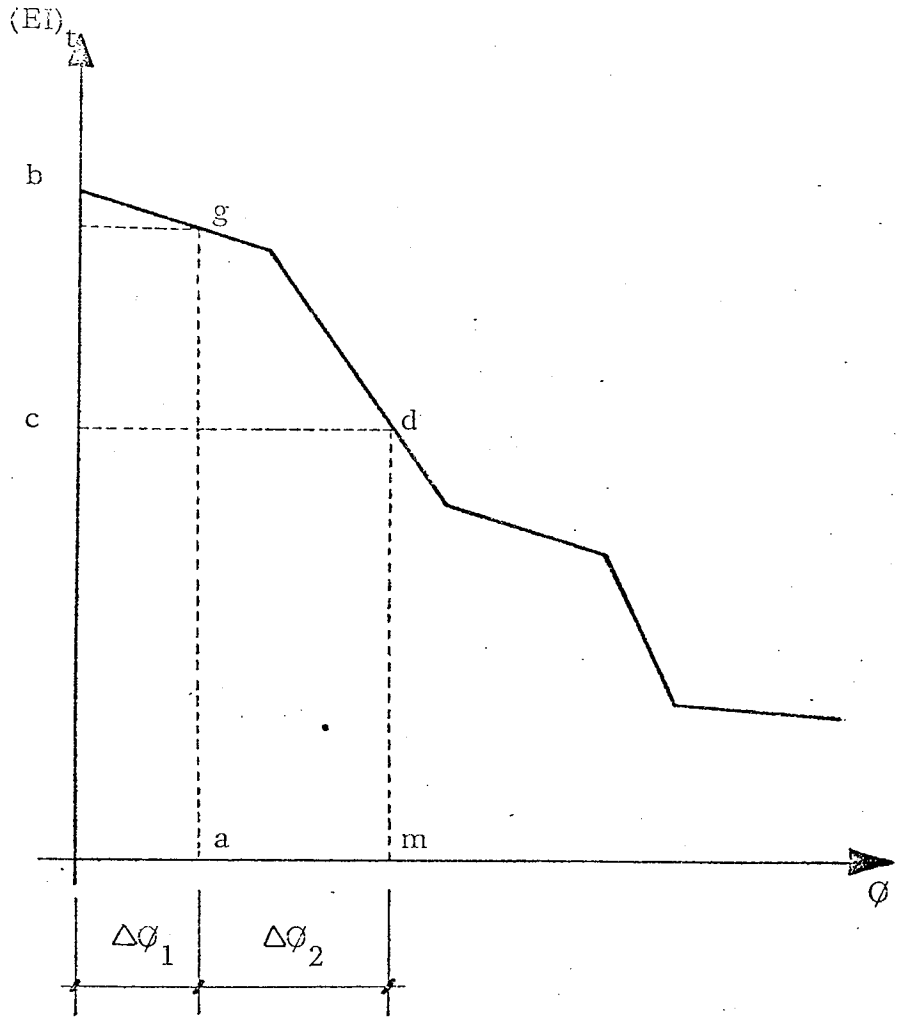

fig. 3.3 $(EI)_t$ - Ø diagram for a typical member of a frame

During the analysis of the frame subject to the loads $\Delta\underline{L}_2$ acting alone, the instantaneous flexural rigidity given by Oc in the diagram can be used to represent the tangent modulus for the submembers in both the overall and member stiffness matrices, $\underline{K}_1$ and $\underline{k}_1$. The stiffness equations are solved again. These are now in the form :-

$$\Delta\underline{X}_2 = \underline{K}_1^{-1} \Delta\underline{L}_2 \qquad (3.12)$$

A new set of joint displacements $\Delta\underline{X}_2$ are obtained. The member forces $\Delta\underline{P}_2$ are now given by :-

$$\Delta\underline{P}_2 = \underline{k}_1 \underline{A} \Delta\underline{X}_2 \qquad (3.13)$$

and once again, the induced curvatures $\Delta\underline{\varnothing}_2$ of the submembers are given by :

$$\Delta\underline{\varnothing}_2 = \Delta\underline{M}_2 / (EI)_{t1} \qquad (3.14)$$

Under the loads $\Delta\underline{L}_1 + \Delta\underline{L}_2$ acting together, the total curvature produced in a submember is given by $\Delta\underline{\varnothing}_1 + \Delta\underline{\varnothing}_2$. This is represented on fig. 3.3 by Om. A new set of values $(EI)_{t2}$ corresponding to the total curvatures in the submembers may then be found, and are given by the ordinate Oh.

This process of using the current $(EI)_t$ value to solve the structure for a new set of displacements $\Delta\underline{X}_i$ under an increment of loads $\Delta\underline{L}_i$ acting alone, can be continued upto failure. After each load increment, j, the total load, displacement, member forces and curvature are given by :-

(a) the total loads

$$\underline{L}_j = \sum_{i=1}^{j} \Delta\underline{L}_i \qquad (3.15)$$

(b) the total displacements

$$\underline{X}_j = \sum_{i=1}^{j} \Delta\underline{X}_i = \sum_{i=1}^{j} \underline{K}_{i-1}^{-1} \Delta\underline{L}_i \qquad (3.16)$$

(c) the total member forces

$$\underline{P}_j = \sum_{i=1}^{j} \Delta \underline{P}_i = \sum_{i=1}^{j} \underline{k}_{i-1} \underline{A} \, \Delta \underline{X}_i \qquad (3.17)$$

(d) the total curvature

$$\underline{\phi}_j = \sum_{i=1}^{j} \Delta \underline{\phi}_i = \sum_{i=1}^{j} \left(\Delta \underline{M}_i / (EI)_{t(i-1)} \right) \qquad (3.18)$$

By this procedure, the loading of a frame can be increased upto failure. This state is reached when the determinant of the most recent overall stiffness matrix $\underline{K}_i$ is equal to zero. At this stage, the analysis is terminated.

3.3.3 It is clear that this method will incur some drifting from the true equilibrium path at the end of each load increment. This is because the tangent flexural rigidity $(EI)_{t(i-1)}$ computed from the total curvature after the $(i-1)$th increment, has been used to represent the flexural rigidities of the submembers while the loading increases from $\underline{L}_{(i-1)}$ to $(\underline{L}_{(i-1)} + \Delta \underline{L}_i)$. In reality, however, the flexural rigidity changes during the application of $\Delta \underline{L}_i$. This may result in an overestimation of the true stiffness of a frame. However, it is assumed that this drifting may be reduced to a tolerable level by using small values of load increment throughout the analysis.

3.3.4 Reinforced concrete is an ideal structural material because the properties of a section can be adjusted readily to provide almost any required resistance to applied stresses. This may be achieved by one or a combination of the following methods :-

(a) by increasing the depth and breadth of a section.

(b) by increasing the percentage of tensile reinforcement.

(c) and by adding compressive reinforcement.

As a result of this flexibility, it is possible for a reinforced concrete structure to consist of members with varying properties. Consideration is now given to some causes of this variation.

The size and number of reinforcing bars may vary along the length of the members. This results in varying percentages of tensile reinforcement, and hence, varying M-ϕ properties. The percentage of reinforcement may vary due to the following factors :

(1) Curtailment of main reinforcement at points where the bending moments are small.

(2) Where bond requirements result in an overlapping of bars.

(3) Where clauses in the codes of practice require certain reinforcement detailing.

When reinforced concrete frames are loaded laterally and vertically, two points of contraflexure exist in the cross members. The bending moments produced are such that the top or bottom of a member is in flexural tension at some point along its length. If there is a difference in the position and percentage of reinforcement at these "tensile" regions, then a change in section is present.

For certain frames, architectural constraints may require the section depth to vary along the length of a member. This will also result in a member of varying properties.

It is possible that for most reinforced concrete frames, one of the above situations will occur. Allowance for these changes of properties along a member must, therefore, be made. This may be achieved by dividing the full members of a frame into smaller members, each of which defines a particular section property.

3.4 Particular factors to be considered in the formation of the incremental computer analysis for reinforced concrete frames

3.4.1 The analysis presented above must be translated into a suitable form before a computer program can be written. One of the assumptions made for carrying out the analysis is that for the purposes of calculating the curvature of a submember, the bending moment along its entire length is constant and equal to the larger of the bending moments at its ends. Fig. 3.4 shows the bending moment diagram for a pin-ended portal frame. If joints are inserted at the numbered points shown, and the lengths of frame between these joints termed members, it may be seen that the bending moment is not constant along a member. This is particularly seen to be the case between joints 4 and 5.

Under these conditions, the assumption is unrepresentative of the actual behaviour of the frame. This will result in an underestimation of its load carrying capacity, because the representative bending moment of each member is too large. This will produce larger curvatures and hence reduce the flexural rigidity of the members.

This situation can be improved by dividing the members of a frame into smaller submembers. If this is performed on the member between joints 4 and 5 as shown in fig. 3.5 (a), and the larger of the bending moments of each submember taken to represent the bending moment of the entire submember, then the loss of accuracy becomes insignificant. By decreasing the length of the submembers, the accuracy of the assumption is thus improved.

It is obvious from fig. 3.4 that the gradient of the bending moment diagram is of great importance. For a relatively flat diagram as indicated in fig. 3.5 (b), fewer subdivisions are necessary to describe the state of bending in a member accurately.

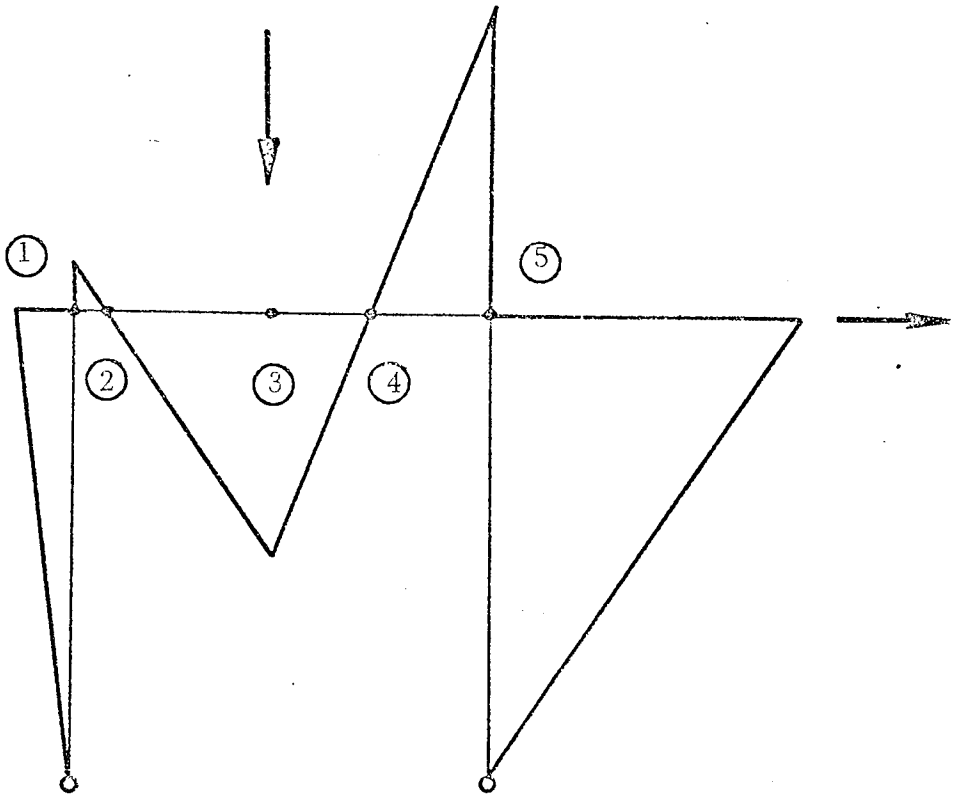

Figure 3.4 Bending moment diagram for a portal frame

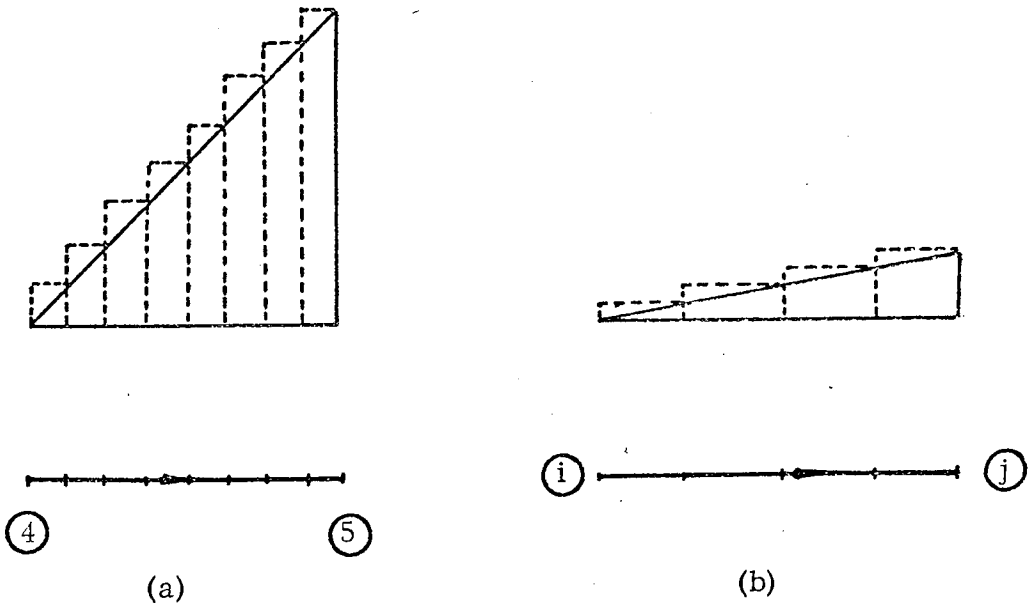

Figure 3.5 Subdivision of a member.
(a) for a steep bending moment diagram
(b) for a shallow bending moment diagram

The larger and not the average of the bending moments in a submember is taken to be representative of the state of bending as this avoids the possibility of a short length of a member reaching its ultimate state without being detected.

The use of this subdivision technique increases the number of degrees of freedom of a frame. A greater number of stiffness equations will therefore require solution, and consequently, more computer time and storage space is used. It is therefore necessary from the economic aspect to limit the number of subdivisions used in a frame. However, any reduction in the number of subdivisions must not interfere with the accuracy of the analysis.

3.4.2 To assess the effect of the number of subdivisions used in a frame with regard to the accuracy of representation, a series of computer analyses were carried out on Frame F1 (see later). The results are presented in fig. 3.6 as the load deflection curves for sway of the frame. The range of subdivisions used were from the full members of the frame to 106 submembers. In the case of the latter analysis, 317 simultaneous equations were solved for each load increment. From the graph, it can be seen that as the number of subdivisions increase, the collapse load becomes larger while the deflections at particular loads decrease. This indicates an increase in the stiffness of the frame. It may also be noticed that for values of subdivision greater than 28, there is no significant change in the results obtained for the load deflection response. For Frame F1, a value of 28 subdivisions may therefore be used with confidence.

If larger frames are subdivided in the same ratio to that used above, a similar degree of accuracy from the subdivision aspect may be assumed.

3.4.3 It would be desirable to further reduce the number of subdivisions whilst maintaining a similar degree of accuracy. This may be achieved by

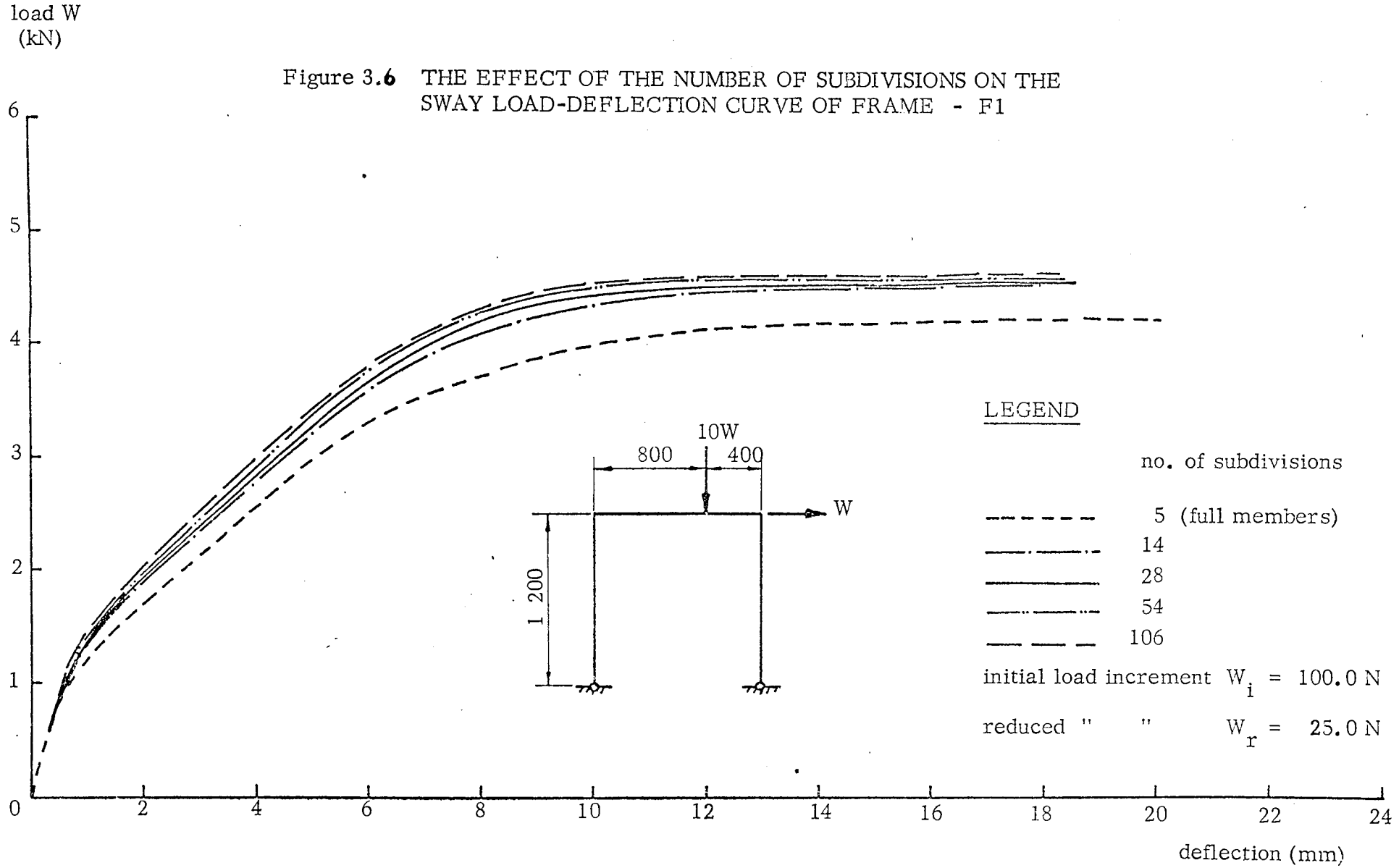

Figure 3.6 THE EFFECT OF THE NUMBER OF SUBDIVISIONS ON THE SWAY LOAD-DEFLECTION CURVE OF FRAME - F1

the following approximation. Fig. 3.7 shows a typical bending moment diagram for a portion of a frame. In this proposed method, a value of bending moment which lies between the values M_1 and M_2 is used to represent the bending moment along the whole length of a member. This bending moment is calculated by the following expression :-

$$M_k = M_1 + k\,(M_2 - M_1) \qquad (3.19)$$

where $M_2 > M_1$ and k is a factor by which the difference in the end moments are factored, to represent the bending moment of a member when computing its curvature. In the analysis extra joints are inserted, apart from the main joints, at points of zero bending moment. These points are easily determined by a single load increment analysis of an undivided frame. The slightly subdivided frame is analysed as previously described, but the curvature of each member is calculated using the factored bending moment M_k.

For Frame F1, a number of values of k were tried, the results are presented in fig. 3.8 as the sway load-deflection curves. The results are also compared with a fully subdivided frame analysis. The best value of k is taken to be 0.93. This modified analysis provides an economic method for testing different configurations and section sizes prior to a fully subdivided analysis.

3.4.4 The magnitude of the load increment used in an analysis is of great importance and its effect on the accuracy of the analysis will now be investigated. It has been shown previously that the overall non-linear behaviour of a reinforced concrete frame can be obtained by summing its response to the application of small increments of load. As the magnitude of these increments becomes smaller, the accuracy of utilizing the value of $(EI)_t$ obtained from the current total curvature, in the formation of the stiffness

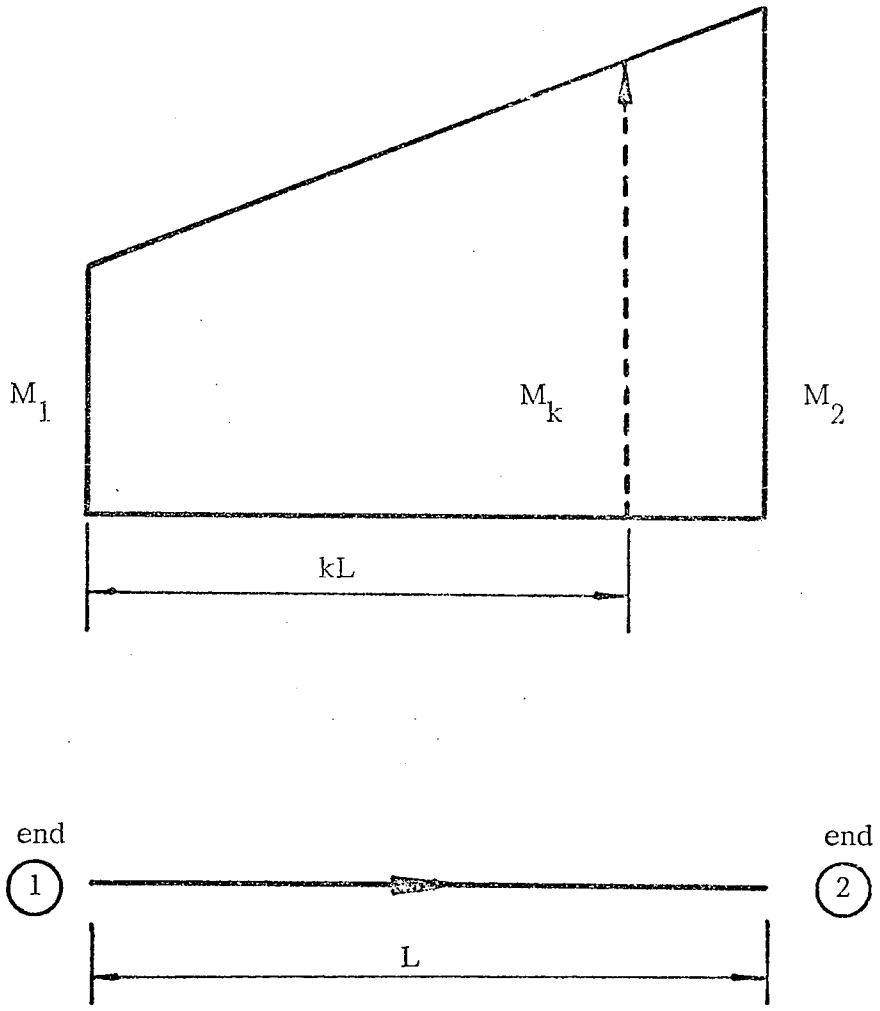

Figure 3.7 Typical bending moment diagram for a portion of a frame

Figure 3.8 THE EFFECT OF BENDING MOMENT FACTOR (k) ON THE SWAY LOAD-DEFLECTION CURVE OF FRAME - F1

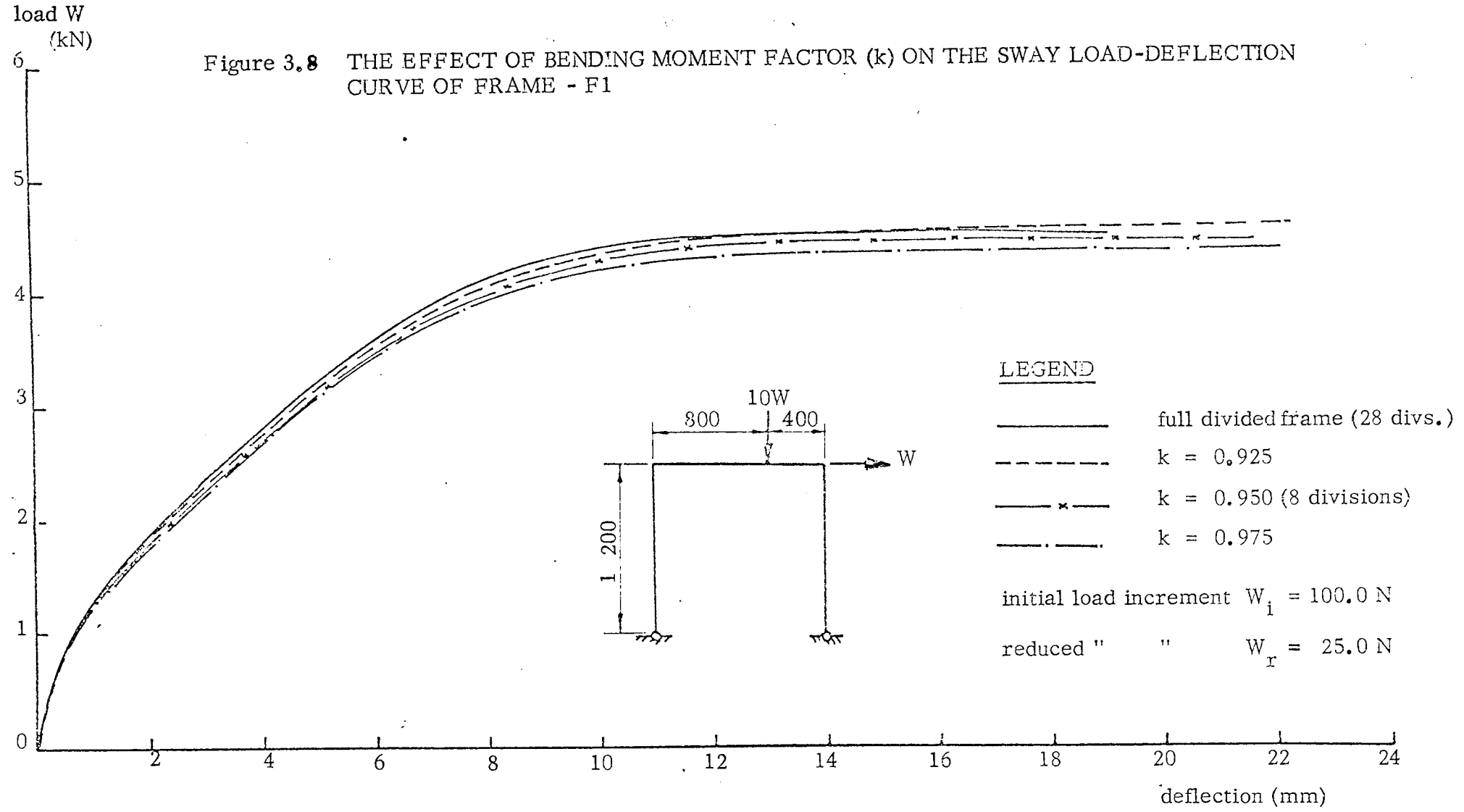

equations at the next load increment, is enhanced.

However, for each load increment applied to a frame, the stiffness equations must be assembled and solved. If the increments are very small, the computer time necessary for a complete analysis is large and may be uneconomic. It is therefore necessary to examine the effect of the magnitude of load increment used in an analysis.

Consider the typical $(EI)_t$-ϕ diagram of a reinforced concrete member shown in fig. 3.8. Initial load increments produce small increases in the curvature of the members of a frame because the members are initially very stiff. As the loading increases, the stiffness of a member reduces according to its total curvature. At a particular stage in the loading, L_i, the total curvature of a member is ϕ_i and the corresponding flexural rigidity $(EI)_{ti}$. If a further increase in load from L_i to L_{i+1} causes an increase in the total curvature of a member from ϕ_i to ϕ_{i+1}, then from fig. 3.9, it is apparent that the stiffness of the member has been overestimated for this curvature increase. This is because $(EI)_{ti}$ has been assumed to represent the flexural rigidity of a member for the entire increase in curvature from ϕ_i to ϕ_{i+1}. In reality, however, EI is reducing in magnitude. At regions where $(EI)_t$ varies rapidly with curvature, e.g. between points A and B on fig. 3.9, the inaccuracy resulting from using large load increments may be quite significant.

This overestimation of the stiffness of a frame is accentuated at the total load at which the first yield of steel develops anywhere in the frame. At this stage, large increases of curvature result from small increases in applied loading. It is therefore necessary to further reduce the magnitude of the load increment at this stage in the analysis.

To examine the effect of the magnitude of load increment on a

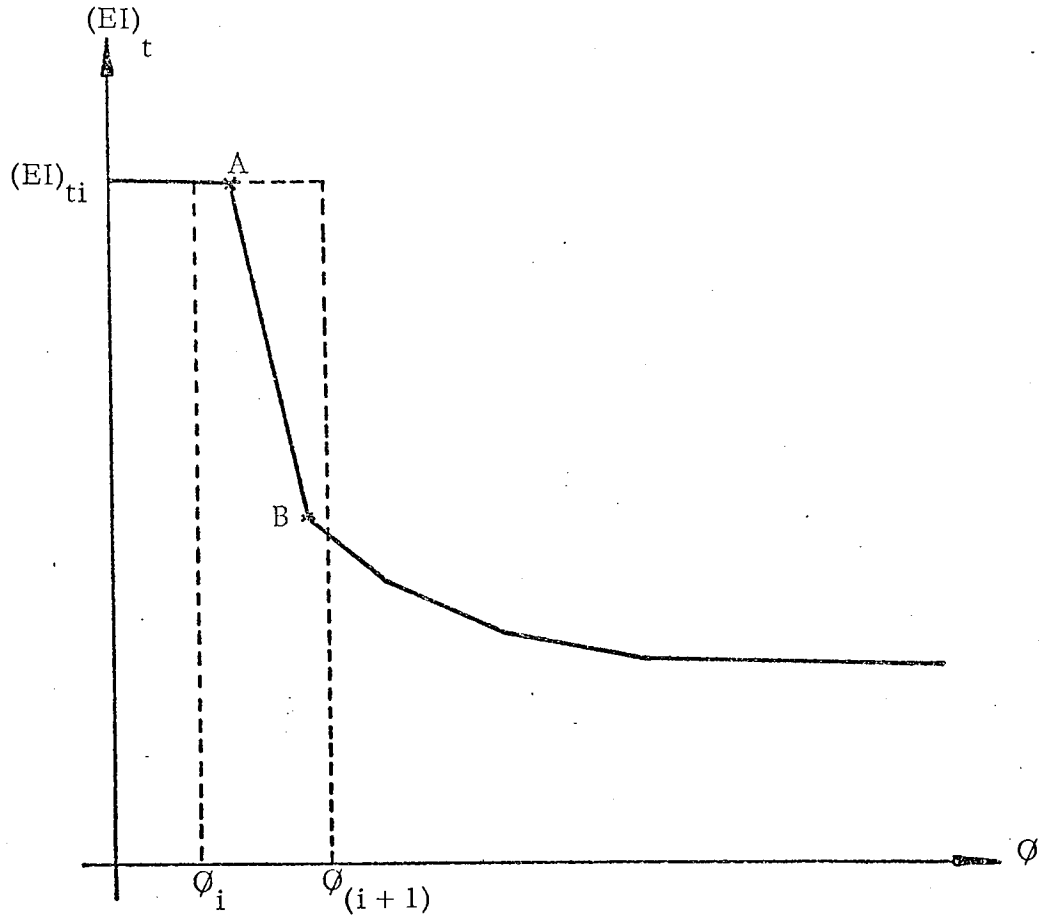

Figure 3.9 $(EI)_t$ - Ø diagram of a member

typical analysis, two sets of computer analyses were carried out for Frame F1. In the first of these, the load increment was varied between 0.1% and 10% of the experimental collapse load. The range of loading of interest in this set was upto that at which first yield of tensile steel occurred anywhere in the frame. The results are presented in fig. 3.10 in the form of the sway load-deflection curves. The first yield of steel occurs at approximately 3kN side load.

From the graph, it may be seen that as the magnitude of load increment decreases, the deflections corresponding to particular summed loads increase. This is because the overestimation of a frame's stiffness is reduced, i.e. a value of flexural rigidity nearer the true value is being utilised. It can also be seen from this figure that for values of load increment less than 100 N ($\triangleq$2% of the collapse load), no significant change in the results occurs.

For the second set of analyses, the load increment was kept constant at 2% of the collapse load upto the total load at which first yield of steel occurred in the frame. Subsequently, the load increment was varied between 5% and 100% of this initial value. The results obtained are expressed as the sway load-deflection curves in fig. 3.11. Again, it may be seen that deflections increased as the magnitude of the load increment was reduced. The load deflection curves did not change significantly when the load increment was reduced below 25% of its initial value.

From the two sets of analyses, it is indicated that no significant change occurs in the results, if the load increments are made smaller than 2% of the collapse load initially and 0.5% after the steel has yielded.

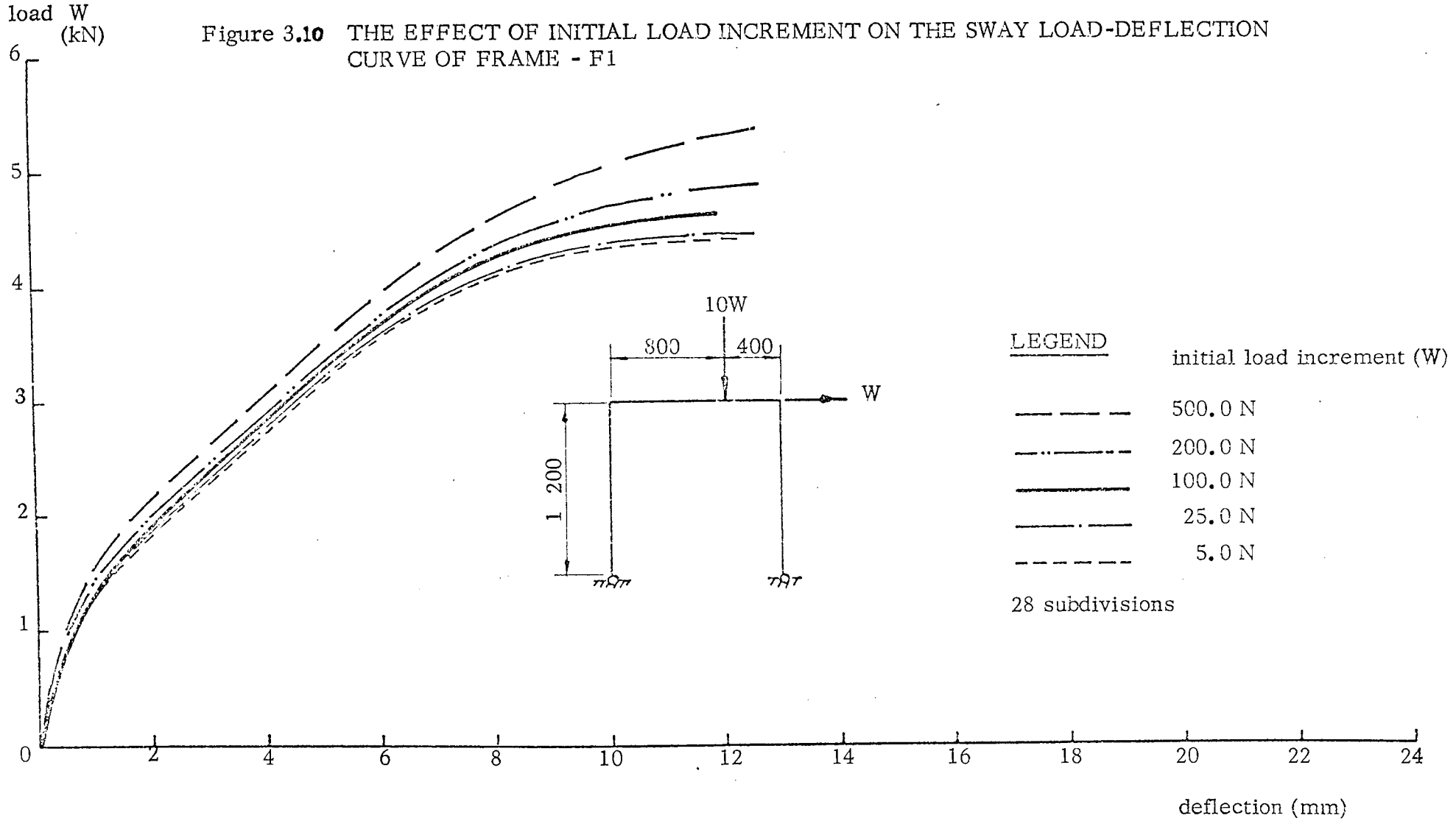

Figure 3.10 THE EFFECT OF INITIAL LOAD INCREMENT ON THE SWAY LOAD-DEFLECTION CURVE OF FRAME - F1

Figure 3.11 THE EFFECT OF REDUCED LOAD INCREMENT ON THE SWAY LOAD-DEFLECTION CURVE OF FRAME- F1

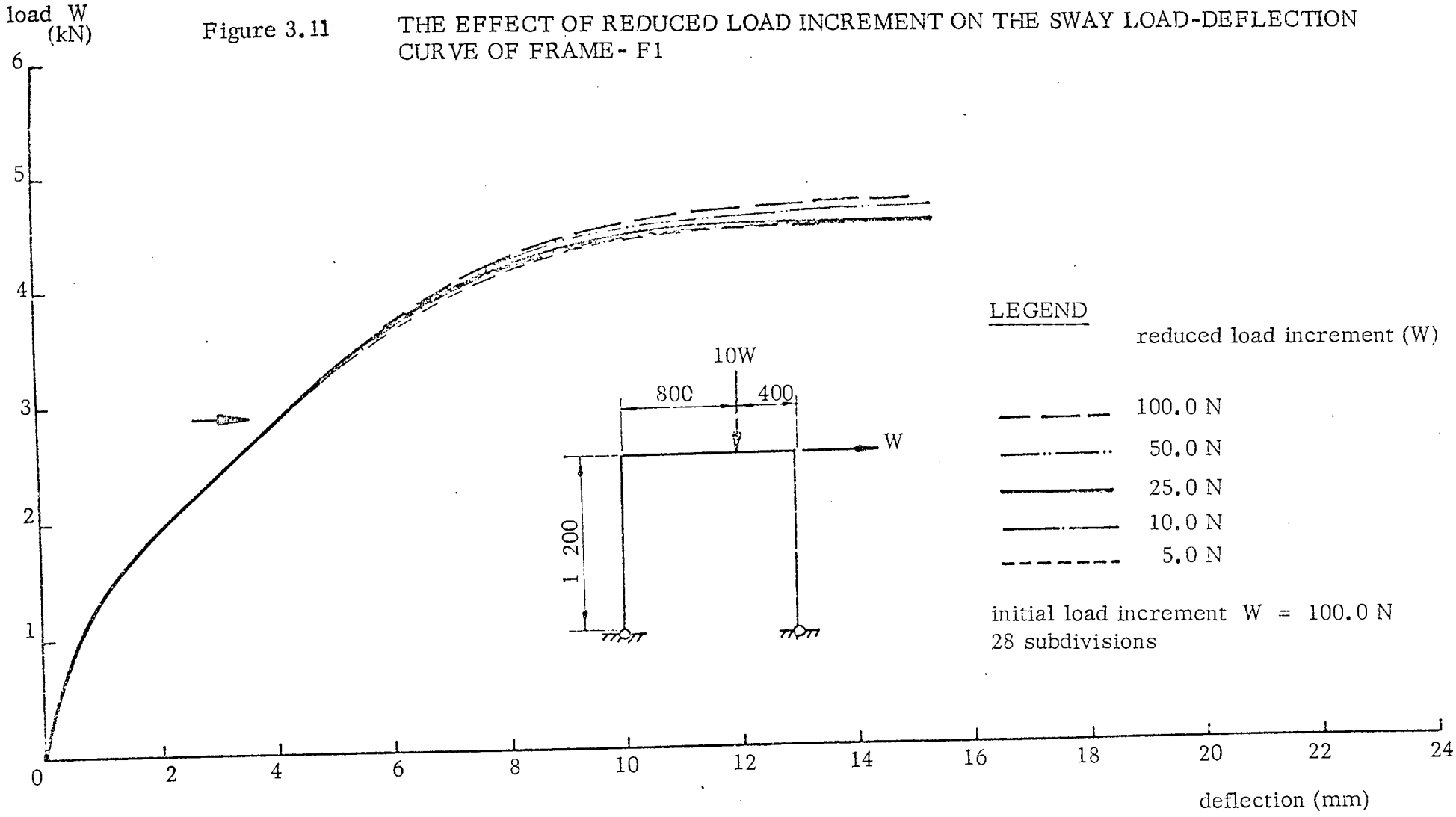

3.5 A computer program for the non-linear incremental analysis of reinforced concrete frames

A computer program was written in FORTRAN IV for the non-linear analysis of reinforced concrete frames by an incremental method. The main steps followed by the program are given in the flow diagram of fig. 3.12. This procedure is described in more detail below.

3.5.1 Firstly, the data concerning the geometry of the frame and the properties of its submembers are read in. The next data to be read is the magnitude of both the initial and reduced load increments. The arrays which store the joint displacements $\underline{X}$, the load vector $\underline{L}$ and the member forces $\underline{P}$, are all made equal to zero. This eliminates the possibility of an incorrect number being stored.

For the analysis, the $(EI)_t$ - $\emptyset$ properties of the submembers are represented by a piece-wise linearized curve. The values of $(EI)_t$ and $\emptyset$ at the critical points of this curve are stored in two separate, two-dimensional arrays. From this curve, the values of instantaneous flexural rigidities corresponding to the curvatures in the submembers can be obtained by interpolation. The initial values of $(EI)_t$ and $\emptyset$ (which is zero) are assigned to each submember.

The number of locations required to store the overall stiffness matrix $\underline{K}$ of the frame is then computed and the array which stores the matrix is made equal to zero. The first increment of loads $\Delta \underline{L}_1$ is then applied to the frame and the $\underline{K}$ matrix is constructed in the manner referred to in section 1.5.7 of this thesis. In this matrix, the flexural rigidity of each submember is represented by the initial $(EI)_t$ value. The joint equilibrium equations are then solved by the compact elimination technique. This technique is also referred to in section 1.5.7. The solution is for the frame with only the

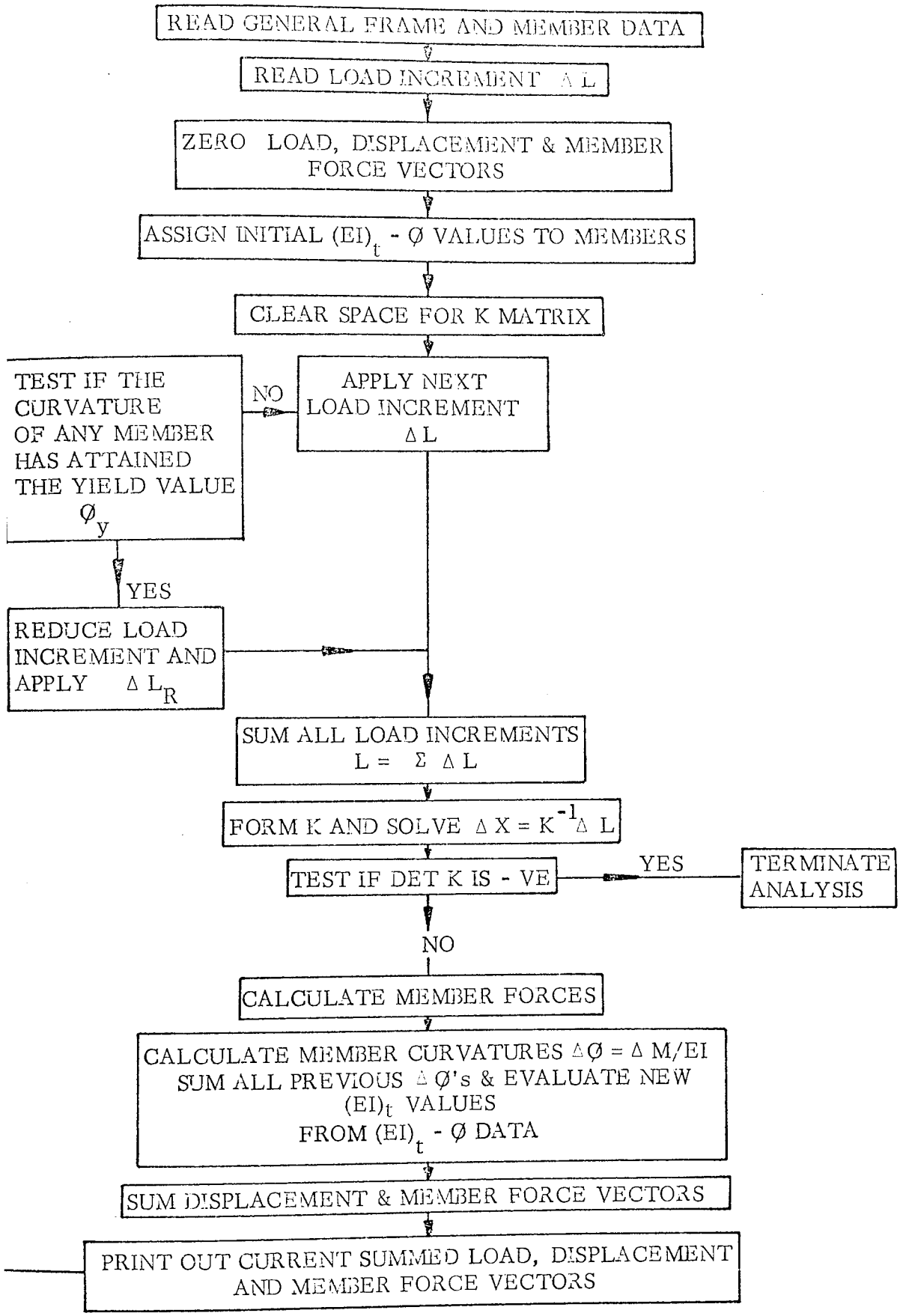

Figure 3.12 Flow diagram for Incremental Program

first increment of loads $\Delta\underline{L}_1$ applied. A test is then performed to ascertain if the determinant of the $\underline{K}$ matrix is negative. If the determinant is positive, the analysis is continued and the submember forces $\Delta\underline{P}_1$ produced by the first load increment are computed.

For each submember, the curvature $\Delta\underline{\emptyset}$ produced by the larger of the bending moments $\Delta\underline{M}$ acting at its ends is computed using the equation $\Delta\underline{\emptyset} = \Delta\underline{M}/EI$, where EI is the initial value of $(EI)_t$. The total value of curvature of a submember is then found by adding $\Delta\emptyset$ to all the previous values of curvature increments. Using the piece-wise linear (EI) - $\emptyset$ data of each submember, the values of $(EI)_t$ corresponding to the summed values of curvature are then found by interpolation. These values will replace the initial $(EI)_{t's}$ as the flexural rigidities of each submember.

The increments of displacement and member forces are then summed and the resulting values are printed together with the total load vector. The total curvature vector ($\sum\Delta\emptyset$) is then tested for each submember to ascertain whether any submember has reached a value of curvature equivalent to that at yield of its tensile reinforcement. If this curvature has been attained anywhere in the frame, the load increment is reduced to $\Delta\underline{L}_R$, otherwise the next full value of the load increment $\Delta\underline{L}$ is applied. This increment, together with all the previous load increments, are summed to give the total loads acting on the frame.

The $\underline{K}$ matrix of the frame is then constructed. In this matrix, the flexural rigidity of each submember is represented by that value computed for the total curvature of the member at the end of the previous load application. The stiffness equations are then solved for the unknown joint displacements resulting from the application of the second load increment ΔL_2. The sign of the determinant of the overall stiffness matrix is determined and if it is

positive, the whole procedure is continued. This procedure is repeated for further load increments until the determinant of the overall stiffness matrix is negative. At this stage, the analysis is terminated.

3.5.2 In appendix (1), the frame reference system and the data used for each frame in the above computer program are presented.

3.6 Results

The portal frames tested, and the results of which are reported in Chapter 5, have been analysed by the incremental method. The $(EI)_t - \phi$ properties of the submembers used in the analyses were those obtained by theory and experiment (Chapter 6). The results are presented in Chapter 7.

3.7 General Discussion of the incremental method

3.7.1 The computer analysis described in this Chapter is an incremental-variable-stiffness procedure which involved repeated solution of the joint equilibrium equations under successive values of applied load increments. After each solution of these equations, the increment of curvature produced in every submember in a frame was computed. It was then possible to obtain the total curvature of each submember and hence the corresponding value of instantaneous flexural rigidity. These values of $(EI)_t$ were then used to represent the flexural rigidity of the submembers throughout the next increase in loading.

3.7.2 It was realised that by utilizing these values of $(EI)_t$ in the solution of the stiffness and member force equations at the next load increment, a certain amount of drifting from the true equilibrium path would result. This is because the flexural rigidity is not constant, but varies during the increase in load. However, it was assumed that if the load increments were kept small, the loss of accuracy in assuming a constant flexural rigidity would be reduced signi-

ficantly. This would in turn reduce the drift.

In order to ensure that equilibrium conditions are satisfied, an iterative procedure such as the Newton Raphson method, must be used in conjunction with the incremental analysis. This will then ensure that for each increase in load, the correct value of flexural rigidity is adopted. It is, therefore, suggested that the following technique should be used in order to ensure that equilibrium is being maintained throughout an analysis.

The main requirement of this iterative technique is that the true values of EI are being used for each load increment application. This requirement is assured by performing a tolerance test on the values of submember curvature obtained at successive rounds of an iterative cycle. The EI values are adjusted according to the total curvature at each step of the cycle. When the tolerance test is satisfied for every submember, convergence is then achieved, and the next load increment can be applied.

To assist in the description of the proposed method, the reader is referred to the flow diagram of fig. 3.13. The following vectors are used in this modified procedure.

$\emptyset_f$ - a vector which stores the total curvature of each submember at the end of the previous load increment f.

$\emptyset'_i$ - a vector which stores the total curvature after each round of the iterative cycle. The magnitude of this vector is equal to $\emptyset_f$, plus the various values of curvature increment computed at each round of the iteration.

$\emptyset''_i$ - another vector which stores the total curvature at the previous round of the iteration.

In the following text, the subscript f refers to the total number of load increments applied at any stage of the analysis and i refers to the current number

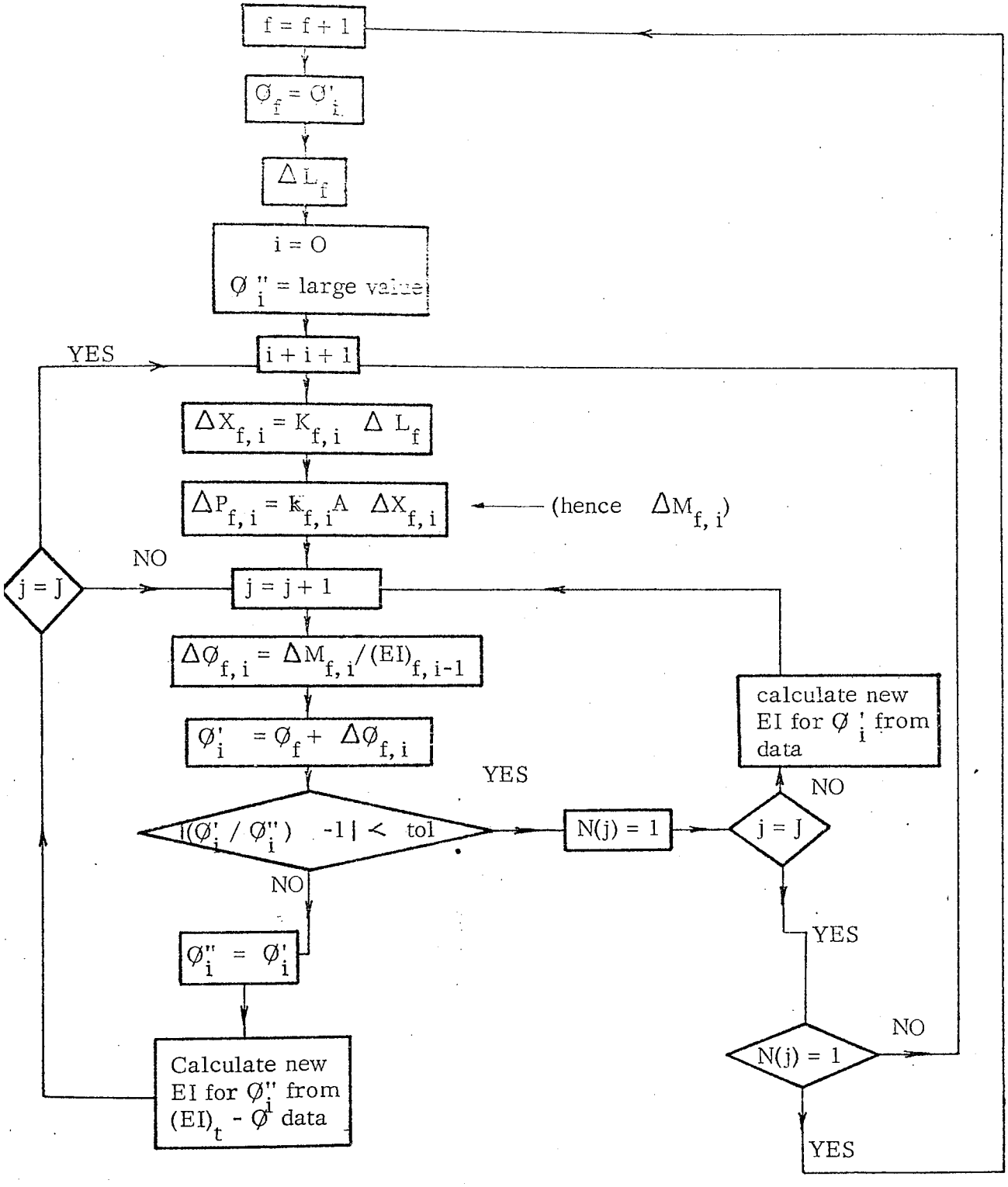

f - current number of increments
i - iteration count
j - submember subscript
J - total number of submembers
N - array of converged submembers

Figure 3.13

of iterations in a cycle.

Consider the application of an increment of loads $\Delta \underline{L}_f$ to a frame. The vector $\emptyset'$ is made equal to the total curvature $\emptyset_f$ after the previous load increment. For the first round of the iteration, a large value is assigned to $\emptyset''$. This is to ensure that the tolerance test is not satisfield at the first round of the iteration. The iterative cycle is then initiated and for the load increment $\Delta \underline{L}_f$, the joint equilibrium equations are assembled and solved. In the overall stiffness matrix $\underline{K}$, the flexural rigidities of the submembers are represented by the $(EI)_t$ values computed at the previous load increment i.e. $(EI)_{f,o}$.

From the resulting joint displacements, the member forces can be found. The bending moments produced by the load $\Delta \underline{L}_f$ are now known and hence, the representative moment $\Delta M^*_{f,1}$ of each submember can be obtained. The curvature of each submember is then given by :-

$$\Delta \emptyset_{f,1} = \Delta M_{f,1} / (EI)_{f,1} \qquad (3.20)$$

This value is added to the previous total value of curvature $\emptyset_f$ at the previous load increment such that,

$$\emptyset'_1 = \emptyset_f + \Delta \emptyset_{f,1} \qquad (3.21)$$

A tolerance test is then performed on the current and previous total curvatures in the following way :

$$\left| (\emptyset'_1 / \emptyset''_1) - 1 \right| < \text{tolerance} \qquad (3.22)$$

This tolerance test, however, will not be satisfied for the first round of the iteration since $\emptyset''$ has been given a large value. Before the next round of the iteration $\emptyset''_2$ is made equal to $\emptyset'_1$ and the new instantaneous flexural rigidities $(EI)_{f,1}$ for each submember corresponding to the total curvatures $\emptyset'$, are computed.

* The first subscript refers to the current number of increments and the latter to the iteration number.

In the next round of the iteration, the stiffness equations are again solved whilst subject to the same load increment $\Delta \underline{L}_f$. In the $\underline{K}$ matrix, the flexural rigidity of each submember is represented by $(EI)_{f,1}$. The new value of the increment of curvature can then be found and is given by :-

$$\Delta \emptyset_{f,2} = \Delta M_{f,2} \cdot (EI)_{f,1} \qquad (3.23)$$

This value is added to $\emptyset_f$ to give the total curvature at the second round of the iteration which is $\emptyset'_2 = \emptyset_f + \Delta \emptyset_{f,2}$, and will be greater than $\emptyset'_1$.

The tolerance test is repeated for each submember in turn and if the test is satisfied, then the iteration for that submember is converged. If the iteration of all the submembers does not converge, the cycle is continued in the same manner described above until this requirement is satisfied.

When convergence has been achieved for each submember, the new values of $(EI)_t$ are computed as before. These values will be used to represent the flexural rigidities of the submembers in the first round of the iteration for the next load increment. The vector $\emptyset_f$ is then equated to the most recent value of $\emptyset'_i$ and will represent the total values of curvature after f increments of load.

The next load increment $\Delta \underline{L}_{(f+1)}$ is applied to the frame and the iterative process continued. This procedure is continued until the determinant of the most recent overall stiffness matrix is negative. At this point, the analysis is terminated. In all other aspects, this modified analysis is similar to the method presented previously.

It may be assumed that by adopting this technique, the correct value of $(EI)_t$ is being used to represent the flexural rigidities of all the submembers for each increase in applied load. However, it must be stressed here that because of the discontinuous nature of the $(EI)_t$ - $\emptyset$ diagram, difficulties in obtaining

convergence may result. To avoid this, it is necessary to apply small increments of loads.

CHAPTER 4

NON-LINEAR ANALYSIS OF REINFORCED CONCRETE FRAMES BY AN ITERATIVE LOAD FACTOR METHOD

4.1 Introduction

The program of Majid and Anderson (18) described in Chapter 1 is a very powerful method for the non-linear elastic plastic analysis of frames. The application of this program is, however, restricted to materials which exhibit the idealised moment-curvature relationship of fig. 1.2. The material must also be capable of practically unlimited plastic hinge rotation. The program cannot, therefore, be used for the analysis of frames manufactured from brittle materials, such as reinforced concrete. In Chapter 2, the moment-curvature relationship of reinforced concrete was shown to be far from the idealised bi-linear relationship that can be assumed for steel.

The program described in this Chapter is a development of Majid and Anderson's program which enables a non-linear analysis on similar lines to be performed for reinforced concrete frames.

4.2 Properties of Reinforced Concrete

4.2.1 The moment-curvature relationship of reinforced concrete has been fully described previously. Experimental observation from the beam tests reported in Chapter 6 has shown a smooth non-linear relationship between moment and curvature. For practical purposes, this smooth curve is assumed to be a series of straight lines. To increase the accuracy of representation, more lines are used in the 'transition' regions of the relationship. If the relationship is obtained from theoretical considerations, three straight lines define it reasonably. Each of the straight lines represents a part of the slope of the moment-curvature relationship, and thus the flexural rigidity, EI.

In Majid and Anderson's method, the first line of the moment-curvature diagram represented the flexural rigidity of a section in the initial 'elastic' state. After the attainment of the fully plastic moment M_p of the section, the flexural rigidity changed to zero. The plastic hinge so formed was given unlimited plastic deformation capacity.

Reinforced concrete is a highly non-linear material and does have a limit on its plastic deformation capacity. In the tri-linear representation of the moment-curvature relationship shown in fig. 2.6, it is noticed that the flexural rigidity has a finite value for each of the three lines. The nodes which join these straight lines are termed "critical points". For reinforced concrete members in which a bending moment corresponding to one of these critical points is attained, a reduction in flexural rigidity occurs, rather than the formation of a plastic hinge.

4.2.2 The analysis described below determines the load factors at which each critical point is reached for every submember of a frame. To represent the moment-curvature relationship accurately, many straight lines are needed. Therefore, for an accurate representation, many critical points are present, and thus, the method becomes uneconomic with regard to computational time. It is thus desirable to adopt a representation which yields a result that is both accurate and economical.

4.3 Difficulties arising in the non-linear analysis of reinforced concrete frames

4.3.1 The problems which arise in the analysis of reinforced concrete frames by the method described in this Chapter are similar to those discussed in the previous Chapter. A full member of a frame is again divided into submembers, for which the larger of the bending moments acting at their ends is assumed to be representative for the entire length of a submember. This is for the purpose of calculating its curvature. The non-linear effects due to axial load are accounted for by the use of an iterative technique which will be

described below.

4.3.2 The effect of axial load on member stiffness and frame instability for the magnitude of load encountered in the portal frame tests reported in Chapter 5 is small. Axial load effects are, however, included in the analysis to extend its application to frames where these effects are significant.

4.4 Non-linear analysis by the iterative load factor method

4.4.1 The analysis decribed in this Chapter traces the non-linear load deflection history of a frame upto and including the state of collapse. The analysis moves from one critical point to the next. Load factors at which these critical points are attained are computed. These are the lowest load factors for each prediction of the next critical point. The flexural rigidity of the 'critical section' is adjusted, and the search for the next critical point, extrapolated.

4.4.2 The procedure followed by the analysis is described below. Initially, the frame is assumed to be linear. The iterative cycle is set up and the overall stiffness matrix is constructed utilising the initial submember flexural rigidities, and zero axial load. The so-formed stiffness equations are solved to determine the unknown joint displacements, ($\underline{X} = \underline{K}^{-1}\underline{L}$), under an initial load factor of unity. The bending moment and axial force in each submember are calculated using these joint displacements in the member stiffness equations, $\underline{P} = \underline{k}\,\underline{A}\,\underline{X}$.

The load factor at which the bending moment of each submember reaches its first or next critical point is computed by a linear extrapolation, for two successive load factors. The lowest of all these load factors is the load factor F_2 at which the next critical point is expected to be reached anywhere in the frame.

The axial loads computed above are used to extrapolate the axial load in all the submembers under the next load factor. The ϕ-functions are calculated

using these extrapolated axial loads. These functions are then utilised to modify the stiffness coefficients in the formation of the stiffness equations in the next cycle of the iteration. The joint equilibrium equations are solved again, with the current load factor F_2 imposed upon the external loads. The new axial forces and bending moments in each submember are calculated using the resulting joint displacements.

The larger of the bending moments in each submember at the previous and current cycle of iteration and load factors F_1 and F_2 are used to interpolate or extrapolate the load factor at which the next critical point is reached in each submember. The lowest of all these load factors is again the expected load factor F at which the next critical point is predicted to occur anywhere in the frame. Using the axial loads in the submembers under the load factors F_1 and F_2, the axial load in each member for the load factor F are extrapolated.

The load factors are then updated, i.e. F replaces F_2 as the current value and F_2 replaces F_1 as the previous value of the load factor. The iterative cycle is repeated until the current load factor at the previous cycle of iteration F_2 and the lowest predicted load factor F for the next critical point are within a small specified tolerance. When this tolerance check is satisfied, the location of the critical region and value of the load factor at which it occurs are evaluated. The flexural rigidity of the submember which is critical is then adjusted to the next value on its moment-curvature relationship.

The critical load factor is then increased by a small amount and the load factors F_2 and F_1 updated. The next iteration is then initiated and for its first cycle, the axial loads in a submember are kept constant at their current value. The whole process described above is repeated to predict the load factor at which the next critical point is attained.

At the prediction of each critical point, a test is made on the sign of the determinant of the most recent overall stiffness matrix. The analysis is terminated when the determinant is negative, indicating that the frame has collapsed.

4.4.3 The iteration process

The iterative cycle is set up to test the convergence of the predicted and current load factors for each critical point. This procedure is necessary, since the axial loads in submembers are not known until the stiffness equations have been solved for the current load factors. To accurately predict the load factor at which a critical point is attained in a submember, the axial load that would occur under the load factor in the submember must be known. The iterative technique enables a linear extrapolation of these axial loads at the predicted load factor to be made. The accuracy of this extrapolation is assured by a tolerance check. This check is performed on the predicted load factor F and the current load factor F_2 in the following manner :

$$\left|(1 - F/F_2)\right| < \text{SPECIFIED TOLERANCE} \qquad (4.1)$$

4.4.4 For each cycle of the iteration, a linear prediction is made of the lowest load factor F at which the next critical bending moment in a frame is reached. To accomplish this, the following procedure is adopted. The induced submember bending moments are calculated using the joint displacements of the frame. The larger of the bending moments at the ends of each submember is taken to be representative of the bending moment for its whole length. Consider the bending moment in a particular submember to have been M_1 at the previous cycle of iteration and to be M_2 at the current cycle. The corresponding load factors are F_1 and F_2. These values together with the value of bending moment, M_{crit}, for the next critical point in the submember are shown in fig. 4.1. With increased load factor, the bending moment tends towards a positive or negative

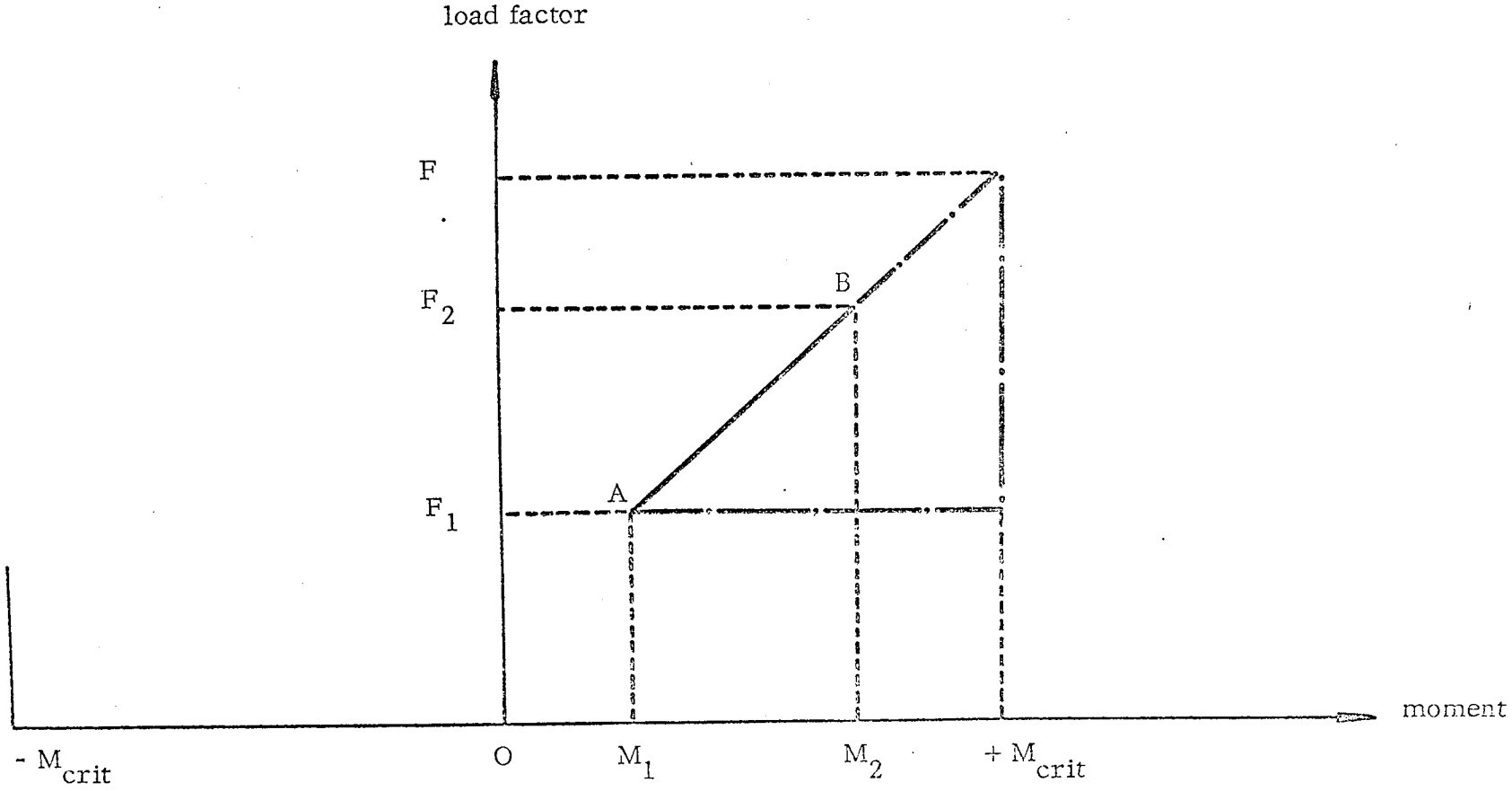

Figure 4.1 Extrapolation of load factor for next M_{crit}

M_{crit}. The sense of this is given by the sign of the gradient of AB in the figure, thus :

$$(F_2 - F_1) / (M_2 - M_1) \qquad (4.2)$$

For a negative ratic of this expression, the bending moment approaches a negative M_{crit}.

4.4.5 From fig. 4.1, a linear extrapolation can be made of the load factor F at which the bending moment in a submember reaches its next critical bending moment. Hence, by similar triangles :

$$F = (F_2 - F_1) / (M_2 - M_1) M_{crit} + (F_1 M_2 - F_2 M_1) / (M_2 - M_1) \qquad (4.3)$$

It was stated earlier that to accurately predict the load factor for a critical point, the axial loads that would act in submembers under it, must be known. This can be achieved by using the iterative procedure in conjunction with a linear extrapolation of the axial loads P_2 and P_1 at the load factors F_2 and F_1 respectively. The axial load P_F in a submember corresponding to the load factor F is given by :-

$$P_F = (F - F_1) / (F_2 - F_1) P_2 - (F - F_2) / (F_2 - F_1) P_1 \qquad (4.4)$$

4.4.6 In an analysis, the situation may arise where the bending moments M_1, M_2 and M_{crit} are nearly equal in value. This could occur when several submembers are approaching their next critical point. In this situation, the probability of making a wrong prediction is very high due to rounding-off errors. To safeguard against this occurance, a tolerance check is made on the product of M_1, M_2 and M^2_{crit}, i.e.

$$\left| 1 - (M_1 M_2) / M^2_{crit} \right| < \text{TOLERANCE} \qquad (4.5)$$

If this check is satisfied, then M_1, M_2 and M_{crit} are all nearly equal and the sign of the current load factor F_2 is assigned to M_{crit}. Thus, if M_1 and M_2 are positive, the iteration is carried out towards $+ M_{crit}$, and if they are both negative, the iteration is towards $- M_{crit}$. When M_1 and M_2 have different

values or a different sign, a wrong prediction cannot be made since the tolerance check will indicate that M_1 and M_2 are different.

4.5 The computer program

4.5.1 The representation of a frame for the computer analysis is as described in Appendix (1). An identical set of schematic diagrams are constructed and the data from these are prepared in an identical manner. In the analysis, the moment-curvature relationship of submembers are presented as data by the same system of two dimensional arrays used for the $(EI)_t$ - ϕ relationship as described in the previous chapter. Each critical point is given a number, and values of bending moment and curvature corresponding to these numbers are presented.

4.5.2 A program was written in FORTRAN IV for the non-linear analysis of reinforced concrete frames by the iterative load factor method. The main steps followed by the program are given in the flow diagram of fig. 4.2. These steps are described below.

The non-linear analysis of a frame starts by reading in data for the problem. The load factor is set to unity and the initial flexural rigidity of each submember is set. The number of locations required for the "main sequence" of the overall stiffness matrix $\underline{K}$ are computed, and a space cleared for them in the store. The iterative cycle is now initiated, and the load vector $\underline{L}$ is factored by the current load factor F. This is followed by the construction of the overall stiffness matrix for which the individual stiffness elements are adjusted in the light of the axial loads acting in each member by the ϕ-functions. Initially, the axial loads are set to zero. The stiffness equations are then solved, (i.e. $\underline{X} = \underline{K}^{-1}\underline{L}$) to determine the joint displacements $\underline{X}$. A test is then made on the determinant of the $\underline{K}$ matrix, if it is negative, the analysis is terminated.

For each submember, the induced axial loads and bending moments are

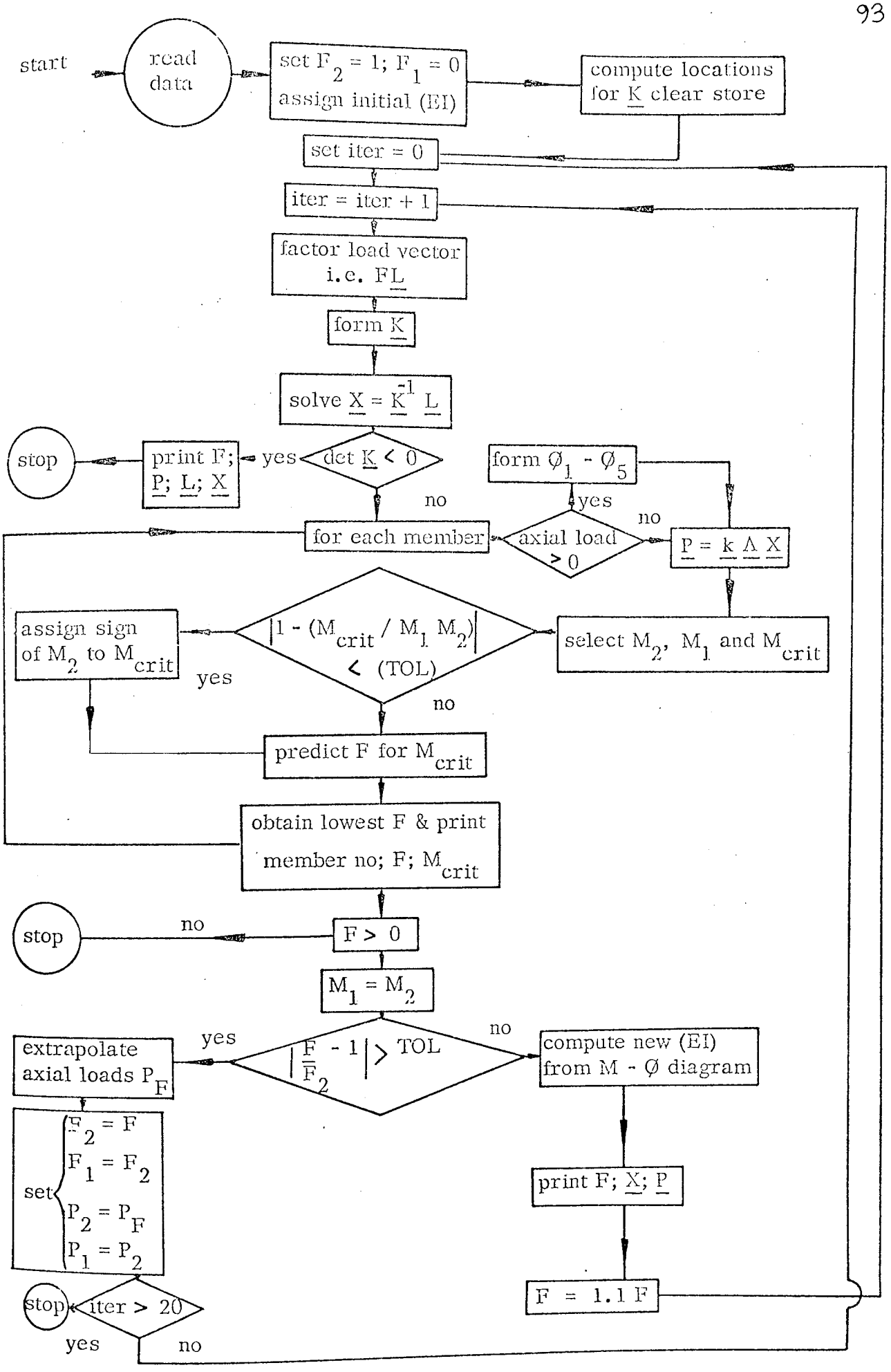

Figure 4.2 Flow diagram for iterative load factor program

calculated. If the previous axial load is greater than zero, these member forces are computed utilising the corresponding Ø functions. The larger of the bending moments M_2 and M_1 in each submember at the current and previous cycle of the iteration, together with the value of bending moment, M_{crit}, for the next critical point are found. To avoid the possibility of a wrong prediction, the tolerance check discussed in 4.4.6 for the bending moments M_2, M_1 and M_{crit} is performed. The load factor F at which the next critical point in a submember occurs is then predicted. The value of the lowest of these predicted load factors, F, is then printed out together with the values of critical bending moment, and the member in which it occurs. The bending moments are then updated.

The value of lowest predicted load factor, F, is compared with its value F_2 at the previous iteration in the tolerance check of equation (4.1). If F is not within the tolerance, the axial loads are extrapolated as in equation (4.4) and the values of load factor, and axial loads at the previous and current cycles are updated. To assess whether convergence is taking place, a test is performed on the number of iterations made so far. If this is greater than 20, it is assumed convergence will not take place, and the analysis is terminated. However, if less, the iterative cycle is continued. If the predicted load factor F is within a tolerance with its previous value, a critical point is realised. The flexural rigidity of the critical submember is then adjusted. The position of the critical point, the joint displacements $\underline{X}$, and values of the axial loads and bending moments at the present and previous rounds of iteration are printed. The load factor is then increased by a small amount and the iteration for the next critical point initiated.

The analysis is terminated when the determinant of the $\underline{K}$ matrix is negative, indicating that the frame has collapsed.

4.6 Conclusions and Discussion

4.6.1 The set of portal frames that were tested, and the results of which are reported in Chapter 5, have been analysed by the method presented in this chapter. In Chapter 7, these results are compared with those acquired by the incremental analysis of Chapter 3, and those obtained experimentally. It will be shown that the load factor analysis yields load-deflection curves which are discontinuous and indicate a less stiff response to the load when compared with the other methods.

The procedure described in this chapter is a development of the program by Majid and Anderson (18). Their program, however, was specifically formulated for the analysis of steel structures. The only similarity that the method presented in this thesis bears with reference (18) is in the manner in which load factors are predicted for each critical point in a frame. A true development of their method cannot be made if the concept of a gradually reducing flexural rigidity is adopted rather than the assumption that plastic hinges develop in the material.

4.6.2 In the analysis presented above, a value of load factor is computed for the attainment of all critical points in a frame while it is loaded to collapse. When a critical point has been reached in a member, the stiffness of that member and also the stiffness of the frame is reduced. The modified overall stiffness matrix of the frame was then used to predict the load factor F for the next critical point under a full loading from zero to F. Consider the load-displacement curve of a frame given in fig. 4.3. Initially, the overall stiffness of the frame is K_1. At the first critical point, the displacement of the frame is d_1 and the load factor F_1. This point is represented by A in the figure. At this stage of the analysis, the overall stiffness of the frame is reduced to K_2. This value of stiffness is then used for another complete analysis, i.e. from zero load

to the load factor at the next critical point F_2. This behaviour is represented by OB in fig. 4.3. In this manner, the analysis is repeated upto collapse. The results reported in Chapter 7 will show that a cycling of load factors occurred in each of the load factor analyses. Reasons for this behaviour will be given below.

4.6.3 In reality, the procedure discussed above is not strictly representative of the true behaviour of a frame under increasing load. This is because the modified overall stiffness matrix of a frame which results after each critical point has been reached is only representative of the stiffness for the increase in load from that at the previous critical point to the next critical point. This stiffness is represented by K'_2 in fig. 4.3, i.e. between the load factors F_1 and F_2. The assumption that the modified overall stiffness matrices are representative of the stiffness of a frame from zero load, after each critical point has been reached, is, therefore incorrect.

As the state of stiffness was not represented correctly, the analysis would yield a discontinuous load displacement curve.

4.6.4 If the true behaviour of a frame is to be followed, a modification must be made to the above method. It is suggested that an incremental procedure is utilized with this approach. This procedure will enable the modified stiffness matrix to be used only for the increase in load between consecutive critical points. The analysis will be continued after each critical point by predicting the increment of load factor necessary for the next critical point to occur. This is while the load factor increases from that value at the previous critical point. For this computation, the stiffness of the frame is represented by the modified K matrix which resulted from the reduction in stiffness of a member at the previous critical point. This stage of the analysis is represented by AB on the load-displacement curve of fig. 4.3.

To obtain a more representative prediction of the true behaviour of a frame loaded to collapse by a load factor method, the following procedure is suggested. This must be used in conjunction with the method previously described in this chapter.

Initially, the stiffness of a frame is represented by the overall stiffness matrix K_1. In this matrix, the initial value of flexural rigidity of each member is used. The lowest load factor ΔF_1 at which the first critical point is reached anywhere in the frame is then predicted in the same manner to that discussed previously in this chapter. This load factor and the corresponding displacement Δd_1 are shown in fig. 4.4.

The flexural rigidity of the submember is then reduced and the new overall stiffness matrix of the frame K_2 is calculated.

After the first critical point, the total bending moments in each submember of the frame are known and may be represented by the vector $\underline{M}_1$. The next stage of the analysis requires the lowest increment of load factor ΔF_2 to produce the bending moments at which the subsequent critical point occurs in the frame. If the bending moment at the next critical point for each submember is $\underline{M}_{crit(2)}$, then the increment of moment $\Delta\underline{M}_2$ which must be produced in each submember so that its next critical point is reached, may be given by :-

$$\Delta\underline{M}_2 = \underline{M}_{crit(2)} - \underline{M}_1 \qquad (4.6)$$

The lowest increment of load factor for $\Delta\underline{M}_2$ in any of the submembers is then predicted in the usual way. The total load factor and displacement at this point in the analysis are represented by B on fig. 4.4.

The new overall stiffness matrix K_3 can then be found. This will represent the stiffness of the frame for the increase in load factor ΔF_3 which will produce the next critical point. At each critical point, the increments of member forces (hence, bending moment) and displacements are computed. The

increase in moment $\Delta \underline{M}_i$ required for each member to reach the moment, $M_{crit\,(i)}$ at its next critical point, i, is given by the following expression :-

$$\Delta \underline{M}_i = \underline{M}_{crit\,(i)} - \underline{M}_{(i-1)} \qquad (4.7)$$

where $\underline{M}_{(i-1)}$ is the total bending moment at the (i - 1)th critical point.

The total load factor, displacements and member forces at any critical point i in the analysis are given by :-

1) load factor $$F_i = \sum_{j=o}^{i} \Delta F_j \qquad (4.8)$$

2) displacements $$d_i = \sum_{j=o}^{i} \Delta d_j = \sum_{j=o}^{i} K_j \Delta F_j \qquad (4.9)$$

3) member forces $$P_i = \sum_{j=o}^{i} \Delta P_j = \sum_{j=o}^{i} k_j \underline{A} \Delta d_j \qquad (4.10)$$

In the same manner to that described earlier in this chapter, the analysis is continued upto collapse.

The accuracy of the analysis may also be assured by performing an equilibrium check on the internal and external forces of the frame for every few load factor increases.

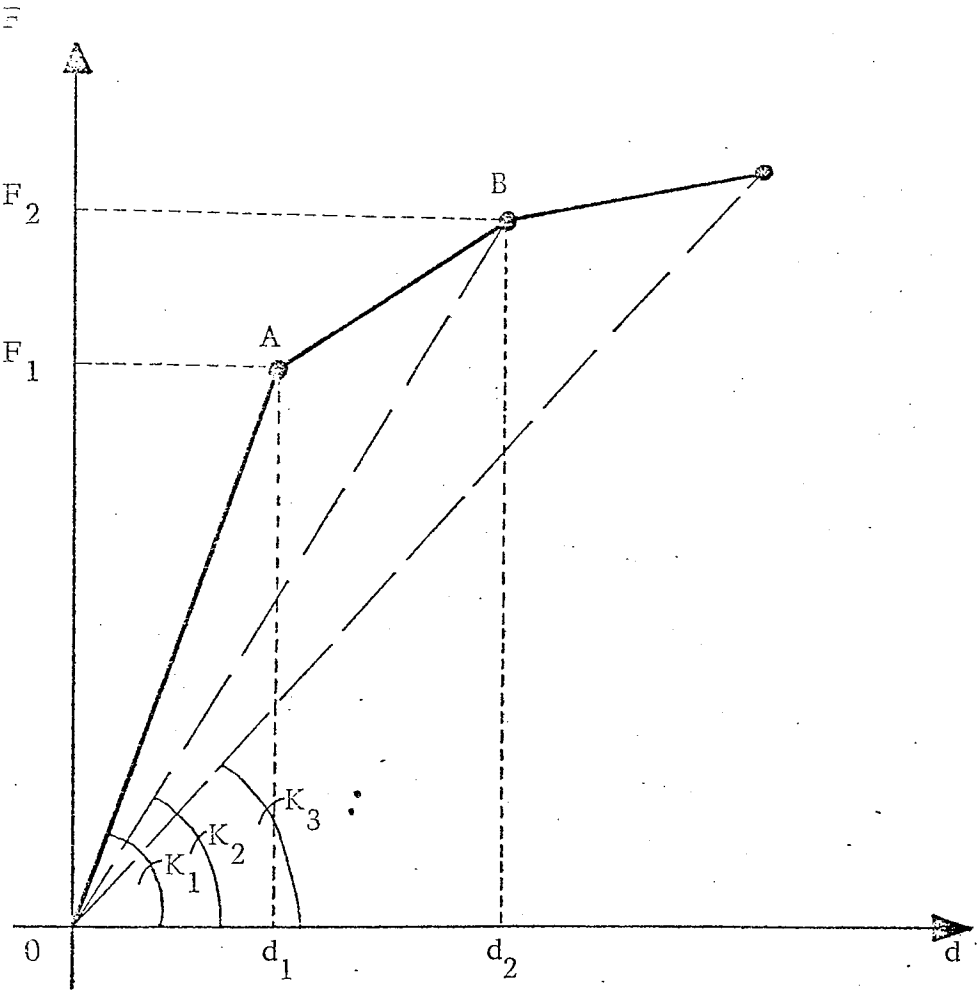

fig. 4.3 load factor-displacement curve for a frame

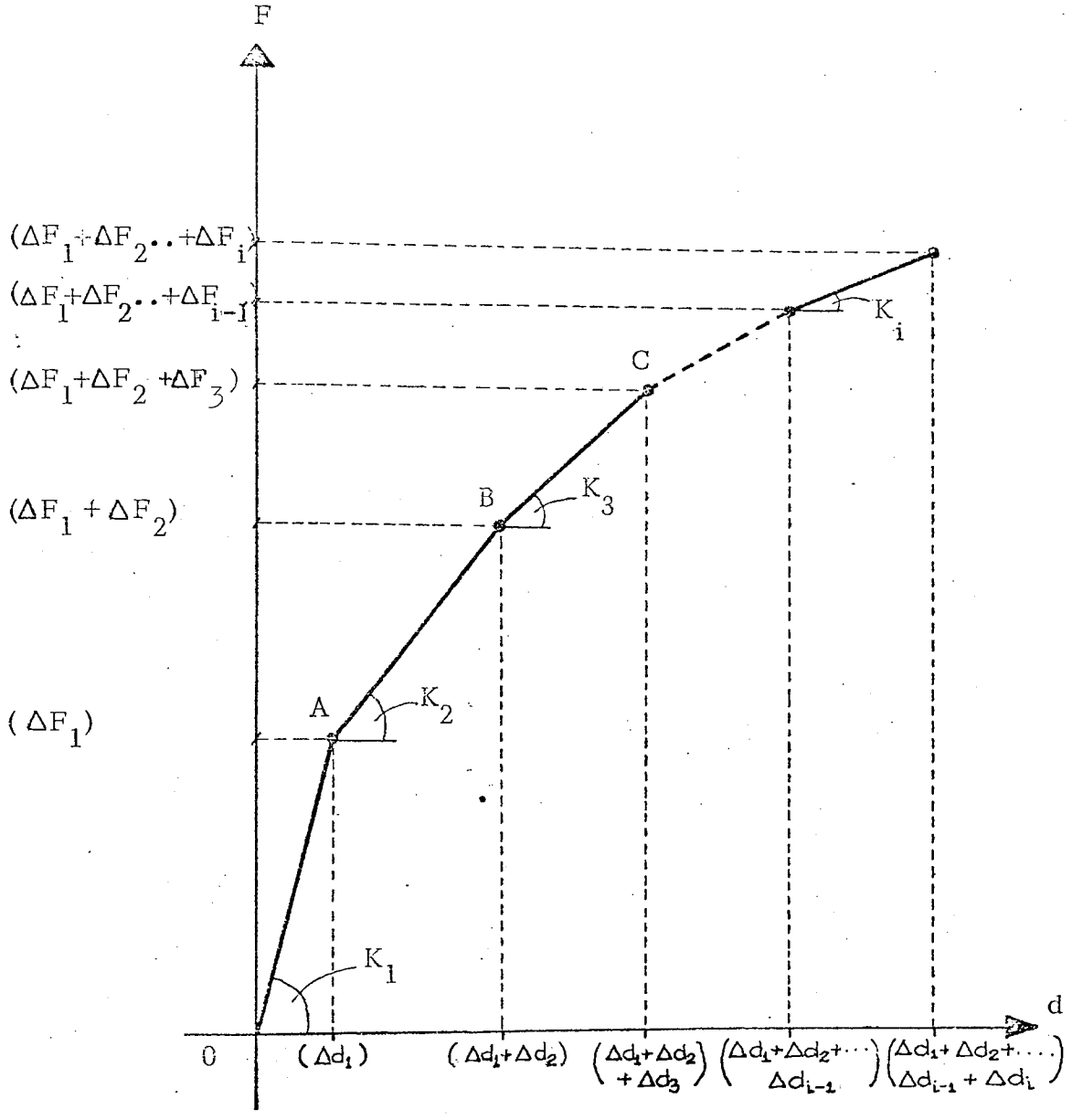

fig. 4.4 load-displacement curve of a frame

CHAPTER 5

TESTS ON REINFORCED CONCRETE PORTAL FRAMES

5.1 Introduction

In this chapter, a series of tests performed on reinforced concrete plane frames will be described. To validate the computer analyses described in previous chapters, a set of twelve pin-ended reinforced concrete portal frames were tested to collapse. To perform the computer analyses of these frames, moment curvature relationships were required for each different section used. These relationships were obtained from tests performed on reinforced concrete beams with the appropriate section. The frames and their associated beams were manufactured from the same materials, and cast simultaneously. Each frame was tested with proportional vertical and side load, this load being added in increments, up to collapse. At each load increment, the resulting displacement of the frame was measured. Each test gave the complete load-deflection history of the frame up to and including the state of collapse.

For the set of twelve frames, nine were single, and three two storey portals. Two storey portal frames were used to increase the number of external redundancies. The main variables used in the complete set were :-

(1) column height.

(2) section depth and reinforcement cover.

(3) percentage of tensile reinforcement of a section.

(4) pitch of vertical shear reinforcement.

5.2 Details of the Frames

5.2.1 The frames were tested to verify the accuracy of the computer analyses. Their sections were not designed for any particular mode of failure. The variables

used throughout the test series were to assess whether the computer could predict the overall behaviour of the frames, whatever their properties.

In all the frames, the longitudinal reinforcement was four continuous bars. These bars were placed two at the top and two at the bottom of a section. With the exception of one section of Frame F11, each section was "under-reinforced". All the frames were provided with shear reinforcement, throughout their length.

5.2.2 The twelve portal-frames tested consisted of seven different sets of frames. The first set contained frames F1, F2 and F3, which were identical. The second set comprised of F4 and F5 which were again identical. The third set of frames F6, F7 and F13 were three identical, two storey portals. The last four sets were frames F9, F10, F11 and F12 respectively, each being different. The details of each set of frames is given in figs. 5.1, 5.2 and 5.3. Reinforced Concrete by virtue of its constituent materials and manufacture is a variable structural material. To assess this variability, the first three sets of the series consisted of more than one frame. The set of frames were manufactured under the same conditions and the variability of their load-deflection curves noted. If this variability was small, then single tests on frames could be performed and the results reported with confidence. The load-deflection response to the sway load of frames F1, F2 and F3; F4 and F5; F6, F7 and F13 are given in figs. (7.1, 7.2, 7.3) respectively. The results obtained, and shown in these figures, do not vary significantly. Hence, the last four sets only contained one frame each.

5.2.3 The frames were made as large as was practical for the available space in the laboratory. Each frame was pin-ended at its feet. This end condition was used for two main reasons. The first is that the load necessary to cause collapse, would not be as high as that required, if the ends were fixed. Secondly, end fixity

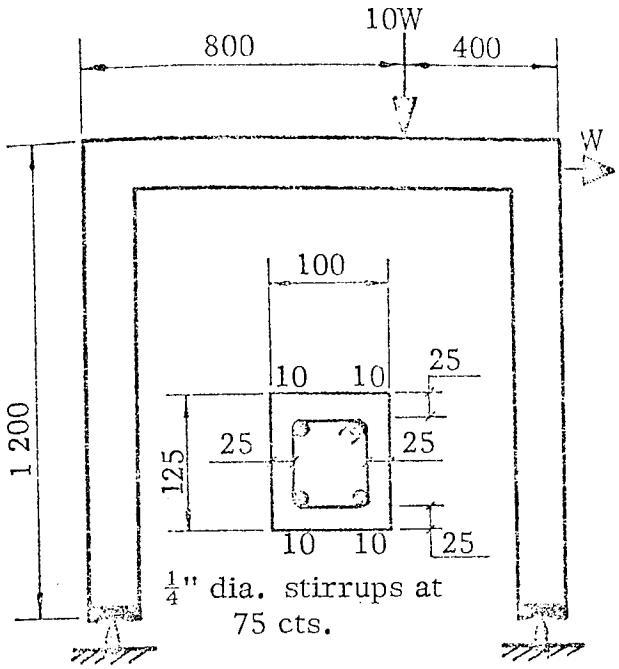

Typical Section

FRAMES F1, F2 & F3

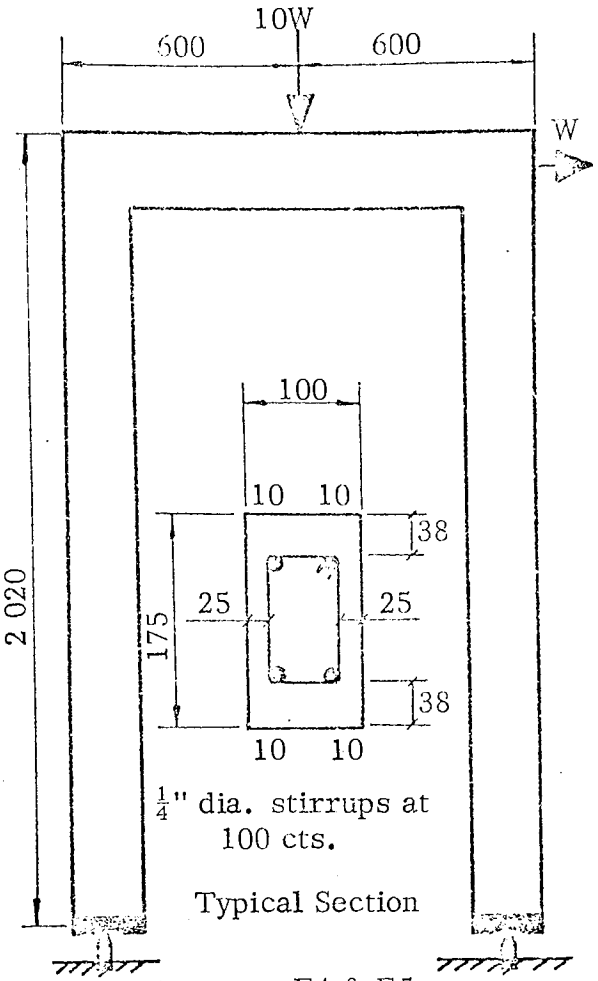

Typical Section

FRAMES F4 & F5

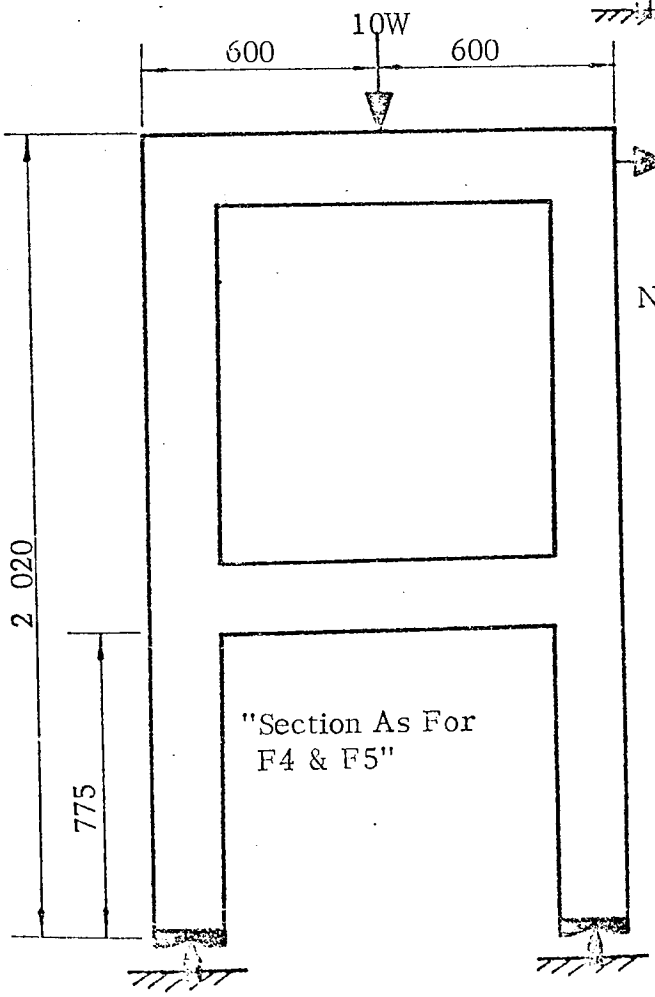

FRAMES F6, F7 & F13

N.B. All dimensions are in mm unless otherwise stated.

Figure 5.1 Details of Frames - (1)

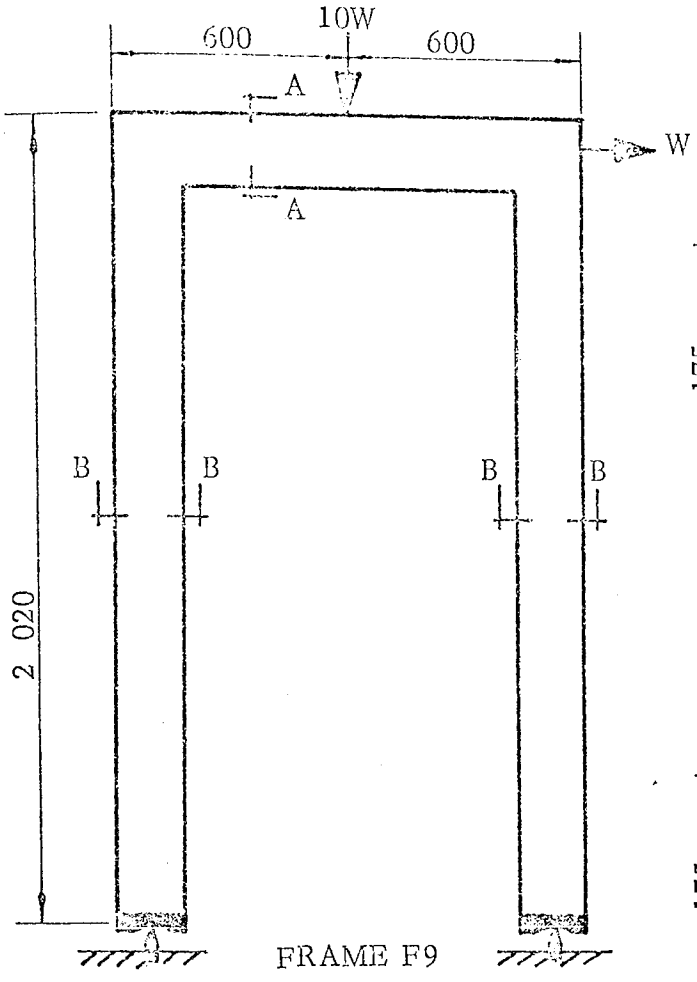

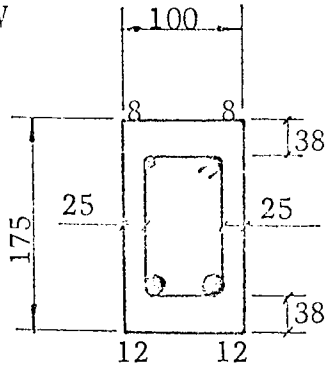

$\frac{1}{4}$" dia. stirrups at 100 cts.

Section A - A

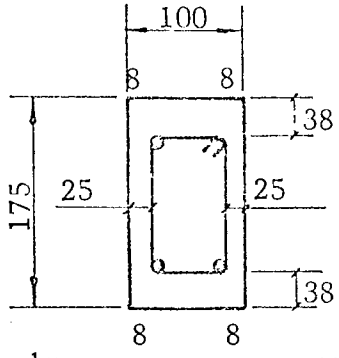

$\frac{1}{4}$" dia. stirrups at 150 cts.

Section B - B

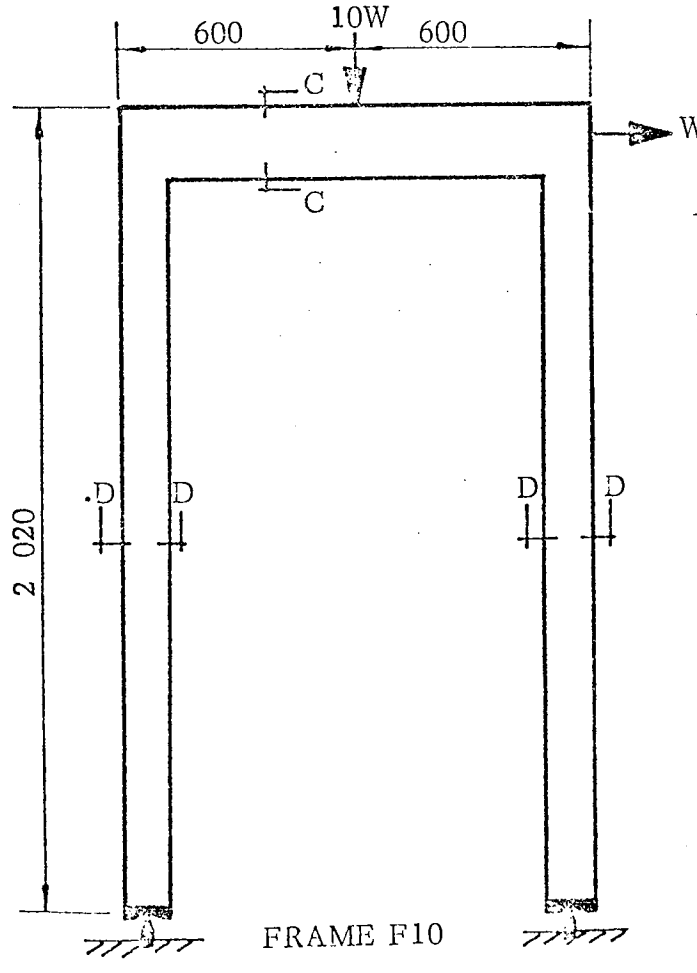

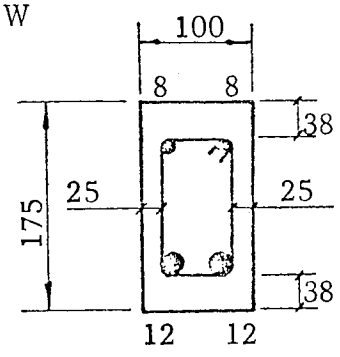

$\frac{1}{4}$" dia. stirrups at 120 cts.

Section C - C

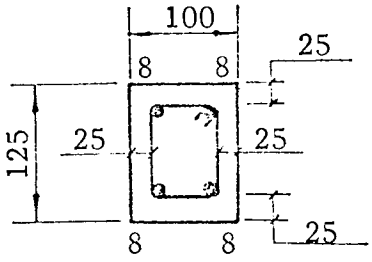

$\frac{1}{4}$" dia. stirrups at 150 cts.

Section D - D

Figure 5.2 Details of Frames - (2)

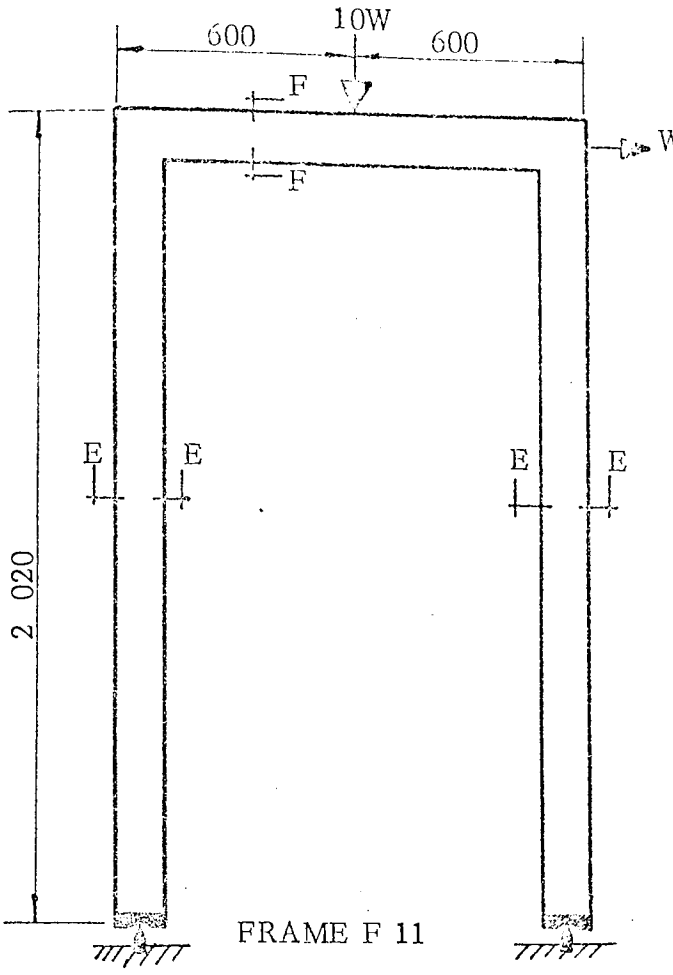

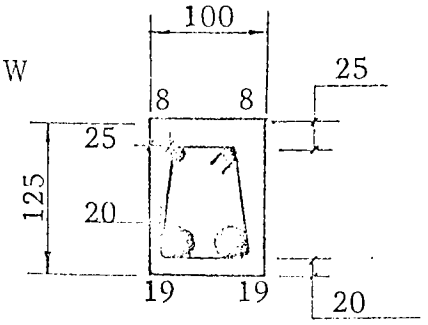

$\frac{1}{4}$" dia. stirrups at 190 cts.

Section F - F

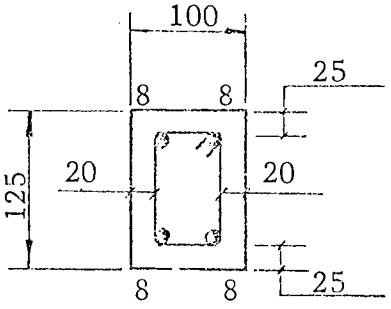

$\frac{1}{4}$" dia. stirrups at 200 cts.

Section E - E

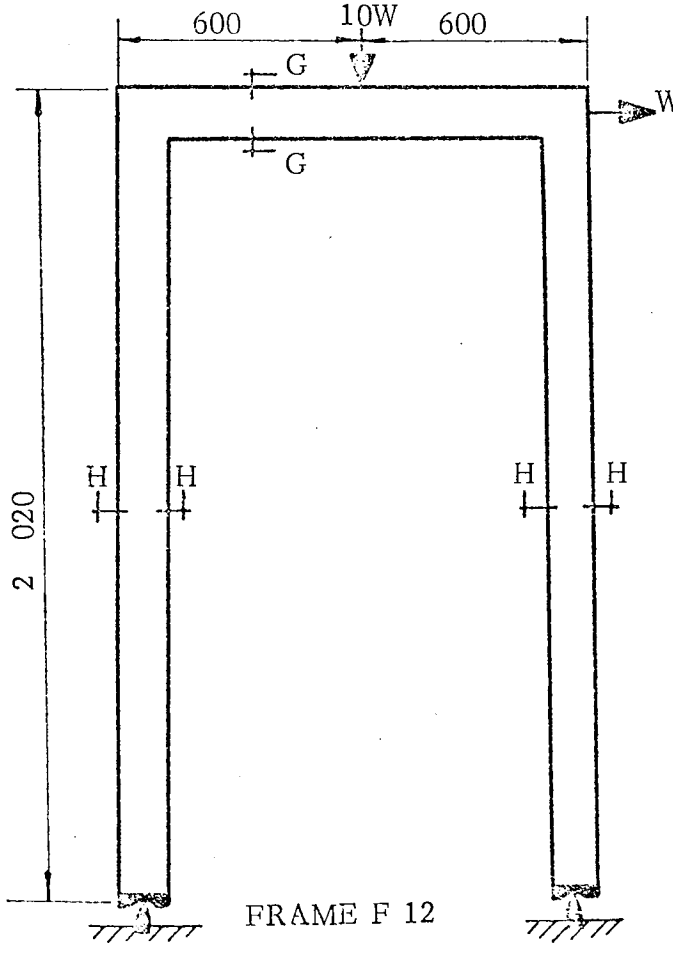

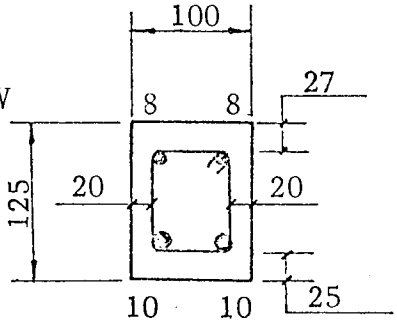

$\frac{1}{4}$" dia. stirrups at 190 cts.

Section G - G

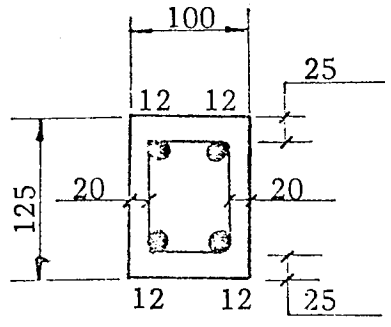

$\frac{1}{4}$" dia. stirrups at 200 cts.

Section H - H

Figure 5.3 Details of Frames - (3)

is very difficult to achieve, and is nearly always used in practical structures, only when heavy raft foundations are provided, at the feet of the columns. To provide a greater degree of indeterminancy, two storey portal frames were tested, again with pin-ends. This was to assess whether the computer programs could cope with more degrees of freedom. The first three sets of frames each had a constant section throughout, i.e. identical top and bottom steel and cover. For these sets, only one beam needed to be tested with each frame to determine the moment-curvature relationship of the section. For the last four sets, the column sections were identical in each frame, however, the top and bottom steel of the transom members, were different. Three beams were tested for each of these frames, to provide the necessary moment-curvature relationships of all their different sections.

5.2.4 A detail of the reinforcement of a typical frame and beam is shown in fig. 5.4. The longitudinal bars are continuous with bends provided at the corners. Where a bar diameter changes at a location in a frame, the two different bars were welded together in a double V weld. The main bars were welded into holes in the metal end blocks at the column feet. Cover was provided to the main bars by placing mortar blocks around the frame, tied to the bars. Special attention was paid to the detailing of corners and joints in the frames. Swann (42) suggested the use of double inclined stirrups welded to the main bars as the best detail to resist opening and closing effects at corners. This detail is shown in fig. 5.4, and was used for all the frames. For the joint of the two storey portals, where the lower transom member met the columns, the detail shown in fig. 5.5 was used. Side load was transmitted to the frames via a 12 mm square bar. This bar was welded to the inclined corner stirrups of the frame as shown in fig. 5.4.

Vertical shear links were provided throughout the length of the frame.

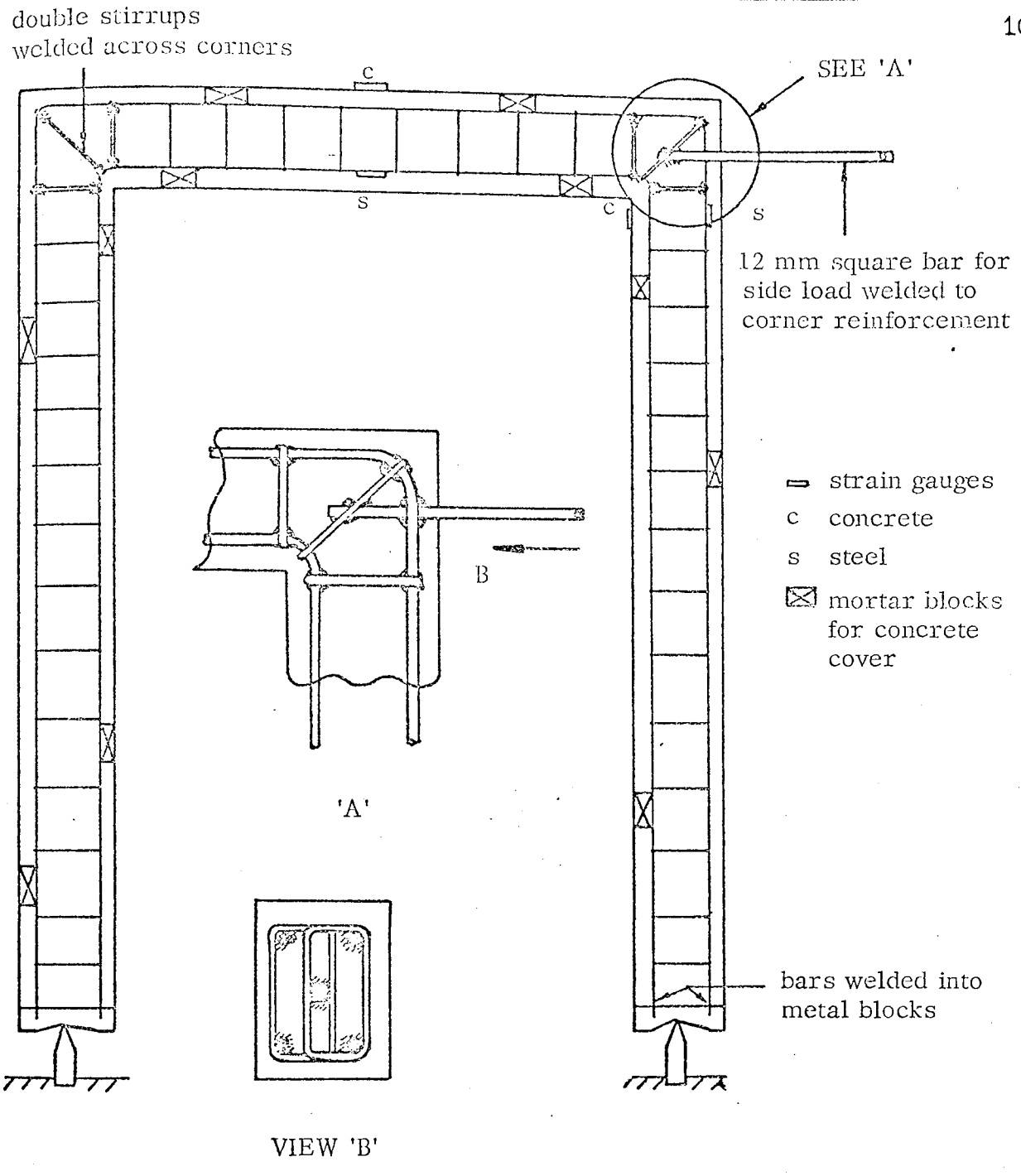

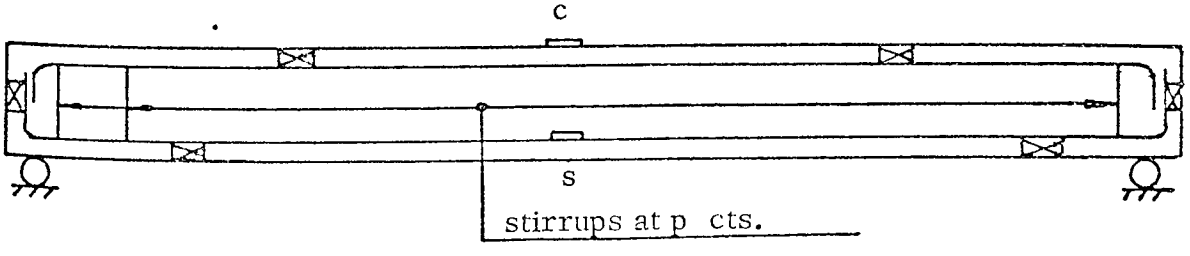

Figure 5.4 Reinforcement details of a typical Frame & Beam

This reinforcement was vertical stirrups of 0.25 in. diameter bars. In the last three tests, the pitch of the stirrups were increased to ascertain whether shear cracking was occurring in members where high shear forces existed.

5.3 Manufacture of Frames and Beams

5.3.1 The cement used throughout the test series was ordinary Portland Cement. Zone III sand and 3/8" crushed gravel were used as aggregates. The seive analysis of both aggregates are given in tables 5.1 and 5.2. The concrete mix used throughout the test series was 1 : $1\frac{1}{2}$: 3 with a water cement ratio of 0.5. These constituents were dry and batched by weight. This mix was chosen as its performance was known from other experimental work being carried out in the Department. The strength of the mix for the hardened concrete is reported in table 6.3

5.3.2 Before the selection of the type and size of reinforcing bars to be used, tests were carried out on thirty, randomly selected samples of each available bar. This was with the exception of the 19.1 mm diameter bar. Tensile tests were performed for each bar in a Denison Universal Testing Machine. The load strain characteristics were plotted automatically using a Baldwin Strain Recorder and strain gauge. The average pertinent values of stress and strain recorded for each bar are reported in table 6.2. All the bars eventually selected exhibited a consistent, reasonably sharp yield point, and strain hardening. Shear reinforcement was randomly selected from a batch of 0.25 in. diameter mild steel bars.

5.3.3 The reinforcing bars were supplied in batches of 8 metre long bars. The lengths of bars required for each particular location in the frames and beams were cut from the same bar. This was to reduce any variability in the properties of sections that may be caused by a change in the reinforcement's properties in

TABLE (5.1)

sieve analysis of ZONE III sand

sieve size or no.		%
retained	3/16	6.899
retained	7	11.040
retained	14	5.201
retained	25	14.640
retained	52	39.995
retained	100	19.400
passing	100	2.824

TABLE (5.2)

sieve analysis of 3/8 crushed gravel

sieve size or no.		%
retained	3/8	2.731
retained	3/16	82.298
passing	3/16	14.971

a batch. The bars were bent and welded to the required shape. Shear stirrups were manufactured to the required sizes. The reinforcement cages were assembled and fixed, by tying the main bars to the stirrups with binding wire. The column feet and corner stirrups were then welded. The 'cages' were placed in oiled formica lined timber moulds, and mortar blocks tied to the main reinforcement, to provide the necessary cover.

5.3.4 With each test, the following control specimens were cast :-

(1) 3 No. 150 mm cubes - to obtain the cube crushing strength of the concrete.

(2) 3 No. capped 300 mm x 150 mm diameter cylinders - for the uniaxial compression test.

(3) 2 No. 300 mm x 150 mm cylinders - for the tensile splitting test (i.e. tensile strength of concrete).

Prior to mixing the concrete, the frame, beams and control specimen moulds were placed horizontally on a 'variable speed' vibrating table. This method of vibration was used to ensure a constant degree of compaction for all specimens. The concrete was mixed in a non-tilting mixer, to avoid segregation in the concrete. The concrete was added evenly to the moulds, and vibration carried out throughout the cast. All the cast specimens were transferred to a controlled humidity curing tank. The concrete was kept wet throughout the curing period. The moulds were stripped after two days.

5.4 Instrumentation

5.4.1 Deflection was measured at points around the frames by 50 mm travel dial gauges. The gauges were fitted to a rigid slotted-angle frame. To prevent false readings due to 'sticking' of the stems of the gauges, they were thoroughly cleaned before each test.

5.4.2 Steel tensile and concrete compressive strains were measured at points

of maximum bending moment in the frames. These were the maximum values anticipated to occur at the loading points, i.e. in the column and transom members. Electrical resistance strain gauges detected the strain. The gauges used to detect steel strains were fixed to the reinforcement and water-proofed before casting. Concrete strain gauges were fixed to a prepared surface of the concrete. Strains were measured using a Peekel strain recorder. This instrument gave a direct reading of microstrain. Dummy strain gauges were positioned to simulate the conditions encountered by the test gauges. This eliminated the possibility of electrical inbalance. Measurement of these strains gave a check on the state of 'critical' sections throughout the experiments.

5.5. The test rig

5.5.1 The frames were tested in a test bed consisting of two end stanchions braced by a top and bottom cross beam. This provided a rigid frame with a clear rectangular space in which to place the test apparatus. The test bed was capable of withstanding very heavy loading, far in excess of that encountered during this test series. To provide the clearance height necessary for the lever system (described later), the bottom cross member of the test bed was raised as high as possible. For the first three tests, extra height was provided by placing the frames on two UC sections (F)*(L) which were bolted to the test bed.

5.5.2. Pin-ended conditions were provided by a knife edge arrangement (E). The knife edges were made out of steel containing 1% carbon and 0.5% chrome, hardened by an oil quenching at 800° C. and tempered back at 250° C. The knife edges were placed in grooves on a 50 mm thick plate which was rigidly fixed to the test bed. Adequate clearance to allow the 'hinge' to rotate was necessary. To assist in providing this clearance, the metal blocks at the feet

* letters refer to those used in Plate (15)

of the columns were splayed. The pin-end arrangement is shown in fig. 5.6.

5.5.3 To prevent lateral movement of the frames, and also to eliminate the possibility of the frame toppling off the test bed, passive lateral support was provided. This took the form of two frictionless rollers located either side of the transom member (W). The rollers allowed the frames to sway without resistance. Each roller had an adjustable bearing at the top and bottom, as can be seen in fig. 5.7 (a). The rollers were supported from the top cross member of the test bed as shown in fig. 5.7 (b).

5.5.4 Two methods exist for applying loads to test models :-

(1) hydraulic loads via jacks and proving rings.

(2) dead load.

For testing frames under vertical and side load, it is necessary for the vertical load to act at the same point during sway. To provide this type of loading hydraulically is difficult, and would necessitate the modification of the standard load apparatus. During a test to collapse on reinforced concrete, creep and cracking occur. To allow time for these phenomena to develop, it is necessary to apply a constant load for a period of time. Hydraulically applied loads generally relax and require readjustment, and do not, therefore, give a constant load. The two requirements of the loading system can be met by using dead load. The main disadvantage of this type of load is in providing the magnitude of load necessary to collapse a frame. A lever system, however, will deliver the necessary load. This type of loading was used throughout the test series.

5.5.5 For practical reasons, the largest lever ratio possible was 10 : 1. The ratio of vertical to side load throughout was also 10 : 1. This simplified the loading procedure in that the same load increments were applied to each of the load

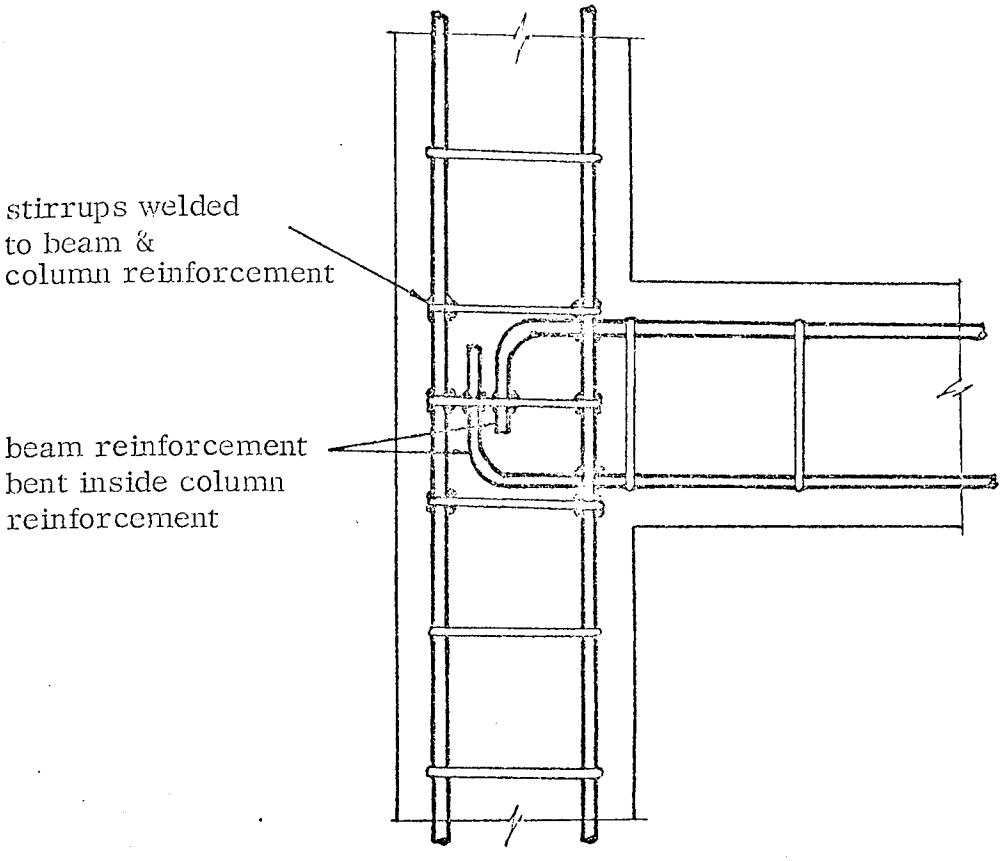

Figure 5.5 Column-lower beam connection

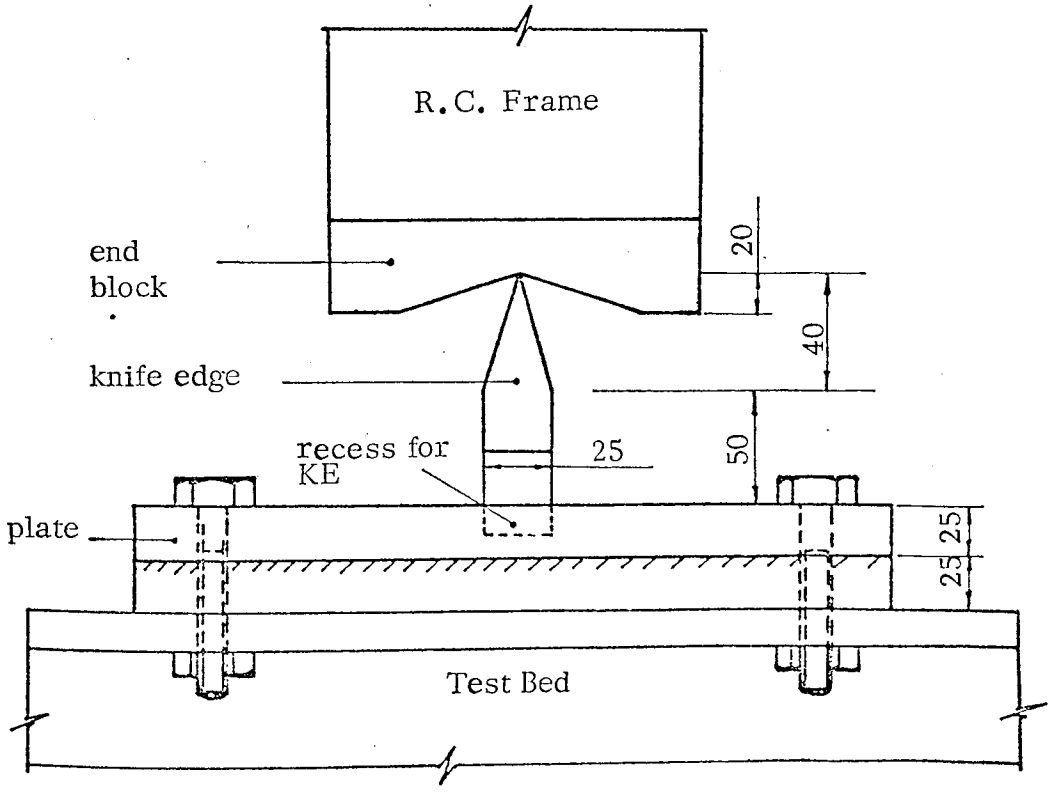

Figure 5.6 Details of the pin-end

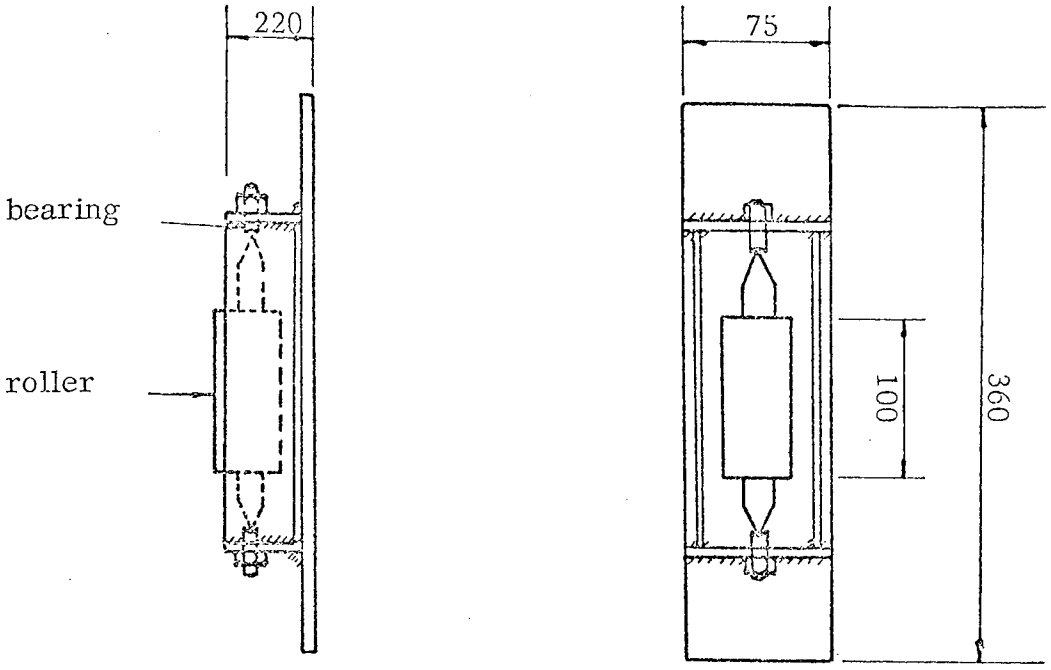

(a)

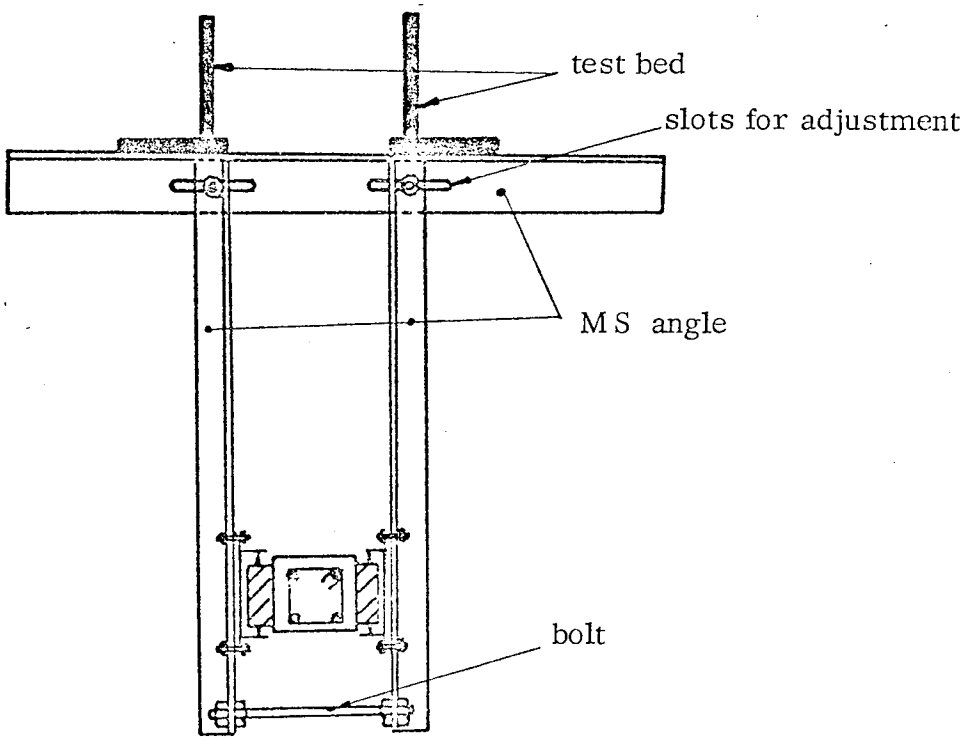

(b)

Figure 5.7 Lateral support system
(a) details of rollers
(b) arrangement of support system

systems. The lever arm itself, (L)**, was required to withstand large bending and shear forces without distortion. A few sections were tested for use in the lever arm, the best was a square hollow section 4" x 4" x $\frac{1}{4}$". The lever arm was required to transmit a vertical levered load with a minimum of losses due to friction at all points of load transfer. The points of application and transfer of load to and from the lever arm were kept on the same horizontal line, see fig. 5.8. To reduce friction, all these transfers were made via knife edges. These were special hardened bushes pressed into the lever arm see fig. 5.8. Load was transferred to and from the knife edges to other parts of the system with rollers and plates. The plates (A)(C)(D)(F)(W), were made of 4" x $\frac{1}{4}$" bright steel and also provided with hardened knife edge bushes. Each of these plate systems consisted of two plates bolted together with enough space between so that the lever arm would pass between them. The internal diameter of the knife edges was greater than the outside diameter of the rollers to reduce the point of contact between the rollers and knife edges.

One of the conditions the vertical load system had to satisfy was that it gave a constant point of application of load which remained reasonably vertical during sway. To allow the lever system to move, wire ropes (B)(E), transferred the load from the arm to the frame and fulcrum. The ropes were $\frac{1}{2}$" diameter and looped at either end. The fulcrum of the lever system was provided by a rigid connection to the test bed (F).

The levered load was applied to the frame by a flattened roller bedded in plaster of paris on the top of the transom member. The roller was flattened to avoid local crushing of the concrete. The load pan was hung at the free end of the arm (W).

The complete lever system is shown in fig. 5.9 and plate (13).

** letters refer to those used in Plate (13)

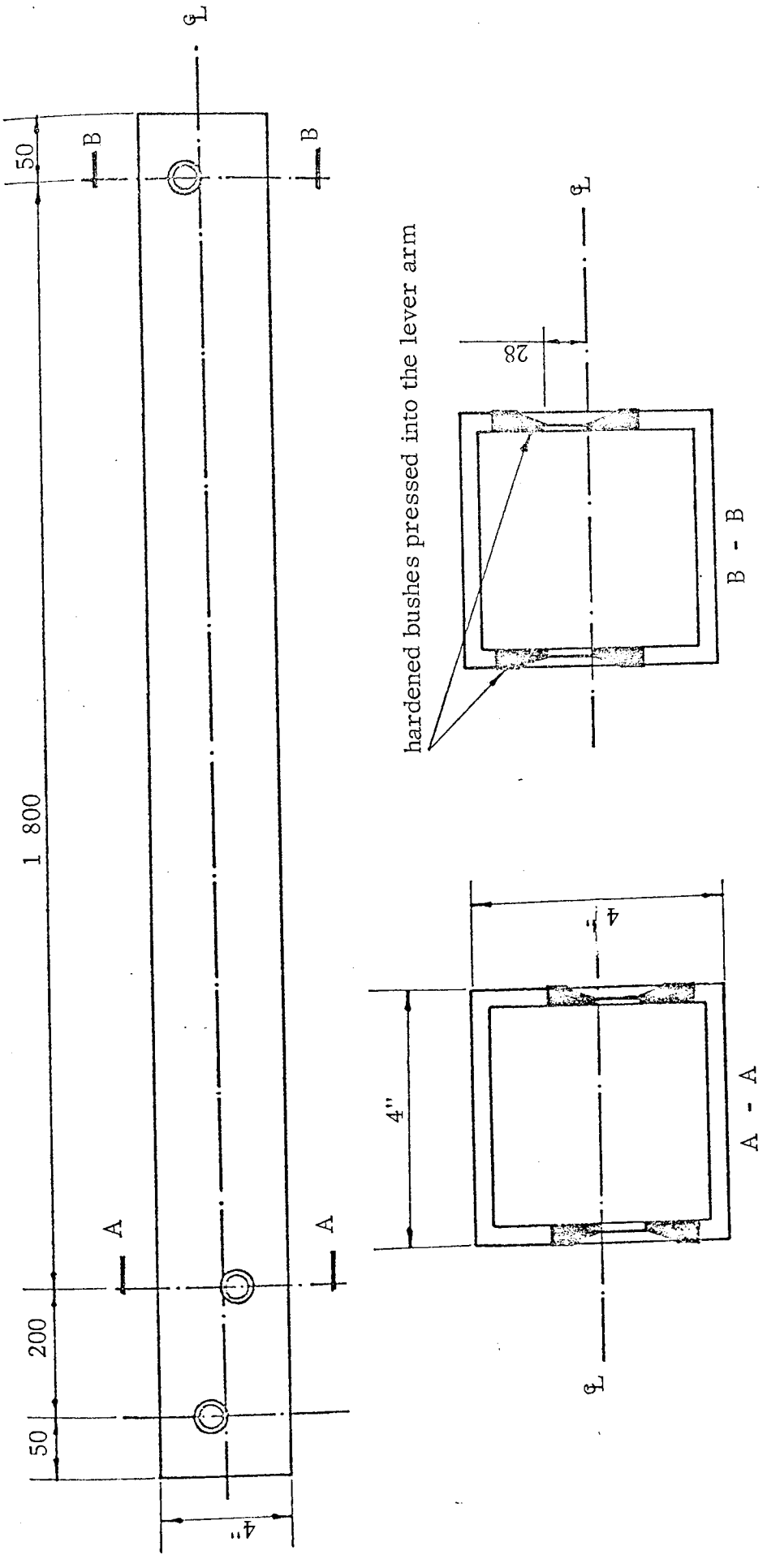

Figure 5.8 Details of the lever arm

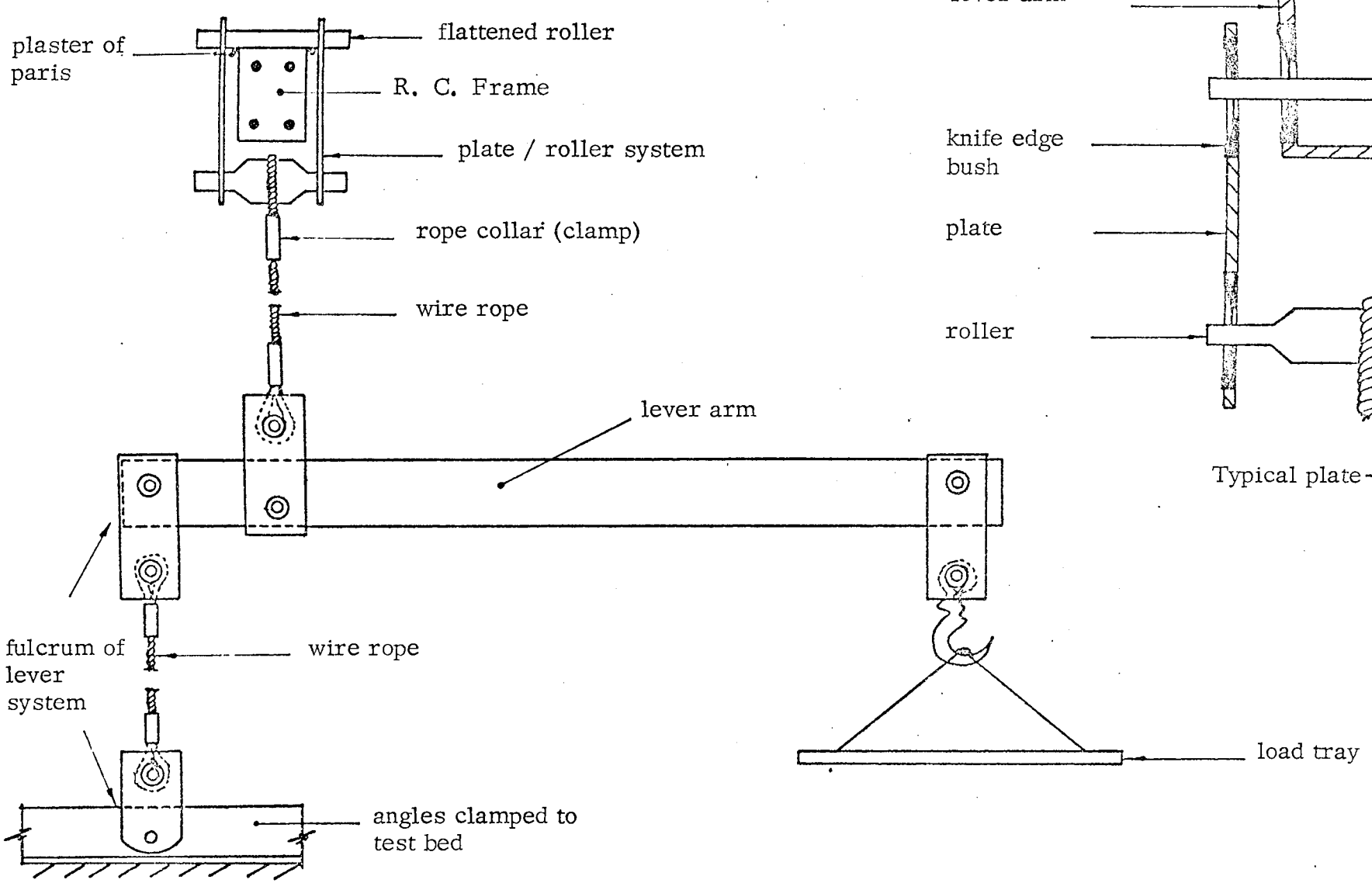

Typical plate-roller system

Figure 5.9 Lever loading system

5.5.6 The side load was also transmitted by a dead load system. As the magnitude of load required here was much less than for the vertical load, no special load system was needed. Load was transferred from the load pan (Z)+ to the frame via a 6 mm diameter stranded wire (V)(Y). This wire looped through a hole in the bar which protruded from the frame. The wire passed over a well oiled pulley (W) which was rigidly fixed to the test bed. The length of the wire was 1.5 metres and horizontal to minimise any vertical component of load during sway. The load pan was identical to the one used in the lever system. This allowed similar pre-weighed boxes of chains to be added simultaneously at both load points. This assisted in accurate realisation of a proportional loading system. The side load system is detailed in fig. 5.10, and shown in plate (14).

5.6 Testing the apparatus

To test the apparatus for both accuracy and capacity, a portal frame was manufactured and loaded. This allowed any modification that was necessary for the apparatus to be made and tested.

5.7 Test Procedure

The frame was lifted into position with a fork lift truck, care being taken not to damage any part of the frame. With the frame in position, a check was made to ensure that the columns were vertical and cross-member horizontal. The frame was held manually, whilst the lateral support was positioned. The rigid slotted angle frame used for supporting the dial gauges, was positioned around the frame, and the gauges attached at the required locations. The stems of the dial gauges were thoroughly cleaned to avoid restriction in their travel. The strain gauge wires were connected to the strain recorder, and the gauges tested. Initial readings of the strain and dial gauges were recorded.

+ letters refer to those used in Plate (14)

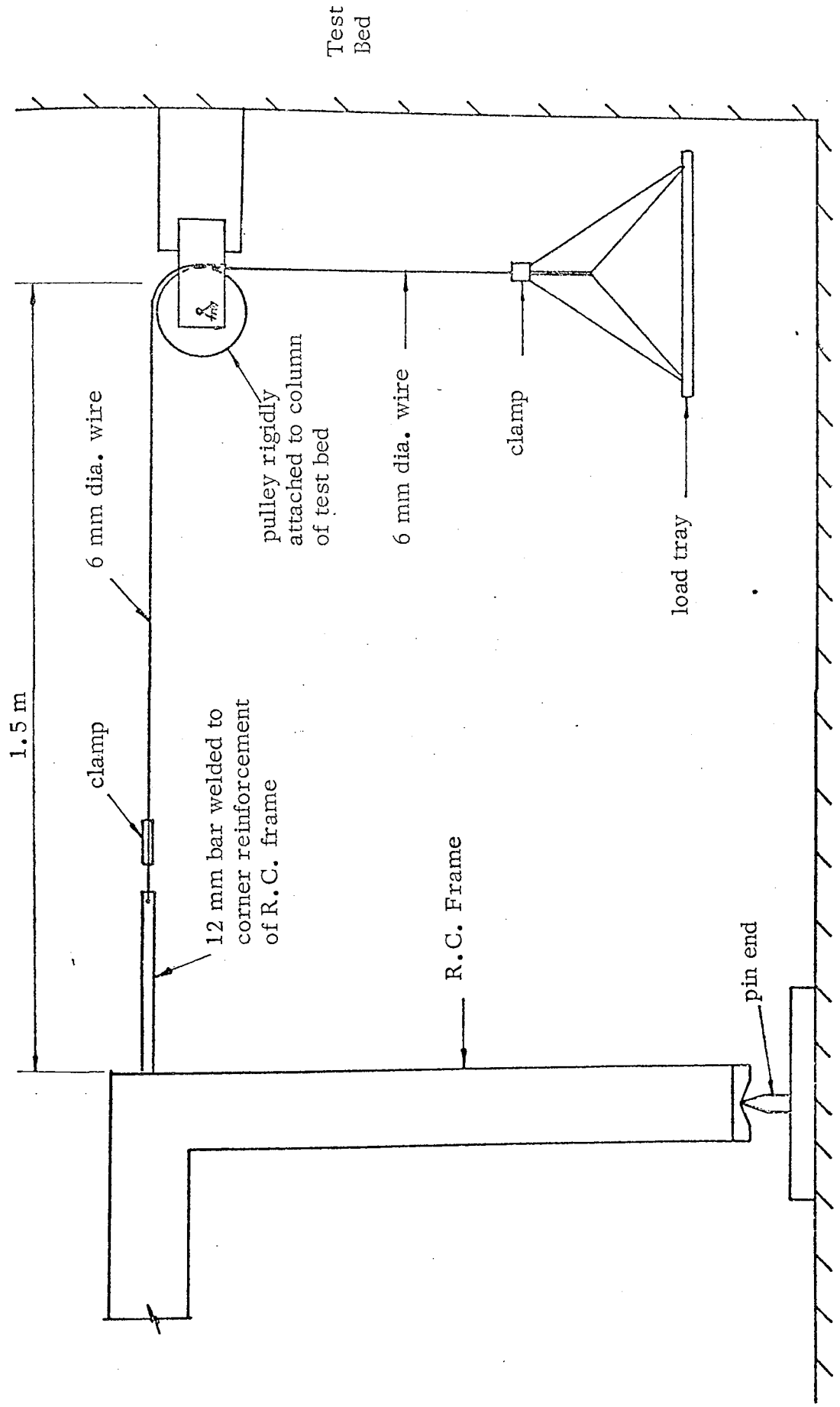

Figure 5.10 Details of side load system

The load systems were carefully applied to the frame, and their self-weight inbalance, corrected. The test set up prior to commencement of a test is shown in Plate (15). Time was allowed for the frame to settle before recording the next set of readings. Load was carefully applied simultaneously at both load points by two people. Measurements were taken only when the dial gauges had settled to a constant rate of 0.01 mm/min. This allowed time for creep and cracking to occur. During each test, graphs of load against deflection were plotted for each load point. From these graphs and the strain readings, the value of subsequent load increments were chosen i.e. when to reduce them in value. This procedure was carried out upto the load at which the frame collapsed. Near failure, the load increments were small. Readings at this stage were taken when the dial gauges had slowed to the rate of 0.05 - 0.1 mm/min.

In addition to the readings mentioned above, points of specific interest, such as the extent of cracking in the concrete, and loads at which the steel tensile reinforcement yielded, were noted. At failure, photographs were taken of the mode of collapse.

The concrete control specimens were tested to ascertain the strength of the concrete at the time of testing. The duration of each frame test, varied between 6 and 8 hours. On completion of each test, the beams were tested as soon as was possible. The collapse mechanism of each frame is shown in Plates (1-12). These will be discussed in Chapter 7 where the results of each test are reported. The behaviour of individual sets of frames is described. The values of load-deflection upto collapse are compared with the results obtained from computer analyses. The strain guages were used to detect the strain in the concrete and steel as the loading was increased. With knowledge of the state of strain, it was possible to adjust the magnitudes of applied load to ensure that the loads at the point of cracking of concrete and yield of steel were not missed. The gauges were used for no other purpose and therefore, no results of the readings have been reported in this thesis.

CHAPTER 6

TESTS ON REINFORCED CONCRETE BEAMS TO DETERMINE THEIR MOMENT - CURVATURE RELATIONSHIPS

6.1 Introduction

In this chapter, the tests performed on reinforced concrete beams to determine the moment-curvature relationships of the sections used in the portal frames of Chapter 5 will be described. The results gained from these experiments, and the theory detailed in 2.3 will be compared. The reinforced concrete sections tested correspond in every detail to those used in the portal frames. The beams were tested immediately after the frames were tested. This minimised any gain in strength of the concrete. A total of twenty moment-curvature relationships were required to define the properties of all the sections used in all the frames. To ensure uniformity of the testing procedure, with that adopted for the frame tests, dead loading was used. The beams were all 2.1 metres in length and simply supported.

To examine the effect of axial load on the moment-curvature relationship, two extra tests were carried out on identical beams. The axial load was kept constant throughout each test.

The loading was "first time" for all the experiments.

6.2. Details of the beams

6.2.1 The dimensions of the section for the beams were either 100 mm x 125 mm or 100 mm x 175 mm, breadth to depth. The longitudinal reinforcement consisted of four continuous bars, bent up at the ends, to ensure adequate bond between the concrete and steel. The location of the bars and their cover was indentical to that used for the sections of the portal frames. Shear reinforcement in the form of vertical stirrups of 0.25 in. diameter bar was provided along the entire length of

the beams, their pitch was the same as that used in the portal frames. A typical reinforcement detail of a beam is given in fig. 5.4.

The details of all the beams tested are given in Table 6.1

6.3 Manufacture of Beams

6.3.1 The concrete used in manufacturing the beams was the mix described in 5.3. Table 6.3 gives details of the properties of the concrete mix used for each cast of the frames and beams. The reinforcement was cut from the same lengths of bars used in the portal frame tests. The properties of the reinforcement are given in Table 6.2. The beams were cast and cured under the same conditions as the portal frames. It was assumed, therefore, that the beams were truly representative of the corresponding members in the portal frames.

6.4 Test arrangement

6.4.1 The main requirement of this test series was to obtain the curvature of the beam for each load increment applied upto collapse. The test arrangement and bending moment diagram for a test are shown schematically in fig. 6.1. The loading system is the so-called four point bending test. The 2.1 metre long beams were supported on two 75 mm diameter rollers, spaced at a centre to centre distance of 2.0 metres. The two concentrated loads were applied at points situated 1.0 metres apart, these points were disposed symmetrically in relation to the centre of the beam. This loading gave a region of constant bending moment between the load points, as is seen between B and C in fig. 6.1. For this region, the beam can be assumed to bend in a circular manner.

6.4.2 Assuming circular bending between the load points and small deflections, the moment-curvature relation was found in the following manner. Deflection was measured at both the load points, and the centre of the beam.

The portion of the beam between points B and C in fig. 6.1 is taken to be

TABLE NO. (6.1)

Properties of the sections

Beam No.	b mm	h mm	c_1 mm	c_2 mm	c_3 mm	d_1 mm	d_2 mm	pitch of stirrups mm
1	100	125	25	25	25	10	10	75
2	100	125	25	25	25	10	10	75
3	100	125	25	25	25	10	10	75
4	100	175	38	38	25	10	10	100
5	100	175	38	38	25	10	10	100
6	100	175	38	38	25	10	10	100
7	100	175	38	38	25	10	10	100
13	100	175	38	38	25	10	10	100
9.1	100	175	38	38	25	12	8	100
9.2	100	175	38	38	25	8	8	150
9.3	100	175	38	38	25	8	12	100
10.1	100	175	38	38	25	12	8	120
10.2	100	125	25	25	25	8	8	150
10.3	100	175	38	38	25	8	12	120
11.1	100	125	25	20	*	19	8	190
11.2	100	125	25	25	20	8	8	200
11.3	100	125	20	25	*	8	19	190
12.1	100	125	27	25	20	10	8	190
12.2	100	125	25	25	20	12	12	200
12.3	100	125	25	27	20	8	10	190

Note :

For Frames F9, F10, F11 and F12, three beams were needed, e.g. 9.1 refers to the transom member with the bottom in tension. 9.2 refers to the column section. 9.3 refers to the transom member with the top in tension. The bar diameters are serial numbers not actual diameters (see Table 6.2)

* For 11.1 & 11.3 the cover was variable as the stirrups did not have vertical sides.

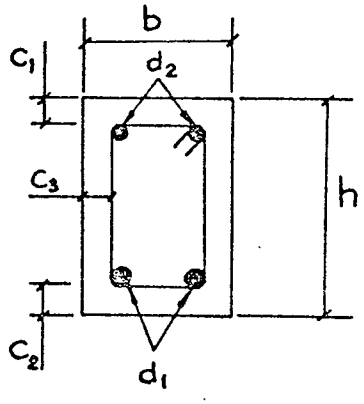

Dimensions in Table

TABLE NO. (6.2)

Properties of the Reinforcement

Bar serial no.	Bar dia. mm	Yield stress N/mm^2	Yield strain x 10^3	Ult. stress N/mm^2	Young's Mod. kN/mm^2
8	8.0	399.0	1.885	535.0	211.5
10	9.8	322.0	1.540	484.0	215.4
12	12.1	307.3	1.487	486.0	206.4
19	19.1	309.0	1.430	475.0	223.0

TABLE NO. (6.3)

Properties of the concrete

Frame test no.	Age of Conc. days	Cube crushing strength N/mm^2	Cylinder crushing strength N/mm^2	Cylinder splitting strength N/mm^2
1	28	46.5	40.8	3.3
2	28	48.0	42.9	3.2
3	28	52.2	41.7	3.4
4	30	46.8	38.0	3.2
5	30	53.8	41.7	3.7
6	30	47.5	36.0	3.3
7	30	48.5	39.5	3.5
13	30	48.5	37.0	3.2
9	36	51.0	43.6	3.2
10	36	50.4	39.0	3.1
11	36	48.0	33.0	3.0
12	36	51.6	34.0	3.0

Note : The modulus of elasticity of the concrete has been taken as $29kN/mm^2$, this is in the light of experimental work carried out on the mix by other investigators in the Department

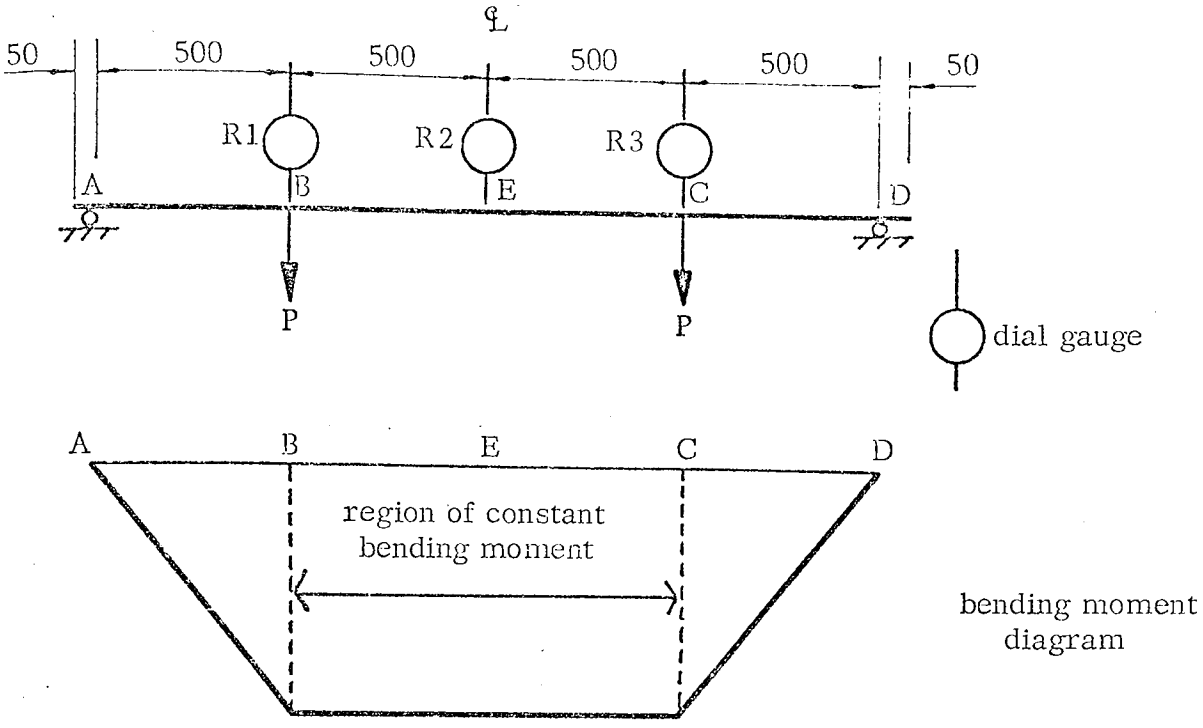

Figure 6.1 The test arrangement and bending moment diagram for a beam test

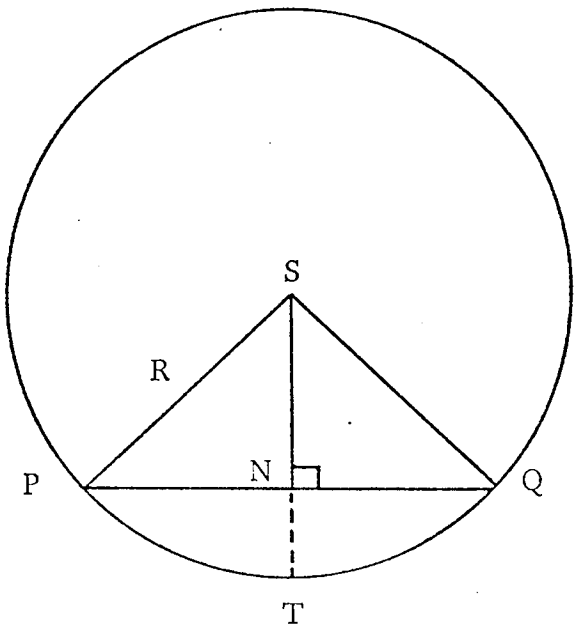

Figure 6.2 Deflected position of a beam

of part of the circle, centre S, radius R shown in fig. 6.2. The centre of the beam deflects to point T, this is relative to the average displacement of the load points which are represented by P and Q on the circle. The curvature 1/R, for each increment of applied bending moment is found in the following way :-

Consider the right angled triangle SNQ in fig. 6.2

By Pythagoras $$(SQ)^2 = (SN)^2 + (NQ)^2 \qquad (6.1)$$

But $$SQ = SN + NT \qquad (6.2)$$

Substituting equation (6.2) in (6.1) we get :

$$(SN)^2 + (NT)^2 + 2(SN)(NT) = (SN)^2 + (NQ)^2 \qquad (6.3)$$

Now NT is small and hence $(NT)^2$ may be neglected, thus,

$$2(SN)(NT) = (NQ)^2$$

Therefore, $$SN = (NQ)^2 / 2(NT) \qquad (6.4)$$

Substituting equation (6.4) in (6.2) gives :

$$SQ = (NQ)^2 / 2(NT) + NT \qquad (6.5)$$

From which if $(NT)^2$ is again neglected we obtain :

$$SQ = (NQ)^2 / 2(NT) \qquad (6.6)$$

Now Curvature $\emptyset$ = $$\frac{1}{R} = \frac{1}{SQ} = \frac{2NT}{(NQ)^2} \qquad (6.7)$$

N.B. NT is the deflection of the beam relative to the average deflection of the load points and is given by :-

$$NT = R2 - (R1 + R3) / 2$$

where, R2 is the central deflection and R1 and R3 are the deflections at the load points.

6.4.3 The curvature of the beam may also be calculated from the state of strain in the section. An equation which relates curvature to the strain at the extreme

compressive fibre in the concrete e_{cc}, the strain at the centroid of the tensile steel e_{st} and the effective depth of the section d may be given by :-

$$\phi = (e_{cc} + e_{st}) / d \qquad (6.8)$$

6.5 The test rig

6.5.1 The test rig used to give the test arrangement detailed in 6.4 will be described here. A similar test bed to that used for the portal frame experiments was utilised for the beam tests. To provide sufficient height for the lever system, the simple support blocks were raised on UC sections. The supports and sections were rigidly clamped to the test bed. Both support rollers were checked for level before each test. A firm level seating of each beam on its simple supports (A)*(B) was required. This was facilitated by gently lowering the beams onto wet plaster of paris which had been spread on a plate, placed on the rollers. The beams were raised and lowered with a fork lift truck. The support detail is shown in fig. 6.3.

6.5.2 For consistency in experimental technique, especially during the application of the load, dead load was again used throughout the test series. The lever system described in 5.5.5 was utilised. In a beam test no sway occurs, so a rigid fulcrum and load transfer system was employed. The levered load was equally applied at both load points (C)(D) via a rectangular hollow section (4" x 4" x $\frac{1}{4}$") spreader beam (F). This beam was 1.1 metres long and was bushed with hardened knife edges, located as shown in fig. 6.4. The point of contact, at load and load transfer points in the beam, was on the same horizontal line. The levered load was transferred through 90^{o} from the lever arm to the spreader beam by the component (E) shown in fig. 6.5. The transfer of load was accomplished by a similar system of plates and rollers to that described in 5.5.5. The load was applied to the top surface of the beam via 25 mm

* letters refer to those on Plate (16)

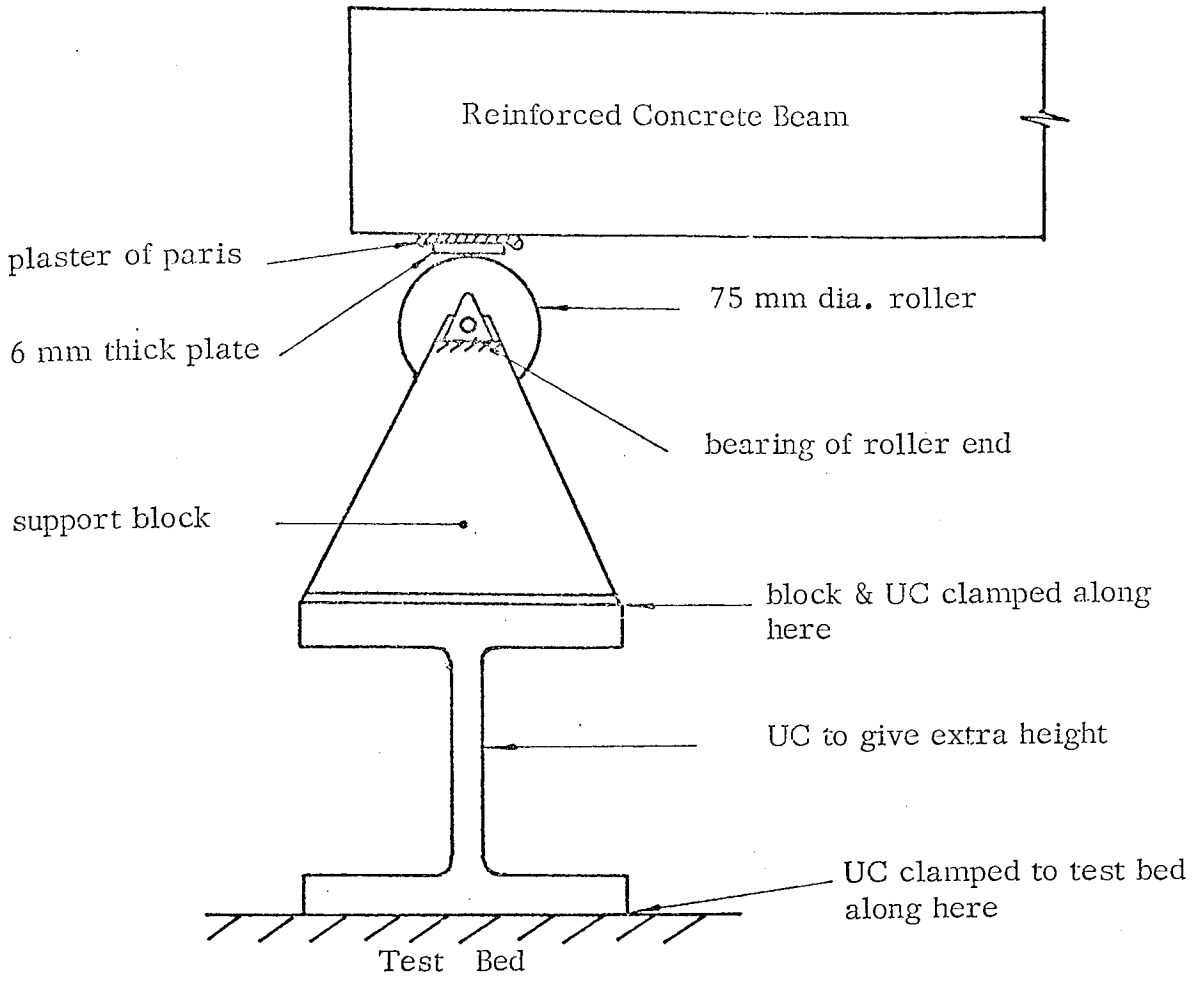

Figure 6.3 Detail of a Simple-Support

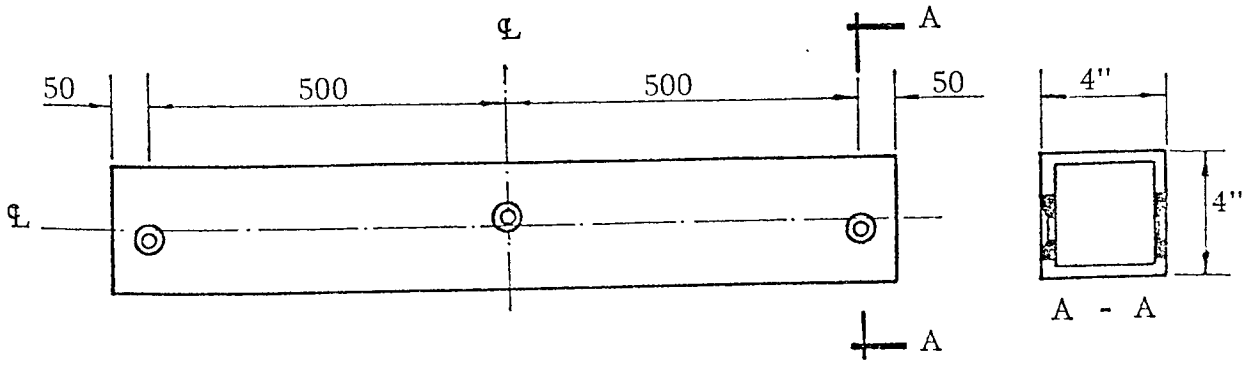

Figure 6.4 Details of Spreader Beam

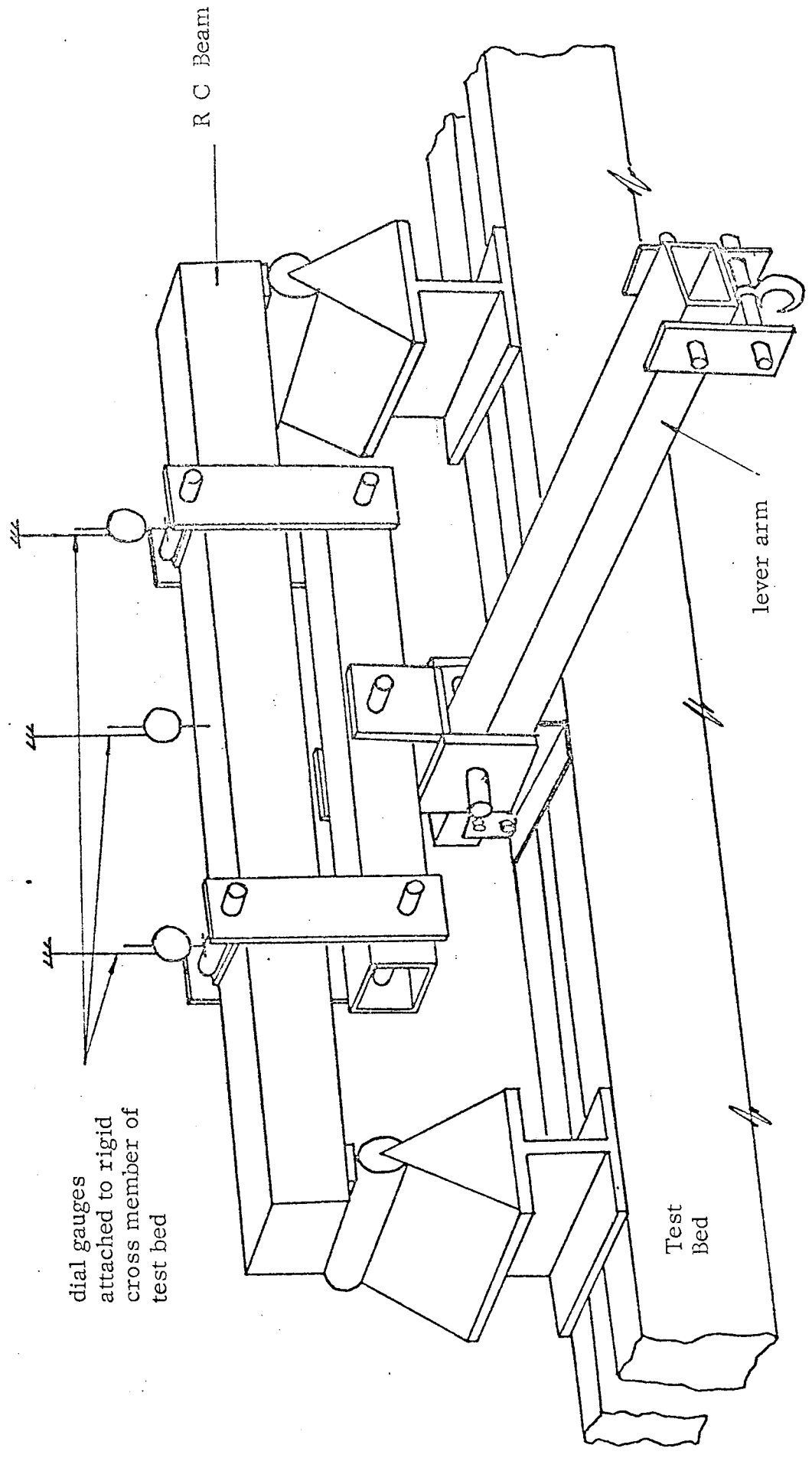

Figure 6.5 Beam Test Apparatus

diameter rollers, seated on 6 mm plates which were bedded in plaster of paris onto the beam. This system gave a uniform application of load. The complete loading system is shown in fig. 6.5 and Plate (16).

6.5.3 Deflection was measured at the centre of the beam and load points by dial gauges (L)(M)(N). These were rigidly fixed to the top cross member of the test bed, and the deflection of the top surface of the beam measured. It would be more accurate to measure the deflection at the centre line of the section. However, this would involve a sophisticated measuring system. For the large radii of curvature anticipated, the accuracy obtained by measuring the deflection of the top of the beam was assumed to be more than satisfactory.

6.6 Test Procedure

Prior to commencement of each test, initial no load readings were taken of the strain gauges with the beam supported along its entire length. These readings enabled zero corrections to be made, for the self weight load induced by the beam and load apparatus. The beam was then located on its supports and the load apparatus applied. The dial gauges were positioned, and when they had settled, initial self weight readings of strain and dial gauges were recorded. To define the initial behaviour fully up to cracking, and through the transition stage to the cracked state of the section, load increments were kept small. Dial and strain gauge readings were measured when the dial gauges had settled to a rate of 0.01 mm/min. During each test, a graph of load vs deflection for the centre of the beam was plotted. This graph described the behaviour of the beam, and by reference to it, the value of subsequent load increments were determined. Larger load increments were added, after the initial stage upto the first yield of tensile reinforcement. Measurements of strain and deflection were taken, again only after sufficient time had been allowed for the dial gauges to settle. This allowed the effects of creep and cracking to take place. After yield, the load

increments were reduced, and measurements were recorded when the gauges had settled to a rate of 0.05 mm/min.

In addition to the above measurements, the extent of the tensile cracking of the concrete was noted. From this, an estimate of the position of the neutral axis at any stage in the loading could be made. From the above measurements, the moment-curvature relationship of a section was found.

6.7 Comparison of measured and theoretical moment-curvature relationships

6.7.1 The results obtained for the moment-curvature relationships of reinforced concrete sections by experiment and theory will be presented and compared. The values used in the theoretical construction of the diagrams will be stated, and comparisons made of the values at the main stages of the moment-curvature relationships, obtained by the methods described in Chapters 2 and 6.

6.7.2 The material properties necessary to construct the moment-curvature relationship of a section, by the theory described in 2.3 are stated in 2.4. The values used in the construction of the M-Ø relationships for the sections of interest in this thesis are given below :-

1) For the tensile strength of concrete, split cylinder tests were carried out for each cast made. The split cylinder strength was used for the tensile strength of concrete for the purpose of calculating the bending moment at which the concrete cracks (see Table 6.3)

2) The short term modulus of elasticity E_c. The average value obtained for the modulus of elasticity for the concrete mix used throughout the series was taken as that obtained from previous and current research work carried out with the mix in the Department (54), for which :-

$$E_c = 29\ 000\ N/mm^2 \qquad (6.9)$$

3) The tensile stress and strain values at yield of steel, the modulus of elasticity of both tensile and compressive reinforcement were taken as the values

obtained from the control tests on the reinforcing bars. The values are quoted in Table 6.2.

4) The increased tensile strength of the steel due to strain hardening was taken as 10% of the yield strength. This was a conservative estimate of the real increase.

5) The ultimate compressive strain of concrete was taken as that quoted in CP110(1). $e_{cu} = 0.0035$ (6.10)

6.7.3 The values of $(EI)_c$, $\emptyset_y$ and $\emptyset_u$ of each of the sections tested can be obtained approximately by drawing the three best straight lines to represent the curve. The slope of these lines will represent the EI values at the three stages in the behaviour. The curvatures at cracking and yield are given by the point of intersection of these lines, and $\emptyset_u$ is given by the curvature at which the concrete begins to crush. To define the moment-curvature relationship of a reinforced concrete section, the flexural rigidity in the cracked state of concrete $(EI)_c$ is of specific interest. The values obtained for this quantity by the equations of 2.3 and by experiment will be compared. In 2.3, the following equations were defined for calculating $(EI)_c$:- $(EI)_c = (-2.5r^2 + 13.9r - 1.1).b.d^3.10^3 kgf\,cm^2$ (6.11)

$$(EI)_c = 0.85\, E_c\, I_e \qquad (6.12)$$

The results obtained for $(EI)_c$ by the above equations and experiment are given in Table 6.4. When more than one experimental result is available for a section, the average result acquired is quoted. From the Table it can be seen that in the majority of cases, the value of $(EI)_c$ is always overestimated with respect to the experimental result, by using equation (6.12). Equation (6.11), however, in most instances gives a truer representation of the experiental value of $(EI)_c$. It is this value which has been used inthe theoretical construction of the moment-curvature relationship.

6.7.4 In 2.3, it was stated that the curvature at first yield of steel in a section may be obtained by either of the following equations :-

$$\emptyset_y = ((M_y - M_c) / (EI)_c) + \emptyset_c \qquad (6.13)$$

TABLE NO. (6.4)

Comparison of the cracked flexural rigidity by experiment and theory

Beam No.	$(EI)_c$ by equation (6.12) $Nmm^2 \times 10^{-10}$	$(EI)_c$ by equation (6.11) $Nmm^2 \times 10^{-10}$	$(EI)_c$ by experiment $Nmm^2 \times 10^{-10}$
1, 2, 3	13.57	12.37	13.10
4, 5, 6, 7, 13	30.00	26.05	25.00
9.1	36.80	34.40	34.10
9.2	20.80	18.50	21.30
9.3	20.80	18.50	18.00
10.1	36.80	34.40	38.00
10.2	10.10	9.34	9.89
10.3	20.80	18.50	18.10
11.2	10.13	9.34	9.02
11.3	10.13	9.34	9.01
12.1	13.50	12.40	12.60
12.2	17.20	14.60	14.40
12.3	9.66	8.90	9.50

N.B. No results are quoted for 11.1 as this section was over-reinforced

$$\phi_y = (e_{cc} + e_{sy}) / d \text{ (by theory)} \qquad (6.14)$$

where the symbols are as defined in Chapter 3. The values obtained for ϕ_y for each section, by both the above equations and from experimental observation are given in Table 6.5. From this Table, it is noticed that generally there is good agreement between both of the theoretical and the experimental values of ϕ_y. The experimental values of curvature at yield are generally higher than those obtained by both the equations. The flexural rigidity in the cracked state and the bending moment at yield are found independently. The curvature at yield has been expressed in terms of these values by equation (6.13), and it is therefore this value which has been used for the theoretical construction of the M-ϕ relationships.

6.7.5 The curvature at the ultimate state is found from the assumed strain diagram of the section at failure. The extreme concrete fibre compressive strain is at its ultimate value of 0.0035, and the neutral axis is assumed to be at the level of the centroid of the compressive reinforcement. The curvature at the ultimate state ϕ_u is found from equation (2.17). The results obtained for ϕ_u by this equation and experimentally are presented in Table 6.6. There is again quite good agreement between the theoretical and experimental values. This indicates that the assumptions made are reasonable.

6.8 Moment-curvature relationships of the sections

The moment-curvature relationships for all the sections used are given in figures (6.6 - 6.15). Each figure gives the curves for both experimental and theoretical relationships. Generally, from these graphs good agreement is seen between the experimental and theoretical curves, the main difference, however, being abrupt changes on the theoretical curve compared with the smooth transitions of the experimental curve. This results in an underestimation of the flexural rigidity throughout these transition regions.

TABLE NO. (6.5)

Comparison of the curvature at yield for experiment and theory

Beam No.	ϕ_y by equation (6.12) $\times 10^6$ 1/mm	ϕ_y by equation (6.13) $\times 10^6$ 1/mm	ϕ_y by experiment $\times 10^6$ 1/mm
1,2,3	27.15	25.80	28.00
4,5,6,7,13	16.80	17.70	18.00
9.1	19.10	18.50	21.00
9.2	17.86	19.90	19.00
9.3	17.81	19.75	20.00
10.1	19.38	18.50	20.00
10.2	29.13	29.00	29.00
10.3	18.20	20.00	19.00
11.2	29.40	29.00	31.00
11.3	28.50	26.70	30.00
12.1	27.90	26.90	28.00
12.2	33.27	27.10	34.00
12.3	29.80	28.90	28.00

N.B. No results are quoted for 11.1 as this section was over-reinforced

TABLE NO. (6.6)

Comparison of the ultimate curvature by experiment and theory

Beam No.	$\emptyset_u$ by theory x 10^6 1/mm	$\emptyset_u$ by experiment x 10^6 1/mm
1, 2, 3	116.0	110.0
4, 5, 6, 7, 13	81.0	90.0
9.1	83.0	80.0
9.2	83.0	78.0
9.3	80.0	74.0
10.1	84.0	91.0
10.2	120.0	90.0
10.3	77.0	100.0
11.2	116.0	101.0
11.3	113.0	128.0
12.1	108.0	108.0
12.2	107.0	108.0
12.3	112.0	125.0

N.B. No results are quoted for 11.1 as this section was over-reinforced

6.8.1 The instantaneous flexural rigidity-curvature diagrams of each section found from experimental and theoretical M-Ø relationships, and used in the analysis of the portal frames tested are given in figures (6.16 - 6.26).

6.9 Conclusions

A comparison has been made between the moment-curvature relationships obtained experimentally and from theoretical consideration of the state of a section at the three main stages upto collapse. The results show good agreement between experiment and theory. The theoretical diagram may be used with confidence to represent the moment-curvature, and hence, the instantaneous flexural rigidity-curvature relationship of a reinforced concrete section. The only deviation from the true behaviour predicted by theoretical consideration is at the transition regions at first cracking of concrete and from first yield of steel to the ultimate condition.

6.10 Tests on reinforced concrete sections subject to axial load

6.10.1 So far in this chapter, the moment-curvature relationships have been found for sections in which no axial loading was present. In 2.7, it was stated that in some structures, heavy axial loading is present in certain members, and its affect on their moment-curvature relationships cannot be overlooked. In this section, the affect of axial load on the properties of the most heavily axially loaded member of the portal frame test series (i.e. lower column of a two storey frame) will be investigated. The maximum magnitude of axial load encountered in these tests was in the region of 40 kN. Two beams of the section used in the two storey frames were manufactured and tested for their moment-curvature relationships. Each beam was subject to constant axial loading of either 40 kN or 20 kN. The latter value of load was used to represent the average value during the complete loading from zero to collapse.

6.10.2 Test Arrangement

With the exception of the axial loading, the test arrangement was identical to that described in 6.4. Axial load was applied at the centre point at each end of the beams. The arrangement is shown schematically in fig. 6.27.

6.10.3 Test Rig

Axial load was applied to the beam via an hydraulic jack/proving ring system (S)**. The reactions to the applied load were provided by the rigid stanchions of the test bed (F)(G). The load was transferred axially to the beam via rollers and radiused end blocks (F)(C), which fitted over the ends of the beams. This arrangement gave a single point of contact from the load apparatus to the beam. The arrangement is shown in fig. 6.28. In all other aspects, the test rig was as described in 6.5. The rig prior to a test is shown in Plate (17).

6.10.4 Test Procedure

With the beam in position on its supports, the axial load was applied. Care was taken to ensure that the load was applied centrally to the beam. The load was maintained constant throughout the test. Initial readings due to the self weight of the beam and transverse loading apparatus were taken of the dial and strain gauges. The test procedure detailed in 6.6 was then followed upto collapse.

6.10.5 In the computation of bending moment for each transverse load, no effect of the eccentricity of the centroid of the axial load with respect to the neutral axis position was taken. It was assumed that for the greater part of the test, the neutral axis remained close to the centroid of the beam.

6.11 Results of axial load tests

The moment-curvature relationships obtained from the above tests are

** letters refer to those used in Plate (17)

compared with the relationship found for the section of F13, with no axial load present. The curves are given in fig. 6.29. From this figure, it is seen that the curves obtained where axial load is present have a larger initial stiffness than for the curve where no axial load is present. This is because the beams which are subjected to axial load have initial compressive forces acting, and tensile forces do not develop so readily. This increase in stiffness is maintained upto the yield of tensile reinforcement. The reserve of strength after yield is not as great for the axially loaded beams when compared with the beam with no axial load. In the case of the beam with the 40 kN load, the moment-curvature relationship shows an increase in strength, the 20 kN loaded beam, however, is marginally stronger than the unloaded beam.

In the test, the column is not subjected to the full 40 kN axial load from start to finish of the loading history, but has an increasing load. The 20 kN curve, therefore, gives a truer picture of its axial load history. The M-ϕ relationships obtained from these tests have been used for the column members in an incremental analysis of frame F13, the results of which are given in the next Chapter.

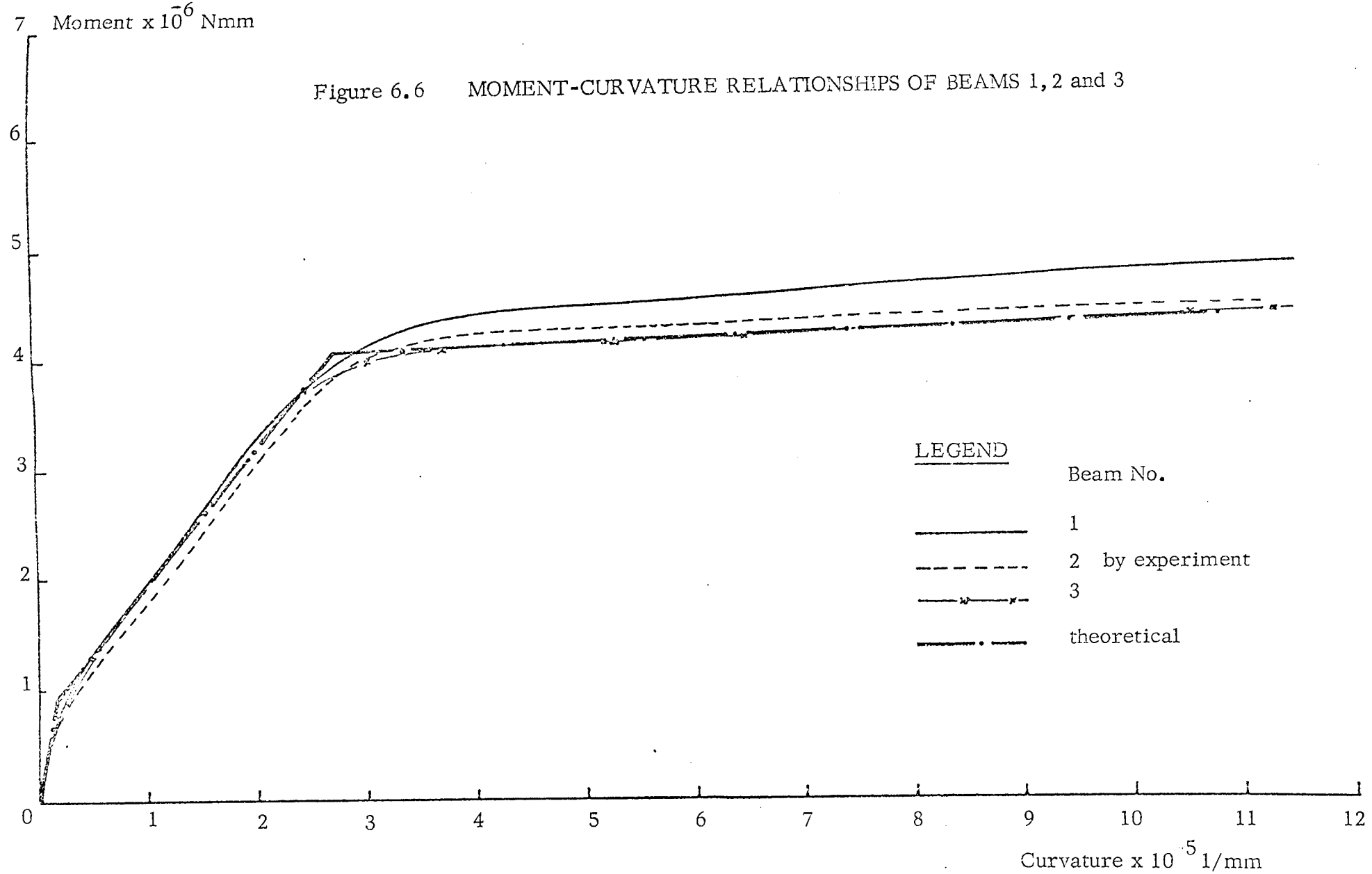

Figure 6.6 MOMENT-CURVATURE RELATIONSHIPS OF BEAMS 1, 2 and 3

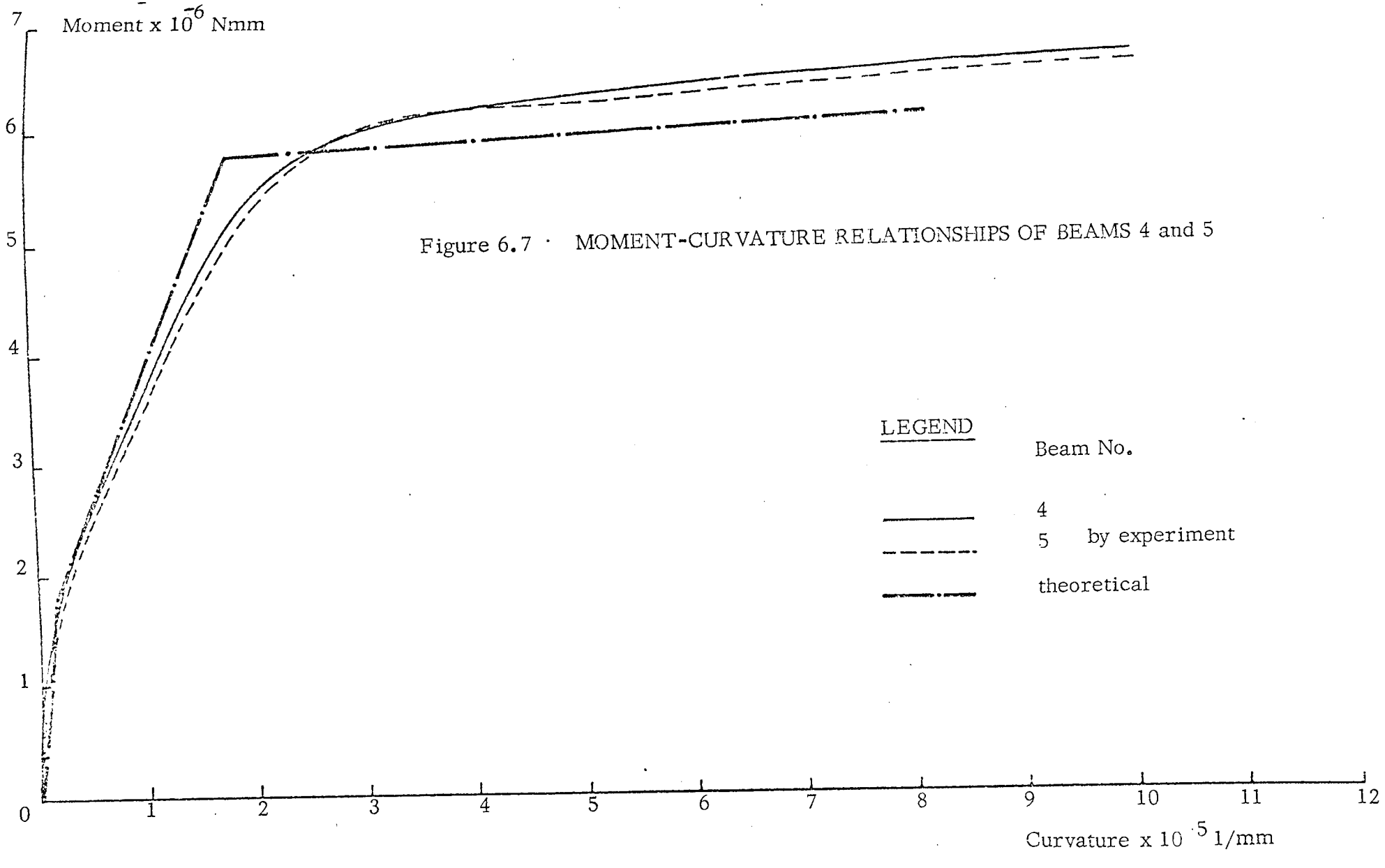

Figure 6.7 · MOMENT-CURVATURE RELATIONSHIPS OF BEAMS 4 and 5

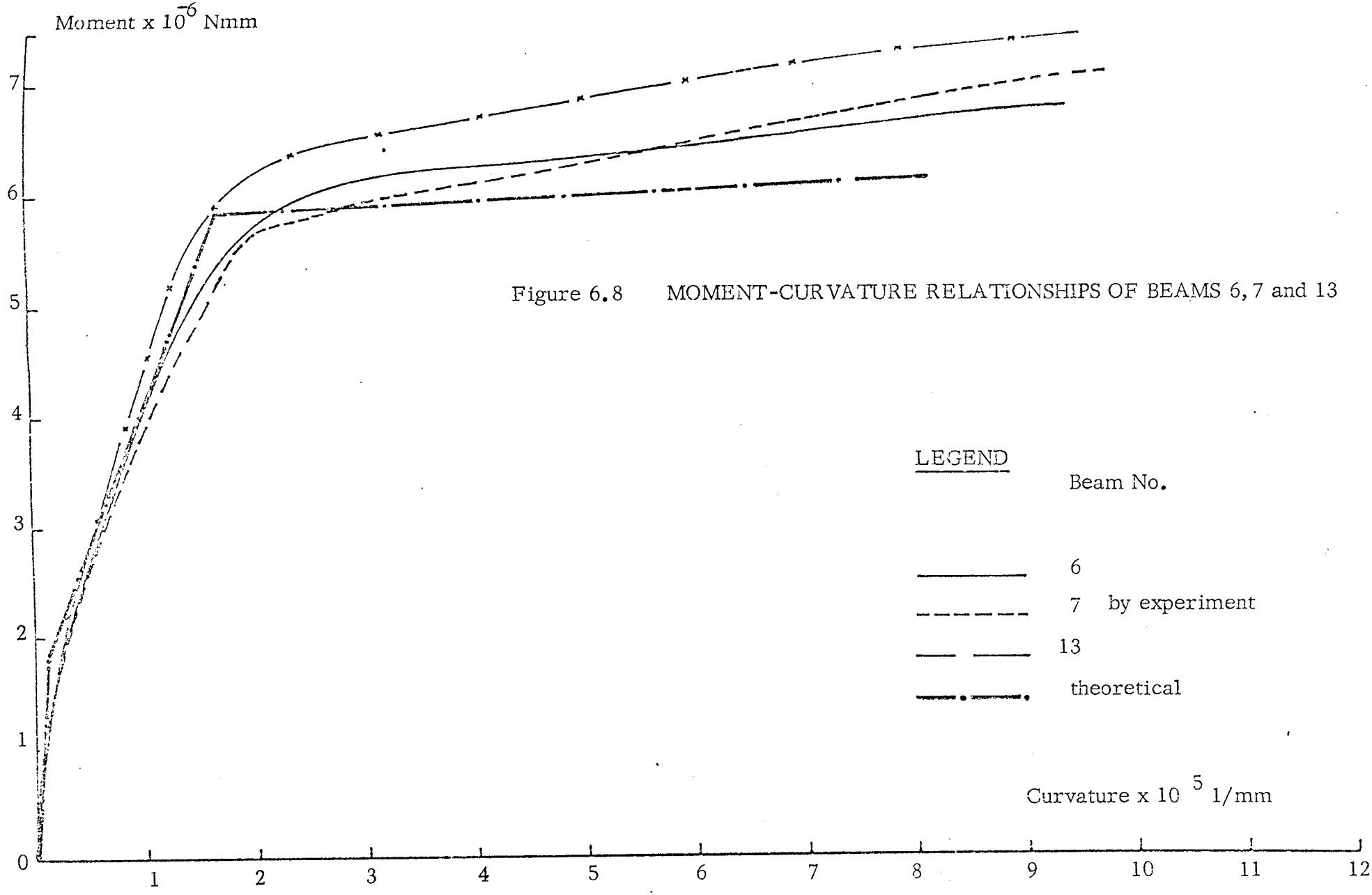

Figure 6.8 MOMENT-CURVATURE RELATIONSHIPS OF BEAMS 6, 7 and 13

Figure 6.9 MOMENT-CURVATURE RELATIONSHIP OF BEAM 9.1

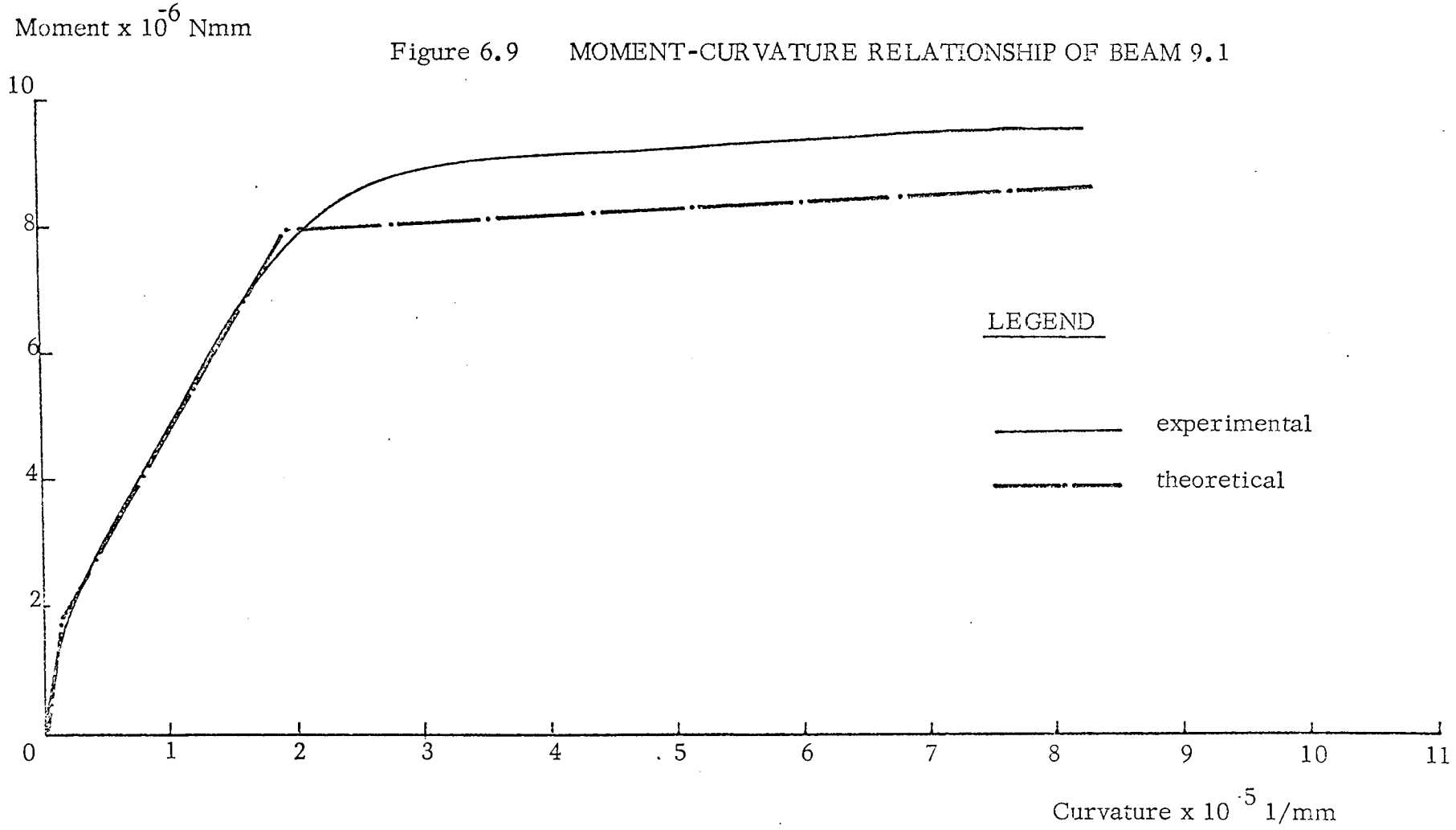

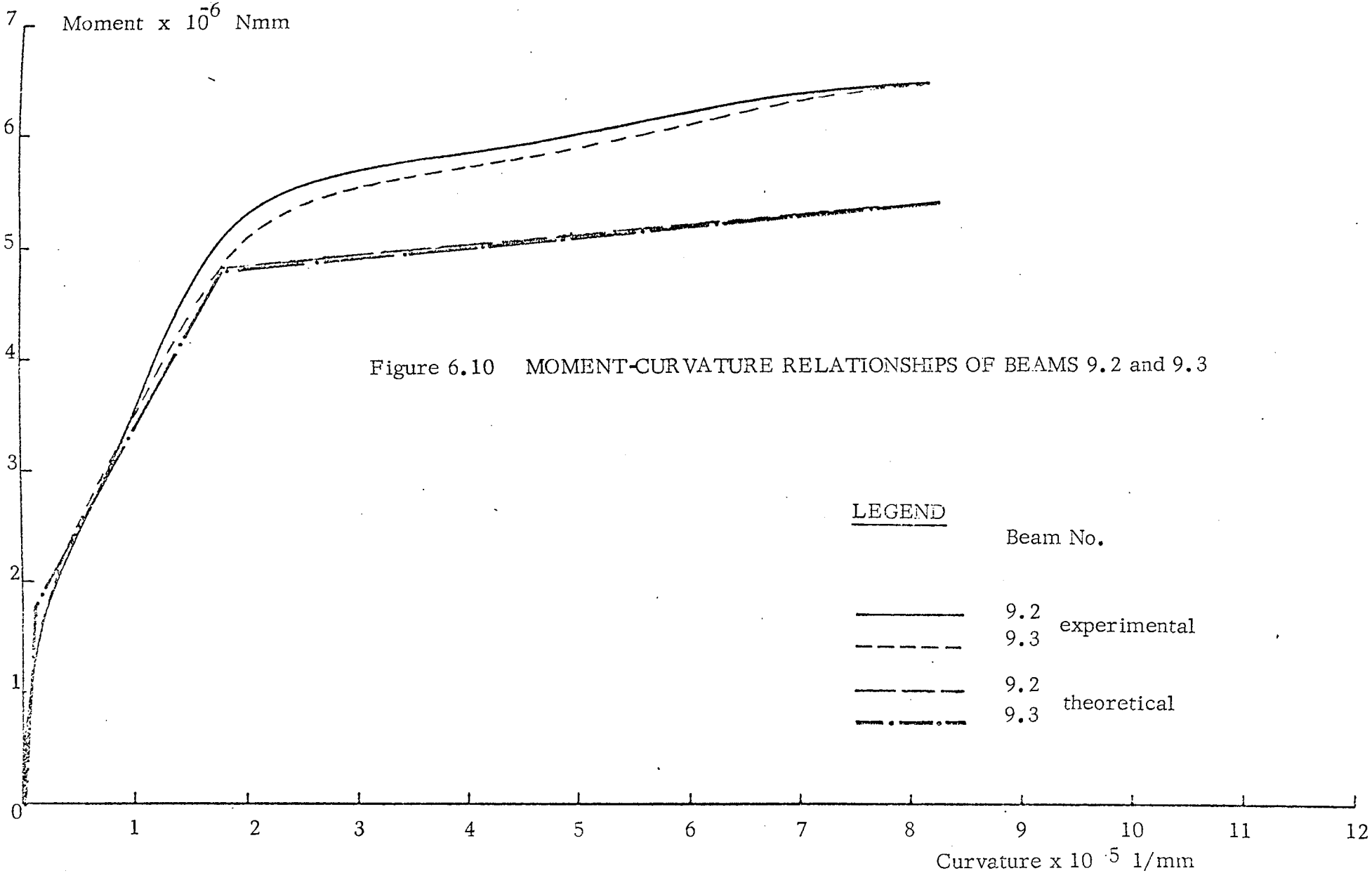

Figure 6.10 MOMENT-CURVATURE RELATIONSHIPS OF BEAMS 9.2 and 9.3

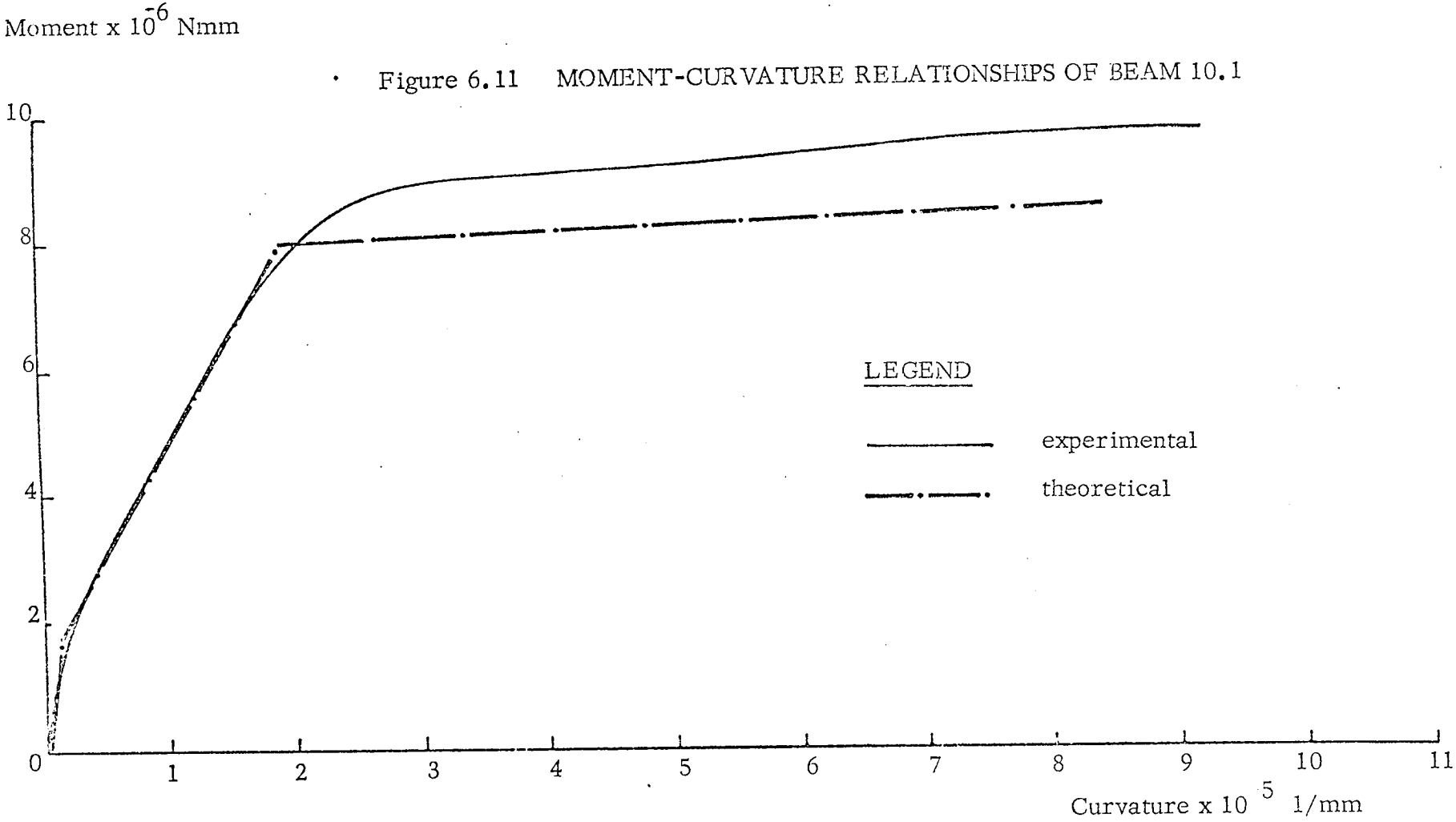

Figure 6.11 MOMENT-CURVATURE RELATIONSHIPS OF BEAM 10.1

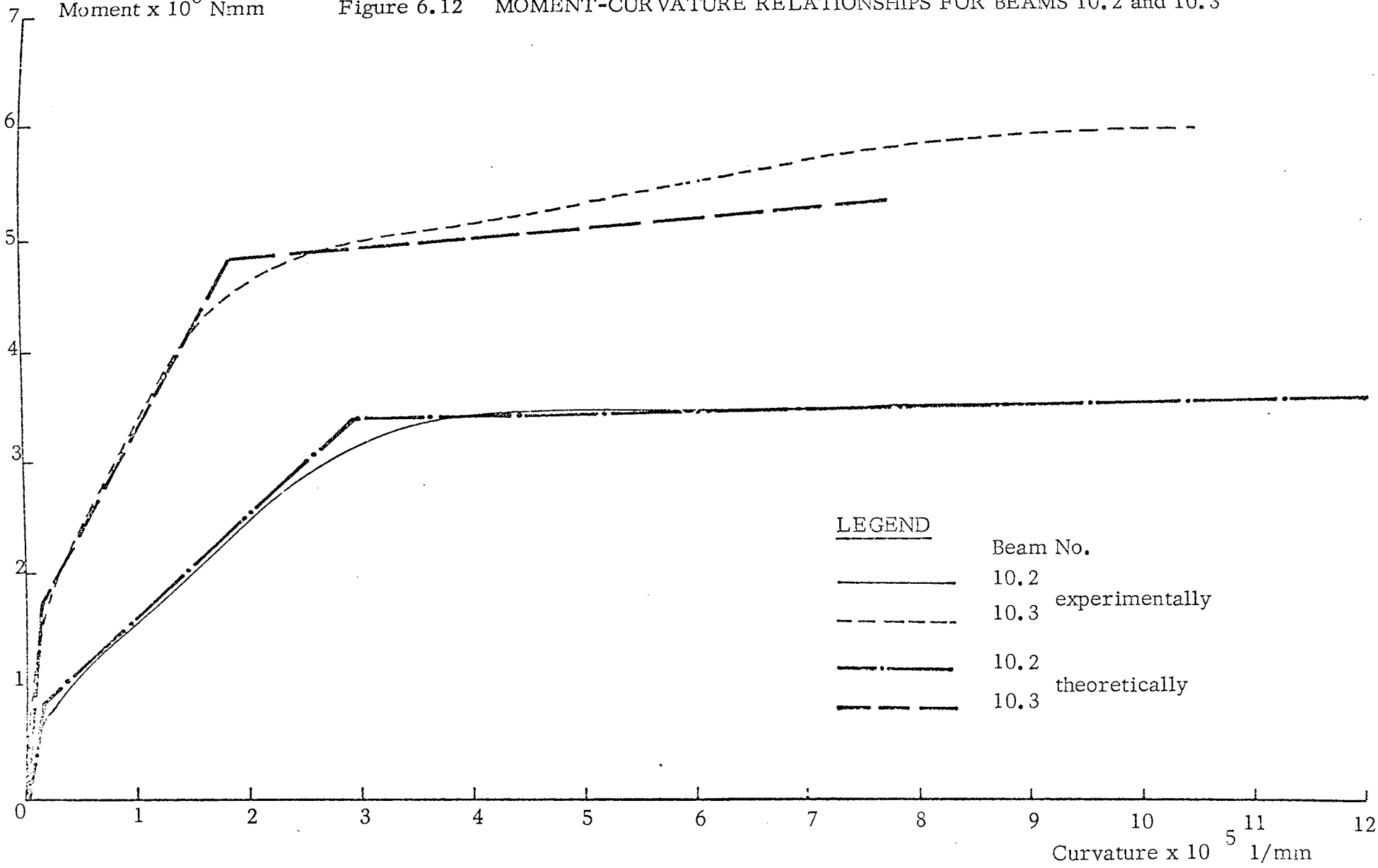

Figure 6.12 MOMENT-CURVATURE RELATIONSHIPS FOR BEAMS 10.2 and 10.3

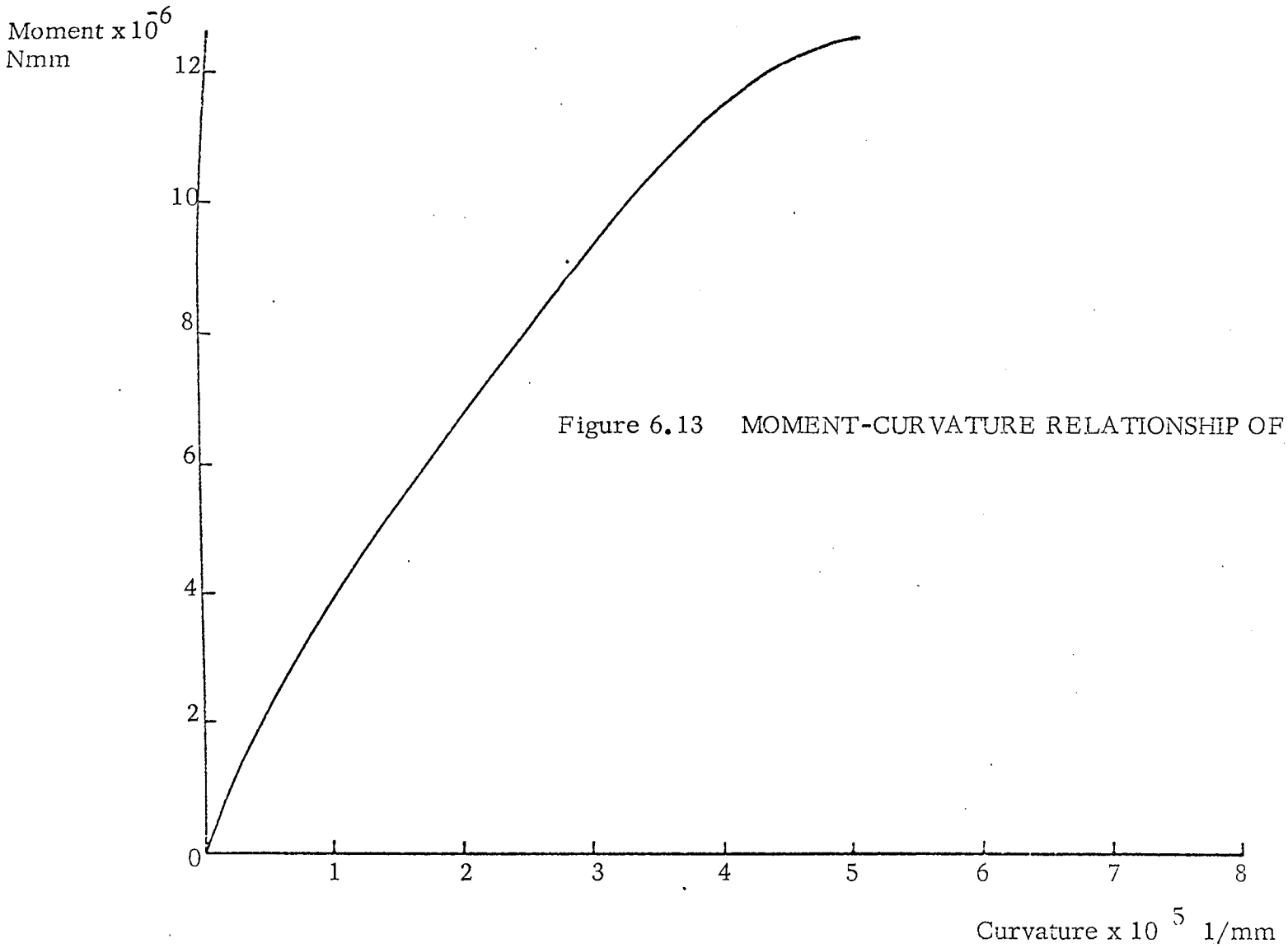

Figure 6.13 MOMENT-CURVATURE RELATIONSHIP OF BEAM 11.1

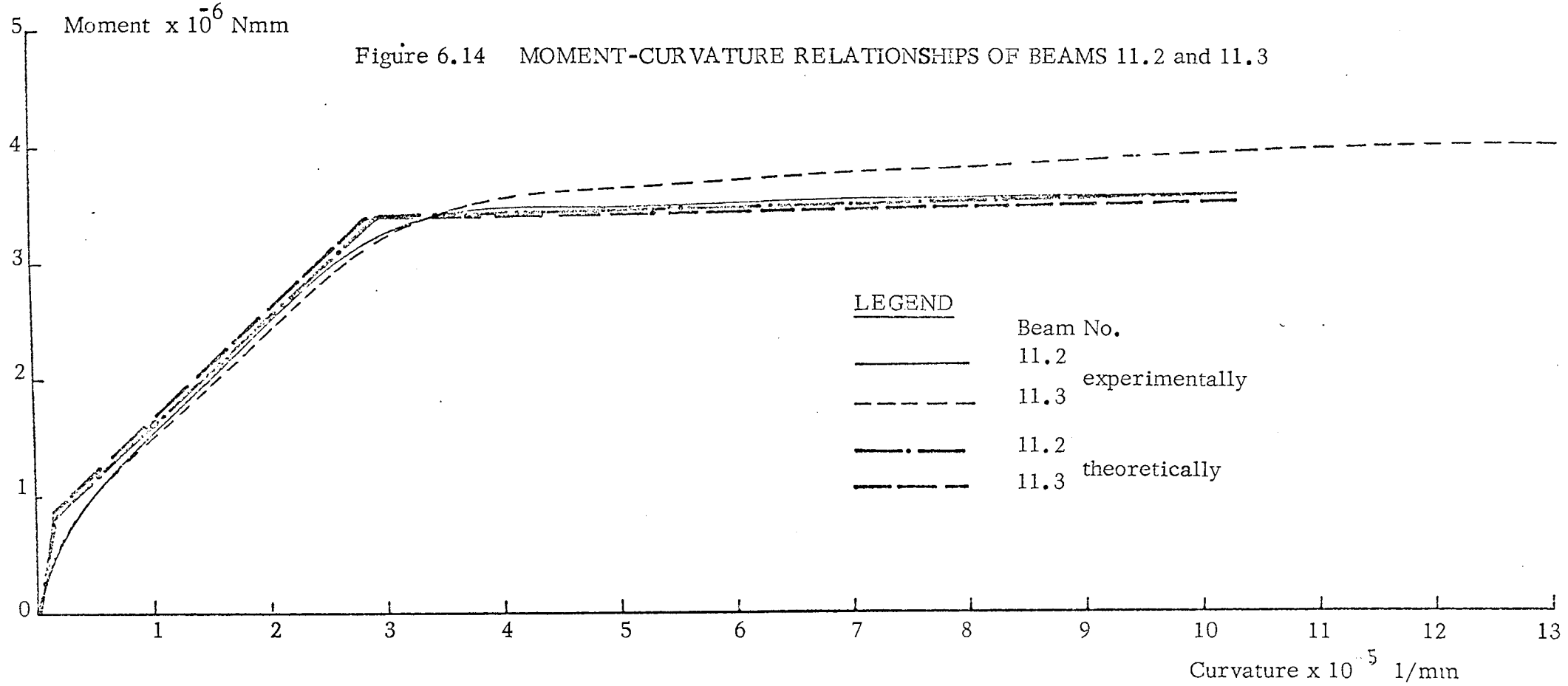

Figure 6.14 MOMENT-CURVATURE RELATIONSHIPS OF BEAMS 11.2 and 11.3

Figure 6.15 MOMENT-CURVATURE RELATIONSHIPS OF BEAMS 12.1, 12.2 and 12.3

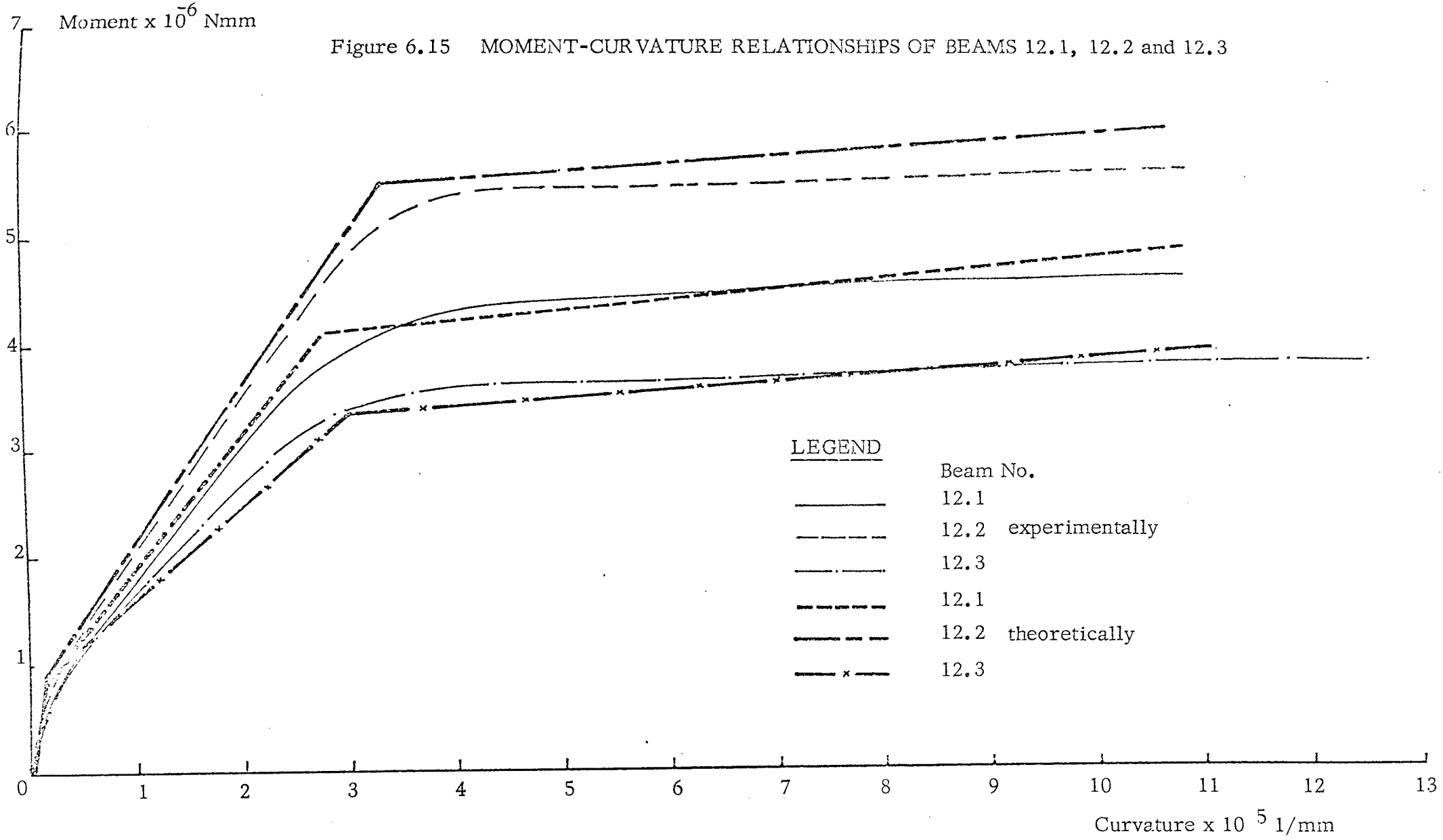

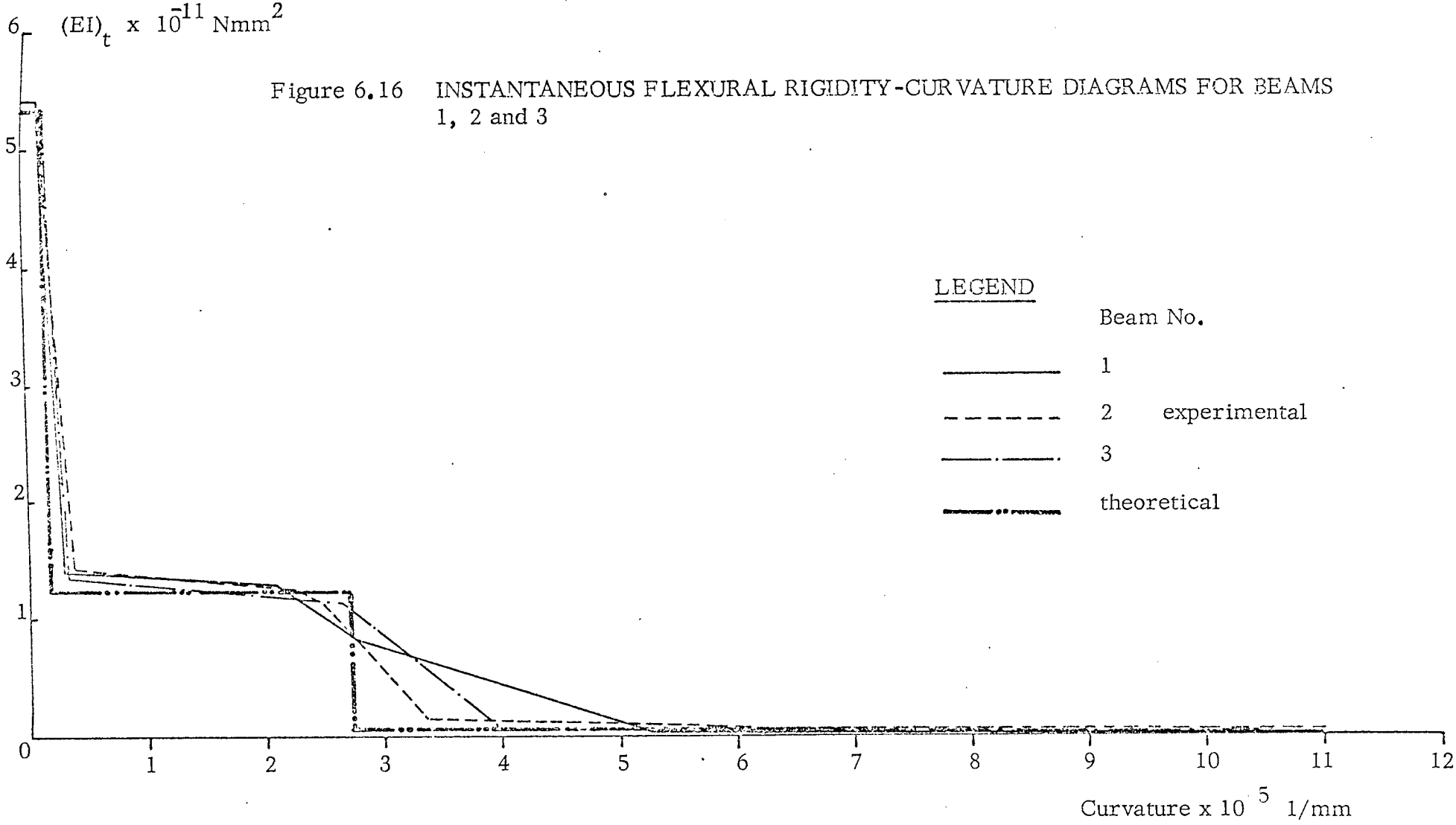

Figure 6.16 INSTANTANEOUS FLEXURAL RIGIDITY-CURVATURE DIAGRAMS FOR BEAMS 1, 2 and 3

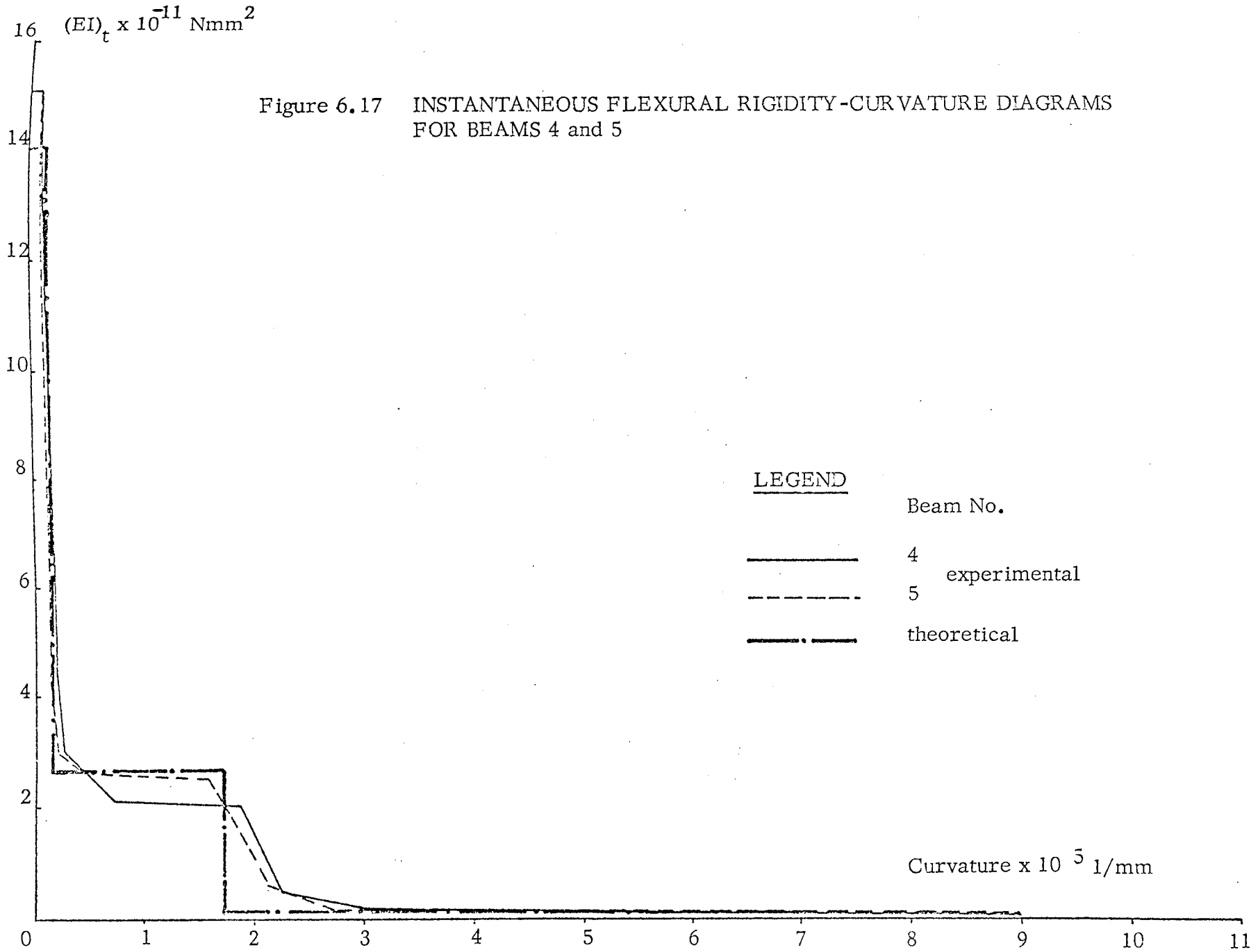

Figure 6.17 INSTANTANEOUS FLEXURAL RIGIDITY-CURVATURE DIAGRAMS FOR BEAMS 4 and 5

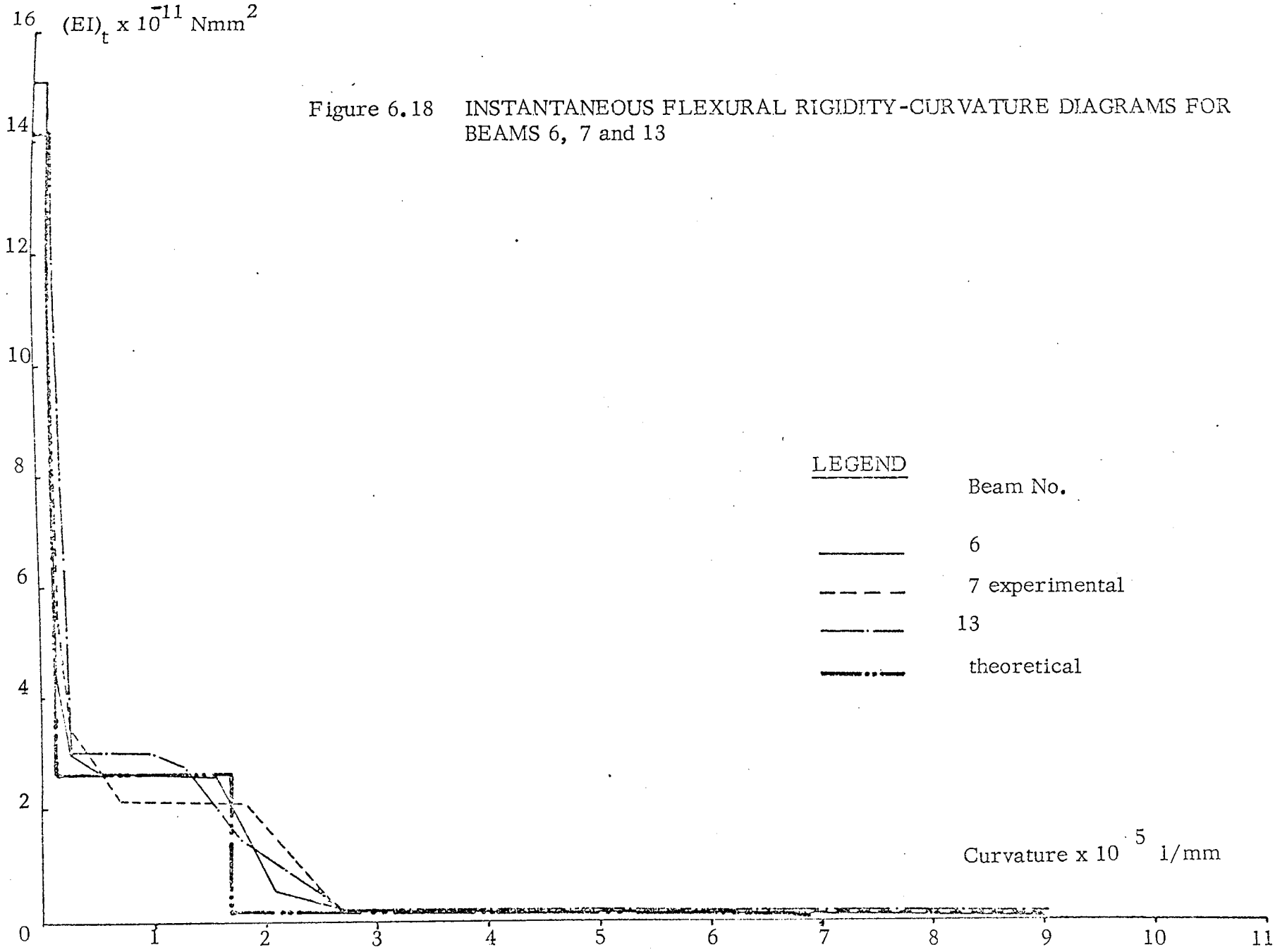

Figure 6.18 INSTANTANEOUS FLEXURAL RIGIDITY-CURVATURE DIAGRAMS FOR BEAMS 6, 7 and 13

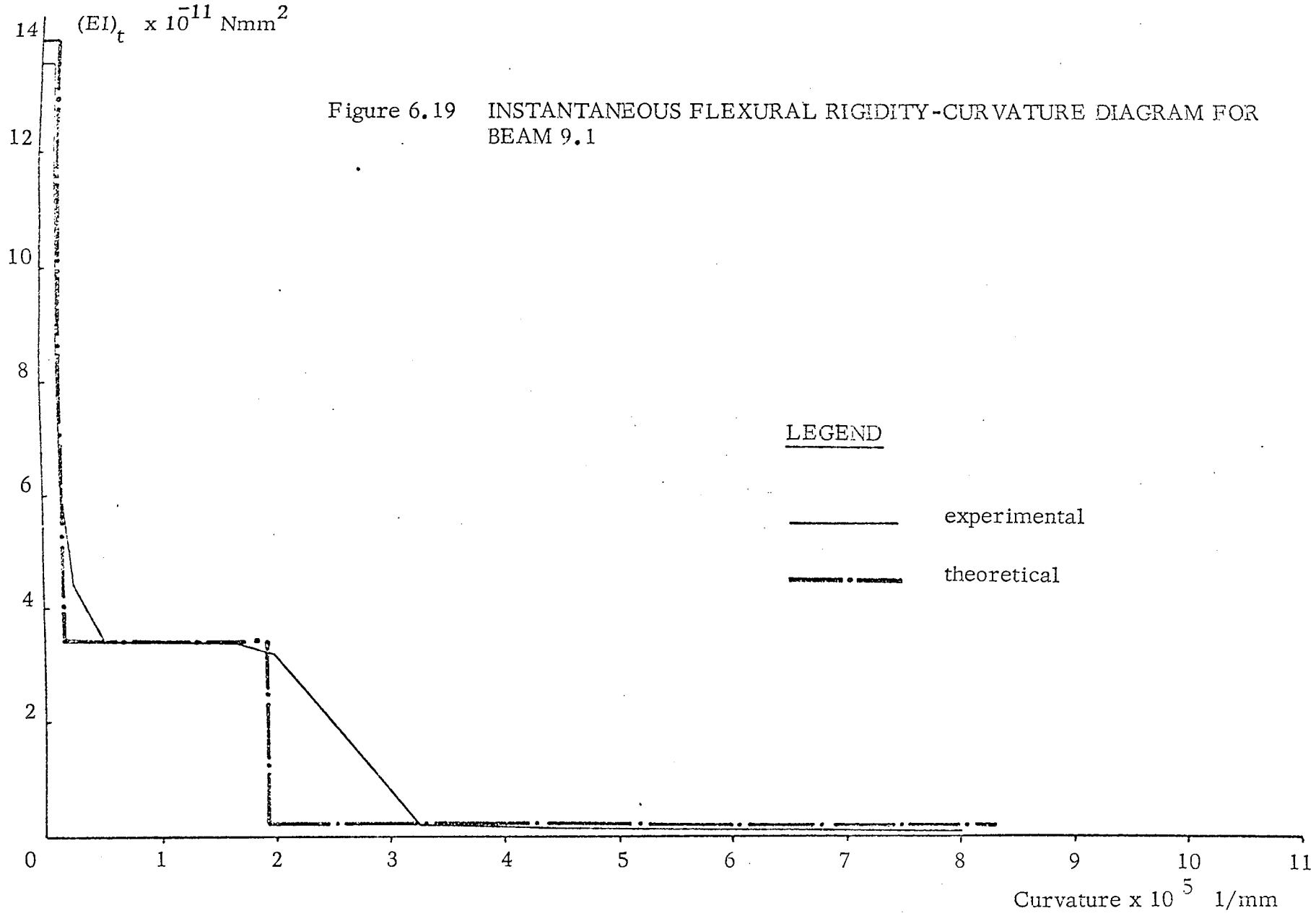

Figure 6.19 INSTANTANEOUS FLEXURAL RIGIDITY-CURVATURE DIAGRAM FOR BEAM 9.1

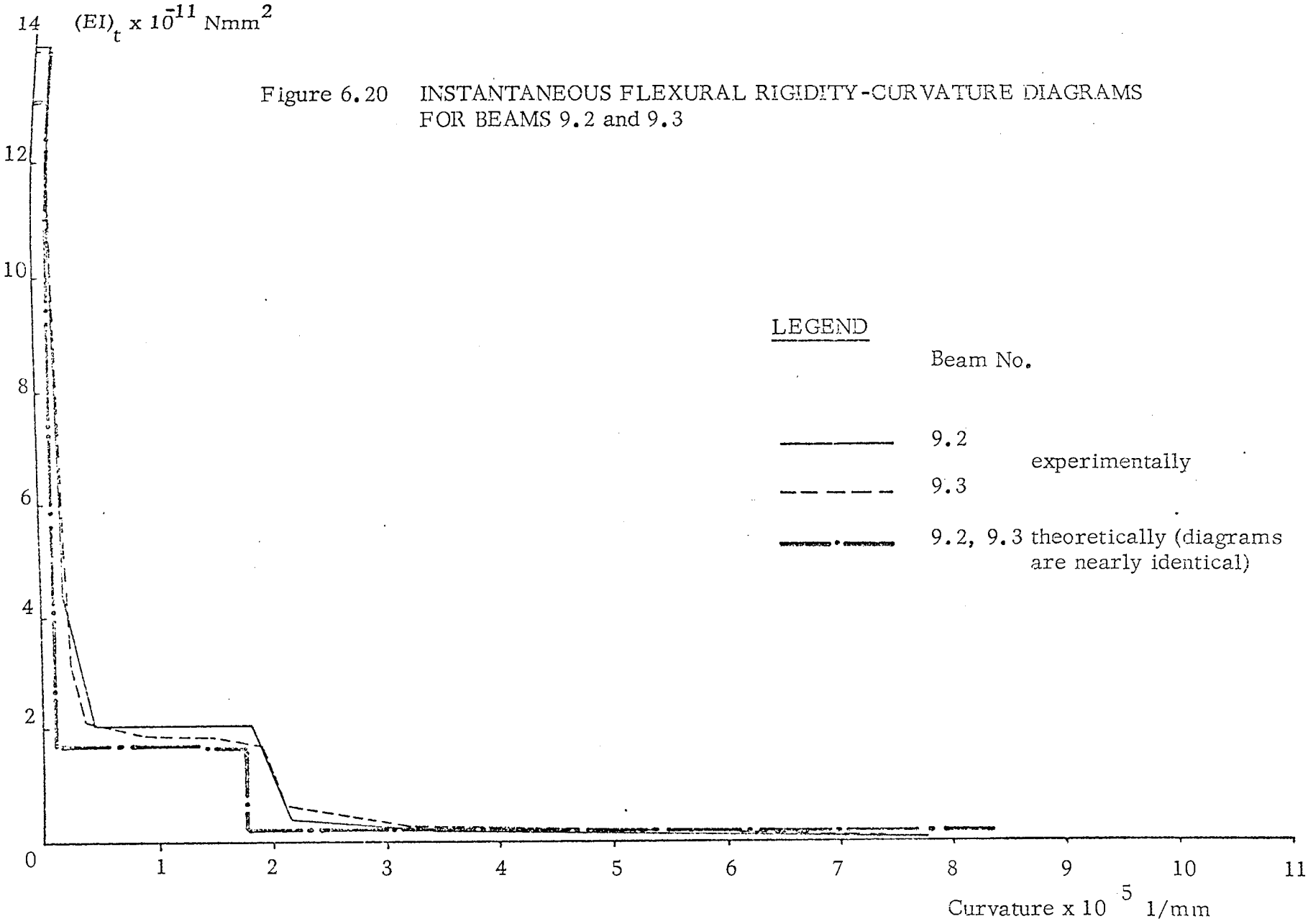

Figure 6.20 INSTANTANEOUS FLEXURAL RIGIDITY-CURVATURE DIAGRAMS FOR BEAMS 9.2 and 9.3

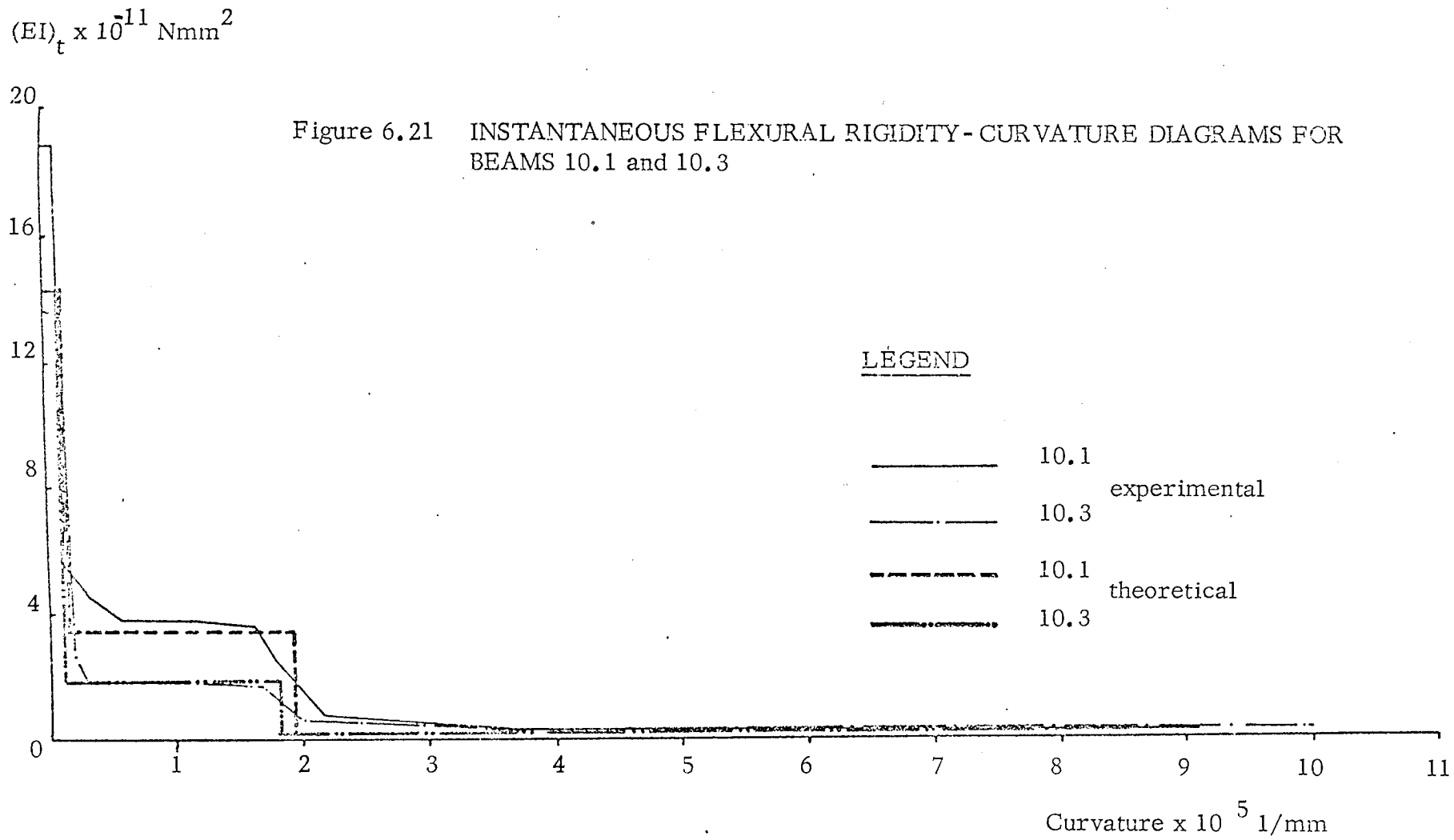

Figure 6.21 INSTANTANEOUS FLEXURAL RIGIDITY - CURVATURE DIAGRAMS FOR BEAMS 10.1 and 10.3

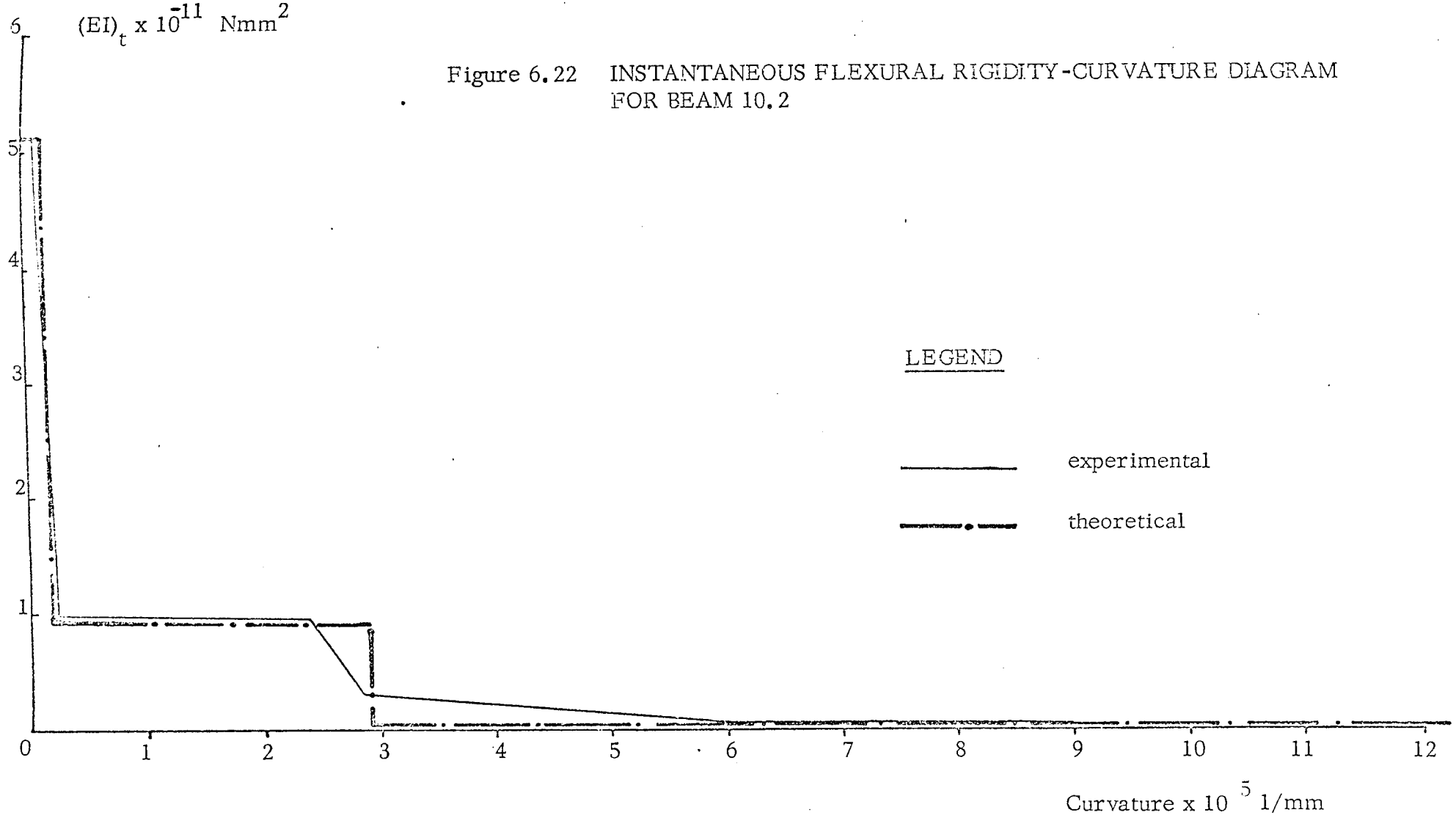

Figure 6.22 INSTANTANEOUS FLEXURAL RIGIDITY-CURVATURE DIAGRAM FOR BEAM 10.2

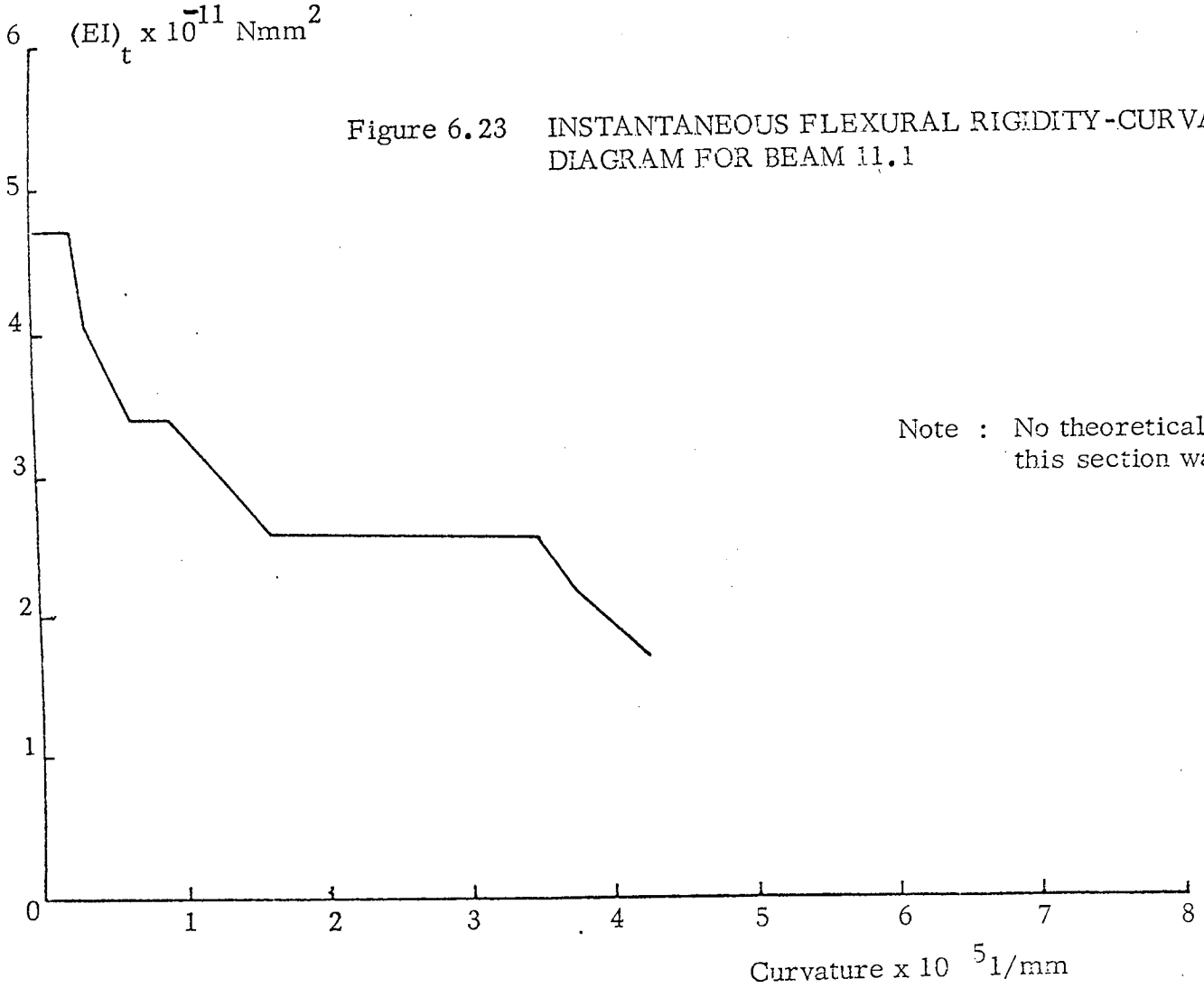

Figure 6.23 INSTANTANEOUS FLEXURAL RIGIDITY-CURVATURE DIAGRAM FOR BEAM 11.1

Note : No theoretical curve is given as this section was over-reinforced

Figure 6.24 INSTANTANEOUS FLEXURAL RIGIDITY-CURVATURE DIAGRAMS FOR BEAMS 11.2 and 11.3

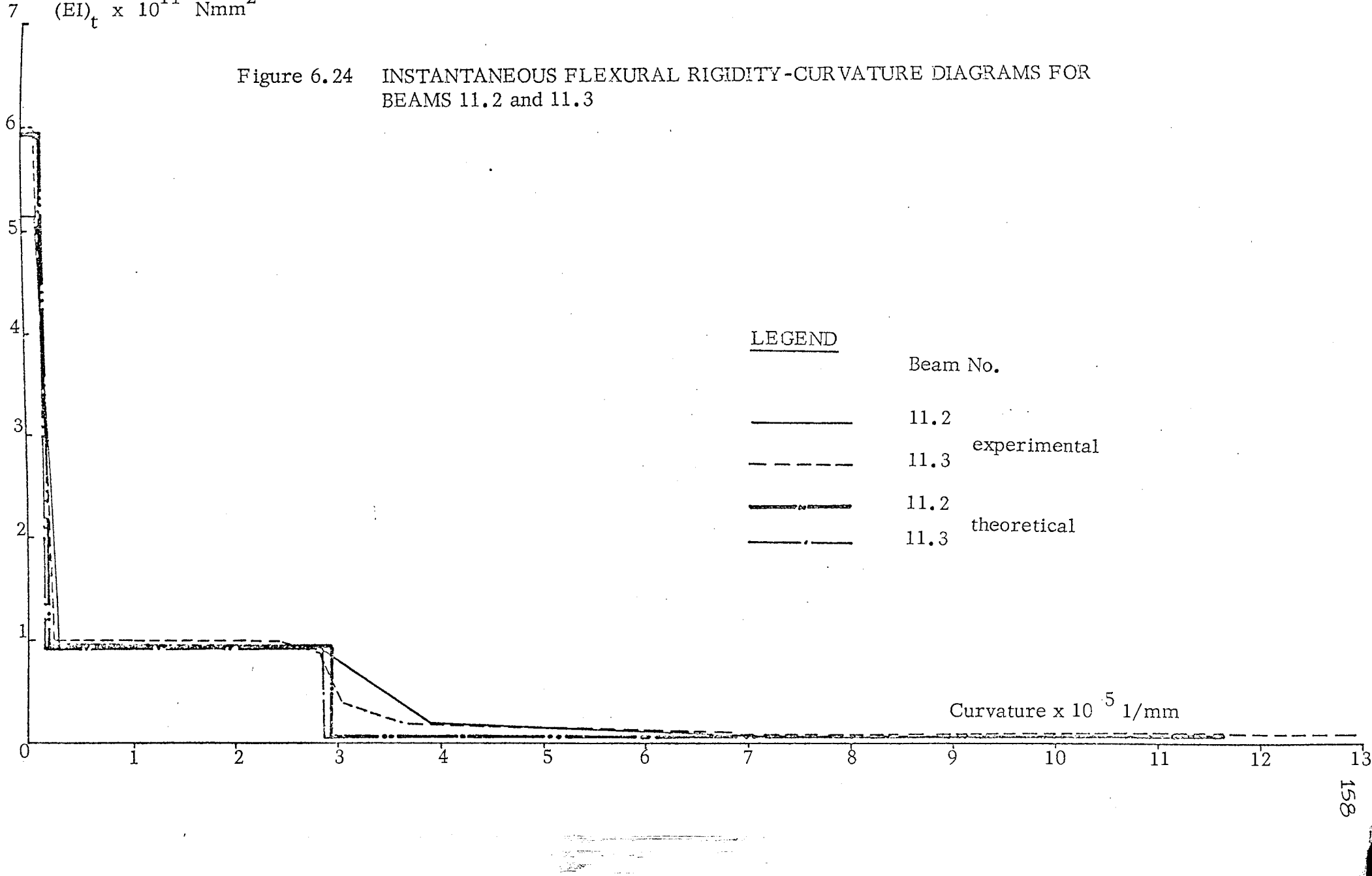

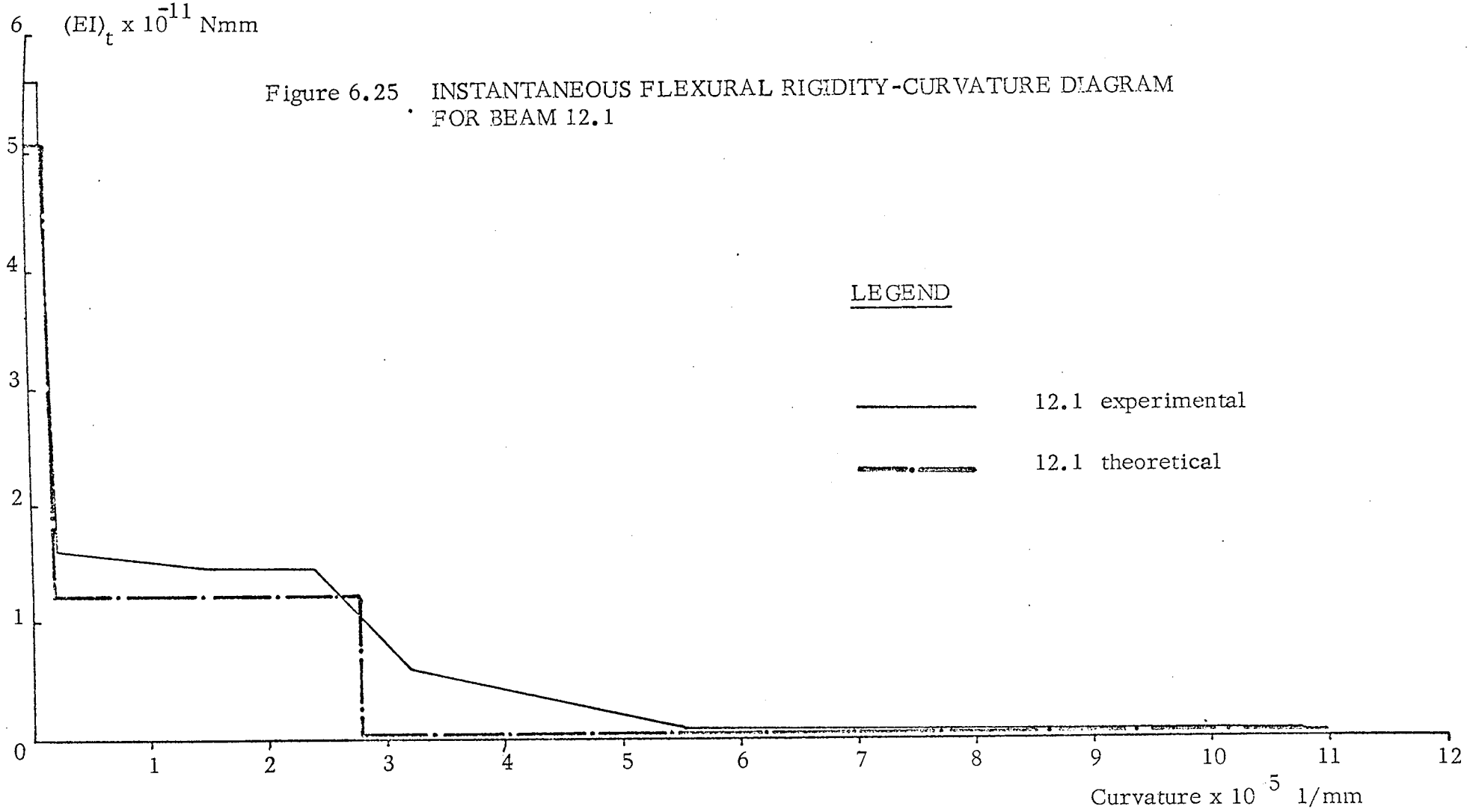

Figure 6.25 INSTANTANEOUS FLEXURAL RIGIDITY-CURVATURE DIAGRAM FOR BEAM 12.1

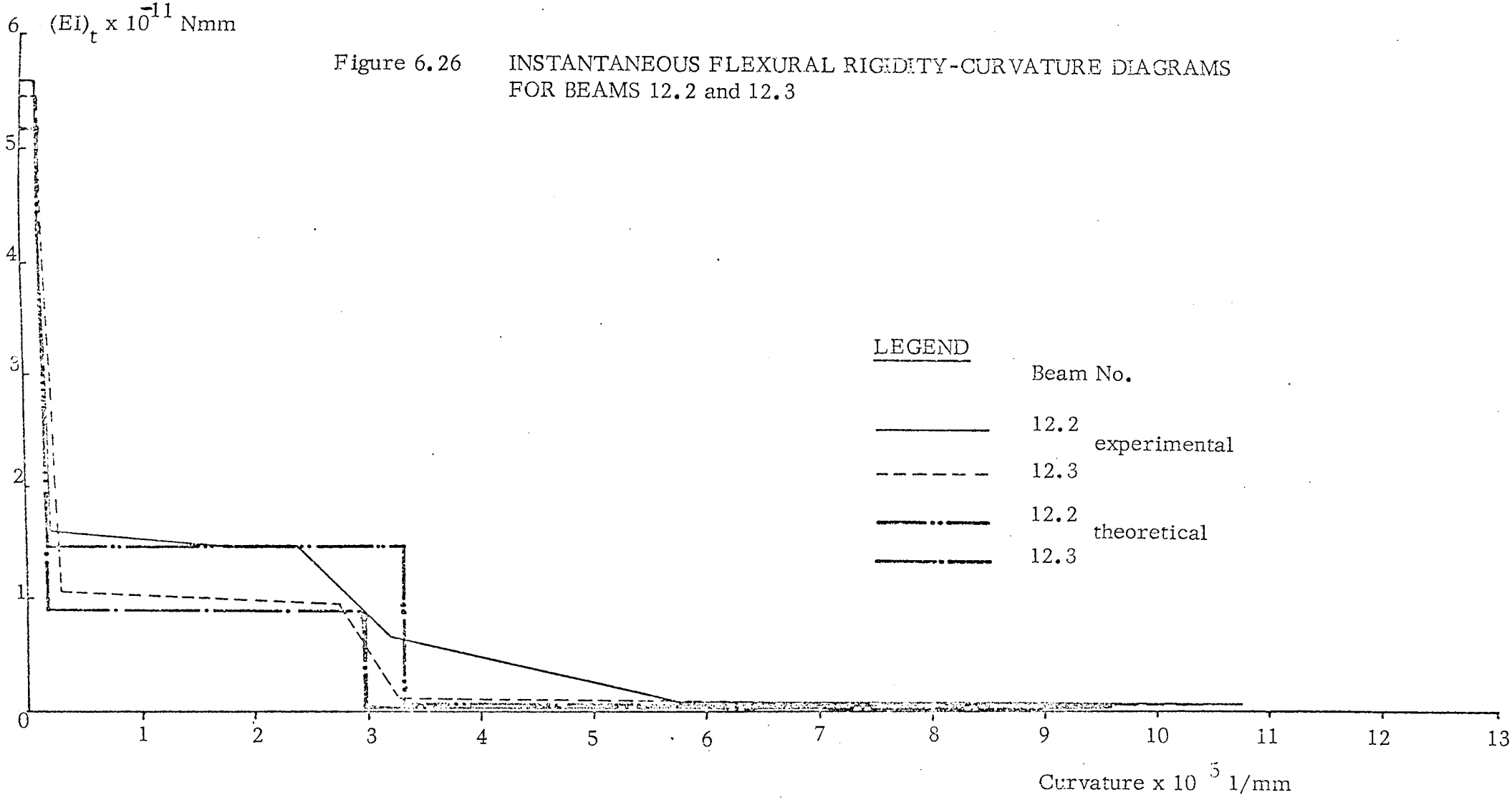

Figure 6.26 INSTANTANEOUS FLEXURAL RIGIDITY-CURVATURE DIAGRAMS FOR BEAMS 12.2 and 12.3

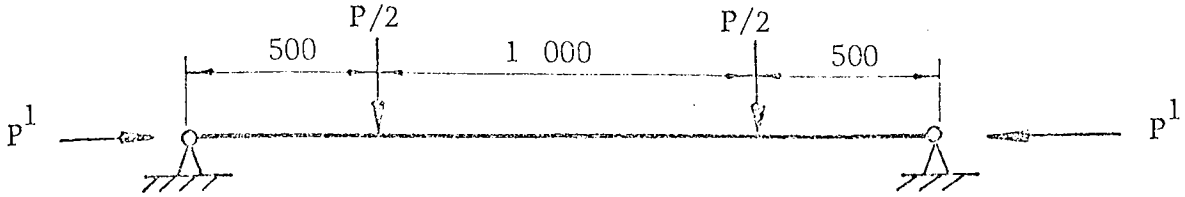

Figure 6.27 Test Arrangement of beam test with axial load

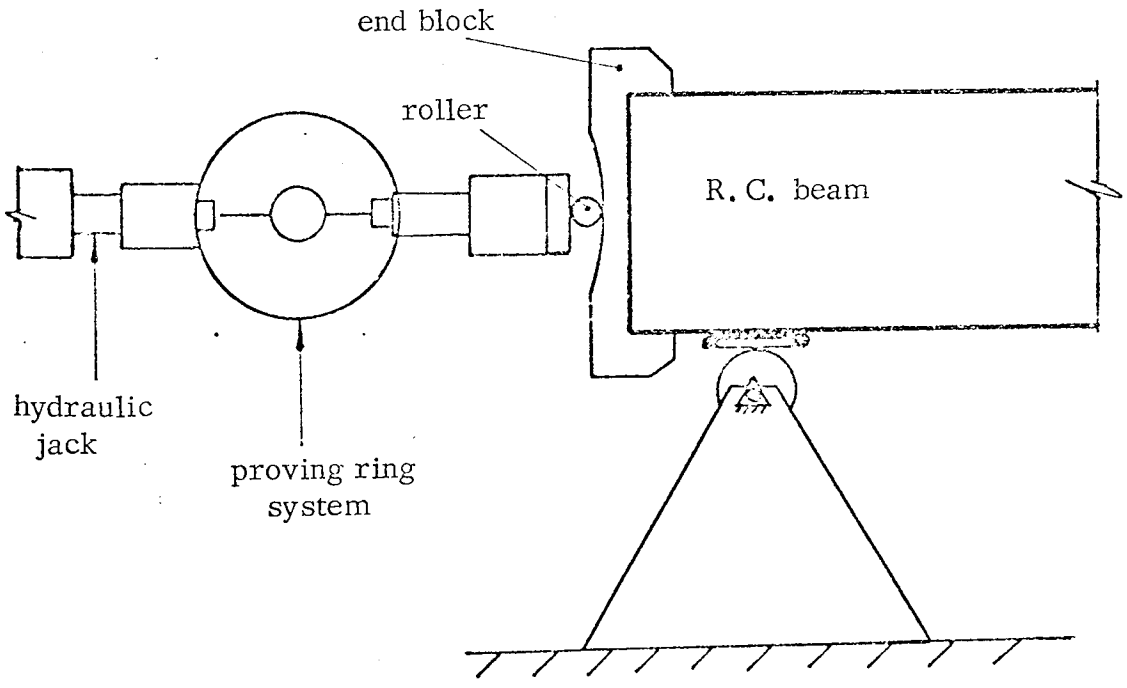

Figure 6.28 Axial load application

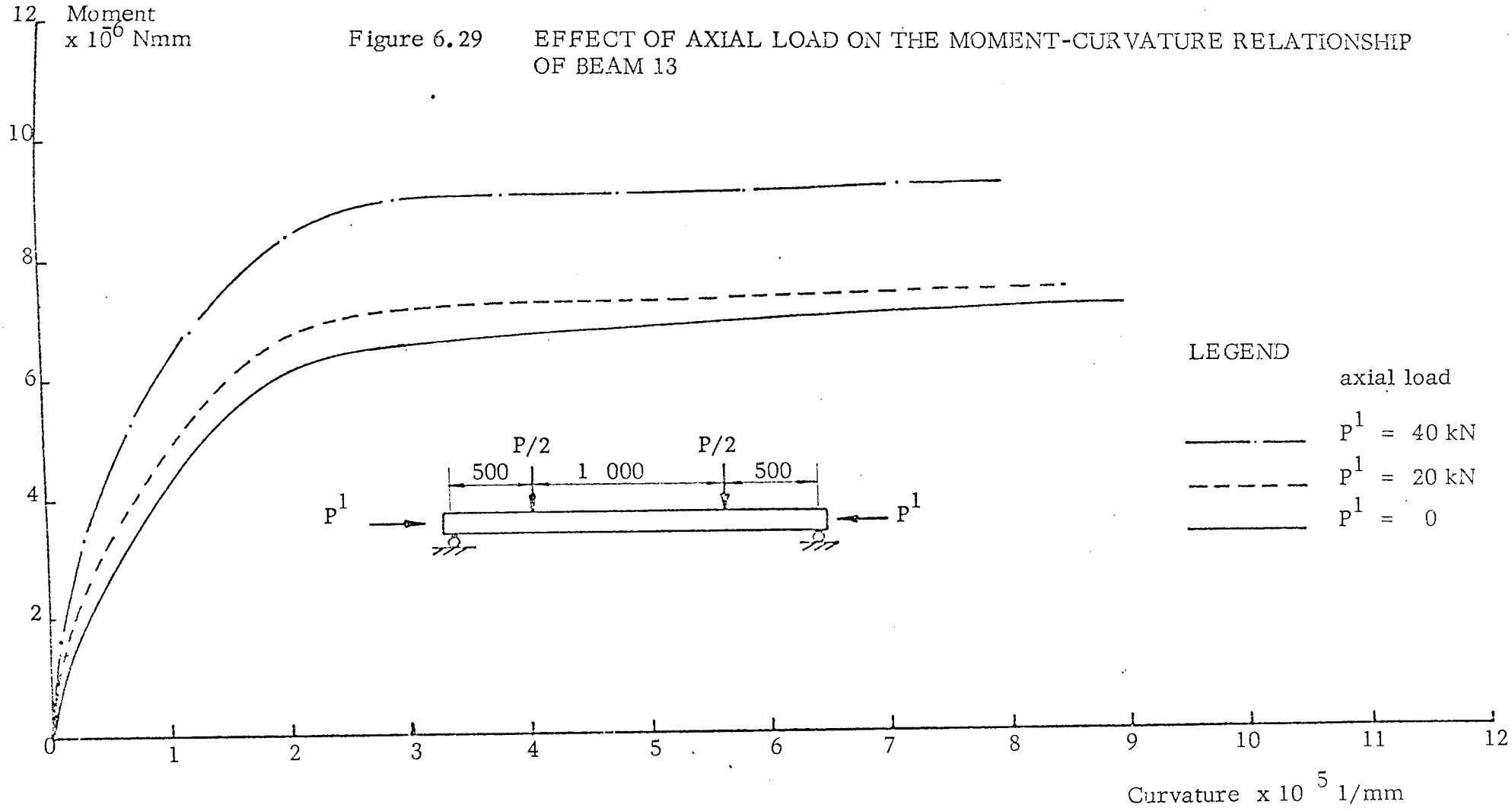

Figure 6.29 EFFECT OF AXIAL LOAD ON THE MOMENT-CURVATURE RELATIONSHIP OF BEAM 13

CHAPTER 7

COMPARISON OF RESULTS AND GENERAL REMARKS

7.1 Introduction

In all, twelve reinforced concrete portal frames were tested, the properties and dimensions of which are given in Chapter 5. These twelve frames are divided into seven different sets. The first set comprises of frames F1, F2 and F3, the second, F4 and F5, the third, F6, F7 and F13, and the final four sets correspond to frames F9, F10, F11 and F12 respectively. Each frame was tested to collapse, and the complete load-deflection history was obtained, together with a photograph of their collapse mode. The results acquired from these tests and the computer analyses of Chapters 3 and 4 together with those predicted by the rigid-plastic theory are presented and compared in this Chapter. This comparison will be of their collapse loads and sway load-deflection curves. The curves obtained for the sway load-deflection of sets 1, 2 and 3 will be compared to assess the variability in their results. The collapse mode of each frame will be compared with that predicted by the rigid-plastic theory. A comparison of the load-deflection curves and collapse loads by experiment, computer analyses and rigid-plastic theory is then made.

7.2 The consistency of the results in sets 1, 2 and 3

7.2.1 The first three sets of the test series each comprised of identical frames. The object of testing these identical frames was to assess the consistency in their overall behaviour. The results of these tests are presented in graphical form by their load-deflection curves under sway loading, and also, in tabular form (Table 7.1) where the collapse loads are reported. Each set will be dealt with separately.

TABLE NO. (7.1)

Comparison of collapse loads in the first three sets

Set No.	Frame No.	Collapse load W (kN)	% Difference in range of collapse loads
1	F1	4.52	3.1%
	F2	4.38	
	F3	4.39	
2	F4	4.76	4.5%
	F5	4.55	
3	F6	7.47	1.5%
	F7	7.36	
	F13	7.38	

7.2.2 Set 1 (F1, F2 and F3)

The sway load-deflection curves obtained for the tests on these frames are shown in fig. 7.1, from which a good agreement can be seen between the curves. The frame F1 was stiffer in the elasto-plasto and plastic stages of the curve. In Table 7.1, the difference in the values of collapse loads obtained is shown to be 3.1%. This indicates that the collapse loads are also in good agreement. The differences in the collapse loads and the deflection response at a load of 4 kN (see fig. 7.1) may be attributed to the variation in the properties of the reinforcement and concrete. Experimental errors incurred in the transfer of load from the lever system and possibly a restriction to the travel of the dial gauges or movement of their support frame may also have contributed to the slight differences recorded.

Figure 7.1 SWAY LOAD DEFLECTION CURVES FOR FIRST SET (FRAMES F1; F2; F3) BY EXPERIMENT

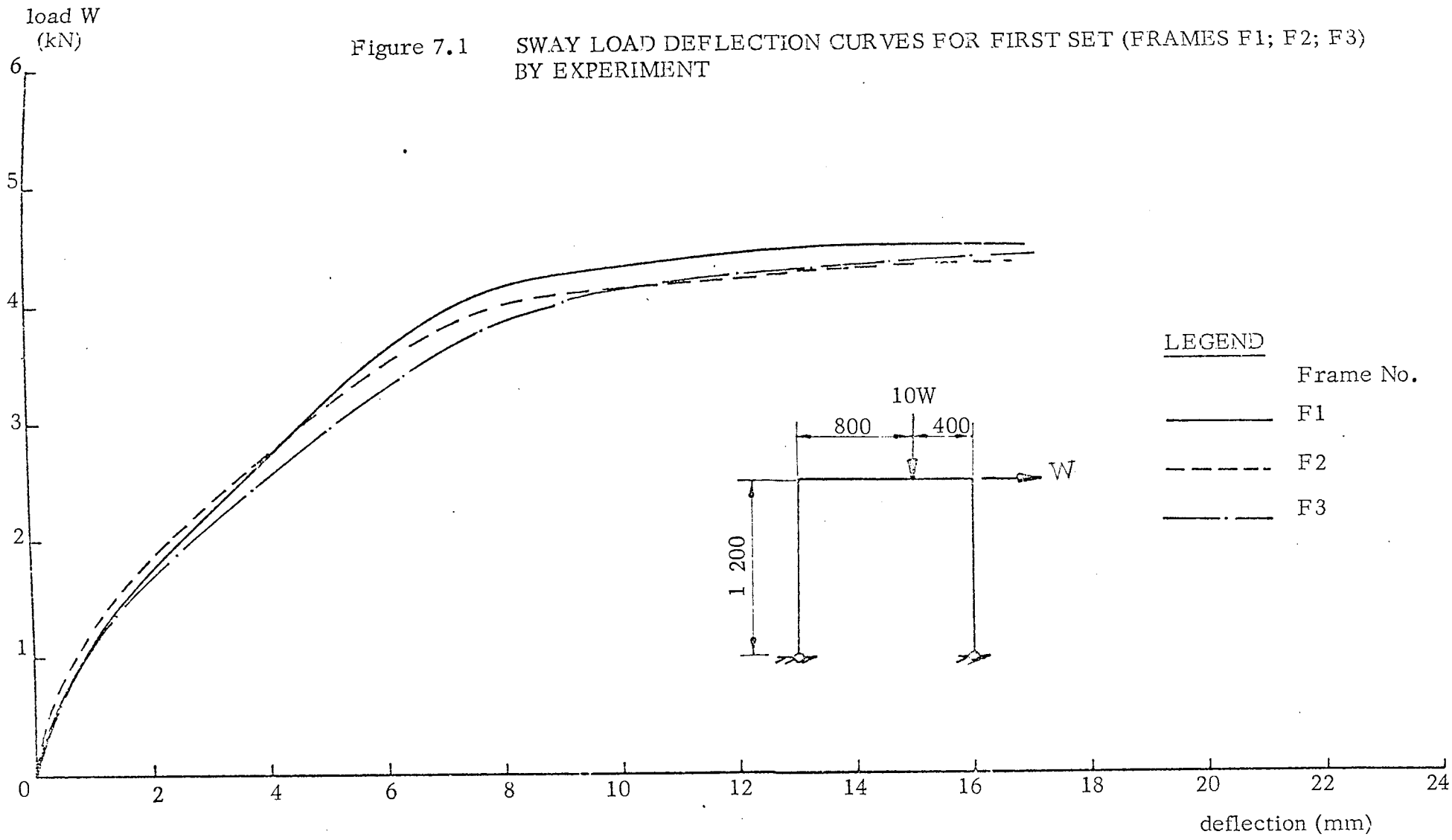

7.2.3 Set 2 (F4, F5)

The curves for this set are given in fig. 7.2, where a good agreement can again be seen between the curves. The percentage difference in the collapse loads of this set is 4.5%. Frame F4 shows a slightly greater stiffness throughout its loading history. The difference in results may again be attributed to the causes stated in section 7.2.2

7.2.4 Set 3 (F6, F7 and F13)

Set 3 comprises of three two-storey portal frames, the load-deflection curves under sway loading are given in fig. 7.3. In Table 7.1, the difference in collapse loads is given as 1.5%. From this, and fig. 7.3, a very close agreement between the results obtained for the frames in this set is shown.

7.2.5 From the results and comparisons made above, it may be assumed that there is no signficant variation between individual tests on the frames reported. Individual tests may, therefore, be used to represent the behaviour of a particular frame with a good degree of accuracy, provided care is taken to ensure reasonably constant conditions of manufacture.

7.3 Description of experimental results with particular regard to their failure modes

7.3.1 Utilising the ultimate bending moment values obtained by the beam tests of Chapter 6, for the sections used in the frames, the failure mechanisms and collapse loads for each frame have been found theoretically by the rigid-plastic theory. The calculations of the collapse loads for the various failure mechanisms are given in Appendix (2). These collapse loads, together with the values of ultimate bending moment, M_u, of each section of the frame are reported in Table 7.2. Also in this Table, the difference between the values of collapse loads obtained experimentally and by the rigid-plastic theory are

Figure 7.2 SWAY LOAD DEFLECTION CURVES FOR SECOND SET (FRAMES F4; F5) BY EXPERIMENT

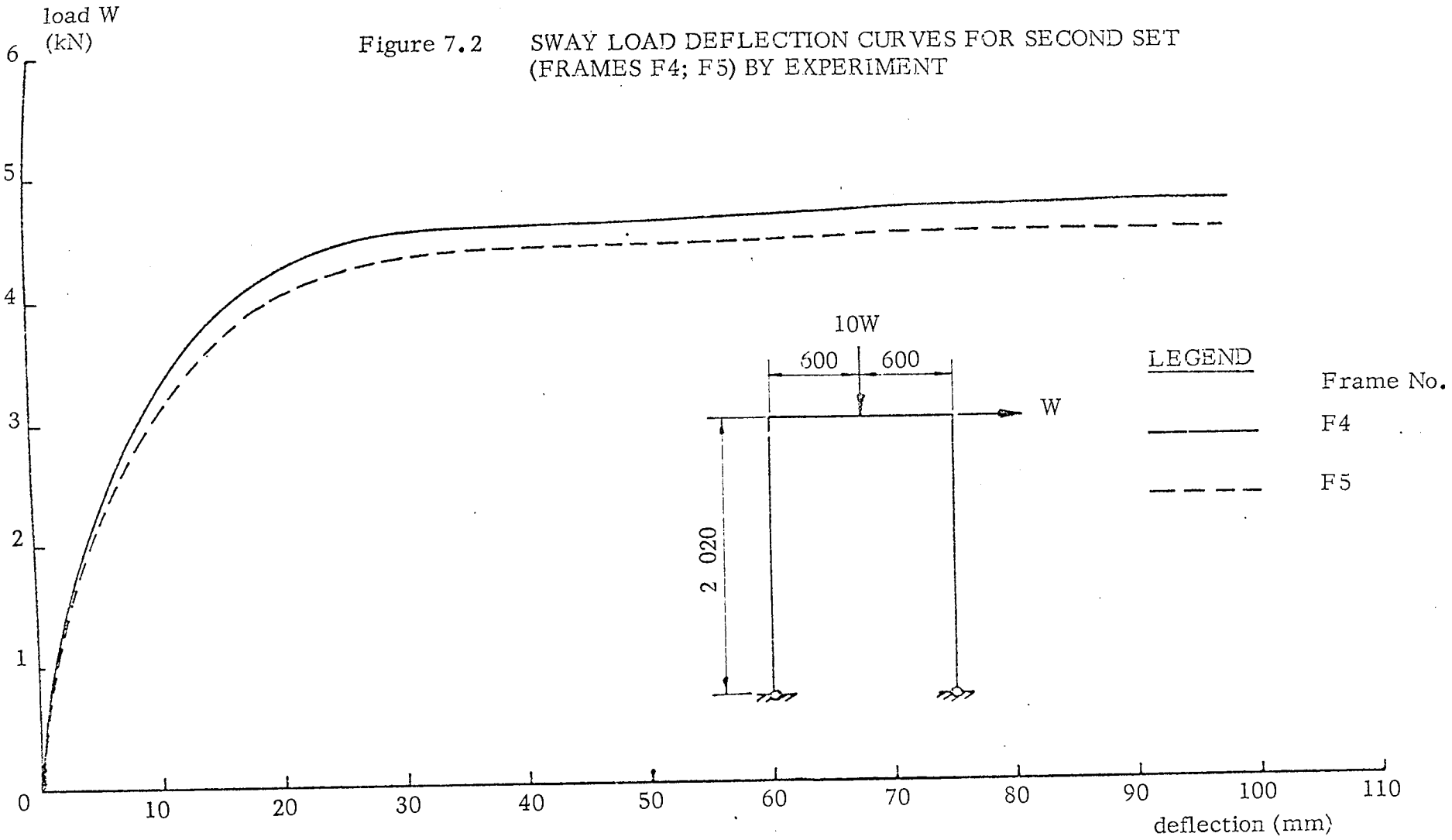

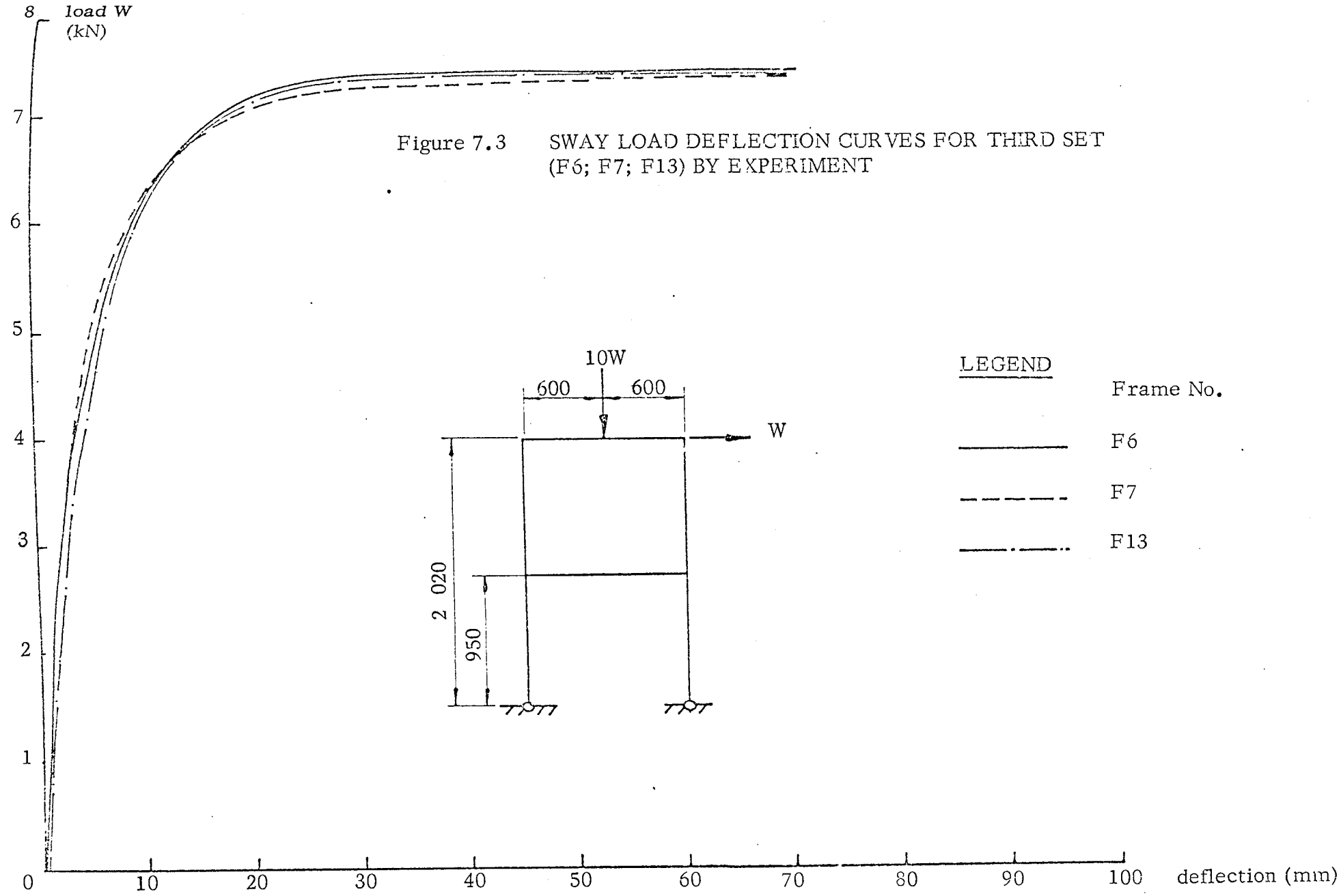

Figure 7.3 SWAY LOAD DEFLECTION CURVES FOR THIRD SET (F6; F7; F13) BY EXPERIMENT

TABLE NO. (7.2)

Ultimate bending moments, collapse loads by theory and experiment

Frame No.	Ultimate Moment M_u (kN mm)	Rigid-Plastic Collape Load W_R (kN)	Experimental Collapse Load W_E (kN)	% ± Difference in W_E & W_R
F 1	4 900	3.67	4.52	18.8
F 2	4 600	3.45	4.38	21.0
F 3	4 500	3.37	4.39	23.0
F 4	6 750	3.82	4.76	19.6
F 5	6 600	3.75	4.55	17.6
F 6	6 800	5.30	7.47	29.0
F 7	7 000	5.47	7.36	25.5
F13	7 400	5.78	7.38	21.7
F 9	9 700	4.60	5.29	13.0
	6 500			
	6 500			
F10	9 800	3.66	3.70	1.1
	3 600			
	6 000			
F11	12 600	3.68	3.50	5.1
	3 600			
	4 000			
F12	4 600	2.30	3.06	25.0
	5 600			
	3 800			

The three values quoted for frames F9, F10, F11 and F12 correspond to :

(1) M_u of the beam member with the bottom fibre in tension

(2) M_u of the column

(3) M_u of the beam member with the top fibre in tension

quoted. The mechanisms are compared below with those actually occurring in each frame and shown in Plates (1 - 12).

7.3.2 The failure mode of each frame in the first set was identical. The mechanism predicted by the rigid-plastic theory is shown in fig. 7.4 which is that actually occurring in frames F1, F2 and F3 and given in Plates (1, 2 and 3). This is a combined beam and sway mechanism, with plastic regions ('hinges') located beneath the vertical load in the cross beam and at the head of the column near the loaded joint. The first section to reach its ultimate state was that beneath the vertical load. Failure took place when the second plastic region was formed in the column. No local failure was seen at this joint, this indicated that the joint detail was satisfactory. From Table 7.2, it is seen that for this set, the collapse loads predicted by the rigid-plastic theory range between 17% and 21.5% below those obtained by experiment. These differences are discussed later in section 7.4.

7.3.3 For the second set (F4, F5), the mode of failure shown in Plates (4, 5) was again identical to the combined beam and sway mechanism predicted by the plastic theory fig. 7.5. As with the first set, two plastic regions were formed, one beneath the vertical load and the second at the head of the column near the loaded joint. The ultimate state was reached in the beam member first and failure, again took place, when ultimate conditions were reached in the column. Again, no localised failure effects such as bearing failure of concrete at the joints was seen. The rigid-plastic theory predicted collapse loads which were between 17% and 20% below the experimental values.

7.3.4 The two-storey frames of set 3 have a greater degree of statical indeterminancy. Difficulty was encountered in tracing the onset of plasticity in this set. The collapse modes of these frames are shown in Plates (6, 7, 8). It is possible that failure took place before the lower beam ends reached their

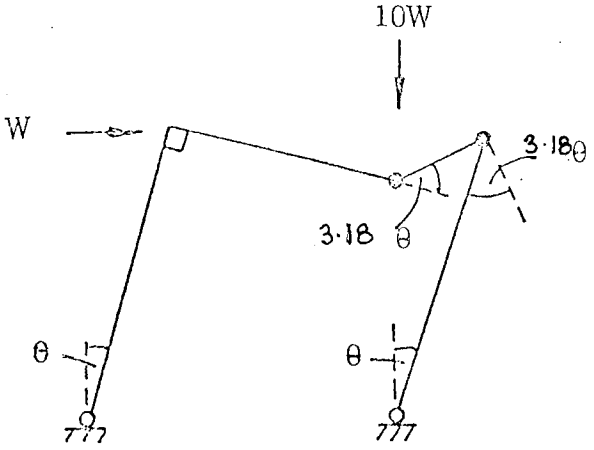

Figure 7.4

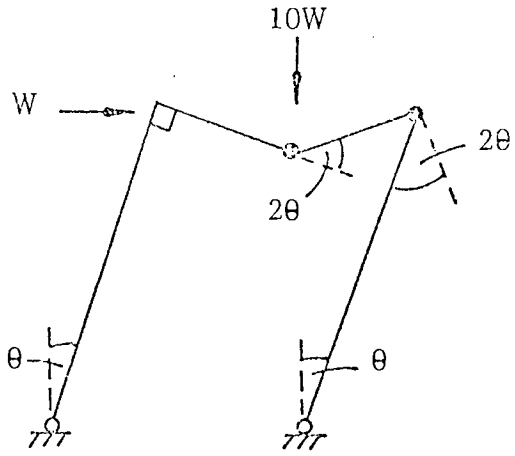

Figure 7.5

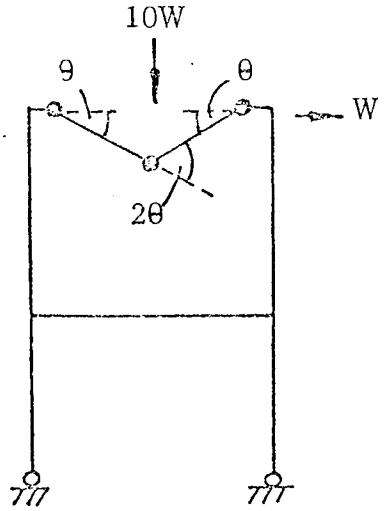

Figure 7.6

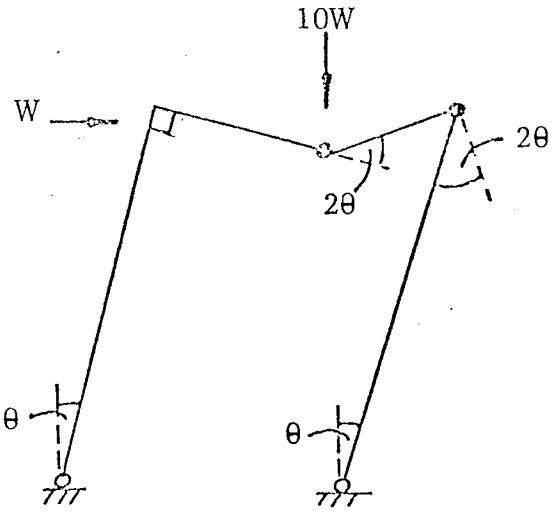

Figure 7.7

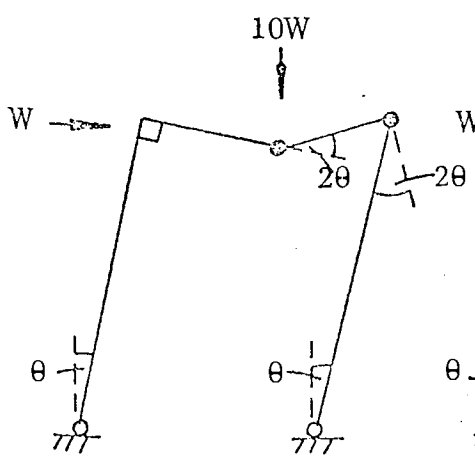

Figure 7.8

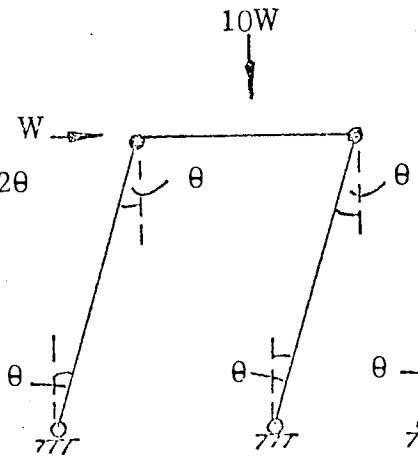

Figure 7.9

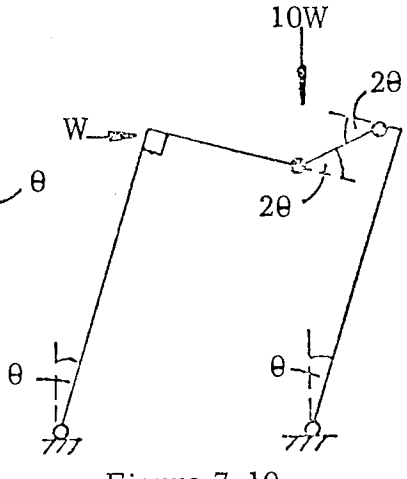

Figure 7.10

ultimate states. The plastic theory predicted an upper beam mechanism (see fig. 7.6) at failure. It was noticed that the plasticity of the connection between lower beam and column took place in the joint itself and the columns, indicating that the joint may not have been strong enough to transmit the larger bending moments to the lower beam. For this set, the rigid-plastic theory collapse loads were between 22% and 29% below those found by experiment.

7.3.5 For the first three sets of the test series, each frame had a constant cross-section and ultimate bending moment, M_u, throughout. For the latter four sets, the cross-sections of beams and columns varied. This was either with depth and/or percentage of reinforcement. In the cross beam member, there are two values of M_u depending upon whether the top or the bottom fibres are in tension. The column M_u's were identical for both faces in tension.

Frame F9 had a constant concrete section with varying reinforcement. The columns were reinforced with less steel than the beam. The collapse mode of this frame is shown in Plate (9). An identical mechanism is predicted by the rigid-plastic theory fig. 7.7. This is a combined beam and sway mechanism, with plastic regions beneath the vertical load and in the column near the loaded joint. The M_u values either side of this joint are approximately the same (see Table 7.2), so this plastic region may have occurred at either side of this joint. The first section to reach its ultimate moment was that beneath the vertical load. Failure again took place when the second section reached its ultimate state. The experimental collapse load was 13% higher than that predicted by the rigid-plastic theory.

7.3.6 Frame F10 had a varying concrete section. The beam's depth was greater than that of the columns. The ultimate bending moment of the column sections were far less than those of the beam sections. The failure mode is given in Plate (10). The theoretical mode is again identical (see fig. 7.8), and

of the combined beam and sway mechanism type. It is worth stating here that from the calculations of the collapse mechanism, the collapse load of the sway type of mechanism was very close to that of the combined mechanism. For the combined mechanism, the collapse load is 3.66 kN and for the sway mechanism, 3.70 kN. These values are very close to the actual collapse load of the frame, the difference being 1.1%.

7.3.7 Frame F11 was of a constant concrete section, the beam member was 'over-reinforced' and thus, possessed little ductility. The column was lightly reinforced, its M_u being 3.5 times smaller than that of the beam section. The second ultimate moment of the beam, i.e. with the top in tension, was slightly larger than the column's M_u. The collapsed frame shown in Plate (11) is not truly representative of the actual failure, as the beam member had to withstand some further load after failure, as the vertical load system was still applied to this member. The failure mode was of the sway type predicted by the rigid-plastic theory, fig. 7.9. At the unloaded corner joint, there appeared to be some local failure due probably to the high percentage of tensile reinforcement there. The shear reinforcement was spaced widely apart, and it is possible that some shear failure also took place. The rigid-plastic theory predicted a collapse load which was 5.1% greater than that obtained experimentally.

7.3.8 Frame F12 was again of constant concrete section, the ultimate moment of the columns being greater than both those of the beam. The failure mode of this frame is shown in Plate (12). An identical mode was predicted by the plastic theory, fig. 7.10 and is a combined beam and sway mechanism. The two plastic regions were both in the beam member, one beneath the vertical load, the other in the beam to one side of the loaded corner joint. The first of these to reach its ultimate state was that beneath the vertical load. Failure took place when the second 'hinge' was formed. The experimental

collapse load is 25% larger than the rigid-plastic collapse load.

7.3.9 The values obtained for the experimental and rigid-plastic collapse loads will now be discussed. To aid the discussion, reference will be made to a typical load-deflection curve of a frame subject to proportional loading such as given in Fig. 7.24. The rigid-plastic behaviour of a frame is represented by the line AB, and the rigid-plastic collapse load factor is F_{RP}. Due to the non-linear P - Δ effects prevalent in a frame, the true rigid-plastic curve has a "drooping" form represented by AB' in the figure.

In reality, the non-linear load deflection curve of a frame is expected to have the form represented by OEG. For this curve, the failure load of a frame is given by the load factor F_E. From this diagram, it is apparent that the true collapse load of a frame should be less than that predicted by the rigid plastic theory which neglects P - Δ effects.

From table 7.2, it can be seen that the rigid-plastic collapse loads range between 1 and 29% below those obtained by experiment. Reasons for these differences will now be discussed.

There are two main reasons why the experimental collapse loads do not agree with those obtained by the rigid plastic theory. These are due to :-

1) experimental errors

2) the effect of the bending moment-axial load interaction in the column members of a frame.

The most probable experimental error is due to the application of load to the frames. The loading system is described in Chapter 5 where it is shown that a lever system is utilized to transmit the vertical load. One of the requirements of a vertical loading system is that as a frame sways, the loading remains vertical. For small lateral displacements, this requirement can be met reasonably well. However, as these displacements increase, because the lever system

is rigidly attached to the test bed, the wire ropes which transfer the load to the frames displace by an angle θ to the vertical, this is shown in fig. 7.25 (a). This results in the force diagram given in fig. 7.25 (b). In this diagram, it can be seen that the load, which is now inclined, has a horizontal component. This component acts in opposition to the applied sway load W, with the effect of reducing its magnitude.

For the seven sets of frames reported in this thesis, side displacements would have a significant effect of reducing the sway load when their magnitudes were in the region of :-

i) 12 mm for set 1

ii) 20 mm for set 2 - 7

For set 1, a side displacement of 12 mm in the total height of 1200 mm would make $\theta = 0.01$. For the remaining six sets, a side displacement of 20 mm in 2000 mm would also make $\theta = 0.01$.

For $\theta = 0.01$, the induced horizontal component of load will be equal to $10W \sin\theta$ which is approximately 0.1W. This has the effect of reducing the total sway load from W to 0.9W.

Because the vertical load is large in comparison with the sway load i.e. 10 : 1, the reduction in this load due to the vertical component $10W \cos\theta$ is negligible, i.e. 1% compared with the 10% reduction in sway load.

This reduction in the effective sway loading is increased as the sway displacements increase further. It is therefore obvious that the values of the collapse loads obtained experimentally are greater than those which actually occurred during the tests. Also, when significant side displacements were present, the loading was not truly proportional.

The second reason why the experimental results were in excess of those predicted by the rigid plastic theory may be due to the effect of the

presence of low axial loading in the column members of the frames. In Chapter 2, fig. 2.13, the axial load-moment interaction curve is described. It is shown on this curve that when the ratio of axial loads P/P_u is low, there may be an increase in M/M_u beyond unity, i.e., the moment the column can withstand is larger than the ultimate bending moment of the column under no axial loading. During the tests "plastic hinges" were formed in the column members. The axial loads P imposed in the columns of the frames were small in comparison to ultimate compressive strengths P_u of the columns.

e.g. For the two storey portal frames F6, F7 and F13 :

$f'_{cu} = 48 N/mm^2$ & $A_c = 17500\ mm^2$

Now the maximum axial forces in the column were approximately equal to 40 kN. The ultimate strength of each column ignoring the reinforcement is given by :-

$$P_u = 48 \times 17500 = 840\ kN$$

Hence, the ratio of axial load to ultimate axial load in the column is given as :-

$$P/P_u = 40/840 \doteq 0.05$$

This value is small and may therefore have resulted in an increase in the resistance moments of the columns. Larger moments than those ultimate values used in the computation of the rigid plastic collapse loads may well have been present at these particular plastic hinge regions. This effect would contribute to some of the difference in the values of collapse load obtained for all the frames by the rigid-plastic theory and experiment.

7.3.10 The modes of failure of each frame have been discussed and compared with those obtained by the rigid-plastic theory. The theory on all occasions but for the two-storey frames predicts the actual collapse mode. It has been demonstrated that for most of the frames, the rigid-plastic collapse load is smaller than that obtained by experiment.

For frames F10 and F11, the slenderness of the columns was increased

and the ultimate moments of resistance decreased. This meant that large sway displacements were induced at lower values of load. It is possible that due to the P - Δ effect, the experimental collapse loads of these frames were reduced in comparison to those predicted by the rigid-plastic theory and therefore may account for the close proximity of these collapse loads.

7.4 Comparison of results by experiment and computer

The results obtained by the experimental tests performed on the portal frames of Chapter 5, and by the two computer analyses presented earlier in this thesis are compared below. A comparison is made of the load-deflection response under the sway load and the collapse loads by the different methods. Each frame will be examined separately.

7.4.1 The subdivision of frames and values of load increment for the incremental analysis were selected in accordance with the conclusions drawn for the tests reported in Chapter 3. The representations of moment-curvature and instantaneous flexural rigidity-curvature relationships used in the various analyses of the portal frames are given together with the frame subdivision and details in Appendix (1).

For the load factor method, since the effect of axial load is small for the range of axial loads encountered in this thesis, a value of tolerance for successive load factors has been taken as 0.001. This reduces the number of iterations, and hence, computer time necessary for predicting each critical load factor.

From tests performed using various bending moment factors in an incremental analysis with reduced frame subdivision (Section 3.4.3), a value of 0.93 was selected for the factor. This value has been used in this type of analysis for each frame.

7.4.2 Five methods are used to describe the various computer analyses, and

experimental investigation of the behaviour of the reinforced concrete frames of Chapter 5. A definition of each method is given below.

METHOD 1 This method refers to the actual experimental investigation of the portal frames of Chapter 5.

METHOD 2 This method is the incremental computer analysis of the fully subdivided frames. The $(EI)_t$ - Ø relationship used is that acquired from the beam tests of Chapter 6.

METHOD 3 This method is again the incremental computer analysis of fully subdivided frames, the $(EI)_t$ - Ø relationship used, however, is that constructed from the theory of Chapter 2.

METHOD 4 An incremental computer analysis using a reducted frame subdivision, and a bending moment factor (Section 3.4.3). The beam test $(EI)_t$ - Ø data is utilised by this method.

METHOD 5 The load factor computer analysis of Chapter 4. The fully subdivided frame is used together with the moment-curvature relationships obtained from the beam tests.

The collapse loads obtained for each frame by the above methods are given in Table 7.3. These loads correspond to the sway load W.

7.4.3 Frame Set 1 (F1, F2 & F3)

The curves obtained by methods 1 - 5 for the sway load-deflection of frames F1, F2 and F3 are shown in figures 7.11, 7.12 and 7.13 respectively. For frames F1 and F3, there is good agreement between the experimental curve and that of method 2, for the complete loading history. The collapse loads by these methods for F1 are nearly identical (see Table 7.3), and for F3, method 2 gives a value which is 4.5% lower than the experimental value. For F2, the agreement between methods 1 and 2 is not so close for the load-deflection response after a load of 3.5 kN and the eventual collapse load given

TABLE NO. (7.3)

Values of collapse loads by Methods 1 - 5

Frame No.	Experiment 1 kN	Computer Analyses				Rigid-Plastic kN
		2 kN	3 kN	4 kN	5 + kN	
F 1	4.52	4.525		4.600	3.100	3.67
F 2	4.38	3.950	3.400	4.100	3.075	3.45
F 3	4.39	4.200		4.300	3.050	3.37
F 4	4.76	4.675	3.525	4.525	3.150	3.82
F 5	4.55	4.375		4.375	3.125	3.75
F 6	7.47	7.350		***	4.820	5.30
F 7	7.36	7.325	5.250	***	4.810	5.47
F13	7.38	7.150		***	5.130	5.78
F 9	5.29	5.200	3.950	5.175	3.775	4.60
F10	3.70	3.500	3.375	3.450	2.500	3.66
F11	3.50	3.650	2.950	3.600	2.400	3.68
F12	3.06	2.650	2.250	2.700	2.025	2.30

+ In method 5, the loads given are those corresponding to the maximum load factor attained

*** This method did not furnish a true representation of behaviour after the first ultimate bending moment had been reached in the frames

Figure 7.11 COMPARISON OF THE SWAY LOAD-DEFLECTION CURVES FOR FRAME - F1 BY EXPERIMENT AND COMPUTER ANALYSIS

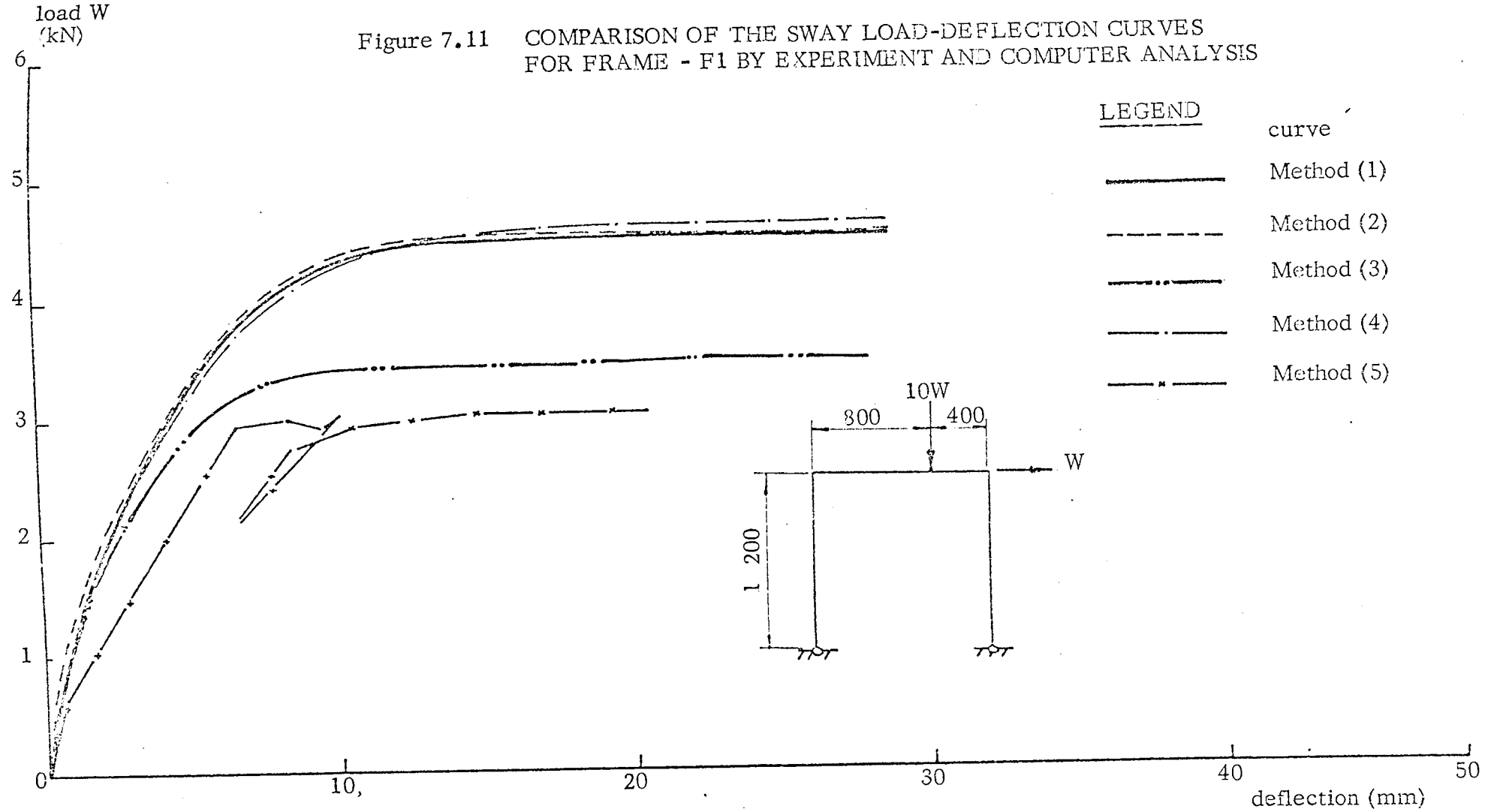

Figure 7.12 COMPARISON OF THE SWAY LOAD DEFLECTION CURVES FOR FRAME-F2 BY EXPERIMENT AND COMPUTER ANALYSES

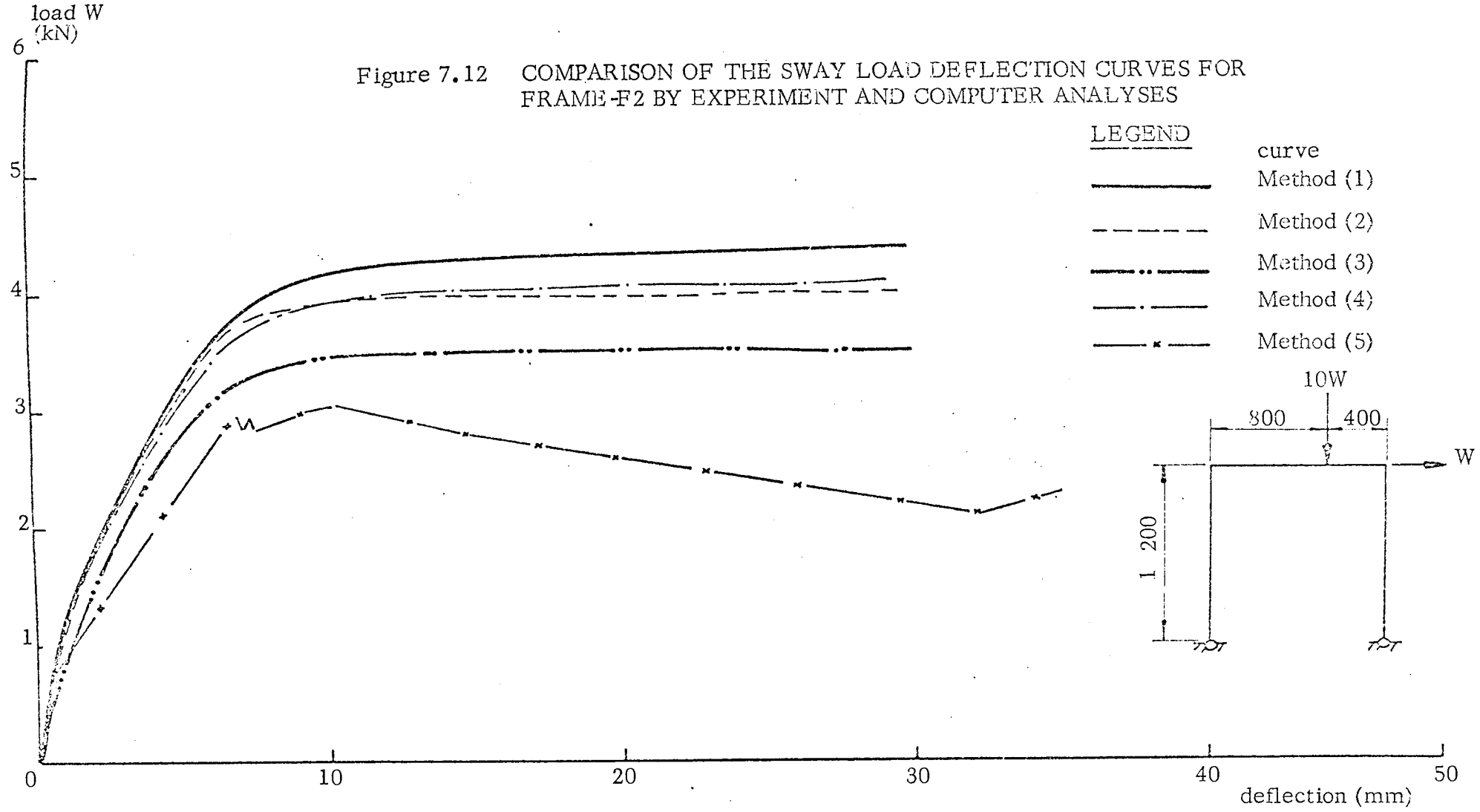

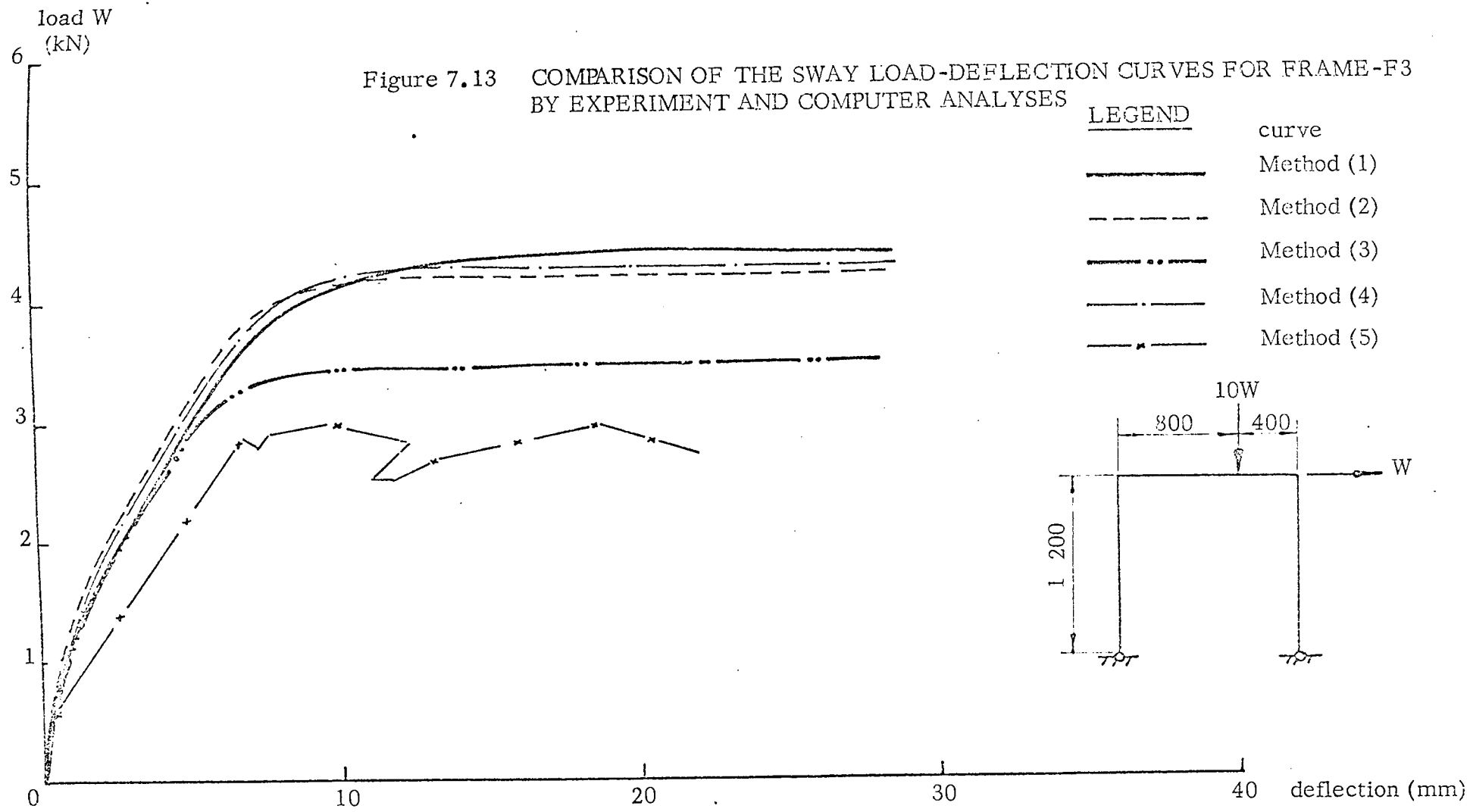

Figure 7.13 COMPARISON OF THE SWAY LOAD-DEFLECTION CURVES FOR FRAME-F3 BY EXPERIMENT AND COMPUTER ANALYSES

by method 2 is 9.8% below the experimental value. The curves obtained by method 4 agree closely with those of method 2 for all the set and the collapse loads given by method 4 range between 1.6% and 2.3% higher than those of method 2. These values may be reduced by selecting a larger value of bending moment factor.

Method 3 which utilises the theoretical $(EI)_t$ - $\emptyset$ relationship gives a curve which closely follows those of methods 1, 2 and 3 initially, upto first yield of steel in the frame. The curve then flattens out far more rapidly and gives eventual collapse loads which range between 12% and 25% below the experimental values. This can primarily be attributed to the sharp reduction in stiffness that is assumed by the theory, when the tensile reinforcement yields. In practice, the change in stiffness at this stage is gradual, and thus, the decrease in the frame's stiffness is not so rapid. Another factor which influences this lower result is the conservative estimate of the effect of strain hardening in the tensile reinforcement. The result is, however, on the safe side.

Method 5 which is the load factor computer analysis yields a curve which is discontinuous in nature. Reasons for this discontinuity are given in Chapter 4. The load-deflection curves by this method follow those of method 3, giving a less stiff response to load. The load deflection curve follows those of other methods upto first yield of steel in the frame. After this stage, the curve flattens abruptly, and also falls. The collapse loads obtained by this method are approximately 30% lower than the experimental values for F1, F2 and F3.

7.4.4 Frame set 2 (F4, F5)

The load-deflection curves of frames F4 and F5 by methods 1 - 5 are shown in figures 7.14, 7.15. The incremental analysis of method 2 gives a

Figure 7.14 COMPARISON OF THE SWAY LOAD-DEFLECTION CURVES FOR FRAME-F4 BY EXPERIMENT AND COMPUTER ANALYSES

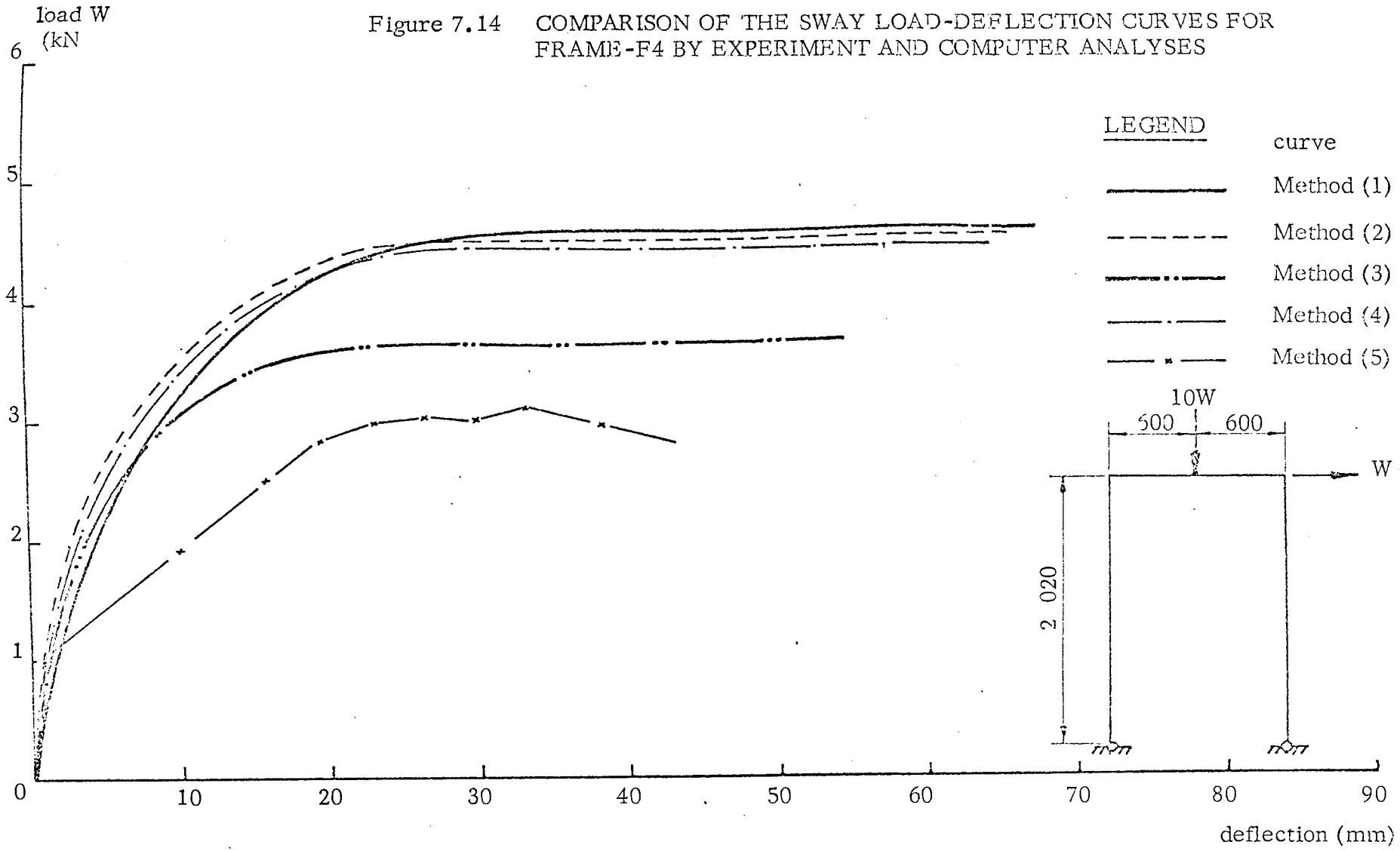

Figure 7.15 COMPARISON OF THE SWAY LOAD-DEFLECTION CURVES FOR FRAME-F5 BY EXPERIMENT AND COMPUTER ANALYSES

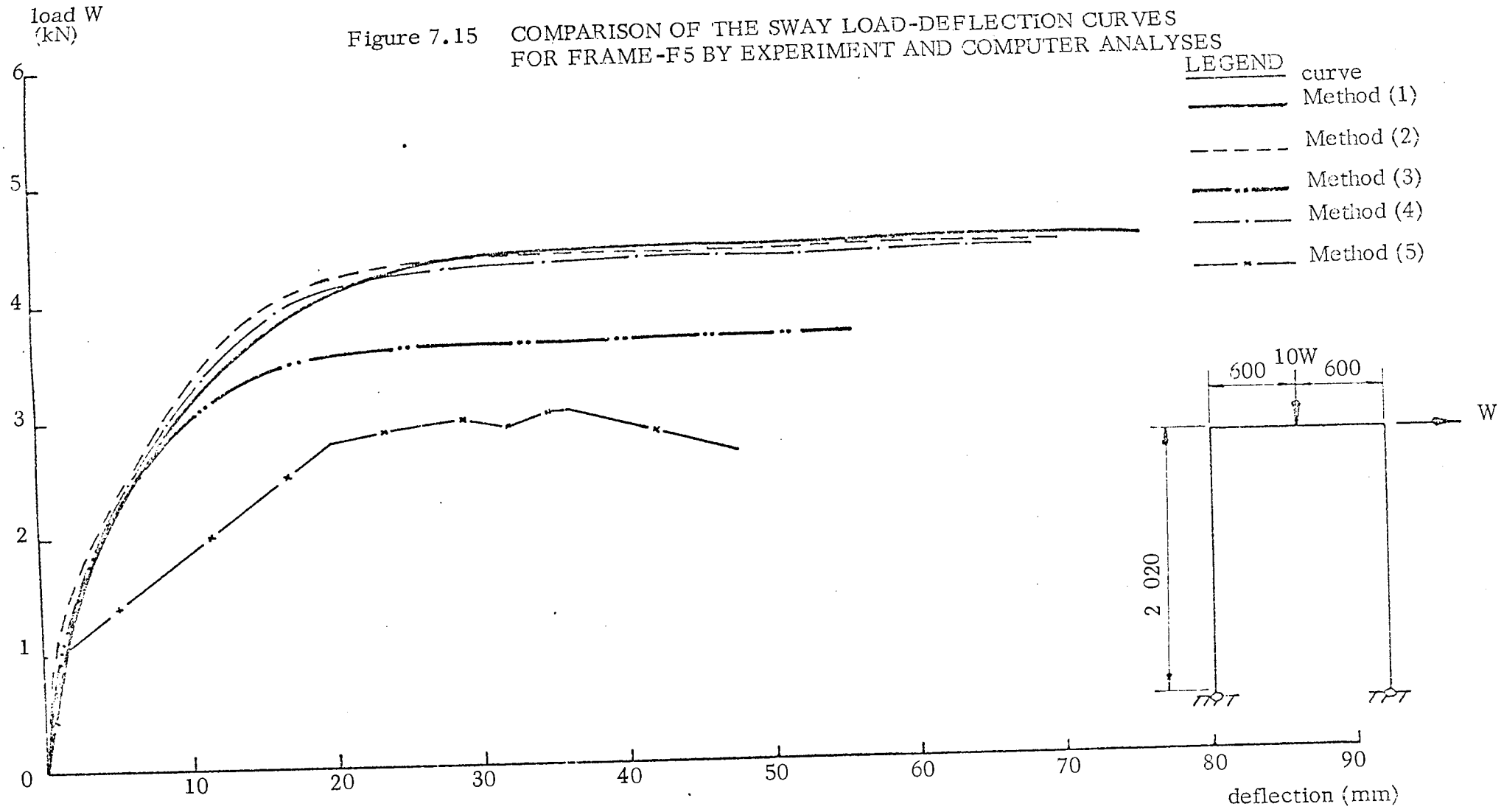

curve which follows that by experiment, very closely, for frames F4 and F5. In both cases, the initial response of the frames are stiffer by the computer analysis than by experiment, this difference is not significant, however. The collapse loads by method 2 are 1.8% and 3.85% respectively below the experimental values for F4 and F5. Method 4 again gives a curve which agrees closely with those of the first two methods, the maximum difference in collapse loads being 3%. The curve of method 3 follows those obtained by methods 1, 2 and 4 upto the first yield of steel in the section of the frame. After this stage, as was the case in the first set, the curve flattens fairly rapidly, yielding collapse loads between 22% and 26% below the experimental values. The reasons for this difference may be attributed to those stated in section 7.4.3 above.

The load factor analysis of method 5, again gives a curve which is discontinuous in nature. Upto first cracking of concrete, this method agrees with the rest, but then exhibits less stiffness upto first yield of steel. At this point, the curve flattens abruptly. The collapse loads given by this method 5 are 34% and 31.5% respectively below the experimental values for F4 and F5.

7.4.5 Frame set 3 (F6, F7, F13)

The sway load-deflection curves for the two-storey portal frames F6, F7 and F13 are given in figures 7.16, 7.17, 7.18 respectively. In each case, the curves of the incremental computer analyses, 2, 3 and 4 exhibit a greater initial stiffness, when compared with the curve of method 1. This difference is maintained upto values of load, near to collapse. The extent of this is not significant, however, and part of it may be attributed to experimental error, such as faulty dial gauge readings or error in the application of load from the lever system. The collapse loads of methods 1 and 2 are close and this is true for each frame in this set, the maximum difference being 3.1% for the values quoted in Table 7.3. Method 4 predicts the behaviour well upto first attainment of

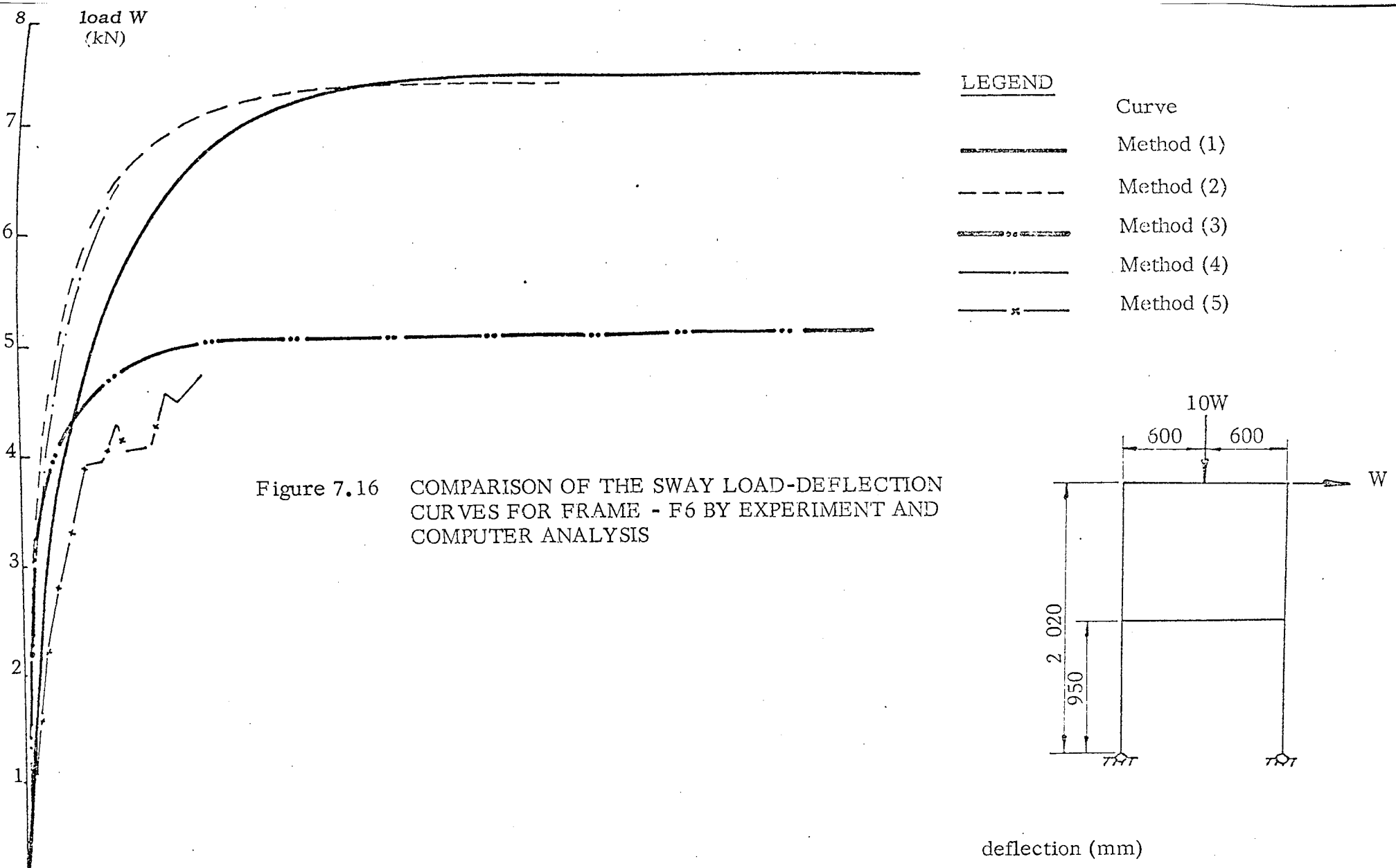

Figure 7.16 COMPARISON OF THE SWAY LOAD-DEFLECTION CURVES FOR FRAME - F6 BY EXPERIMENT AND COMPUTER ANALYSIS

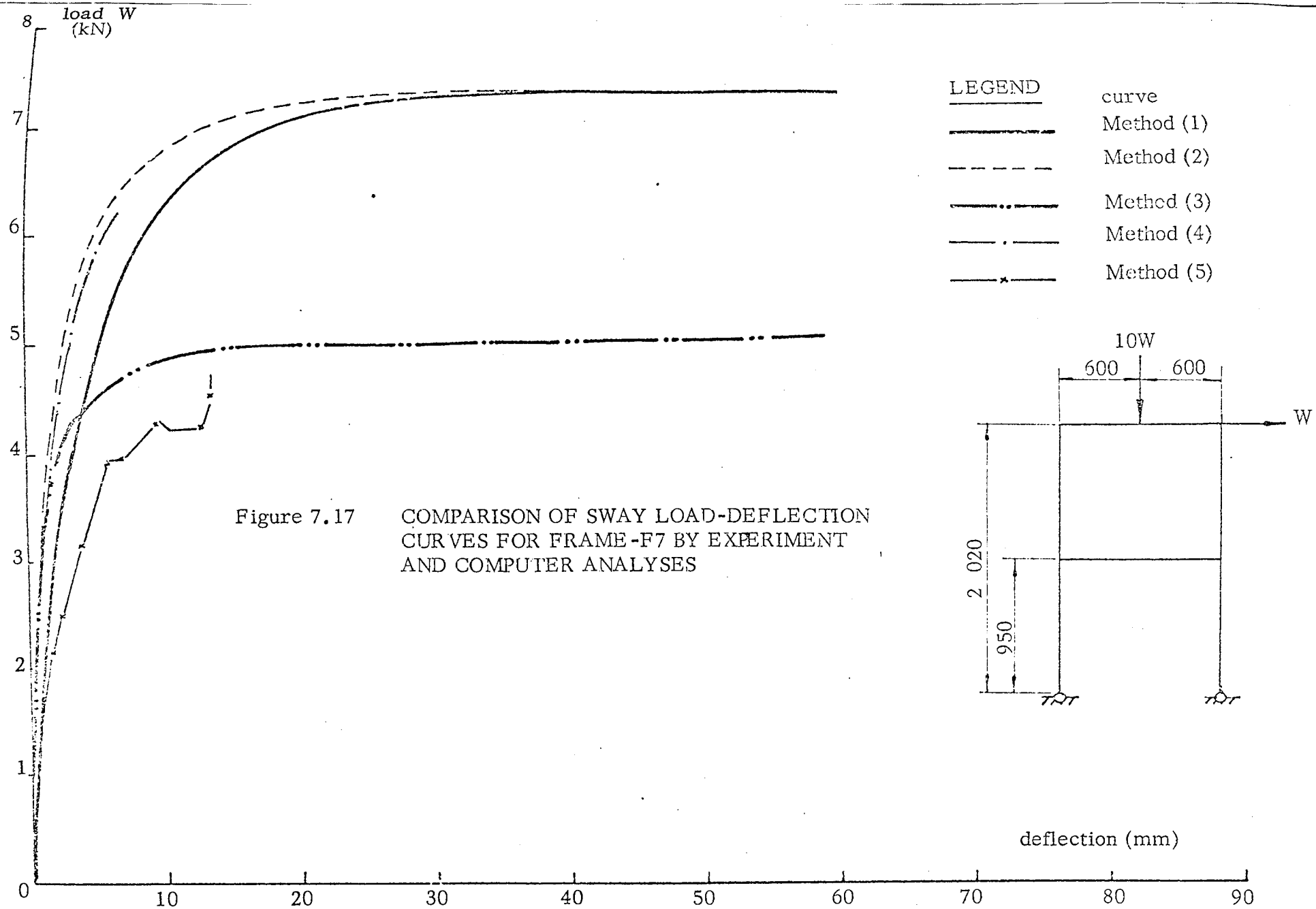

Figure 7.17 COMPARISON OF SWAY LOAD-DEFLECTION CURVES FOR FRAME-F7 BY EXPERIMENT AND COMPUTER ANALYSES

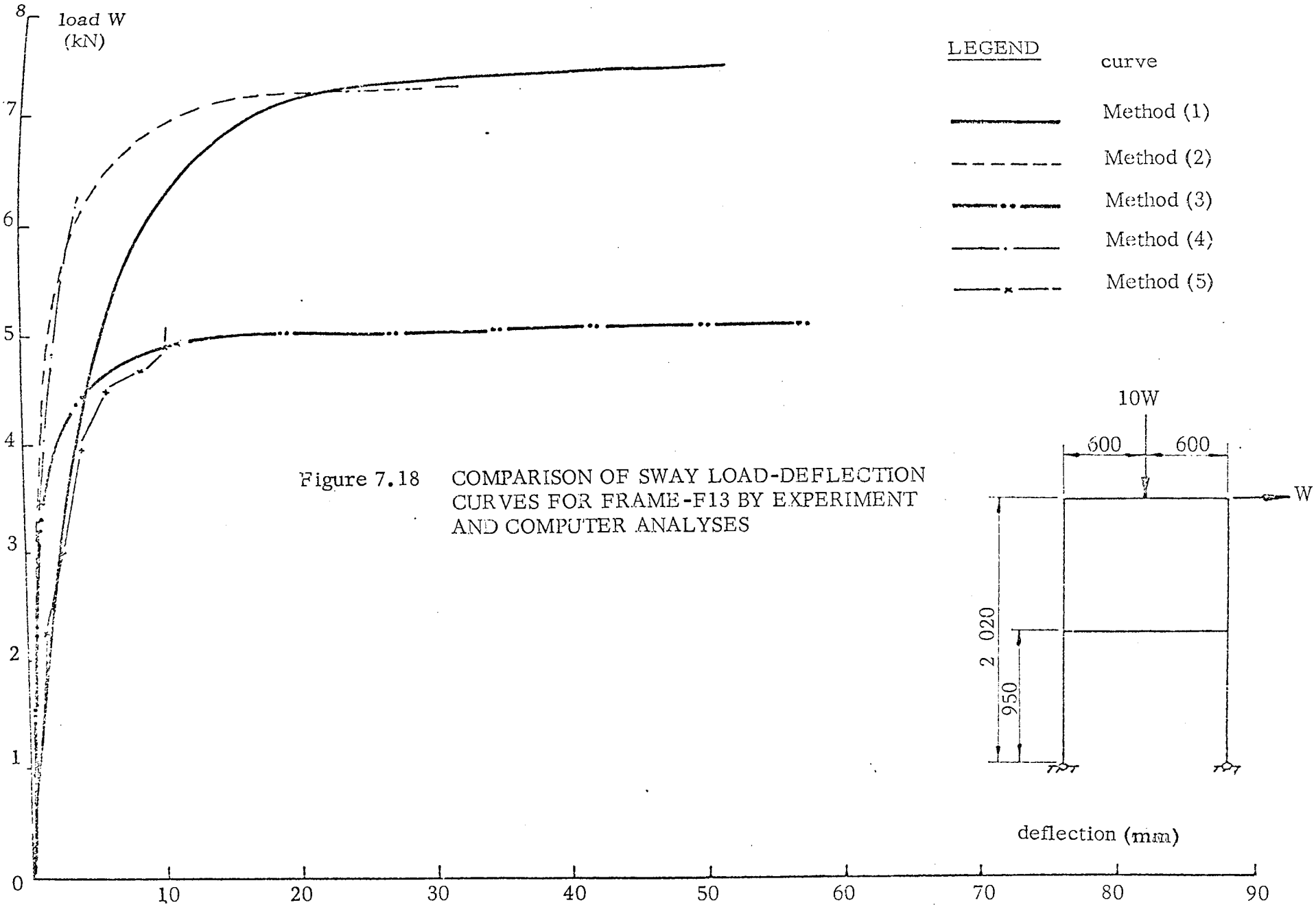

Figure 7.18 COMPARISON OF SWAY LOAD-DEFLECTION CURVES FOR FRAME-F13 BY EXPERIMENT AND COMPUTER ANALYSES

ultimate bending moment in the frame. After further loading, the method does not follow the true behaviour pattern.

As was the case for frame sets 1 and 2, the curves of method 3 in figures 7.16, 7.17 and 7.18 follow those of methods 1, 2 and 4 closely upto the first yield of steel. The subsequent flattening of this curve is far more marked in this set, however. The collapse load by this method is an average of 29% below the experimental value.

The curves obtained by method 5 follow the experimental curves quite closely upto a load of 4 kN, at which the deflections increase. The curves are then discontinuous upto the maximum load. These loads are between 30% and 35% below the experimental maximum loads.

7.4.6 The sway load-deflection curves of frame F9 by methods 1 - 5 are given in fig. 7.19. The agreement is close for the curves of methods 1, 2 and 4 right upto collapse, the computer analyses giving slightly lower values of deflection for the same load. Method 2 gives a collapse load which is 1.7% below the experimental value and 0.5% greater than that of method 4. Method 3 follows the above three methods initially then flattens out at a load of 3.5 kN. The difference in collapse load by this method compared with experiment is 25%.

Method 5, once again, yields a curve which shows a far less stiff response to load and little increase in load carrying capacity after first yield of steel in the frame. The eventual maximum load is 28.5% below the experimental value.

7.4.7 The load deflection curves of F10 by methods 1 - 5 are given in fig. 7.20. For this frame, the agreement between methods 1, 2 and 4 is not as close as for previously described frames. The load deflection curves obtained by all the incremental analyses give larger deflections for loads when compared with the experimental curve. A collapse load which is 5.4% below the experimental value is given by method 2, and this value is 3.6% above that of method 4. The

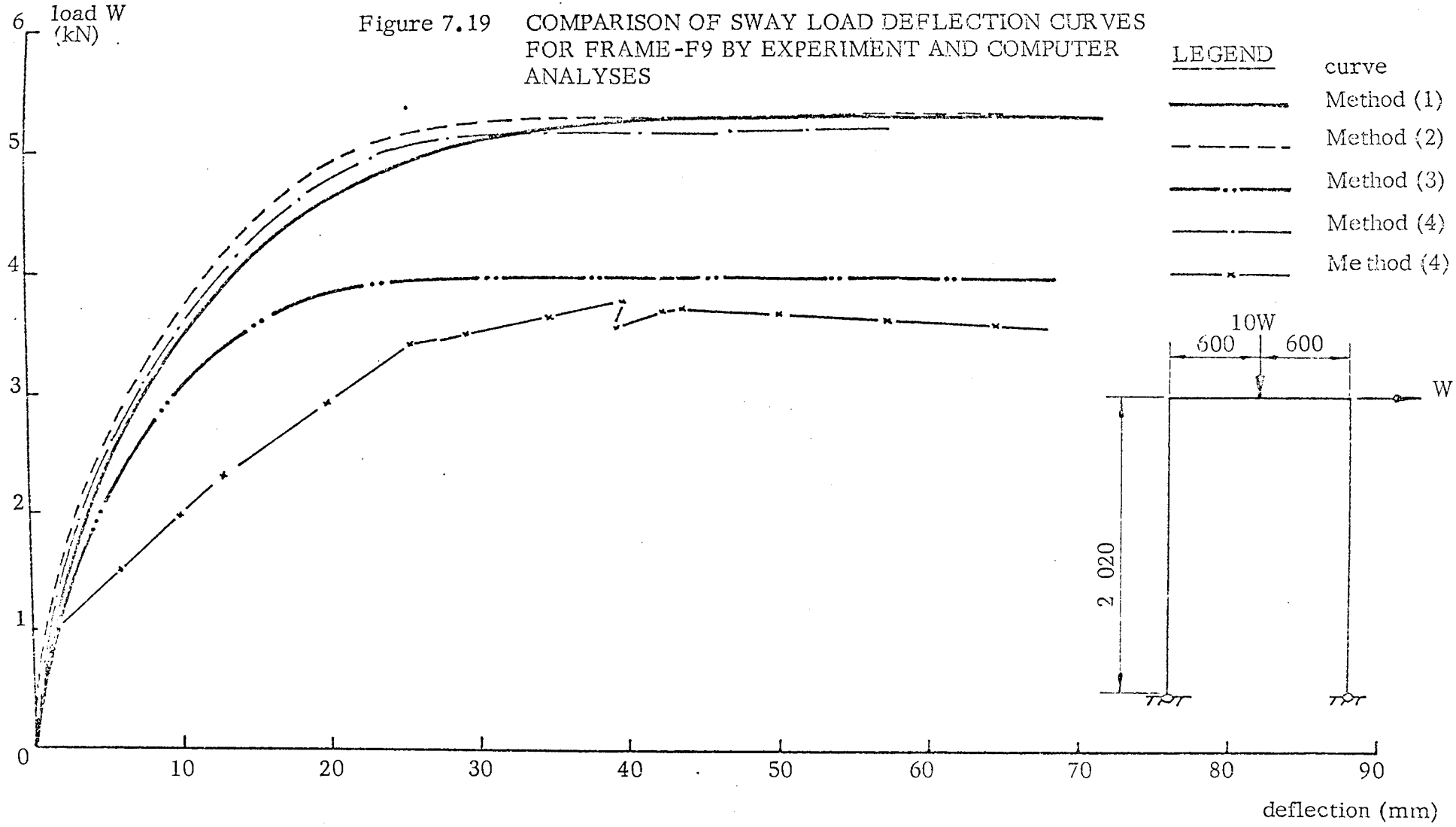

Figure 7.19 COMPARISON OF SWAY LOAD DEFLECTION CURVES FOR FRAME-F9 BY EXPERIMENT AND COMPUTER ANALYSES

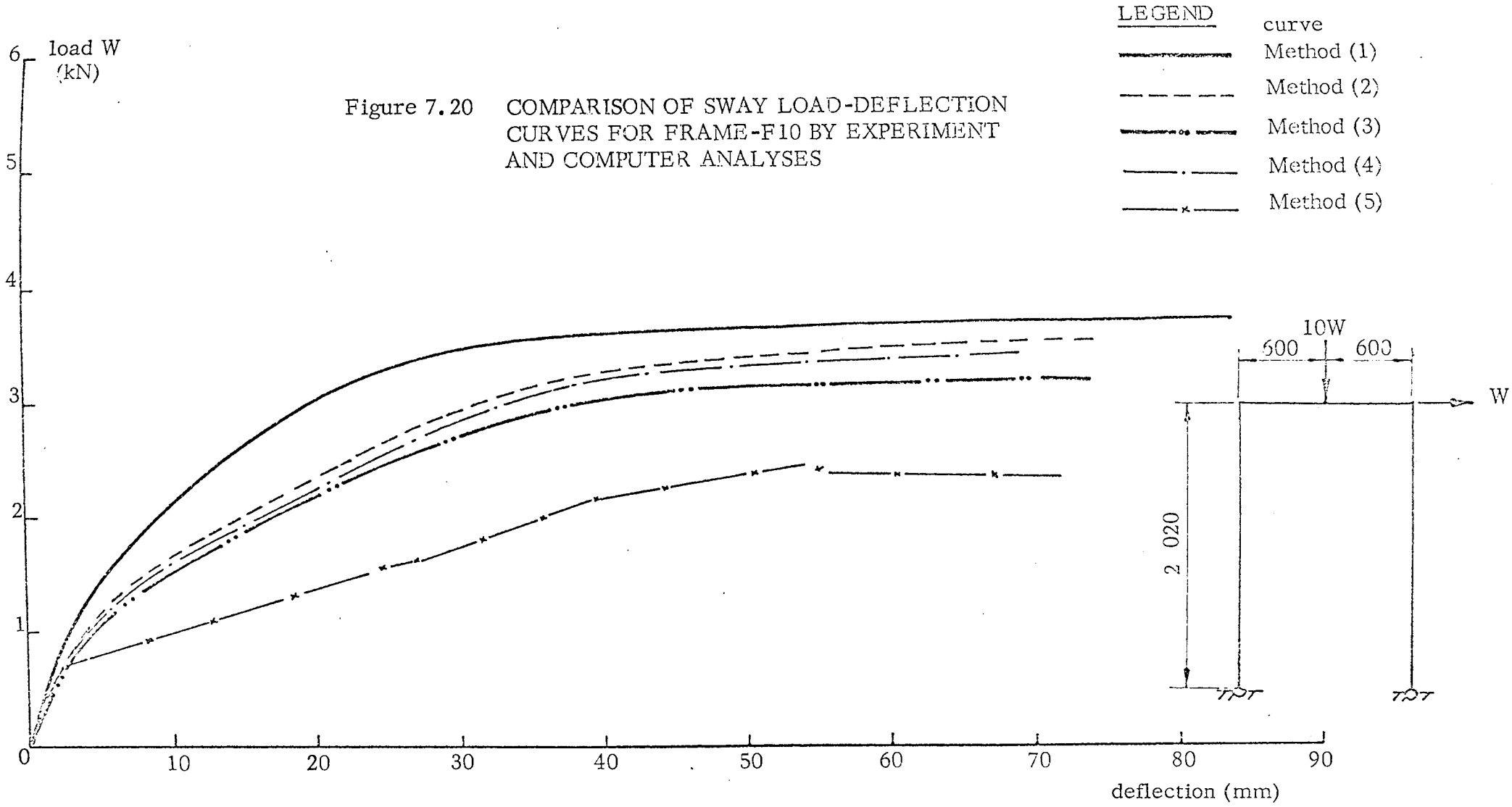

Figure 7.20 COMPARISON OF SWAY LOAD-DEFLECTION CURVES FOR FRAME-F10 BY EXPERIMENT AND COMPUTER ANALYSES

curve of method 3 follows those of methods 2 and 4 quite closely and the collapse load by this method is only 9% below the experimental value.

Method 5 yields a load deflection curve which again does not follow those of the other methods closely. The difference in collapse load with method 1 is 32%.

7.4.8 Fig. 7.21 gives the load deflection curves for frame F11. The incremental computer analysis of methods 2, 3 and 4 agree fairly closely with the experimental curve. The collapse loads of 2 and 4 are slightly greater than the experimental values by the amounts of 4.3% and 2.9% respectively. Method 3 yields a collapse load which is 16% below that of method 1.

Method 5 gives a curve which is less stiff in response to load when compared with the other methods, the difference between the collapse loads of this and method 1 being 31%.

7.4.9 For frame F12, the load deflection curves of methods 1 - 5 are shown on fig. 7.22. Methods 2 and 4 predict the experimental behaviour of the frame quite closely. The difference in the collapse loads are 13%. Method 3 also agrees initially with the above methods upto a load of 2 kN and its collapse load is 26% below the experimental value.

The load factor analysis of method 5 follows that of method 3 reasonably, and yields a collapse load 34% below that of method 1.

7.4.10 A comparison has been made of the results obtained by experiment and the computer analyses. In section 7.3, reference was made to the "drooping" rigid-plastic load deflection curve of a frame. It was shown that the true behaviour of a frame should have the form represented by OEG in fig. 7.24, i.e. with an eventual collapse load less than the rigid-plastic value with no axial load effects included. It was also shown that the values of experimental collapse loads were greater than those actually occurring due to experimental discrepancy and column moment-axial load interaction.

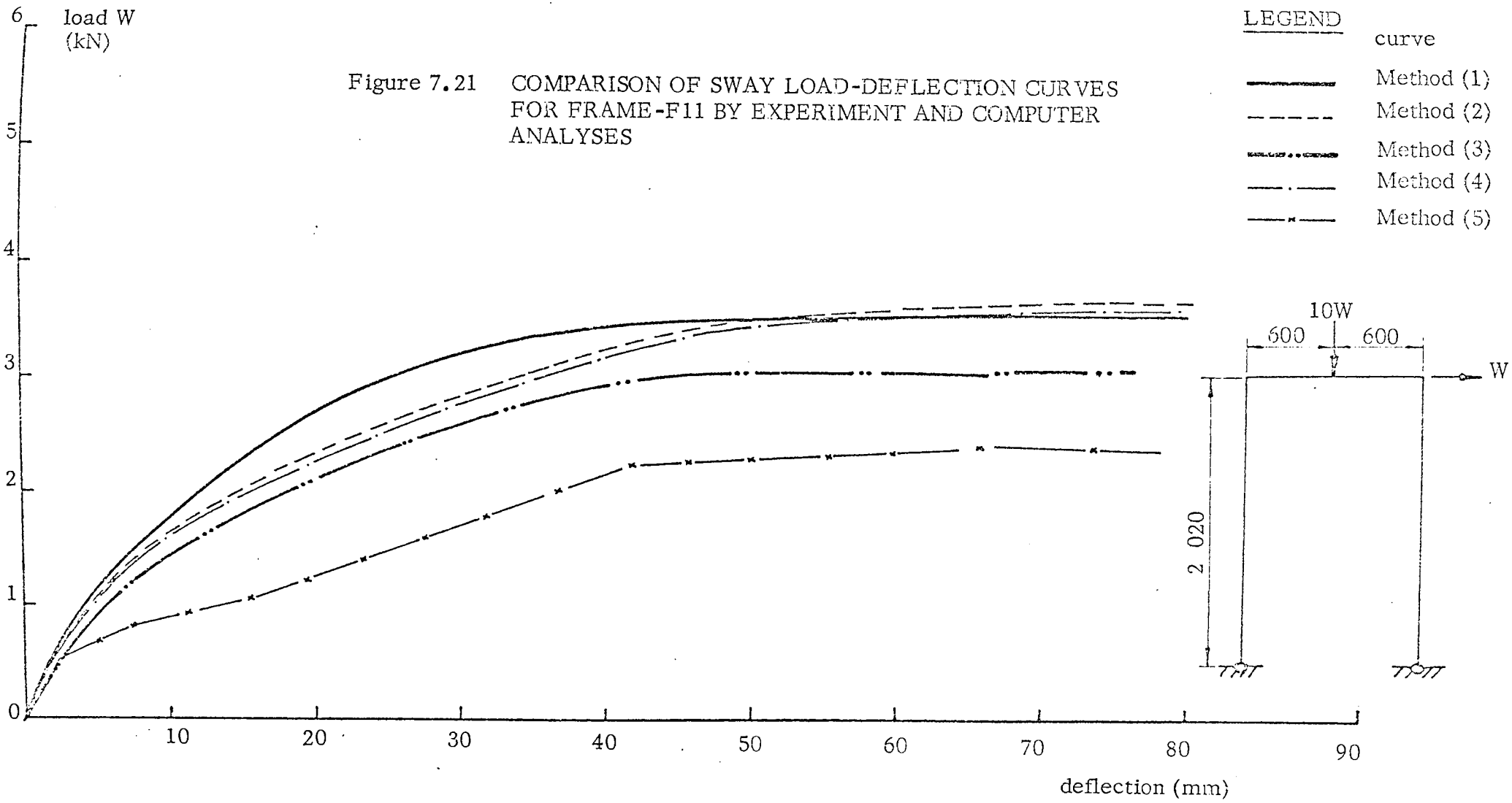

Figure 7.21 COMPARISON OF SWAY LOAD-DEFLECTION CURVES FOR FRAME-F11 BY EXPERIMENT AND COMPUTER ANALYSES

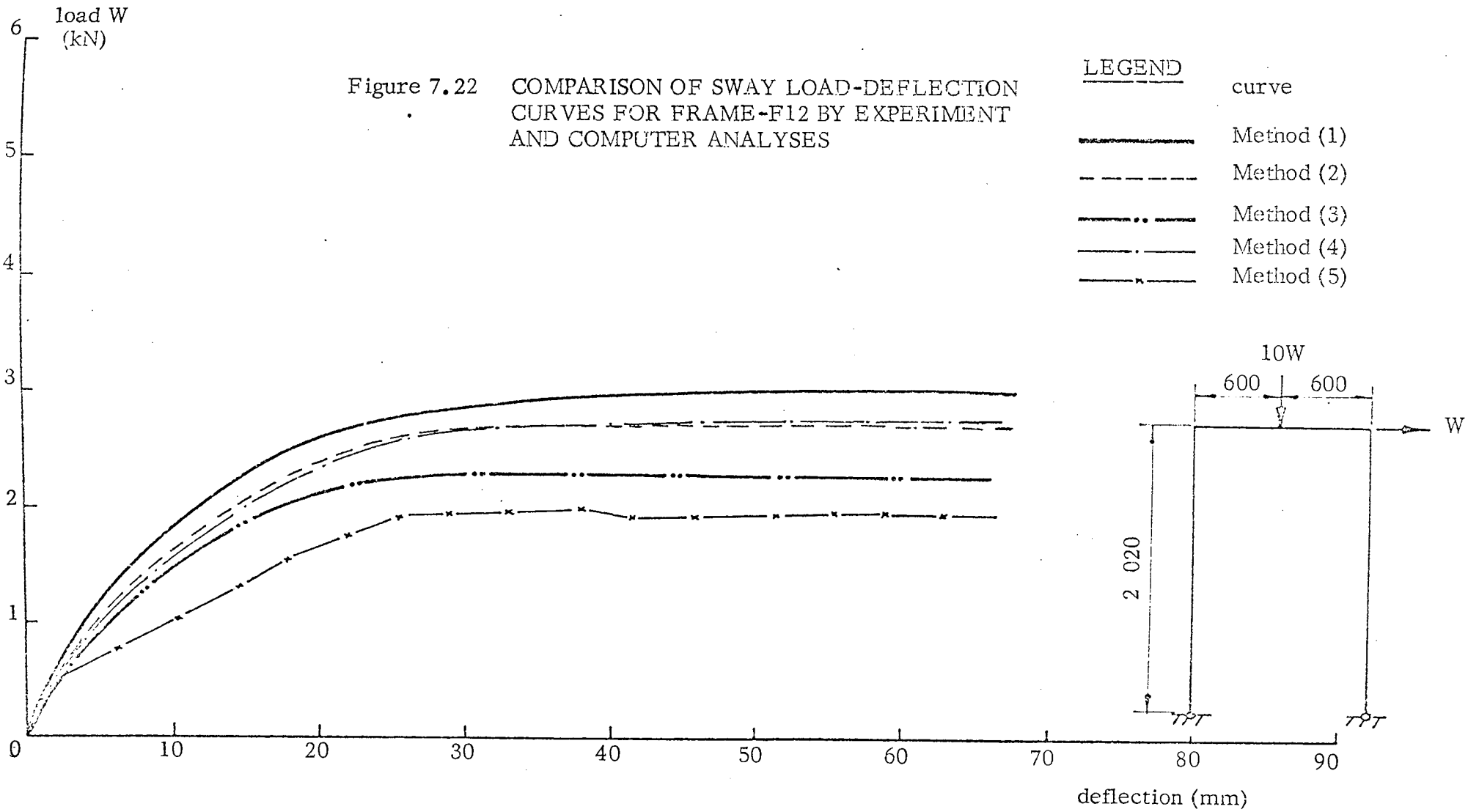

Figure 7.22 COMPARISON OF SWAY LOAD-DEFLECTION CURVES FOR FRAME-F12 BY EXPERIMENT AND COMPUTER ANALYSES

Therefore, where a good agreement exists between the computed and experimental results, the computer analysis is predicting a stiffer overall behaviour than is in fact occurring. This over-estimation of stiffness is most apparent in the incremental analysis which utilises the $(EI)_t - \emptyset$ properties obtained from the beam tests. In Chapter 3, where the incremental analysis is presented, it is assumed that when small increments of load ΔL are applied to a frame, the flexural rigidities of its members obtained from their $(EI)_t - \emptyset$ diagrams at the previous load increment can be representative of their stiffness for the whole increase in load ΔL. If this assumption is not true in reality, then the stiffness of a frame is overestimated for the range of increase in load.

The errors incurred by this overestimation of stiffness may then accumulate and cause a "drift" from the true equilibrium path. The overall result is a deviation from the true behaviour of a frame. It is possible that errors prevalent from an overestimation in the true stiffness of the frame may have contributed to the collapse loads of the incremental computer analysis being in excess of the "true" experimental values..

The incremental analysis which utilised the $(EI)_t - \emptyset$ properties acquired by the method presented in Chapter 2, yields results which are lower than those of method 2. This $(EI)_t - \emptyset$ diagram comprises of a series of vertical and horizontal lines, i.e. EI values are constant for ranges of values of curvature $\emptyset$ between ; $O - \emptyset_c$; $\emptyset_c - \emptyset_y$ and $\emptyset_y - \emptyset_u$. In these regions, the assumption of constant stiffness for the whole increase of ΔL's is accurate. A contributory cause of the low results obtained by use of the theoretical $(EI)_t - \emptyset$ diagram is due to the underestimation of the actual EI values throughout the whole $M - \emptyset$ relationship, especially at the transition regions, i.e. cracking of concrete and yielding of steel. So it is expected that by this method, the overall load-deflection curves will show a less stiff response to load in comparison to method 2.

In the post steel yield states in the experimental tests, the sway displacements were significant. The frames were, therefore, subject to the P - Δ effect. In the computer analyses presented in this thesis, the effect of gross deformations of a frame have been neglected. This assumption may have resulted in the computer analyses predicting a load-deflection response which is stiffer than that actually occurring in a frame due to the P - Δ effect.

The load factor analysis (method 5), described in Chapter 4, in all cases, predicts a collapse load and load-deflection curve which give a far less stiff response to load when compared with the experimental results. The curve is also discontinuous in nature. In Chapter 4, reasons for all these discrepancies are discussed.

7.5 The effect of axial load in the columns on the results of frame F13

To test the effect of heavy axial load on the moment-curvature properties of the most heavily loaded section in the test series (i.e. columns of the two-storey frames), two extra tests were performed on beams of this section, subject to axial loading of 20 kN and 40 kN. These values were selected as being the average and greatest loading, present in these frames. Frame F13 was analysed by method 2 using the $(EI)_t$ - Ø properties obtained from these tests for the column members of the frame. The curves obtained in an incremental analysis are by :-

a) Using the $(EI)_t$ - Ø properties with no axial load acting on the beam.

b) The $(EI)_t$ - Ø properties with 20 kN acting axially on the beam.

c) The $(EI)_t$ - Ø properties with 40 kN acting axially on the beam, and

these are compared with the experimental curve in fig. 7.23. From this figure, it can be seen that there is little difference between the curves obtained by the computer analyses using a), b) and c). The maximum difference in collapse loads is 1.4%. It may thus be concluded that in fact, the presence

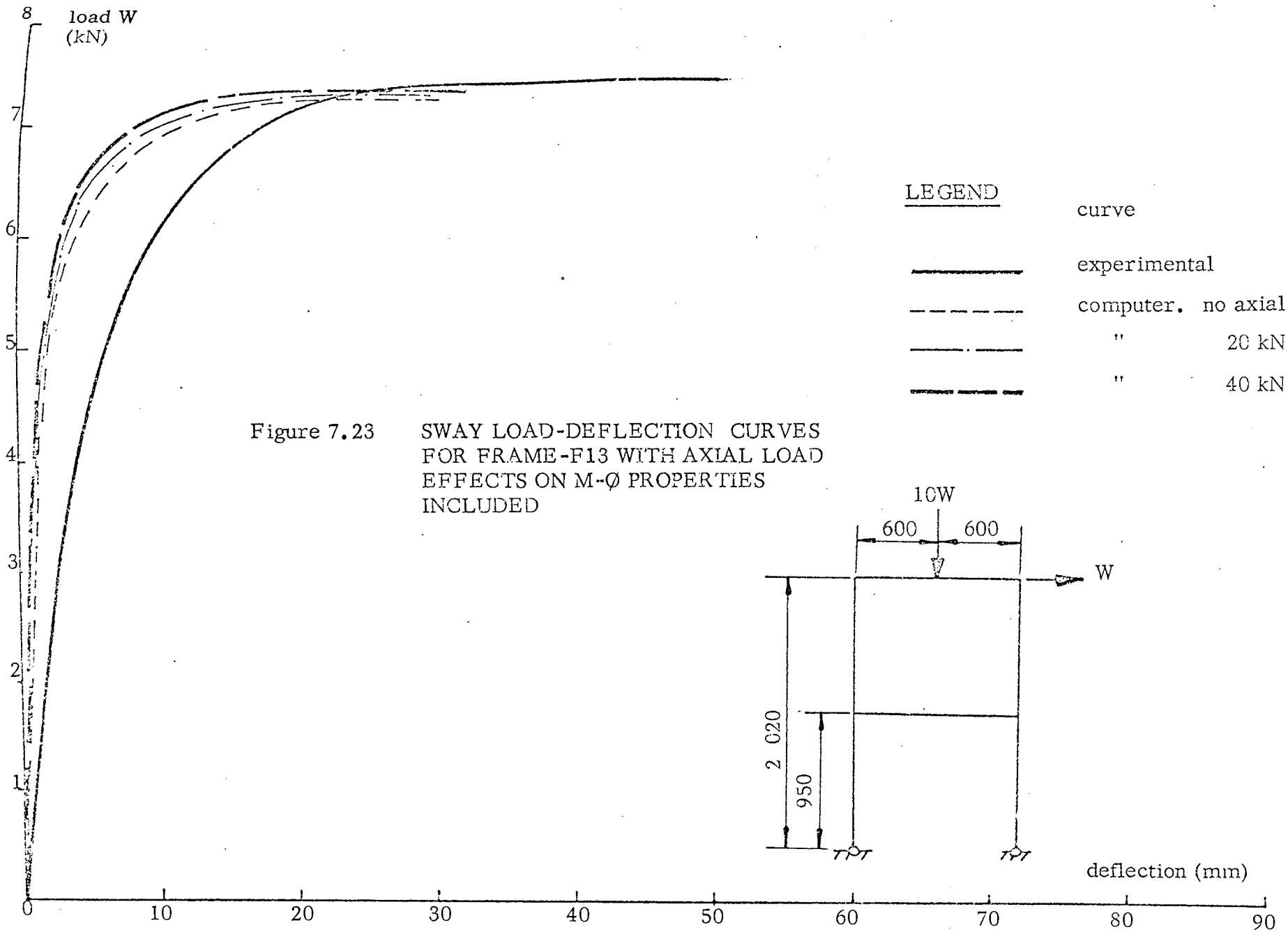

Figure 7.23 SWAY LOAD-DEFLECTION CURVES FOR FRAME-F13 WITH AXIAL LOAD EFFECTS ON M-Ø PROPERTIES INCLUDED

of axial loading has little effect on the overall behaviour of the frames tested and reported in this thesis, with regard to the properties of the members.

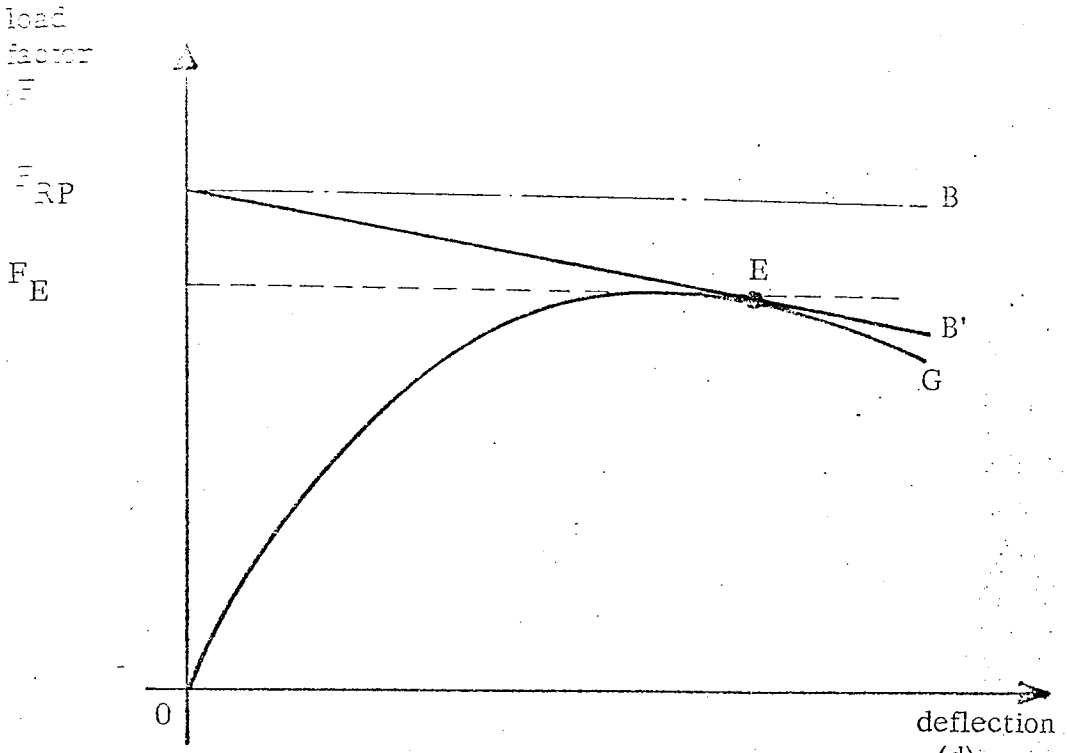

fig. 7.24

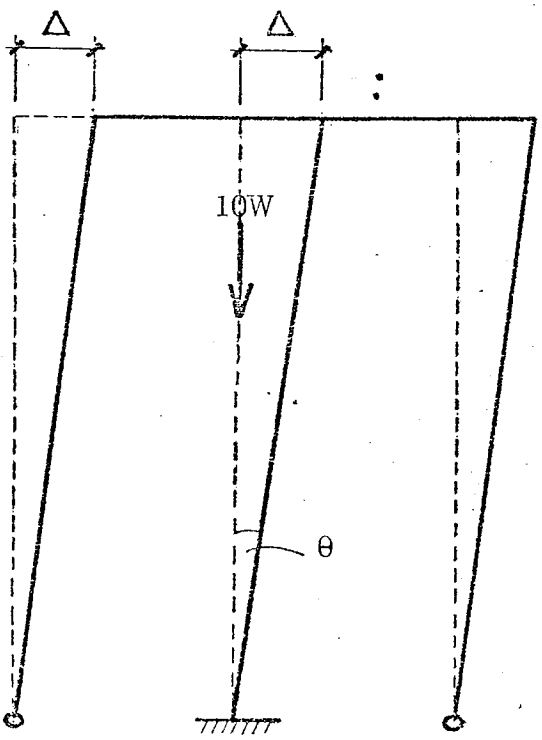

Rigid
Connection

(a)

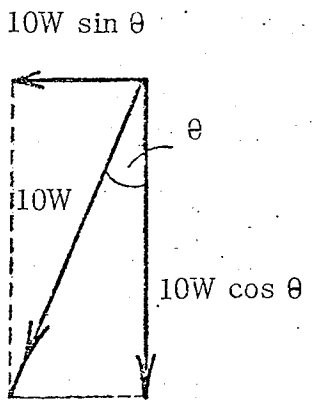

Force Diagram

(b)

fig. 7.25

CHAPTER 8

GENERAL CONCLUSIONS

8.1 Summary

Earlier in this thesis, it was stated that the main objective of the present work was to investigate whether computer analyses, similar to those in existence for predicting the behaviour of steel frames could be developed, specifically for reinforced concrete frames. The behaviour of reinforced concrete, particularly with reference to its bending moment-curvature relationship, was examined. This relationship was shown to be highly non-linear, and in the case of under-reinforced concrete sections, a great deal of reserve strength was shown to be available after first yield of tensile steel. Thus, a concept of gradual reducing flexural rigidity upto collapse was adopted. This was assumed to be more fundamental than the supposition of the formation of plastic hinges at discrete sections. Two methods were presented for determining the moment-curvature relationship of reinforced concrete sections. The first was to carry out tests on beams of the required section, the curvature being measured for each increment of bending moment induced in the beam by the application of external load. The second method was to consider the stress-strain behaviour of a section at first cracking of concrete, first yield of tensile reinforcement and in its ultimate state. By adopting suitable assumptions, a theoretical method was proposed for constructing the relationship. From these moment-curvature relationships, the more convenient instantaneous flexural rigidity-curvature diagrams were obtained.

The first of the analyses presented utilised an incremental technique to account for the non-linearity of the material. By this method, small increments of proportional load are imposed on a frame, and for each increment,

a linear analysis performed. From the resulting bending moment, and hence, curvature distribution, the flexural rigidity of the members of a frame were adjusted. These linear analyses were summed to furnish the overall behaviour of a frame upto collapse. To account for the change in stiffness along the members of a frame, the latter were divided into small submembers. For each submember, the larger of the induced bending moments was assumed to act along the entire length of the submember. The effect of the number of these subdivisions, and the values of load increment imposed on the accuracy of the analysis were examined.

The second computer analysis proposed was a development of Majid and Anderson's program (18). For this, the moment-curvature relationship of reinforced concrete was idealised as a series of straight lines. The nodes at which these lines met, and where a change in slope (i.e. flexural rigidity) occurred were termed critical points. The analysis predicts load factors at which critical point bending moments are attained in a frame. To account for the non-linearity present, an iterative process was employed which required convergence between successive values of predicted load factors. Upon attainment of a critical point, the flexural rigidity of the critical member was reduced accordingly, and the search for the next critical load factor initiated. A similar technique of frame subdivisions was used. Both the computer analyses traced the load deflection history of frames upto and including collapse.

The validity of these analyses were examined by carrying out tests on pin-ended reinforced concrete frames upto collapse. From each test, a complete load-deflection history was obtained. The properties of each section employed in the test series was found by performing tests on beams which were manufactured with the frames. The effect of the largest axial load present in the test series was examined with reference to the moment-curvature relationship, and

complete load deflection behaviour of a frame. Finally, a comparison of the results obtained by the computer analyses, experimental tests and the rigid-plastic theory for each frame was presented.

8.2 Conclusions

The following conclusions can be drawn from the results of this work.

8.2.1 The non-linear moment-curvature relationship of reinforced concrete can be obtained experimentally and from an appropriate theory. In the case of the former, an allowance for the secondary effect of creep may be made, if a sufficient time interval is given between the applications of dead load. The sections used in the frames were not designed, thus, special assumptions were necessary for constructing the moment-curvature relationship theoretically. For most cases, these assumptions proved reliable, when compared with the experimental evidence. The main difference in the relationships by the two methods was that by theory, the curve flattened abruptly after first yield of tensile steel in comparison to the gradual change shown by experiment.

The maximum axial load in a member of the frame test series had some effect on its moment-curvature relationship. The initial and cracked state stiffnesses and bending moment at yield of steel were increased, after yield however, a very small increase in bending moment was present and a reduced amount of reserve strength was indicated.

From the moment-curvature relationship, the instantaneous flexural rigidity-curvature diagram may be found. This curve is more suitable for use with a computer analysis as the flexural rigidity is given directly for values of curvature.

8.2.2 The tests reported in Chapter 5 provided the load deflection curves of the portal frames upto and including collapse. Utilising a dead loading sytem, the secondary effects of creep and cracking of the reinforced concrete were allowed

to take place. This was possible since the magnitude of the applied load remained constant. One disadvantage of this system is that no account can be made of unloading in a frame. It has also been demonstrated in Chapter 7 that when large sway displacements are present, the use of a rigid fulcrum to the lever system caused discrepancies in the true magnitude of the applied loading.

A good agreement was indicated between the results of the tests performed on identical frames, implying that if care is taken in manufacture, single tests will represent the behaviour of specific frames.

Generally, the joint detailing used in the frames was good and hence, a reasonable transmission of bending moments to members could be assumed. Localised effects of failure were only indicated in the over-reinforced section of F11, and in the joints connecting the lower beam to the columns of the two-storey frames. It is possible, however, that this did not contribute to any loss of strength of the frames.

For the range of tests performed, the presence of any high shear stresses did not appear to cause any premature failure.

8.2.3 In Chapter 7, it was shown that the rigid-plastic collapse loads obtained, utilising the ultimate moments M_u of the reinforced concrete sections of the frames, were lower than those obtained by experiment. In most cases, it is expected that the rigid-plastic theory would yield collapse loads greater than those actually occurring if non-linear effects are excluded. The main causes of the differences in these values of collapse loads were discussed in the previous chapter. The first of these was attributed to the experimental discrepancy incurred by the vertical loading system. This caused a reduction in the value of sway load imposed upon a frame due to an induced horizontal component of load as the sway displacements became large. This also meant that the loading was not truly proportional.

It was also suggested that the experimental collapse load may be larger than the rigid plastic collapse load due to the axial load-moment interaction. This 'intereaction' may have caused an increase in the values of ultimate moment of the column members, and hence, collapse loads.

8.2.4 It has been shown that computer analyses may be formed to analyse reinforced concrete frames. The analyses can deal with any shape of moment-curvature relationship. In their present form, the computer programs can deal only with the moment-curvature relationships of sections which are subject to axial loads of fixed value. The programs can deal with varying properties and stiffnesses along the members of a frame. This is achieved by division of the members into smaller sub-members. It has been shown that a relatively small number of subdivisions are required to represent the varying stiffness of frames accurately. By increasing the number, little improved accuracy is achieved, while a large increase in computer time and storage requirement is necessary.

The effect of the value of load increment used in the analysis was investigated. It was shown that values equal to 2% of the eventual collapse load initially, and subsequently, a reduction of 25% after first yield of steel, furnished results which were not improved by use of smaller values.

The incremental analysis which utilises the $(EI)_t - \phi$ relationships obtained from the beam tests has been shown to agree well with the experimental results reported. Since the experimental results are, however, in excess of their "true" values, this would suggest that the incremental analysis yields results which are greater than those actually occurring in a frame. It is possible that this method will give higher values of collapse load since the analysis does not have the facility to allow for the $P - \Delta$ effect. Thus, there may be an overestimation in the true collapse load by this computer analysis.

One of the main assumptions adopted in the incremental analysis is that the flexural rigidities of the members of a frame remain constant for an increase in loading ΔL. This assumption may lead to a slight overestimation of the true behaviour of the frame for each load increment. The cumulative effect of these overestimations may cause a drift from equilibrium resulting in an overestimation of the overall behaviour of a frame.

When the $(EI)_t$ - $\emptyset$ relationship obtained by the method described in Chapter 2 is used in the incremental analysis, the results obtained are lower than the experimental values. By this method, the assumption of constant EI for an increment of load ΔL is true. However, at the transition regions of the M - $\emptyset$ relationships, i.e. cracking of concrete and yielding of steel, this method underestimates the true behaviour of a frame since abrupt changes in EI are assumed at these points.

In Chapter 3, a method has been presented that may ensure that no overestimation in EI of the members of a frame, for an application of load increment, will occur. This is possible by use of an iterative technique which requires the convergence of successive values of induced member curvature in an iterative cycle for each increment of load applied to a frame. In addition to this iterative procedure, it is suggested that an equilibrium check is performed at every three or four load increments to ensure that equilibrium of the internal and external forces is being maintained throughout the analysis.

8.2.5 The modified analysis which uses a factored bending moment distribution in conjunction with reduced frame subdivision gives good results and can be used as a quick, economic method for testing section sizes prior to analysing the fully subdivided frame.

8.2.6 The effect of axial loads on the M - $\emptyset$ relationship of the most heavily loaded section in any of the frames was investigated. The M - $\emptyset$ relationships

thus obtained were used in an incremental analysis of this frame. The load-deflection curves obtained, indicated that these axial loads had an insignificant effect upon the overall behaviour of the frame.

8.2.7 The analysis presented in Chapter 4 viz. the load factor method gave load displacement curves for frames which were discontinuous in nature. The discontinuity was due to a cycling of the values of load factor at which consecutive critical points of the members of a frame were attained. This cycling occurred because the analysis did not follow the true loaded behaviour of a frame. During the analysis, upon attainment of a critical point in a member, the stiffness of that member, and hence, that of the frame is reduced. The modified overall stiffness matrix K' of the frame was then used to predict the load factor, F, for the next critical point under a full loading from zero to F.

This procedure is not strictly true in reality, since the modified K is only representative of the stiffness of the frame for the increase of load from that at the previous critical point to the next critical point. For this reason, the load factor analysis yielded load-displacement curves of a discontinuous form.

A modification to this analysis was presented in Chapter 4 which might ensure that the modified stiffness matrix of a frame is only used for the increase in loading from one critical point to the next.

8.3 Suggestions for future research

8.3.1 Research on the subject covered by this thesis is far from complete. For the analysis presented in Chapter 3, it is suggested that the iterative technique discussed is incorporated into the basic incremental approach. The so-formed analysis, in addition to an equilibrium check, will then ensure that the results obtained from an analysis satisfy equilibrium rigidly, with no residual error due to non-convergence, at each load increment.

For the load-factor analysis of Chapter 4, it is suggested that the modi-

fication discussed is utilised. This will ensure that a true representation of the stiffness of the frame, at any stage in its loading history, is given.

In both the computer analyses presented, the effect of gross deformations of a frame have been neglected. This assumption is valid if a frame has 'stout' proportions, but may not be true for the case of slender sway frames. It is, therefore, suggested that the analyses are modified so that if sway displacements of a frame are significant, an allowance for the inherent P -Δ effect is incorporated.

For the analyses, the dimensions of a frame are those corresponding to its centre line throughout. If the members are deep in section, there will be some 'gusset' action in the frame especially at main joints. This effect will obviously increase the stiffness of a frame at these joints if they are adequately reinforced. It may, therefore, be desirable to investigate the significance of this gusset effect.

If the computer analyses are to be used to analyse slender, multi-storey frames, the action of heavy axial loading present in the lower columns of a frame must be accommodated. This would enable a check against instability to be performed.

8.3.2 On the experimental side, it would be desirable to perform further tests on scaled reinforced concrete frames of practical proportions, i.e. utilising the recommendation of CP110(1). The frames should be detailed by conventional methods to assess the effect of this detailing, especially at joints, on the overall behaviour of the frames. It would be desirable for these frames to have many degrees of freedom. A check on whether the computer analyses were predicting accurately the loads at which plastic hinges were forming, could thus be performed by following accurately, the formation of these plastic hinges throughout the experimental loading history.

If the dead-loading system such as adopted in this work is to be used, the following precautions are suggested.

i) The ratio of vertical to side load is reduced.

ii) If the sway displacements become of such magnitude that they induce a significant horizontal component of load which acts in opposition to the applied side load, then the magnitude of this component is assessed, and the appropriate amount of load added to the side load. This will ensure that the loading is kept proportional throughout the loading history.

8.3.3 The overall strength of practical reinforced concrete structures is significantly increased by the presence of floor slabs and cladding. The extent of this stiffening effect requires investigation. For reinforced concrete buildings, a similar approach to that of Onen (22) is suggested.

APPENDIX (1)

DETAILS OF FRAMES FOR COMPUTER ANALYSES

A1.1 Representation of Frames

The frames were subdivided and load increments chosen in accordance with the conclusions of Chapter 3. For each different frame, two schematic line diagrams are presented. These lines correspond to the centre of each member. The member and joint reference numbers are given in the first of these diagrams. The second diagram shows the subdivided frame with the submember, subjoint and real hinge numbers. The applied loads together with their degrees of freedom on both diagrams are given in the second diagram. The length of each submember and the inclination, sectional area and stiffness properties of each reference member (first diagram) are presented. The stiffness properties of the members quoted are for the following :-

(i) $(EI)_t$ - $\emptyset$ data obtained from the beam tests described in Chapter 6.

(ii) $(EI)_t$ - $\emptyset$ data obtained from the theory of Chapter 2.

(iii) M - $\emptyset$ data obtained from the beam tests of Chapter 6.

A sample data for the incremental computer analysis is presented for Frame F1.

A1.2 Frame Set 1 (F1, F2 & F3)

The frames of this set are identical in geometry and section size, the only variable being the stiffness properties of the members. The schematic diagrams of the frames of this set are shown in fig. A1.1 (a, b & c), the lengths of each submember, in mm, from numbers 1 to 28 are :-

612.5	300.0	150.0	75.0	25.0	50.0	100.0	194.5	193.0	100.0
50.0	25.0	12.0	24.0	48.0	84.0	85.5	48.0	24.0	12.0
20.0	40.0	80.0	160.0	200.0	210.0	213.5	214.0		

The properties of each reference member are given in Table A1.1.

TABLE NO. (A1.1)

Member Reference No.	Area of Section (mm^2)	Inclination
1	12 500.0	270.0
2	12 500.0	90.0
3	12 500.0	0.0
4	12 500.0	0.0
5	12 500.0	270.0

This set of frames consists of members which are of constant cross-section, thus for each frame, just one relationship is necessary to define the stiffness properties of their members. For the incremental analysis of the frames, the $(EI)_t$ - $\emptyset$ relationships used are given below in Tables (A1.2 & A1.3)

(a) From the beam tests of Chapter 6 (figures 6.16, 6.17 & 6.18), 8 points are used to represent the diagrams.

TABLE NO. (A1.2)

Point	FRAME NO.					
	F1		F2		F3	
	$(EI)_t \times 10^{11}$ Nmm^2	$\emptyset \times 10^{-6}$ 1/mm	$(EI)_t \times 10^{11}$ Nmm^2	$\emptyset \times 10^{-6}$ 1/mm	$(EI)_t \times 10^{11}$ Nmm^2	$\emptyset \times 10^{-6}$ 1/mm
1	5.400	0.0	5.400	0.0	5.400	0.0
2	5.400	1.2	5.400	1.2	5.400	1.2
3	1.400	3.0	1.310	2.9	1.298	3.0
4	1.374	13.3	1.245	22.6	1.232	21.5
5	1.305	20.8	1.157	24.7	1.166	26.8
6	0.783	27.8	0.174	33.4	0.062	40.8
7	0.089	52.3	0.057	61.0	0.025	108.0
8	0.060	109.0	0.025	110.0	0.013	111.0

(b) From the theory of Chapter 2, 6 points represent the diagram.

TABLE NO. (A1.3)

Point	$(EI)_t$ x 10^{11} Nmm^2	Ø x 10^{-6} 1/mm
1	5.320	0.00
2	5.320	1.82
3	1.237	1.82
4	1.237	27.15
5	0.039	27.15
6	0.039	116.00

For the load factor analysis, the M - Ø relationships of Frames F1, F2 & F3, fig. 6.6 are represented by five points and the values are given in Table A1.4 below.

TABLE NO. (A1.4)

Point	FRAME NO.					
	F1		F2		F3	
	M x10^5 Nmm	Ø x10^{-6} 1/mm	M x10^5 Nmm	Ø x10^{-6} 1/mm	M x10^5 Nmm	Ø x10^{-6} 1/mm
1	8.00	1.52	8.00	1.52	8.00	1.52
2	39.36	24.56	39.36	26.90	39.36	25.72
3	42.50	31.00	41.00	30.00	41.00	31.00
4	44.00	36.00	41.80	33.40	41.80	35.00
5	49.00	109.00	46.00	110.00	45.00	110.00

A1.3 Data for the Incremental Analysis of Frame F1 using the beam test $(EI)_t$ - Ø properties.

FO1/S028 (Frame serial number)

28 27 2 5 4 2 1 8 5 4 8

No. of submembers; No. of subjoints; No. of real hinges; No. of full members; No. of full joints; No. of loads; Counter; No. of points on $(EI)_t$ - $\emptyset$ curve; Point at which $\emptyset$ in data reaches the elastic plastic stage (i.e. to reduce load increment); Counter for reduced output; No. of submembers for which member forces are required.

4.0 (Value by which load increment is divided for reduced value)

2.9E4 1.0E6

Concrete modulus of elasticity ; terminating (EI) value.

1 2 2 2 3 3 3 3 3 3

3 3 4 4 4 4 4 4 4 4 member reference number for each submember

5 5 5 5 5 5 5 5

1 4 12 20

Joint numbers of main joints (1st diagram) on divided frame also joints at which load displacement values are output.

1 4 5 12 13 20 21 28

submembers numbers for which member forces are output

1 1 2 3 4 5 6 7 8 9 10 11 12 13 14 15 16 17 18

19 20 21 22 23 24 25 26 27

0 2 3 4 5 6 7 8 9 10 11 12 13 14 15 16 17 18 19

20 21 22 23 24 25 26 27 0

(2 arrays of subjoint numbers at first and second ends of each submember).

612.5 300.0 150.0 75.0 25.0 50.0 100.0 194.5 193.0 100.0

50.0 25.0 12.0 24.0 48.0 84.0 85.5 48.0 24.0 12.0

20.0 40.0 80.0 160.0 200.0 210.0 213.5 214.0

length of each submember

12 500.0 12 500.0 12 500.00 12 500.00 12 500.00

Area of each reference member

27.0 90.0 0.0 0.0 270.0

Inclination of each reference member

8	35	-1000.0
10	58	100.0

applied loads

degrees of freedom on both schematic diagrams and values of applied loading

2	82
56	83

real hinge numbers for submembers

5.4 E11	5.4 E11	5.4 E11	5.4 E11	5.4 E11
5.4 E11	5.4 E11	5.4 E11	5.4 E11	5.4 E11
1.4 E11	1.4 E11	1.4 E11	1.4 E11	1.4 E11
1.38 E11	1.38 E11	1.38 E11	1.38 E11	1.38 E11
1.31 E11	1.31 E11	1.31 E11	1.31 E11	1.31 E11
7.83 E10	7.83 E10	7.83 E10	7.83 E10	7.83 E10
8.85 E9	8.85 E9	8.85 E9	8.85 E9	8.85 E9
6.03 E9	6.03 E9	6.03 E9	6.03 E9	6.03 E9
0.0	0.0	0.0	0.0	0.0
1.2 E-6	1.2 E-6	1.2 E-6	1.2 E-6	1.2 E-6
3.0 E-6	3.0 E-6	3.0 E-6	3.0 E-6	3.0 E-6
13.28 E-6	13.28 E-6	13.28 E-6	13.28 E-6	13.28 E-6
20.8 E-6	20.8 E-6	20.8 E-6	20.8 E-6	20.8 E-6
27.84 E-6	27.84 E-6	27.84 E-6	27.84 E-6	27.84 E-6
52.31 E-6	52.31 E-6	52.31 E-6	52.31 E-6	52.31 E-6
109.0 E-6	109.0 E-6	109.0 E-6	109.0 E-6	109.0 E-6

$(EI)_t$ - $\emptyset$ properties

A1.4 Frame Set 2 (F4 & F5)

Again, the frames in this set are identical, the schematic diagrams are shown in fig. A1.2. The lengths of each submember are :-

702.5	600.0	320.0	160.0	80.0	40.0	20.0	10.0	62.5	60.0
125.0	115.0	80.0	40.0	20.0	10.0	10.0	20.0	40.0	242.0
130.5	40.0	20.0	10.0	10.0	20.0	40.0	80.0	160.0	320.0
600.0	702.5								

The properties of the reference members are given in Table A1.5

TABLE NO. (A1.5)

Member Reference No.	Area of Section (mm^2)	Inclination
1	17 500.0	270.0
2	17 500.0	90.0
3	17 500.0	0.0
4	17 500.0	0.0
5	17 500.0	270.0

The frames are of constant cross-section, the $(EI)_t$ - Ø properties of each frame are given in Tables (A1.6 and A1.7)

(a) For the experimental relationships figs. 6.19; 6.20, 8 and 10 points are used to represent the diagrams

TABLE NO. (A1.6)

Point	FRAME NO.			
	F4		F5	
	$(EI)_t \times 10^{11}$ Nmm^2	Ø $\times 10^{-6}$ 1/mm	$(EI)_t \times 10^{11}$ Nmm^2	Ø $\times 10^{-6}$ 1/mm
1	15.20	0.00	15.01	0.00
2	15.20	0.86	15.01	0.87
3	2.97	2.41	4.46	1.24
4	2.06	7.06	2.91	2.47
5	2.02	19.14	2.63	4.37
6	0.55	22.25	2.60	15.90
7	0.21	30.20	0.56	21.10
8	0.07	92.00	0.21	26.80
9	-	-	0.18	42.00
10	-	-	0.04	89.00

(b) For the theoretical relationships, 6 points represent the diagram.

TABLE NO. (A1.7)

Point	$(EI)_t \times 10^{11}$ Nmm^2	$\emptyset \times 10^{-6}$ 1/mm
1	14.070	0.0
2	14.070	1.3
3	2.610	1.3
4	2.610	16.8
5	0.047	16.8
6	0.047	81.0

The 5 point representation of the M - $\emptyset$ relationships of fig. 6.7, used for the load factor analysis are shown in Table A1.8.

TABLE NO. (A1.8)

Point	FRAME NO.			
	F4		F5	
	$M \times 10^5$ Nmm	$\emptyset \times 10^{-6}$ 1/mm	$M \times 10^5$ Nmm	$\emptyset \times 10^{-6}$ 1/mm
1	1.81	1.2	1.88	1.05
2	55.00	19.1	56.50	23.00
3	57.20	22.2	58.00	26.00
4	59.30	30.0	60.50	30.00
5	67.50	92.0	66.0	89.00

A1.5 Frame Set 3 (F6, F7 & F13)

The schematic diagrams for the identical frames of this set are shown in fig. A1.3. The lengths of each submember are :-

442.5	240.0	120.0	60.0	580.0	280.0	140.0	70.0	62.5	60.0
125.0	115.0	80.0	40.0	20.0	10.0	20.0	40.0	80.0	172.0
95.0	60.0	30.0	15.0	20.0	40.0	80.0	160.0	225.0	225.0
220.0	100.0	60.0	120.0	240.0	442.5	30.0	60.0	120.0	226.0
379.0	120.0	60.0	30.0						

The properties of the reference members are given in Table A1.9.

TABLE NO. (A1.9)

Member Reference No.	Area of Section (mm^2)	Inclination
1	17 500.0	270.0
2	17 500.0	90.0
3	17 500.0	90.0
4	17 500.0	0.0
5	17 500.0	0.0
6	17 500.0	270.0
7	17 500.0	270.0
8	17 500.0	0.0

The $(EI)_t$ - Ø properties of the constant section of each frame in this set are given in Table A1.10. 8 points are used to represent the experiment diagrams of figure 6.18.

TABLE NO. (A1.10)

Point	FRAME NO.					
	F6		F7		F13	
	$(EI)_t \times 10^{11}$ Nmm^2	Ø $\times 10^{-6}$ 1/mm	$(EI)_t \times 10^{11}$ Nmm^2	Ø $\times 10^{-6}$ 1/mm	$(EI)_t \times 10^{11}$ Nmm^2	Ø $\times 10^{-6}$ 1/mm
1	15.15	0.00	15.15	0.00	14.20	0.00
2	15.15	0.86	15.15	0.86	14.20	1.10
3	4.57	1.22	5.47	1.70	3.07	2.40
4	2.95	2.54	3.61	2.18	3.07	9.70
5	2.64	4.38	2.11	6.82	2.81	12.90
6	2.61	15.66	2.06	18.60	1.56	17.28
7	0.57	20.81	0.24	26.46	0.24	27.16
8	0.05	86.00	0.07	97.00	0.12	82.00

The 6 point representation of the theoretical $(EI)_t$ - ϕ diagram for the sections of the frames in this set are as quoted in Table A1.7.

The M - ϕ relationships of figure 6.8 are represented by 5 points in Table A1.11.

TABLE NO. (A1.11)

Point	FRAME NO.					
	F6		F7		F13	
	$M \times 10^5$ Nmm	$\phi \times 10^{-6}$ 1/mm	$M \times 10^5$ Nmm	$\phi \times 10^{-6}$ 1/mm	$M \times 10^5$ Nmm	$\phi \times 10^{-6}$ 1/mm
1	17.2	1.7	18.0	1.7	18.0	1.74
2	54.0	15.6	54.7	18.6	57.1	14.80
3	58.0	20.0	56.2	21.0	62.0	17.28
4	60.0	27.0	57.0	25.0	64.5	27.16
5	68.0	86.0	70.0	97.0	74.0	82.00

A1.6 Frame Numbers F9, F10, F11 & F12

The schematic diagrams for these frames are given in fig. A1.4.

The lengths of the submembers of each frame are :-

(i) F9
702.0 600.0 320.0 160.0 80.0 40.0 20.0 10.0 40.0 58.0
134.5 130.0 80.0 40.0 20.0 10.0 10.0 20.0 40.0 233.0
139.5 40.0 20.0 10.0 10.0 20.0 40.0 80.0 160.0 320.0
600.0 702.0

(ii) F10
702.5 600.0 320.0 160.0 80.0 40.0 20.0 10.0 62.5 60.0
145.0 120.0 80.0 40.0 20.0 10.0 10.0 20.0 40.0 288.0
109.5 40.0 20.0 10.0 10.0 20.0 40.0 80.0 160.0 320.0
600.0 702.5

(iii) F11 & F12
722.5 600.0 320.0 160.0 80.0 40.0 20.0 10.0 44.0 30.0
183.5 130.0 80.0 40.0 20.0 10.0 10.0 20.0 40.0 228.0
169.5 40.0 20.0 10.0 10.0 20.0 40.0 80.0 160.0 320.0
600.0 722.5

The properties of the reference members of each frame are given in Table A1.12

TABLE NO. (A1.12)

F9 Member Reference No.	Area of Section $(mm)^2$	Inclination
1	17 500.0	270.0
2	17 500.0	90.0
3	17 500.0	0.0
4	17 500.0	0.0
5	17 500.0	0.0
6	17 500.0	0.0
7	17 500.0	270.0
F10		
1	12 500.0	270.0
2	12 500.0	90.0
3	17 500.0	0.0
4	17 500.0	0.0
5	17 500.0	0.0
6	17 500.0	0.0
7	12 500.0	270.0
F11 & F12		
1	12 500.0	270.0
2	12 500.0	90.0
3	12 500.0	0.0
4	12 500.0	0.0
5	12 500.0	0.0
6	12 500.0	0.0
7	12 500.0	270.0

The frames F9, F10, F11 & F12 each contain varying sections. In all cases 3 $(EI)_t$ - $\emptyset$ relationships are necessary to fully define a frame's properties. For Frames F9 & F10, 10 points are used in Table A1.13 to define the experimental relationships of figures (6.19 - 6.22), and for Frames F11 & F12, 8

points represent the relationships of figures (6.23 - 6.26)

TABLE NO. (A1.13)

Point	SECTION NO.					
	9.1		9.2		9.3	
	$(EI)_t \times 10^{11}$ Nmm^2	$\phi \times 10^{-6}$ 1/mm	$(EI)_t \times 10^{11}$ Nmm^2	$\phi \times 10^{-6}$ 1/mm	$(EI)_t \times 10^{11}$ Nmm^2	$\phi \times 10^{-6}$ 1/mm
1	14.10	0.00	13.10	0.00	13.60	0.00
2	14.10	0.96	13.10	1.01	13.60	1.00
3	6.27	1.64	4.31	2.34	2.98	2.69
4	4.41	2.56	2.14	4.62	2.17	3.64
5	3.45	5.36	2.13	9.22	1.78	9.17
6	3.41	16.88	2.12	13.82	1.76	14.69
7	3.22	19.84	2.10	18.36	1.64	19.00
8	0.71	24.20	0.50	21.54	0.65	21.32
9	0.25	32.57	0.20	33.54	0.28	31.20
10	0.13	80.00	0.13	78.00	0.19	74.00
	10.1		10.2		10.3	
1	18.80	0.00	5.18	0.00	14.00	0.00
2	18.80	0.80	5.18	1.00	14.00	0.90
3	5.56	1.49	0.99	2.20	2.74	2.00
4	3.80	6.00	0.99	5.00	1.86	3.27
5	3.74	13.77	0.99	16.65	1.80	10.10
6	3.58	16.45	0.98	21.61	1.63	17.11
7	2.35	18.10	0.97	24.13	0.55	19.91
8	0.74	21.85	0.29	28.85	0.22	30.10
9	0.16	35.73	0.06	60.88	0.12	70.00
10	0.11	91.00	0.04	90.00	0.08	100.0

	11.1		11.2		11.3	
1	4.72	0.00	5.20	0.00	6.00	0.00
2	4.72	2.60	5.20	1.00	6.00	1.00
3	3.40	6.54	0.90	3.00	0.99	2.60
4	3.40	9.42	0.90	10.00	0.98	19.79
5	2.61	16.07	0.90	20.00	0.86	27.70
6	2.61	35.02	0.90	27.69	0.37	29.86
7	2.19	36.86	0.22	38.93	0.14	36.10
8	1.73	42.54	0.03	101.00	0.05	128.00
	12.1		12.2		12.3	
1	5.38	0.00	5.70	0.00	5.40	0.00
2	5.38	1.00	5.70	1.00	5.40	1.20
3	1.29	2.40	1.64	2.10	1.09	2.80
4	1.29	8.91	1.54	7.99	0.98	13.29
5	1.26	24.42	1.44	14.79	0.89	27.37
6	0.16	32.95	1.44	29.10	0.15	32.57
7	0.06	55.50	0.68	32.15	0.04	72.63
8	0.02	108.00	0.06	108.00	0.02	125.00

The theoretical relationships are represented by 6 points in Table A1.14

TABLE NO. (A1.14)

Point	SECTION NO.					
	9.1		9.2		9.3	
	$(EI)_t \times 10^{11}$ Nmm^2	$\phi \times 10^{-6}$ 1/mm	$(EI)_t \times 10^{11}$ Nmm^2	$\phi \times 10^{-6}$ 1/mm	$(EI)_t \times 10^{11}$ Nmm^2	$\phi \times 10^{-6}$ 1/mm
1	14.26	0.00	13.72	0.00	14.10	0.00
2	14.26	1.33	13.72	1.30	14.10	1.28
3	3.44	1.33	1.85	1.30	1.85	1.28
4	3.44	19.14	1.85	17.87	1.85	17.81
5	0.09	19.14	0.09	17.87	0.09	17.81
6	0.09	83.00	0.09	83.00	0.09	80.00

	10.1		10.2		10.3	
1	14.10	0.00	5.13	0.00	14.10	0.00
2	14.10	1.25	5.13	1.17	14.10	1.12
3	1.85	1.25	0.93	1.71	1.85	1.12
4	1.85	19.39	0.93	29.14	1.85	18.20
5	0.09	19.39	0.02	29.14	0.09	18.20
6	0.09	84.00	0.02	120.00	0.09	77.00
	11.1		11.2		11.3	
1	5.00	0.00	5.13	0.00	5.95	0.00
2	5.00	2.50	5.13	1.66	5.95	1.51
3	3.50	7.50	0.93	1.66	0.93	1.51
4	2.60	14.50	0.93	29.38	0.93	28.52
5	2.60	35.00	0.02	29.38	0.02	28.52
6	1.50	40.00	0.02	116.00	0.02	113.00
	12.1		12.2		12.3	
1	5.20	0.00	5.53	0.00	5.19	0.00
2	5.20	1.67	5.53	1.65	5.19	1.63
3	1.24	1.67	1.46	1.65	0.89	1.63
4	1.24	27.95	1.46	33.30	0.89	29.90
5	0.30	27.95	0.57	33.30	0.01	29.90
6	0.30	108.00	0.57	107.00	0.01	112.00

The 5 point representations of the M - Ø relationships of figures (6.9 - 6.15) used for the load factor analyses of frames F9, F10, F11 & F12 are given in Table A1.15.

TABLE NO. (A1.15)

Point	SECTION NO.					
	9.1		9.2		9.3	
	$M \times 10^5$ Nmm	$\emptyset \times 10^{-6}$ 1/mm	$M \times 10^5$ Nmm	$\emptyset \times 10^{-6}$ 1/mm	$M \times 10^5$ Nmm	$\emptyset \times 10^{-6}$ 1/mm
1	17.90	1.64	17.90	2.00	17.90	1.96
2	81.60	19.84	52.20	18.50	49.80	19.00
3	86.00	23.00	55.00	22.00	52.00	21.00
4	89.00	33.00	57.00	30.00	54.00	30.00
5	97.00	80.00	65.00	78.00	65.00	74.00
	10.1		10.2		10.3	
1	17.90	1.50	8.00	1.60	17.90	1.90
2	81.00	18.00	29.50	25.30	44.90	17.10
3	86.50	21.80	32.00	30.00	47.10	20.00
4	88.50	30.00	33.50	40.00	50.00	31.00
5	98.00	91.00	36.00	90.00	60.00	100.00
	11.1		11.2		11.3	
1	12.40	2.62	8.00	2.00	8.00	2.00
2	27.10	6.54	32.00	27.70	32.00	29.10
3	56.50	16.10	33.00	31.50	34.00	33.00
4	110.00	36.90	34.50	37.50	35.00	40.00
5	126.00	42.54	36.00	101.00	40.00	128.00
	12.1		12.2		12.3	
1	8.00	2.00	8.00	2.00	8.00	2.00
2	36.90	25.20	51.60	33.00	33.50	27.00
3	42.00	34.00	54.00	40.00	34.50	30.00
4	45.00	56.00	55.00	50.00	35.00	35.00
5	46.00	108.00	56.00	108.00	38.00	125.00

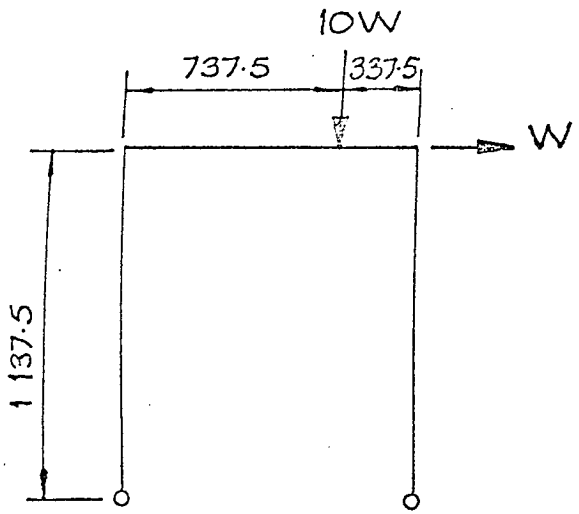

(a)

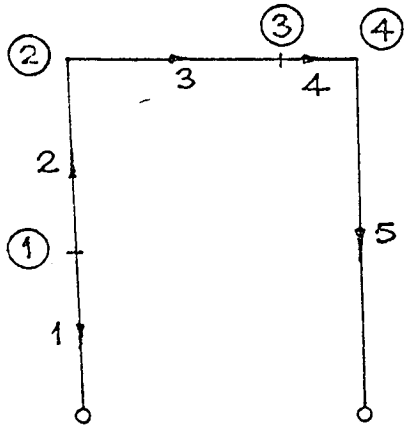

(b)

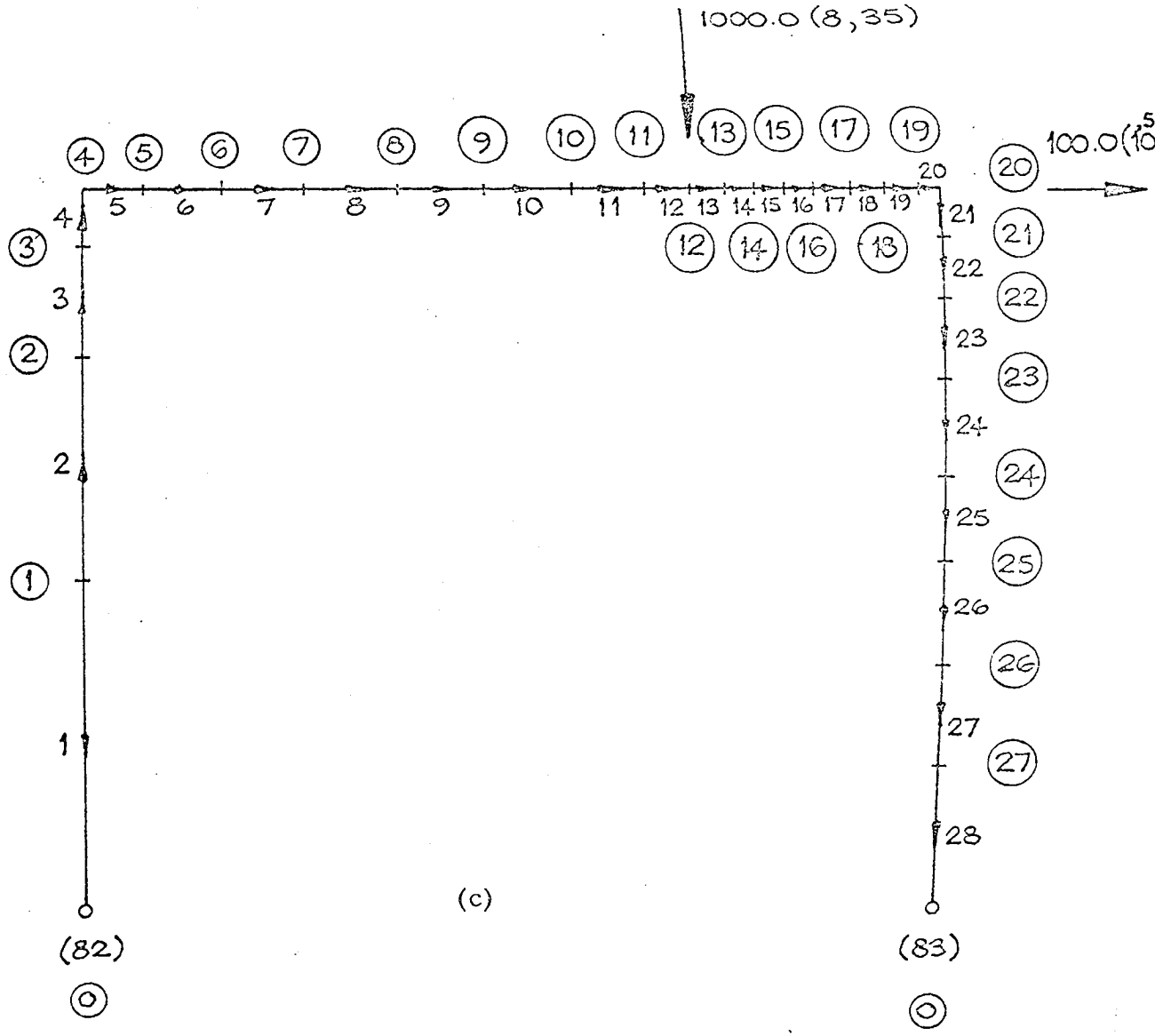

(c)

Figure A1.1

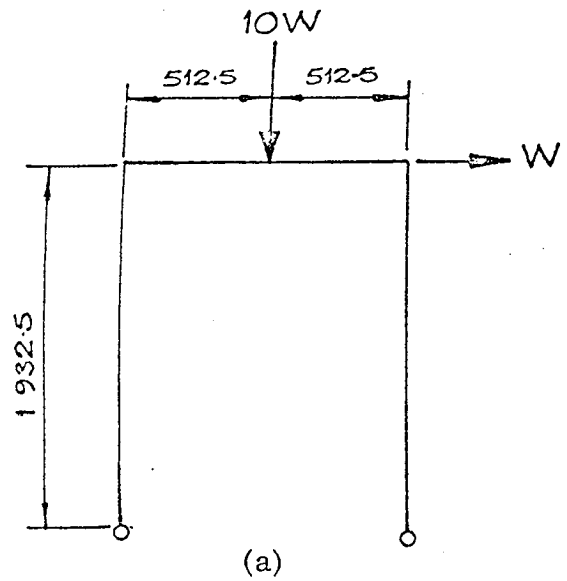

(a)

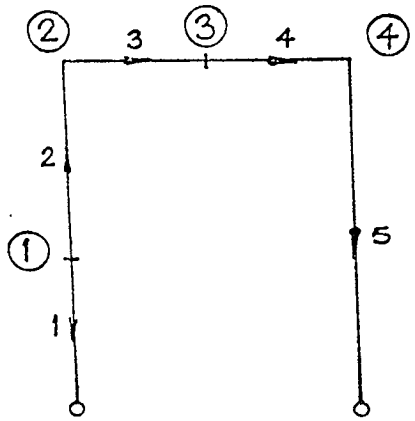

(b)

Figure A1.2

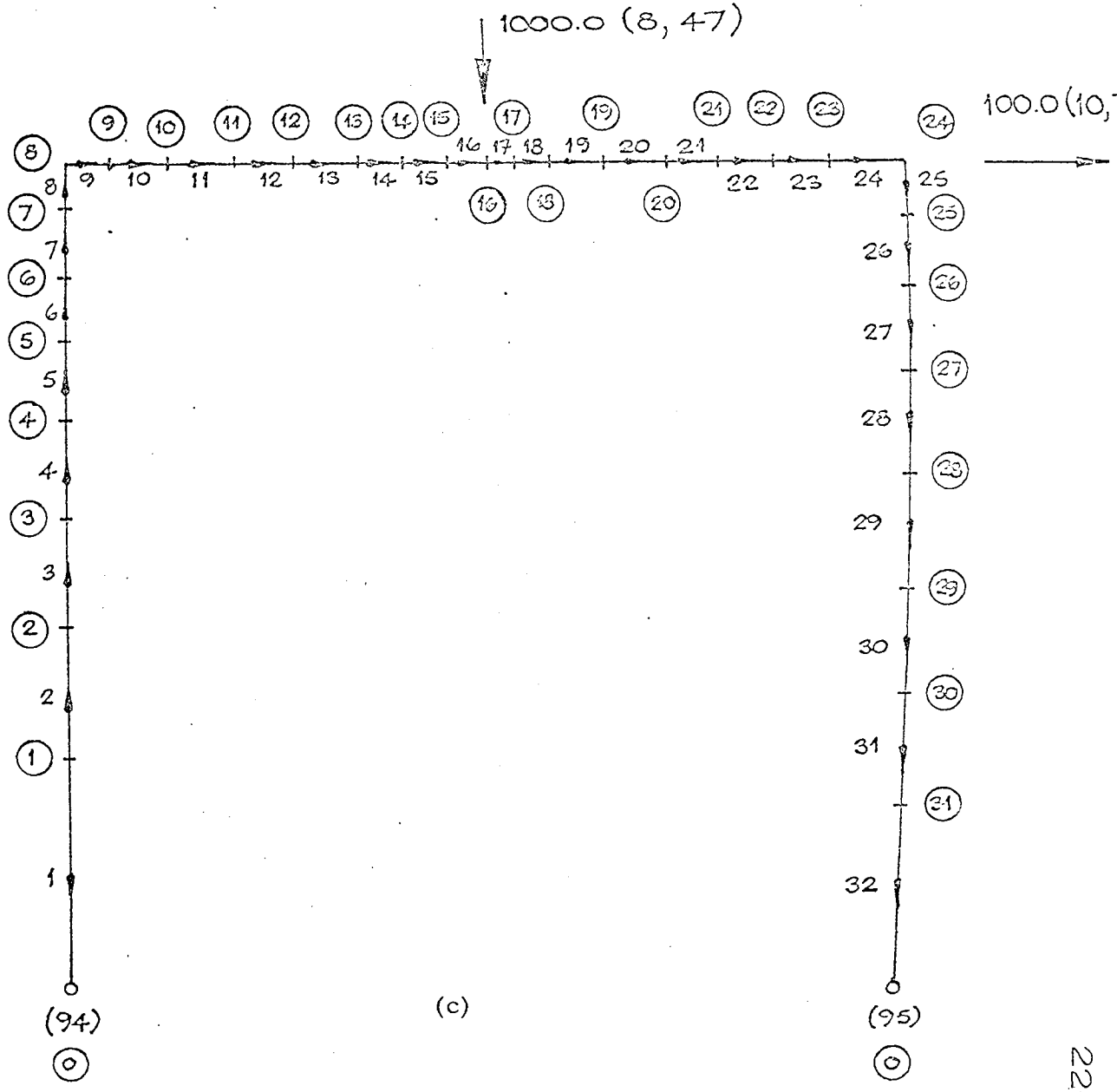

(c)

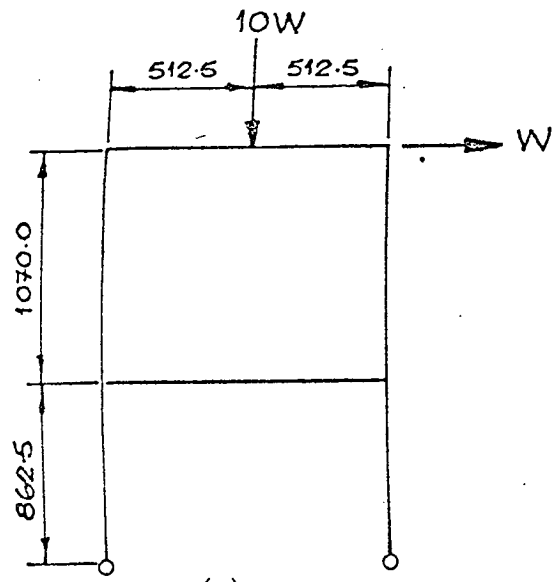

(a)

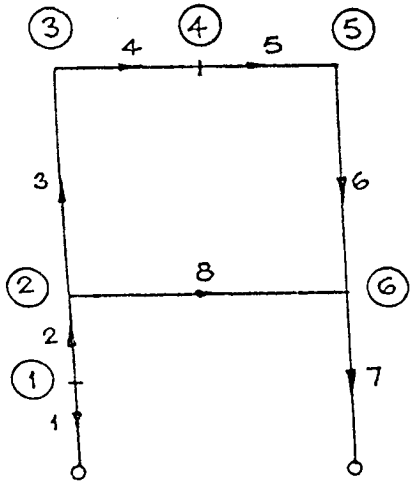

(b)

Figure A1.3

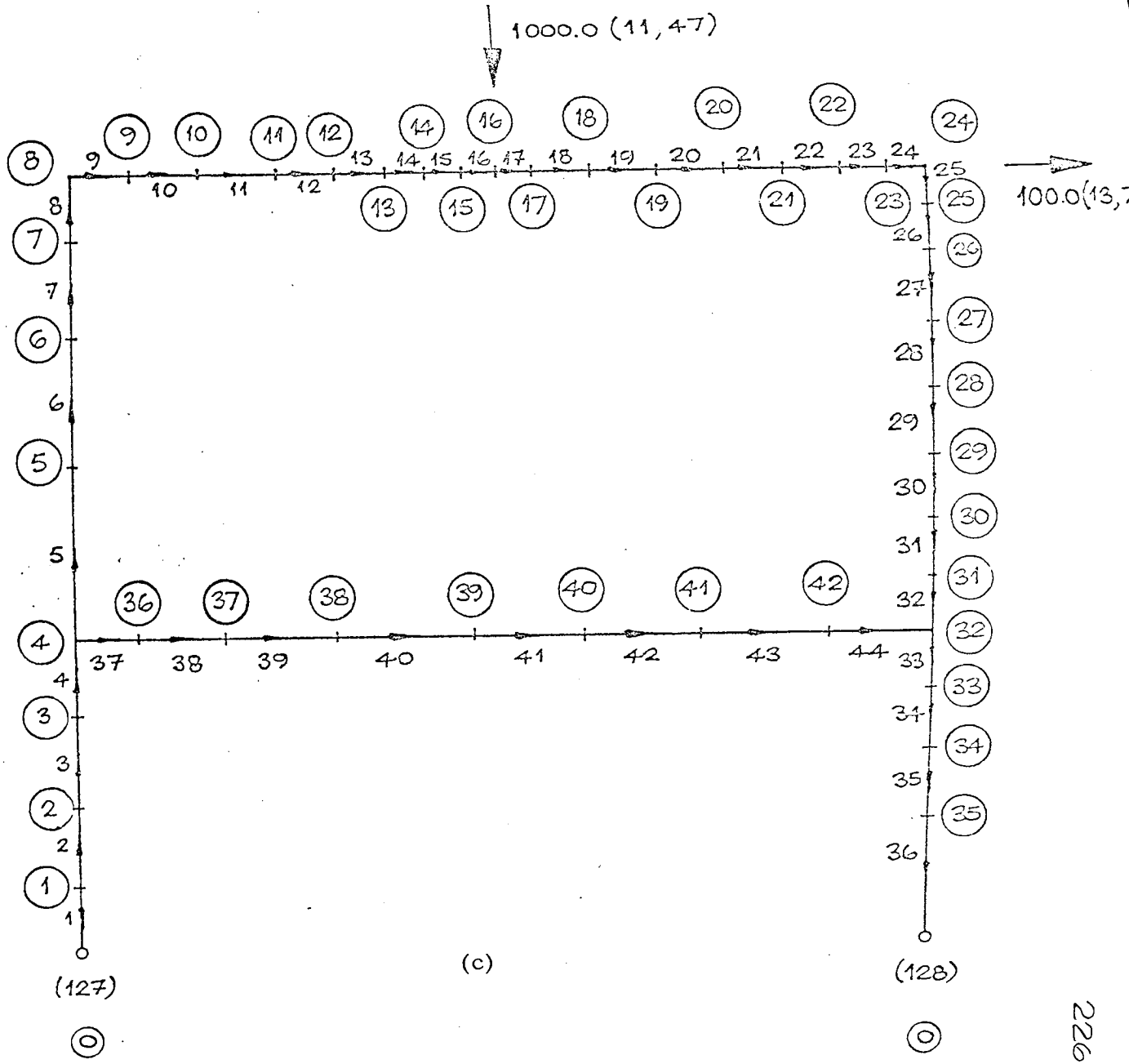

(c)

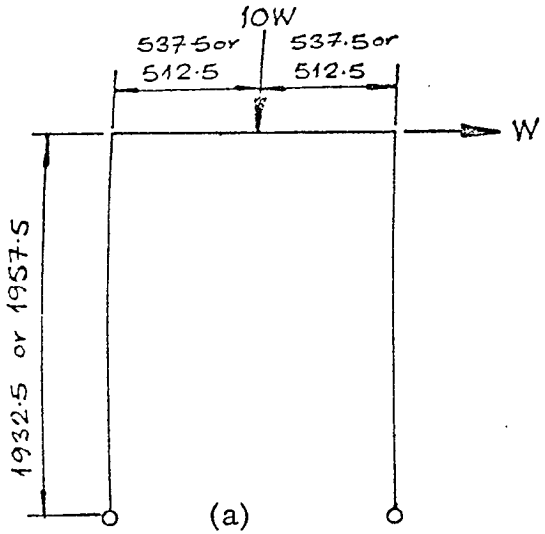
10W
537·5or
512·5
537·5or
512·5
W
1932·5 or 1957·5
(a)

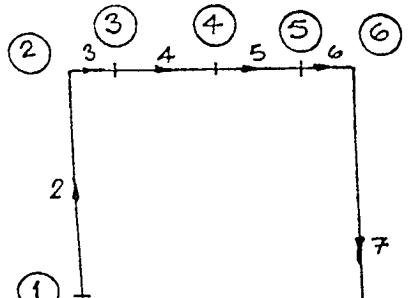
(b)

Figure A1.4

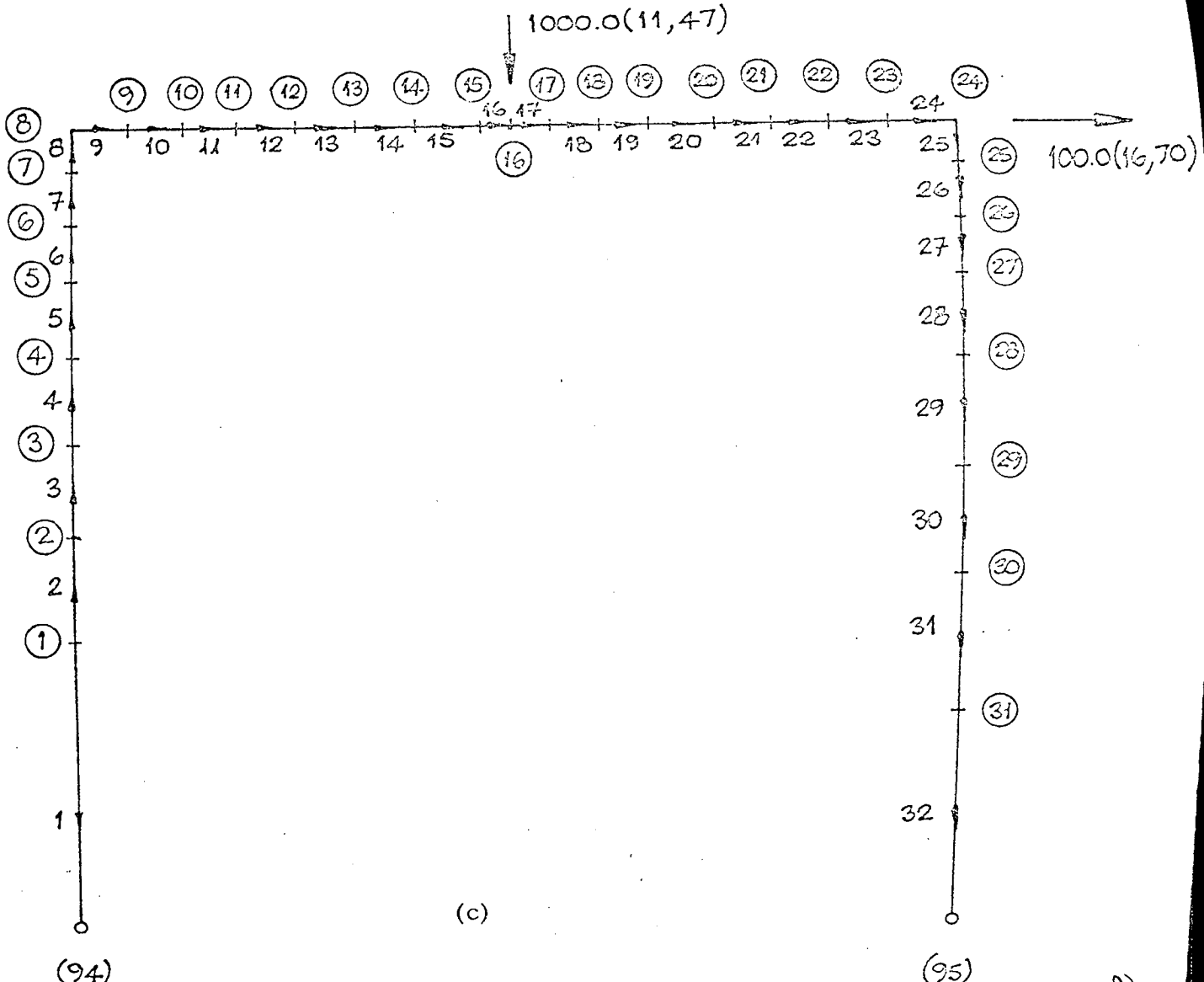
1000.0(11,47)
100.0(16,70)
(c)
(94)
(95)

APPENDIX (2)

Calculations of plastic collapse loads and mechanisms

A2.1 FRAMES F1, F2, F3

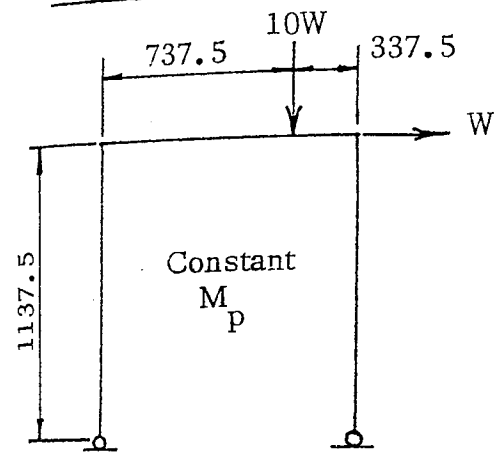

(1) Beam Mechanism

$$10W \times 337.5\,\theta = M_p (2.916)\theta \qquad (1)$$

$$W = 0.865 \times 10^{-3} M_p$$

(2) Sway Mechanism

$$W \times 1137.5\theta = M_p 2\theta \qquad (2)$$

$$W = 1.755 \times 10^{-3} M_p$$

(3) Combined Mechanism

$$10W \times 737.5\theta + W \times 1137.5\theta = 2M_p (\theta + \phi)$$

Now, $\phi = (737.5/337.5)\theta$

$$W = 0.748 \times 10^{-3} M_p$$

The ultimate bending moments of F1, F2, F3 are 49×10^5 ; 46×10^5 Nmm respectively.

The lowest collapse load is given by (3).

For each from the collapse loads are :-

$W_1 = 3.67$ kN

$W_2 = 3.45$ kN

$W_3 = 3.37$ kN

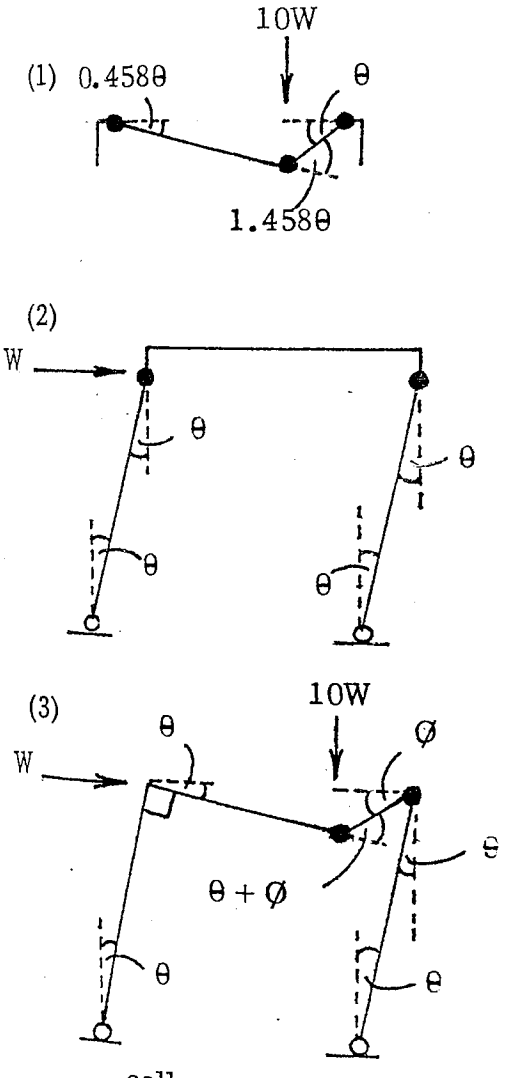

collapse mechanism

A2.2 FRAMES F4, F5

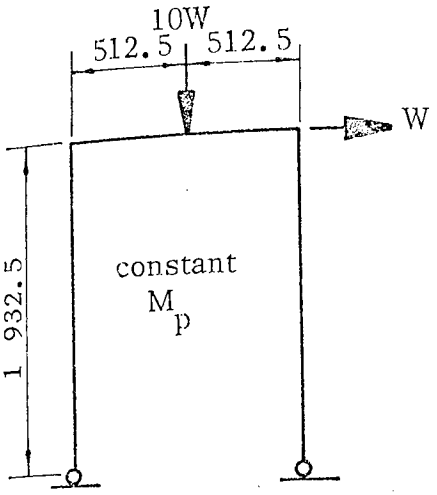

(1) Beam Mechanism

$$10W \times 512.5\theta = 4 M_p \theta \qquad (1)$$

$$W = 0.78 \times 10^{-3} M_p$$

(2) Sway Mechanism

$$W \times 1932.5\theta = 2 M_p \theta \qquad (2)$$

$$W = 1.035 \times 10^{-3} M_p$$

(3) Combined Mechanism

$$5125\ W\theta = 4 M_p \theta$$

$$1932.5\ W\theta = 2 M_p \theta$$

$$\text{cancel hinges} \quad -2 M_p \theta$$

$$7057.5\ W\theta = 4 M_p \theta$$

$$W = 0.566 \times 10^{-3} M_p$$

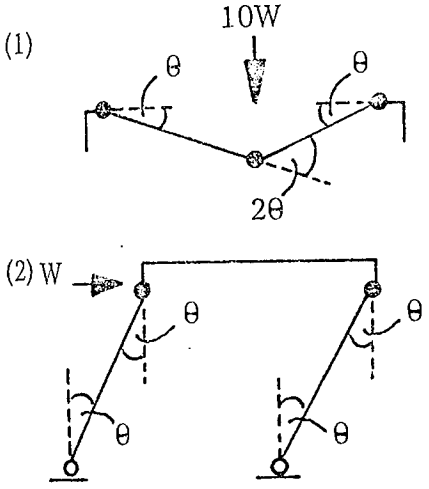

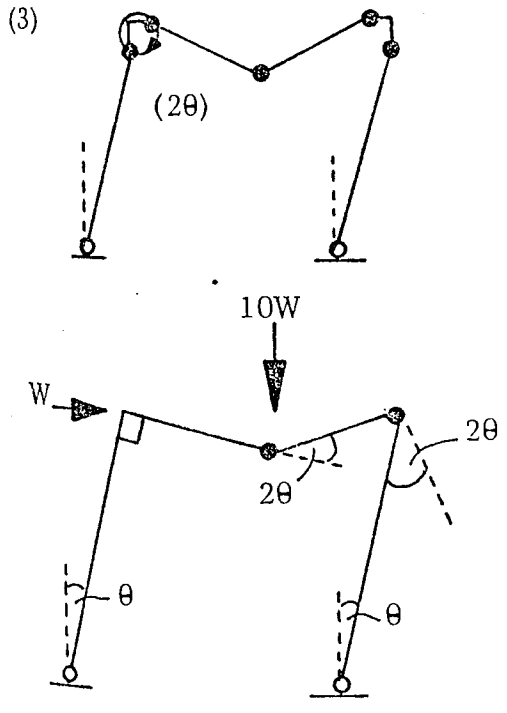

collapse mechanism

The ultimate bending moments of F4, F5 are 67.5×10^5 and 66×10^5 Nmm respectively

The lowest collapse load is given by (3)

The collapse loads of each frame are :-

$W_4 = 3.82$ kN

$W_5 = 3.75$ kN

A2.3 FRAMES F6, F7, F13

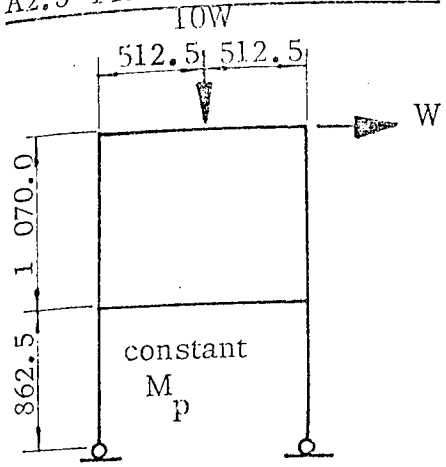

(1) Upper beam

$10W \times 512.5\theta = 4 M_p \theta$ (1)

$W = 0.781 \times 10^{-3} M_p$

(2) Upper sway

$1070 W\theta = 4 M_p \theta$ (2)

$W = 3.74 \times 10^{-3} M_p$

(3) Lower sway

$862.5 W\theta = 2 M_p \theta$ (3)

$W = 2.32 \times 10^{-3} M_p$

(4) Upper beam + upper sway

$5125 W\theta = 4 M_p \theta$

$1070 W\theta = 4 M_p \theta$

cancel hinges $= -2 M_p \theta$

$W = 0.97 \times 10^{-3} M_p$

(5) Upper sway + lower sway

$1070 W\theta = 4 M_p \theta$

$862.5 W\theta = 2 M_p \theta$

cancel hinges $-4 M_p \theta$

add hinges $+2 M_p \theta$

$W = 2.07 \times 10^{-3} M_p$

(6) Upper sway + lower sway + upper beam

$5125 W\theta = 4 M_p \theta$

$1070 W\theta = 4 M_p \theta$

$862.5 W\theta = 2 M_p \theta$

$-2 M_p \theta$

$-2 M_p \theta$

$-2 M_p \theta$

$+M_p \theta$

$+M_p \theta$

$W = 0.85 \times 10^{-3} M_p$

The lowest collapse load is given by (1)

(1)

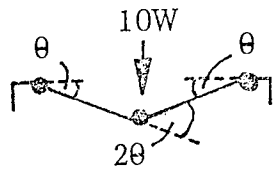

(2)

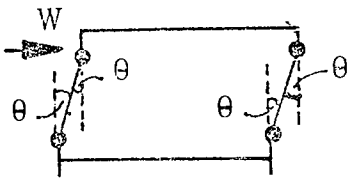

(3)

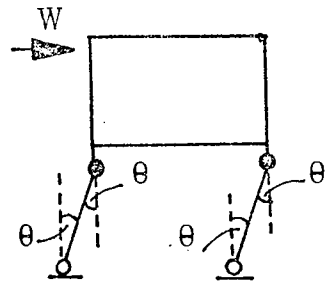

(4)

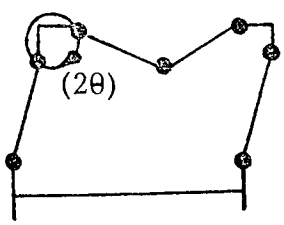

(5)

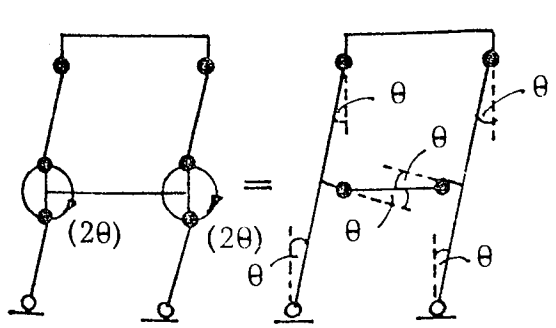

(6)

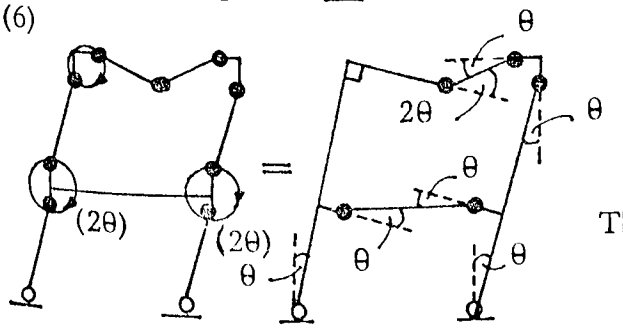

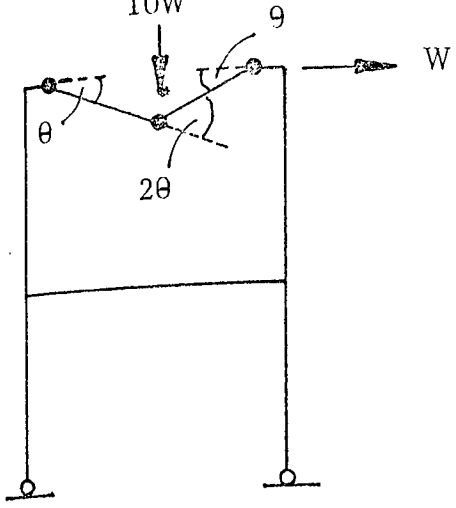

collapse mechanism

The ultimate bending moments of F6, F7, F13 are 68×10^5; 70×10^5; 74×10^5 Nmm respectively

The collapse loads of each frame are :-

$W_6 = 5.3$ kN

$W_7 = 5.47$ kN

$W_{13} = 5.78$ kN

A2.4 FRAME F9

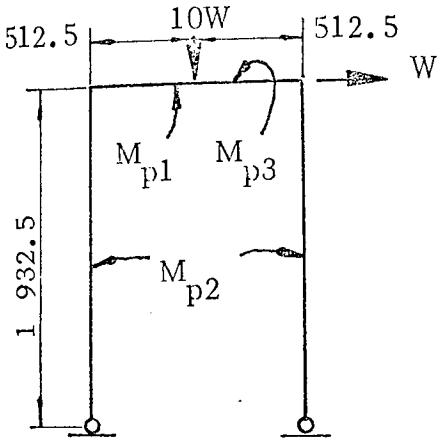

This frame has 3 values of ultimate bending moment.

$M_{p1} = 97 \times 10^5$ Nmm

$M_{p2} = M_{p3} = 65 \times 10^5$ Nmm

$M_{p1} = 1.5\, M_{p2} = 1.5\, M_{p3}$

(1)

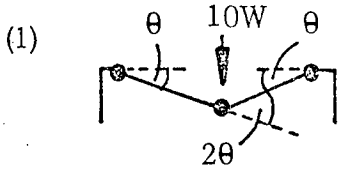

(1) Beam Mechanism

$10W \times 512.5\theta = (M_{p1} + M_{p3}) \times 2\theta$

$5125\, W\theta = 5\, M_{p3}\theta$ (1)

$W = 0.975 \times 10^{-3}\, M_{p3}$

(2)

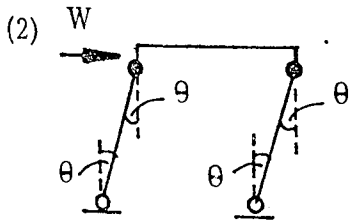

(2) Sway Mechanism

$1932.5\, W\theta = M_{p2} \times 2\theta$ (2)

$W = 1.03 \times 10^{-3}\, M_{p3}$

(3)

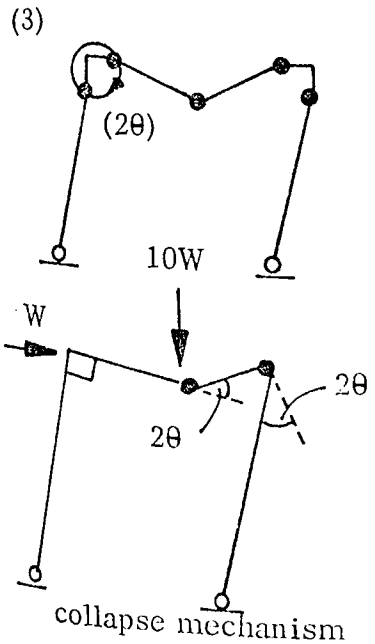

collapse mechanism

(3) Combined Mechanism

$5125\, W\theta = 5.0\, M_{p3}\, \theta$

$1932.5\, W\theta = 2.0\, M_{p3}\, \theta$

cancel hinges $= -2.0\, M_{p3}\, \theta$

$W = 0.708 \times 10^{-3}\, M_{p3}$

The lowest collapse load is given by (3)

$W_9 = 4.6$ kN

A2.5 FRAME F 10

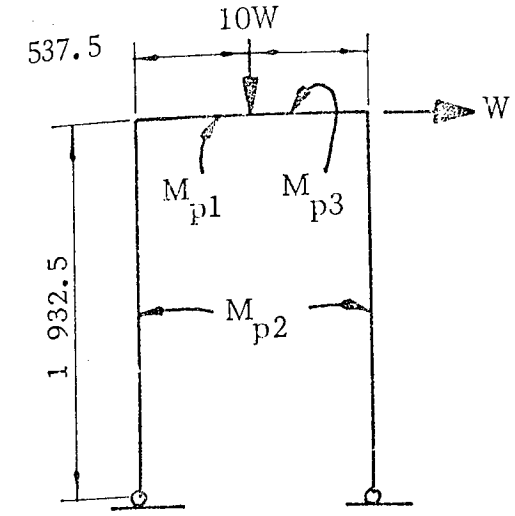

The 3 values of ultimate bending moments are :-

$M_{p1} = 98 \times 10^5$ Nmm

$M_{p2} = 36 \times 10^5$ Nmm

$M_{p3} = 60 \times 10^5$ Nmm

$M_{p1} = 2.72\ M_{p2}$; $M_{p3} = 1.67\ M_{p2}$

(1)

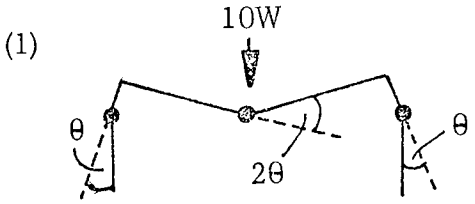

(1) Beam mechanism

$$5375\ W\theta = 2\theta(M_{p1}) + 2\theta(M_{p2}) \quad (1)$$

$$W = 1.383 \times 10^{-3}\ M_{p2}$$

(2)

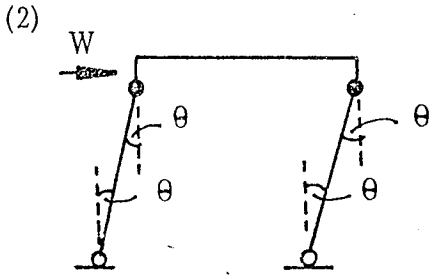

(2) Sway mechanism

$$1932.5\ W\theta = 2\ M_{p2}\theta \quad (2)$$

$$W = 1.032 \times 10^{-3}\ M_{p2}$$

(3)

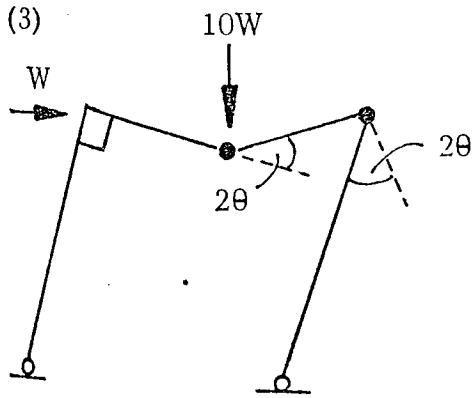

collapse mechanism

(3) Combined mechanism

$5375\ W\theta = 7.44\ M_{p2}\ \theta$

$1932.5\ W\theta = 2.00\ M_{p2}\ \theta$

cancel hinges $-2.00\ M_{p2}\ \theta$

$$W = 1.015 \times 10^{-3}\ M_{p2}$$

The lowest collapse load is given by (3)

$W_{10} = 3.66$ kN

A2.6 FRAME F11

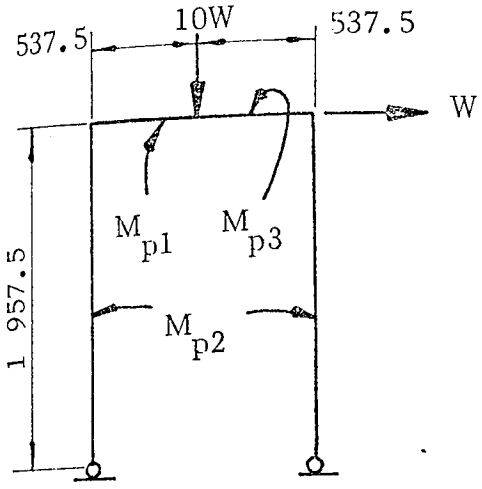

$M_{p1} = 126 \times 10^5$ Nmm

$M_{p2} = 36$ Nmm

$M_{p3} = 40$ Nmm

$M_{p1} = 3.5\, M_{p2}$; $M_{p3} = 1.11\, M_{p2}$

(1) Beam Mechanism

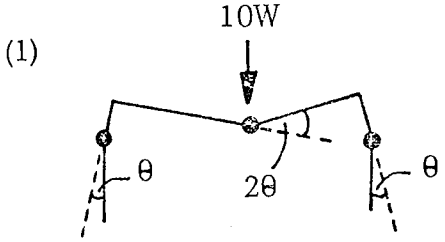

$$5375\, W\theta = 3.5\, M_{p2} \times 2\theta + 2\theta\, M_{p2} \quad (1)$$

$$W = 1.675 \times 10^{-3}\, M_{p2}$$

(2) Sway Mechanism

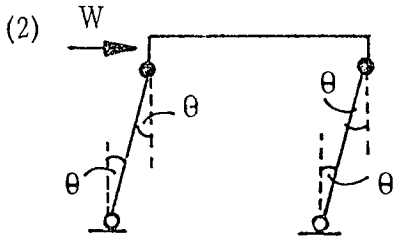

$$1957.5\, W\theta = 2\, M_{p2}\, \theta \quad (2)$$

$$W = 1.02 \times 10^{-3}\, M_{p2}$$

(3) Combined Mechanism

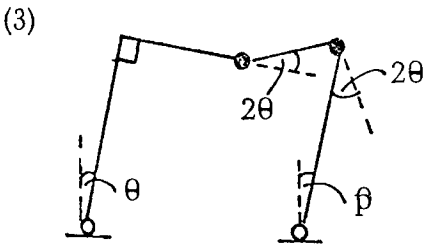

$5375\, W\theta = 9\, M_{p2}\, \theta$

$1957.5\, W\theta = 2\, M_{p2}\, \theta$

cancel hinges $= -2\, M_{p2}\, \theta$

$$W = 1.228 \times 10^{-3}\, M_{p2}$$

The lowest collapse load is given by (2)

$$W_{11} = 3.68 \text{ kN}$$

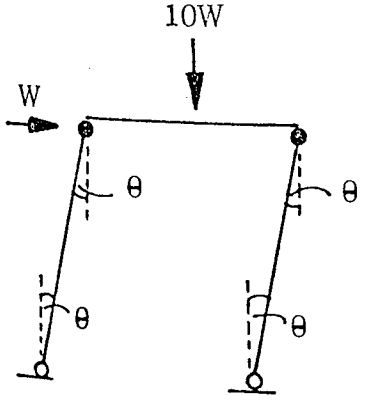

collapse mechanism

A2.7 FRAME F12

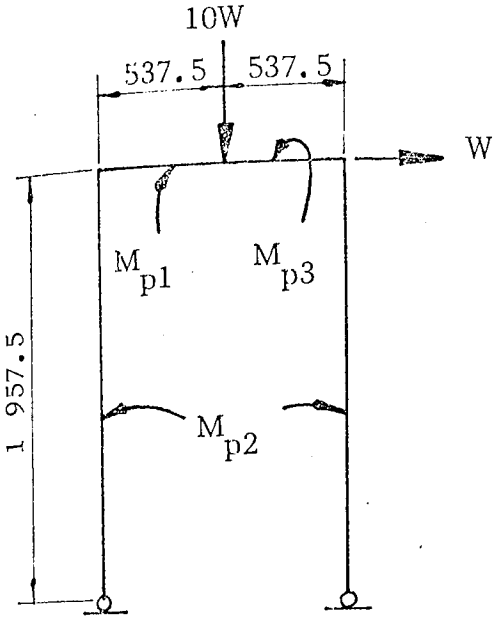

$M_{p1} = 46 \times 10^5$ Nmm

$M_{p2} = 56 \times 10^5$ Nmm

$M_p 3 = 38 \times 10^5$ Nmm

$M_{p1} = 1.21\ M_{p3}$; $M_{p2} = 1.47\ M_{p3}$

(1) Beam Mechanism

$5375\ W\theta = 2\ M_{p1}\theta + 2\ M_{p3}\theta$

$5375\ W\theta = 4.42\ M_{p3}\theta$ (1)

$W = 0.824 \times 10^{-3}\ M_{p3}$

(1)

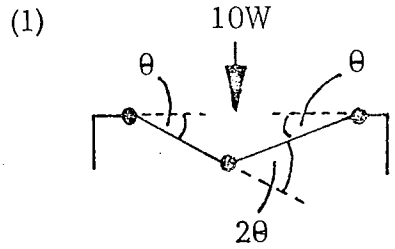

(2) Sway Mechanism

$1957.5\ W\theta = 2\ M_{p3}\theta$ (2)

$W = 1.021 \times 10^{-3}\ M_{p3}$

(2)

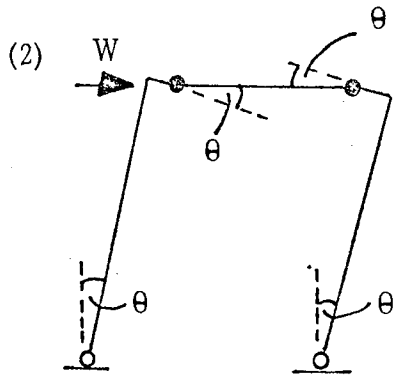

(3) Combined Mechanism

$5375\ W\theta = 4.42\ M_{p3}\theta$

$1957\ W\theta = 2.00\ M_{p3}\theta$

cancel hinges $-2.00\ M_{p3}\theta$

$W = 0.604 \times 10^{-3}\ M_{p3}$

(3)

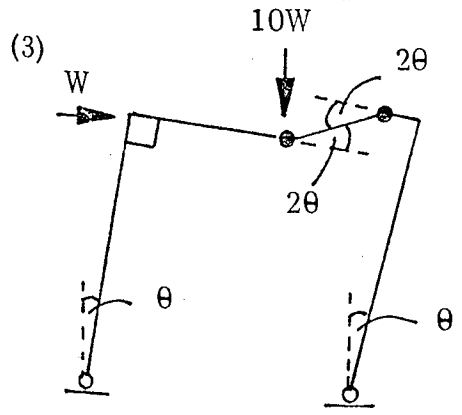

collapse mechanism

The lowest collapse load is given by (3)

$W_{12} = 2.3$ kN

REFERENCES

1. British Standards Institution 'CP110 - The Structural Use of Concrete'. (1972).

2. Baker J. F. 'A Review of Recent Investigations into the Behaviour of Steel Frames in the Plastic Range'. J. I. C. E. 31 188 (1949).

3. Baker J. F., Horne M. R. and Heyman J. 'The Steel Skeleton' Vol. 2, Cambridge University Press (1956).

4. Horne M. R. 'A Moment-Distribution Method for the Analysis and Design of Structures by the Plastic Theory'. Proc. Inst., Civ. Engrs., Vol. 3, Part III (Apr. 1954).

5. Neal B. G. and Symmonds P. S. 'The Rapid Calculation of Plastic Collapse Loads for a Framed Structure'. Proc. Inst. Civ. Engrs., Vol. 1, Part III (Apr. 1952).

6. British Standards Institution 'CP114 - The Structural Use of Reinforced Concrete'. (Amended 1965)

7. British Standards Institution 'British Standard Code of Practice for the Structural Use of Reinforced Concrete' (Draft), (1969).

8. Baker A. L. 'Limit Design of Reinforced Concrete'. Cement and Concrete Association (C. & C. A.) (1970).

9. Livesley R. K. and Chandler D. B. 'Stability Functions for Structural Frameworks'. Manchester University Press, (1956).

10. Wood R. H. 'The Stability of Tall Buildings'. Proc. Inst. Civ. Engrs., Vol. 11, (Sept. 1958).

11. Heyman J. 'An Approach to the Design of Tall Steel Buildings'. Proc. Inst. Civ. Engrs., Vol. 17, (Dec. 1960).

12. Holmes M. and Gandhi S. N. 'Ultimate Load Design of Tall Steel Buildings allowing for Instability'. Proc. Inst. Civ. Engrs., Vol. 30, (Jan. 1965).

13. Driscoll G. C., Beedle L. S., Galambos T. V., Lu L. W., Fisher J. W., Ostapenko A. and Daniels J. H. 'Plastic Design of Multi-Storey Frames'. Dept. of Civil Engineering, Lehigh University, Bethlehem, Pa, (1965).

14. Livesley R. K. 'The Application of an Electronic Digital Computer to Some Problems of Structural Analysis'. Struct. Engr., Vol. 34, (Jan. 1956).

15. Livesley R. K. 'The Application of Computers to Problems Involving Plasticity'. Symposium on the Use of Electronic Computers in Structural Engineering, University of Southampton, (1959).

16. Jennings A. and Majid K. I. 'An Elastic-Plastic Analysis for Framed Structures Load Upto Collapse'. Struct. Engr., Vol. 43, (Dec. 1965).

17. Anderson D. 'Investigations Into the Design of Plane Structural Frames'. Ph.D. Thesis, Manchester University, (1969).

18. Majid K. I. and Anderson D. 'The Computer Analysis of Large Multi-Storey Framed Structures'. Struct. Engr., Vol. 46, No. 11, (Nov. 1968).

19. Livesley R. K. 'Matrix Methods of Structural Analysis'. Pergamon Press, London (1969).

20. Jennings A. 'A Compact Storage Scheme for the Solution of Symmetric Linear Simultaneous Equations'. The Computer Journal, Vol. 9, (Nov. 1966).

21. Majid K. I. and Anderson D. 'Elastic-Plastic Design of Sway Frames by Computer'. Proc. Inst. of Civ. Engrs., Vol. 41, (Dec. 1968).

22. Onen Y. H. 'The Elastic-Plastic Analysis of Complete Building Structures'. Ph.D Thesis, Aston University (1973).

23. Majid K. I. and Croxton P. C. L. 'Wind Analysis of Complete Building Structures by Influence Coefficients'. Proc. Inst. Civ. Engrs. Vol. 47, (Oct. 1970).

24. Davies J. M. 'The Plastic Collapse of Framed Structures Clad with Corrugated Steel Sheeting'. Proc. Inst. Civ. Engrs. Vol. 55, (March 1973).

25. Glanville W. H. and Thomas F. G. 'Moment Redistribution in Reinforced Concrete'. London, H. M. Stationary Office, Building Research Technical Paper No. 22, (1939).

26. Evans R. H. 'The Plastic Theories for the Ultimate Strength of R. C. Beams'. Journ. Inst. Civ. Engrs. (Dec. 1943).

27. Baker A. L. L. 'A Plastic Theory of Design for Ordinary Reinforced and Prestressed Concrete Including Moment Redistribution in Continuous Members.' Mag. of Conc. Research, Vol. 1, No. 2, (June 1949).

28. Baker A.L. L. 'The Ultimate Load Theory Applied to the Design of Reinforced and Prestressed Concrete Frames'. Concrete Publications, (1956).

29. Baker A. L. L. 'Ultimate Load Theory for Concrete Frame Analysis'. Trans. of Amer. Soc. of Civ. Engrs., Paper No. 3386, Vol. 127, Part II, (1962).

30. Baker A. L. L. 'The Inelastic Space Frame'. Concrete Publications, (1967).

31. Report of the Research Committee. 'Ultimate Load Design of Concrete Structures'. Report with discussion, Inst. of Civ. Engrs., (1962).

32. Baker A. L. and Amarakone A. M. N. 'Inelastic Hyperstatic Frame Analysis'. A. C. I., Sp. - 12, Proc. of the Int. Symp. on Flexural Mechanics of Reinforced Concrete, Miami, U.S.A., (1964).

33. Committe European de Beton. 'Recommendations for an International Code of Practice for Reinforced Concrete'. English translation, Cement and Concrete Association (C. & C. A.).

34. Cranston W. B. 'A Computer Method for the Inelastic Analysis of Plane Frames'. C. & C. A. Tech. Report TRA/386, (1965).

35. Cranston W. B. 'Tests on Reinforced Concrete Frames 1 : Pinned Portal Frames'. C. & C. A. Tech. Report TRA/392, (1965).

36. Cranston W. B. and Cracknell J. A. 'Tests on Reinforced Concrete Frames 2 : Portal Frames with Fixed Feet'. C. & C. A. Tech. Report TRA/420,(1969)

37. Hognestad E., Hanson N. W. and McHenry D. 'Concrete Stress Distribution in Ultimate Strength Design'. Journ. Amer. Conc. Inst., Vol. 27, No. 4, (Dec. 1955).

38. Cranston W. B. 'Determining the Relation Between Moment, Axial Load and Curvatures for Structural Members'. C. & C. A. Tech. Report TRA/395, (1966).

39. Cranston W. B. 'A Computer Method for the Analysis of Restrained Columns'. C. & C. A. Tech. Report TRA/402, (1967).

40. Cranston W. B. 'Analysis and Design of Reinforced Concrete Columns'. C. & C. A. Res. Report 20, (1972).

41. Cranston W. B. and Reynolds G. C. 'The Influence of Shear on the Rotational Capacity of Reinforced Concrete Frames'. C. & C. A. Tech. Report TRA/439, (1970).

42. Swann R. A. 'Flexural Strength of Corners of Reinforced Concrete Portal Frames'. C. & C. A. Tech. Report TRA/434, (1969).

43. Sommerville G. and Taylor H. P. J. 'The Influence of Reinforcement Detailing on the Strength of Concrete Structures'. Struct. Engr. No. 1, Vol. 50 (Jan. 1972).

44. Baker A. L. 'Frame Instability'. Concrete, (Feb. 1967).

45. Nahhas U. and Yu C. W. 'The Elastic-Plastic Design of Reinforced Concrete Sway Frames against Instability'. Proc. Inst. Civ. Engrs., Vol. 53, (June 1972).

46. Chin M. W. 'The Failure Loads of High Tensile Steel Structures'. Ph.D Thesis, Manchester University, (1966).

47. Nahhas U. 'The Inelastic Behaviour of Reinforced Concrete Sway Frames with Special Reference to Instability'. Ph.D Thesis, London University, (1970).

48. Wilson E. L. 'Matrix Analysis of Non-Linear Structures'. Proc. of Amer. Soc. of Civ. Engrs. Second Conf. on Elec. Computation, Pittsburg, (Sept. 1960).

49. Cohn N. Z. 'Limit Design of Reinforced Concrete Frames'. A. S. C. E. Vol. 94, ST10, (Oct. 1968).

50. Poologasumdram K. 'Analysis of Three Bay Reinforced Concrete Frames'. Conc. & Const. Eng's. (1961).

51. Monnier Th. 'The Moment Curvature Relation of Reinforced Concrete'. Heron (Netherlands), Vol. 17, No. 2 (1970).

52. Majid K. I. 'Non-Linear Structures'. Butterworths, (1972).

53. Neville A. M. 'Properties of Concrete'. Pitman, (1963).

54. Wainwright P. J. ' Ultimate Strength in Bending and Torsion of Prestressed Beams Reinforced with Longitudinal Steel Only'. Ph.D Thesis, Aston University, (1972)

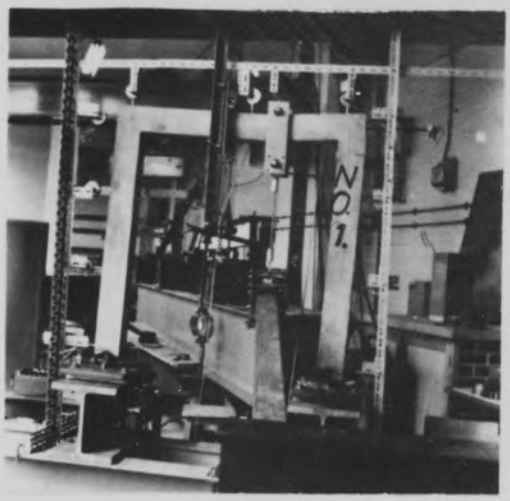

COLLAPSE OF F1

PLATE 1

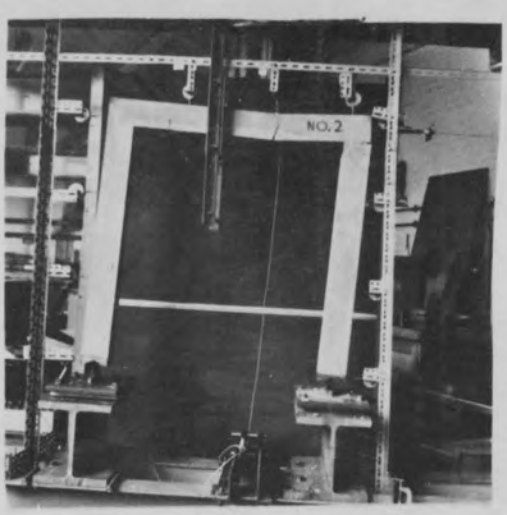

COLLAPSE OF F2

PLATE 2

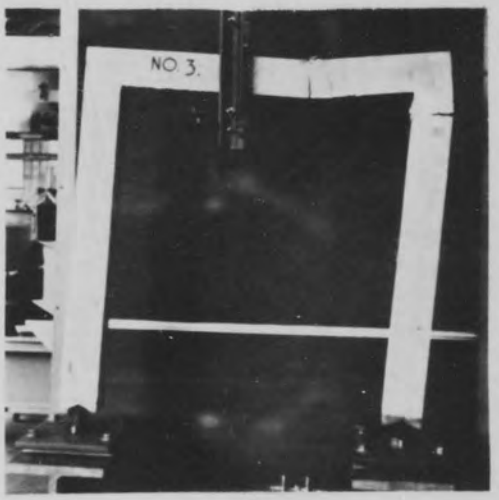

COLLAPSE OF F3

PLATE 3

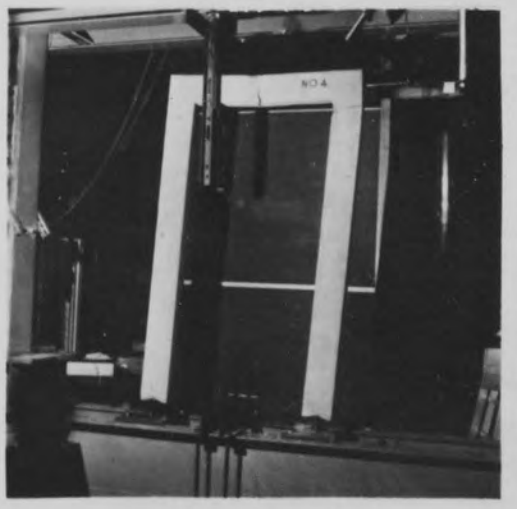

COLLAPSE OF F4

PLATE 4

COLLAPSE OF F5

PLATE 5

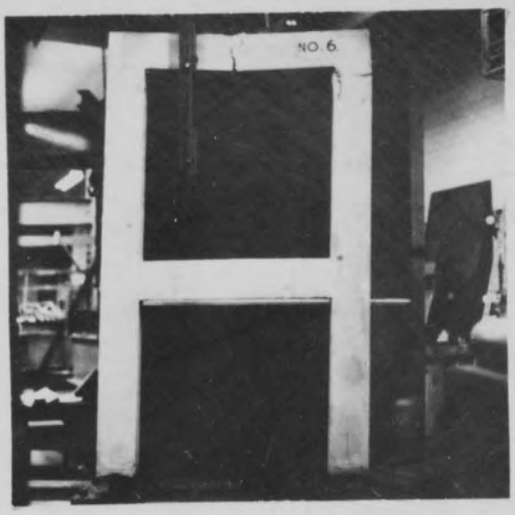

COLLAPSE OF F6

PLATE 6

COLLAPSE OF F7

PLATE 7

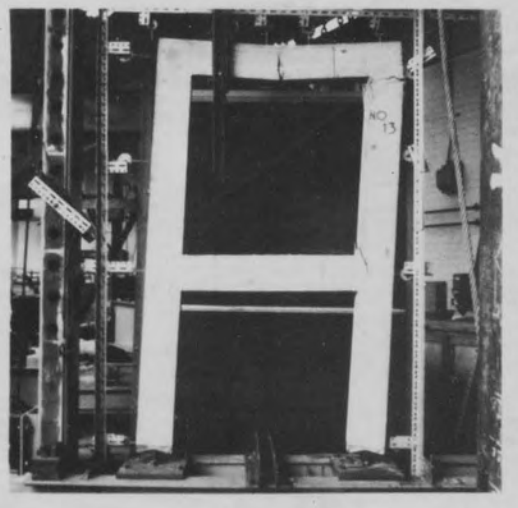

COLLAPSE OF F13

PLATE 8

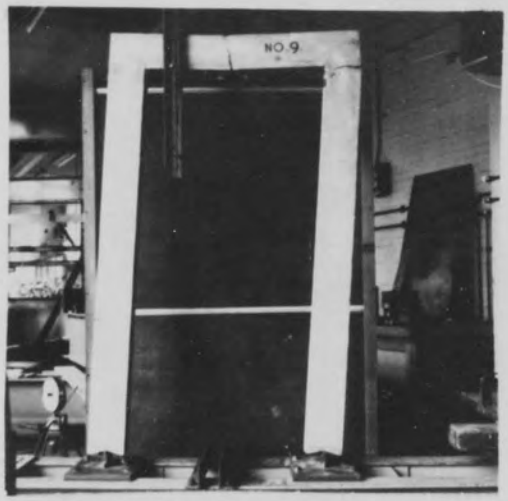

COLLAPSE OF F9

PLATE 9

COLLAPSE OF F10

PLATE 10

COLLAPSE OF F11

PLATE 11

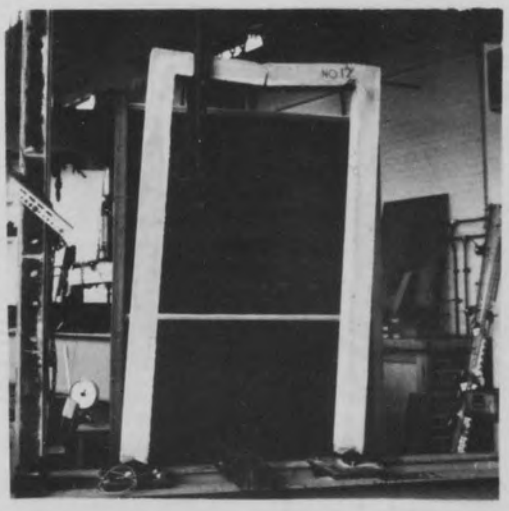

COLLAPSE OF F12

PLATE 12

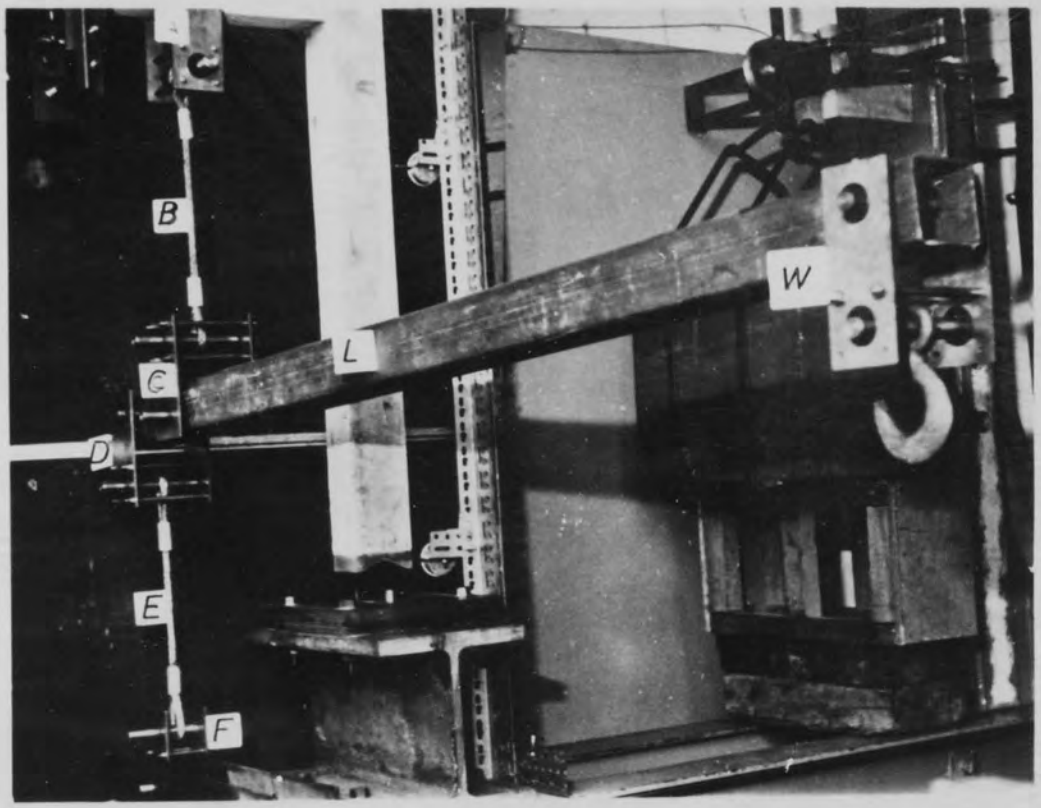

LOAD LEVER SYSTEM

PLATE 13

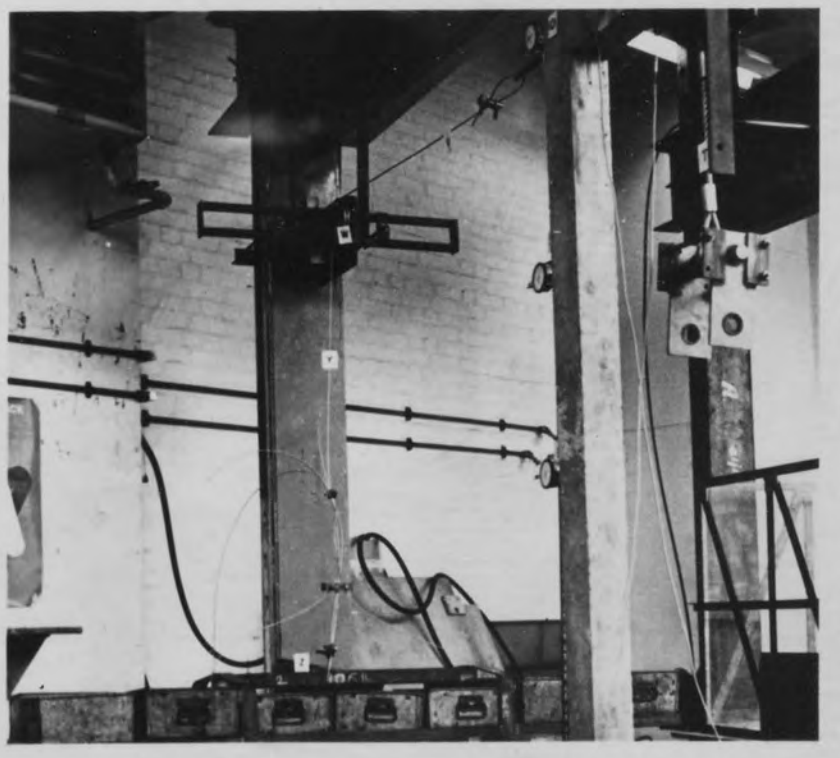

SIDE LOAD SYSTEM

PLATE 14

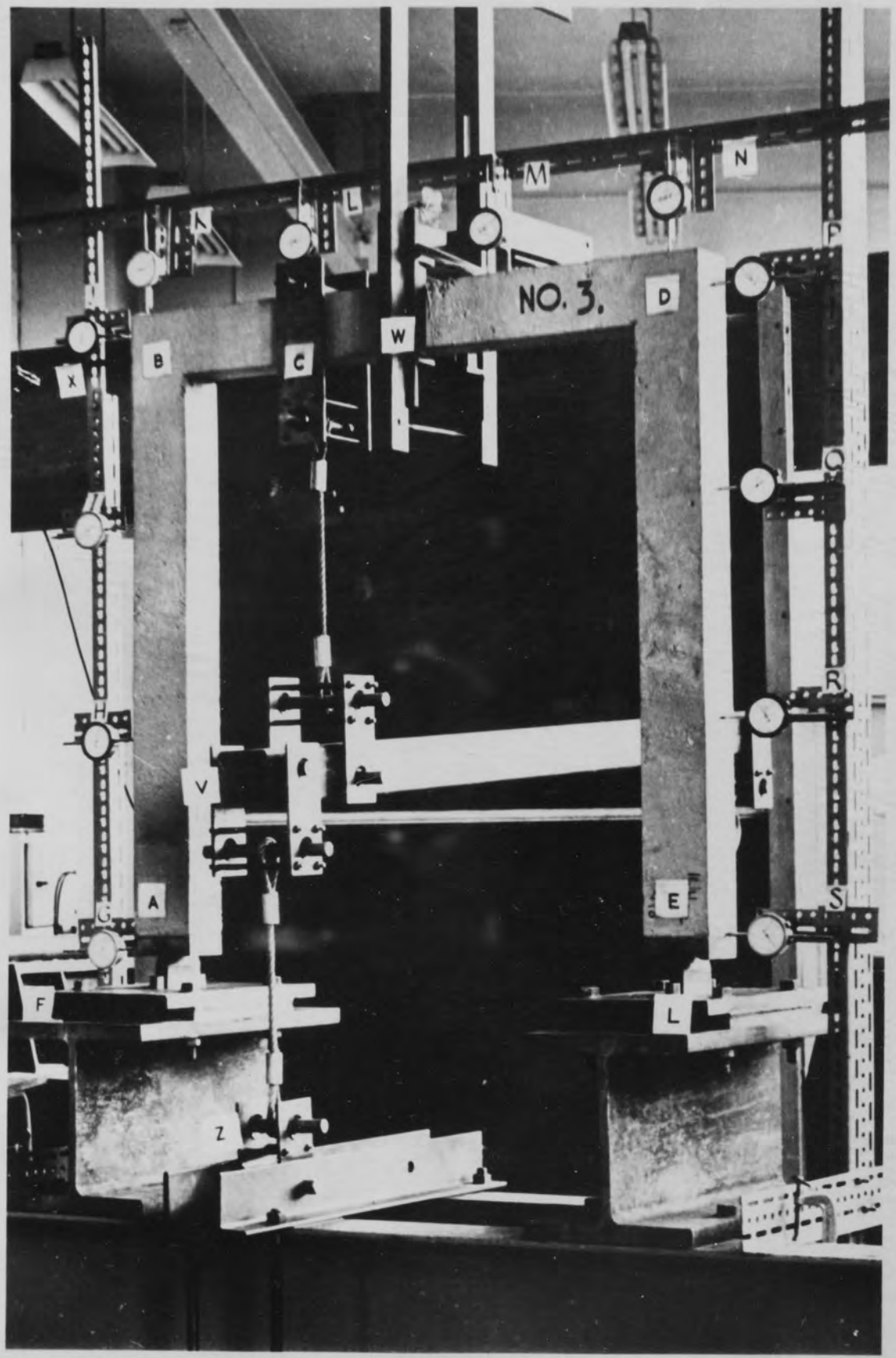

GENERAL VIEW OF A FRAME BEFORE TESTING

PLATE 15

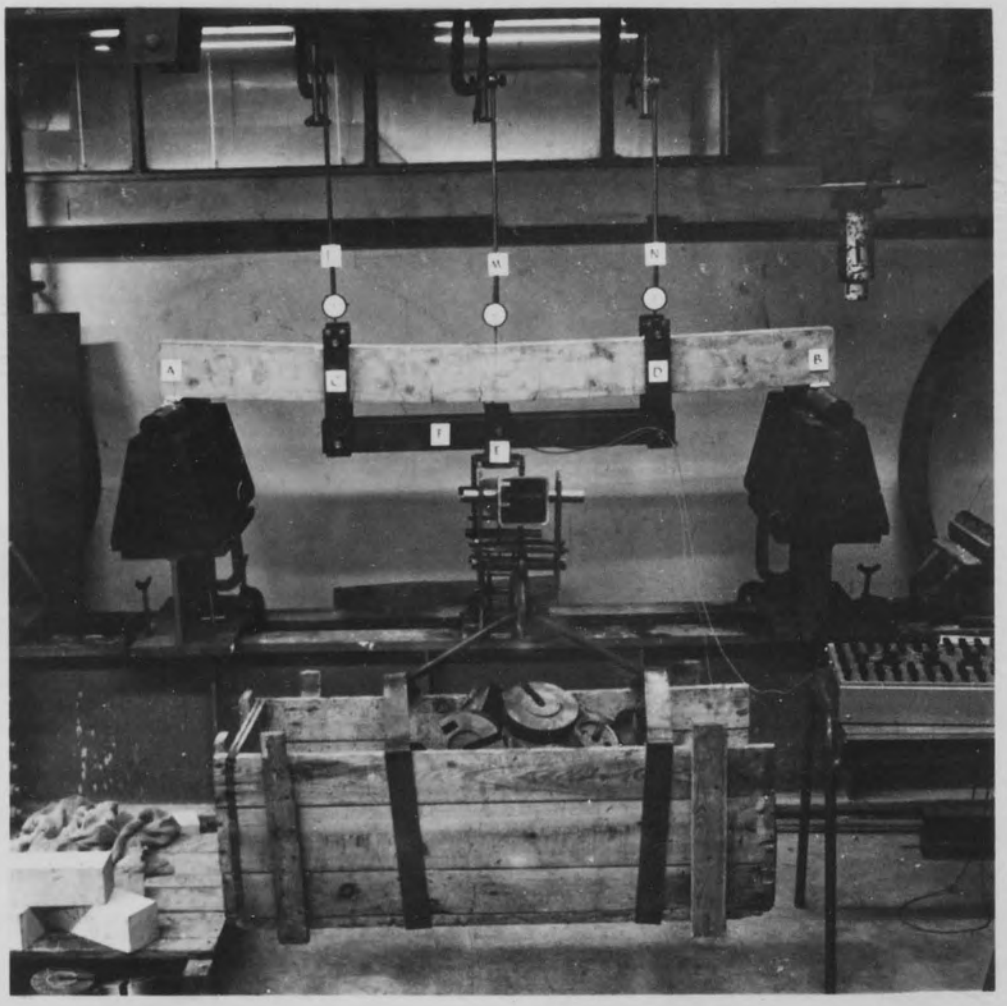

GENERAL ARRANGEMENT OF A BEAM TEST

PLATE 16

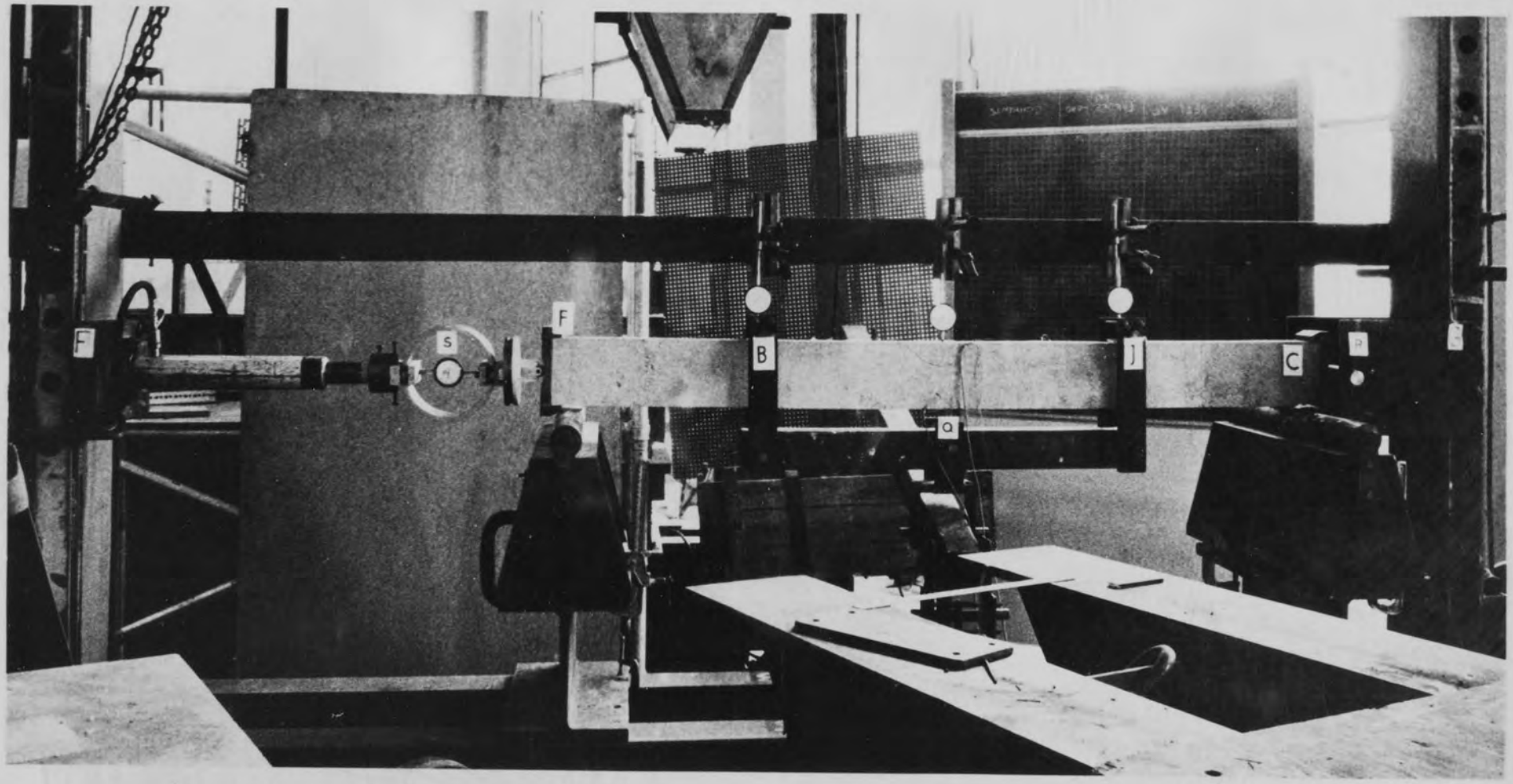

GENERAL VIEW OF A BEAM TEST WITH AXIAL LOAD

PLATE 17